

37

DERA Rohstoffinformationen



**Investigation of tin and tantalum ores
from the Rondônia Tin Province, northern Brazil,
to develop optimized processing technologies**

Impressum

Editors: German Mineral Resources Agency (DERA) at the
Federal Institute for Geosciences and Natural Resources (BGR)
Wilhelmstrasse 25–30
13593 Berlin, Germany
Tel.: +49 30 36993 226
Fax: +49 30 36993 100
dera@bgr.de

Serviço Geológico do Brasil (CPRM)
REPO – Residência de Porto Velho
DGM – Diretoria de Geologia e Recursos Minerais
Tel.: +55 (069) 3901 3722
Fax: +55 (069) 999 561 988
tiago.buch@cprm.gov.br

Authors: Tiago Buch (CPRM), Dr. Herwig Marbler (BGR),
Dr. Simon Goldmann (BGR),
Dr. Frank Haubrich (G.E.O.S. Ingenieurgesellschaft mbH),
Michael Trinkler (Erz&Stein – Gesellschaft für Lagerstätten- und
Rohstoffberatung bR)

Project coordination: Dr. Herwig Marbler (BGR)
Tiago Buch (CPRM)

Contact BGR: Dr. Herwig Marbler: herwig.marbler@bgr.de

Contact CPRM: Tiago Buch: tiago.buch@cprm.gov.br

Layout: deckermedia GbR

Date: October 2018

Cover Images: DERA Berlin

ISBN: 978-3-943566-52-9 (print version)
ISBN: 978-3-943566-53-6 (online pdf version)
ISSN: 2193-5319

Reference: Buch, T., Marbler, H., Goldmann, S., Haubrich, F., Trinkler, M. (2018):
Investigation of tin and tantalum ores from the Rondônia Tin Province,
northern Brazil, to develop optimized processing technologies
DERA Rohstoffinformationen 37: 160 pp.; Berlin.

Berlin, 2018



Bundesministerium
für Wirtschaft
und Energie

The BGR (Federal Institute for Geosciences and Natural Resources) is the central geoscientific authority providing advice to the German Federal Government in all geo-relevant questions. It is subordinate to the Federal Ministry for Economic Affairs and Energy (BMWi).

Investigation of tin and tantalum ores from the Rondônia Tin Province, northern Brazil, to develop optimized processing technologies

Published jointly by the German Mineral Resources Agency (DERA)
and the Geological Survey of Brazil (CPRM)



Forewords

This report is the first work of the Geological Survey of Brazil (CPRM) in partnership with the German Mineral Resources Agency (DERA) as part of the Federal Institute for Geosciences and Mineral Resources of Germany since the 1970's. We are proud to announce the conclusion of the project: Mineral Identity of the Rondônia Tin Province. With the aim of supporting the strategic needs of Germany's high technology industry, this work is a milestone in the bilateral relationship between Brazil and Germany.

Focused on the improvement of mineral processing for tin ore and its by-products in the traditional tin mines of Rondônia, this project is expected to show the potential for tin, tantalum and niobium in the Rondônia Tin Province. We expect that this potential will serve to increase our trade and investment bonds with Germany.

This work was developed with the support of our geologists based in the state of Rondônia and our counterparts in Germany, creating a valuable opportunity for technical cooperation between our institutions. We look forward to implementing more joint ventures with our partner, BGR/DERA, creating more results to foster German investment in our mining sector.



Dr. Maria Glícia da Nóbrega Coutinho

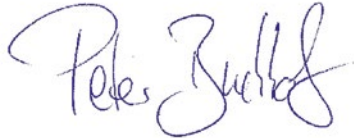
Head of International Affairs, CPRM, Brazil

Brazil is one of the major players in the global raw materials sector. For Germany, Brazil is the most important trading partner in Latin America and also a reliable supplier for a range of metals, industrial minerals and intermediate products. Besides imports of raw materials like iron ore, copper, nickel, aluminum, silicon and several ferroalloys such as ferroniobium, ferromanganese and ferrosilicon, Brazil has important tin and tantalum deposits within the state of Rondônia which could be of interest to the German manufactory industry. Both, tin and tantalum are defined by the European Commission as potentially critical raw materials for the EU.

Together with our Brazilian partner institution CPRM, the geological Survey of Brazil, we show the resource potential of tin and tantalum deposits in the Rondônia Tin Province. The main focus of this study is to highlight beneficiation methods, in order to archive an efficient and sustainable extraction method for tin and tantalum from Rondônia ores. Following China, Japan and the USA, Germany is in fourth place in tin global refined tin consumption and on the ninth place in the demand of tantalum products. Thus, new sources for a sustainable supply of these high tech metals could be of interest to the German industry.

This report not only looks at new procurement opportunities in Brazil, but also discusses the very interesting results of processing tests performed at an industrial scale. For the German-Brazilian co-operation it is of great benefit to integrate interests of the German manufacturing industry with German engineering skills and German mining know-how within the mining sector of Rondônia.

Furthermore, the cooperation between DERA and the CPRM also strengthens the long lasting partnership between Germany and Brazil.



Dr. Peter Buchholz
Head of German Mineral Resources Agency (DERA)
at the BGR, Germany

Content

Forewords	3
Figures	7
Tables	11
1 Introduction	13
1.1 Historical background	13
1.2 Structure of the garimpos and investigated mines	14
1.3 Economic background	15
1.4 Infrastructure	15
1.4.1 Energy supply	15
1.4.2 Logistics and transportation	16
1.4.3 Waterway transportation	16
2 Brazilian mining & environmental code with respect to the Rondônia Tin Province (RTP)	17
3 Geology and mineralogy of the RTP	18
3.1 Geological framework	18
3.2 Geology and mineralogy of the investigated deposits	20
3.2.1 Massangana garimpo	20
3.2.2 Bom Futuro garimpo	21
3.2.3 Santa Bárbara and Cachoeirinha mines	24
4 Methodology and overview of common methods of mining and mineral processing	27
4.1 Methodology of sampling and analytics	27
4.2 Common mining methods	27
4.3 Common methods of mineral processing	28
4.4 Products from mineral processing	30
5 Detailed mineralogical investigations and individual mineral processing methods of the four selected mine sites	33
5.1 Massangana cooperative (CEMAL)	33
5.2 Bom Futuro cooperative (COOPERSANTA)	35
5.3 Santa Bárbara mine (ERSA)	40
5.4 Cachoeirinha mine (METALMIG)	41
6 Mineral processing tests	44
6.1 Origin of the samples	44
6.2 Sample preparation	47
6.2.1 Screening and sample splitting	47
6.2.2 Density separation by heavy liquids (bromoform)	48
6.3 Pre-processing tests	48
6.3.1 Density separation by shaking table	48
6.3.2 Magnetic separation	50
6.3.3 Flotation tests	52
6.4 Mineralogical methods	52
6.4.1 XRD analysis	52
6.4.2 Polished grain thin sections	52
6.4.3 Polarization microscopy	52

6.4.4	Scanning electron microscopy and EDX analysis	52
6.4.5	Mineral liberation analysis – MLA	53
6.5	Geochemical methods	53
6.5.1	Actlabs/Canada	53
6.5.2	Analysis by handheld XRF	53
6.6	Radiation analytics	54
6.6.1	Radiation measurement equipment	54
6.6.2	Radiation measurement	55
6.7	Ore analytics (geochemistry, mineralogy)	56
6.7.1	Mineralogy – EDX, XRD, MLA	56
6.7.2	Geochemistry of heavy and light fractions (bromoform separation)	61
6.8	Processing	63
6.8.1	Processing flow	63
6.8.2	Sieve analysis	64
6.8.3	Density separation	69
6.8.4	Magnetic separation	77
6.8.5	Monazite flotation (experimental set-up)	85
6.8.6	Radiation measurements and separation of radioactive minerals	88
7	Economic approach and evaluation	97
7.1	Massangana	97
7.2	Bom Futuro	99
7.3	Cachoeirinha	100
7.4	Santa Bárbara	101
8	Summary and recommendations	103
8.1	Massangana	103
8.2	Bom Futuro	105
8.3	Cachoeirinha	106
8.4	Santa Bárbara	107
9	References	108
10	Appendix	111
Appendix 1		112
Appendix 2		116
Appendix 3		119
Appendix 4		122
Appendix 5		126
Appendix 6		129
Appendix 7		132
Appendix 8		135
Appendix 9		138
Appendix 10		144
Appendix 11		149

Figures

Fig. 1.1:	Location of the selected deposits in the state of Rondônia.	14
Fig. 3.1:	Mineral provinces of the Amazonian Craton.	18
Fig. 3.2:	Schematic stratigraphy of the alluvial cassiterite deposits.	19
Fig. 3.3:	Stratigraphic section in the Barranco Stream (Oriente Novo Mine) exemplifying the setting of Depositional Sequences I and II.	20
Fig. 3.4:	Geological map of Bom Futuro.	21
Fig. 3.5:	Hard rocks (primary ore) in the Bom Futuro Garimpo with greisen, pegmatite and quartz veins.	22
Fig. 3.6:	Outcrop of sedimentary layers from Depositional Sequence I in the Bom Futuro deposit.	23
Fig. 3.7:	Cross-section of the strata in the southeast region of Bom Futuro.	23
Fig. 3.8:	Profile of supergene cassiterite ore in the Cachoeirinha deposit.	24
Fig. 3.9:	Coarse-grained sand related to Depositional Sequence II in Cachoeirinha.	25
Fig. 3.10:	Mining site in the Santa Bárbara deposit, where an overburden of massive mottled clay covers mineralized sand layers.	26
Fig. 3.11:	Outcrop of Depositional Sequence I in the Cachoeirinha deposit: Conglomerate (left) and coarse-grained sand (right).	26
Fig. 4.1:	a) Garimpeiros checking if the layer contains enough cassiterite to be mined, b) Mining operation with an hydraulic jet in Massangana, c) Mining of alluvium near the Massangana River, in Garimpo Massangana, d) Use of heavy machines to mine in Garimpo Bom Futuro.	28
Fig. 4.2:	a) Jigs outputting clay as tailings in the first gravity concentration, b) and c) Jigs separating the cassiterite and the first and second cama (basin under the jig), d) Shaking table separating the very fine cassiterite.	29
Fig. 4.3:	a) Milling of the ores (primary and secondary) in Bom Futuro, b) Spiral separation of the sieved ore in Santa Bárbara, c) Shaking table separating ore minerals from silicates in Massangana (CEMAL plant), d) Magnetic cross belt separator to produce ilmenite, columbite, monazite and cassiterite at the CEMAL plant.	31
Fig. 4.4:	Final cassiterite concentrate product after magnetic separation at the CEMAL plant.	31
Fig. 4.5:	a) Alloy with Sn grades between 10 to 15%. This product is sold for its high Pb content, making the Sn just a by-product, b) Ingots of high quality Sn that match the LME standard.	32
Fig. 5.1:	Processing scheme of the Massangana plant with sampling locations.	34
Fig. 5.2:	Mineralogical composition from MLA on pre-concentrate from the 1 st cama of jigs at Massangana (TB06B, sample taken during campaign in 2016).	34
Fig. 5.3:	Mineralogical composition from MLA on pre-concentrate from the 2 nd cama of jigs at Massangana (TB06A, sample taken during campaign in 2016).	34
Fig. 5.4:	Mineralogical composition from MLA on tailings from the shaking tables of the CEMAL plant in Massangana (TB43, sample taken during field campaign in 2017).	35
Fig. 5.5:	Processing flow chart for placer ore in the Bom Futuro plant with sampling locations.	36
Fig. 5.6:	Simplified tailings processing scheme of the Bom Futuro plant with sampling locations.	37
Fig. 5.7:	Processing scheme for primary ore of the Bom Futuro plant with sampling locations.	37
Fig. 5.8:	Mineralogical composition from MLA on pre-concentrate from secondary ore at Bom Futuro (TB13B, sample taken during field campaign in 2016).	38

Fig. 5.9:	Mineralogical composition from MLA on pre-concentrate from primary ore at Bom Futuro (TB15C, sample taken during field campaign in 2016).	38
Fig. 5.10:	Particle size distribution for coarse-grained (black line, TB15A) and fine-grained (red line, TB15B) cassiterite concentrate from Bom Futuro.	39
Fig. 5.11:	Details from MLA on coarse-grained and fine-grained concentrate from primary ore at Bom Futuro: Coarse-grained ore material with intergrowth features (left, TB15A) and fine-grained ore material (right, TB15B).	39
Fig. 5.12:	Mineral liberation from MLA for coarse-grained and fine-grained concentrate from primary ore at Bom Futuro.	40
Fig. 5.13:	Simplified mineral processing scheme of the Santa Bárbara plant with sampling locations, the cassiterite concentrate is refined to metallic tin (99.85% Sn) in the ERSA-CSN smelter at Ariquemes.	41
Fig. 5.14:	Mineralogical composition from MLA of pre-concentrate from the spiral separator at the Santa Bárbara plant (sample TB05C, taken during the field campaign 2016).	42
Fig. 5.15:	Mineralogical composition from MLA of pre-concentrate (jig, 2 nd cama) from Cachoeirinha (TB55, sample taken during the field campaign 2017).	42
Fig. 6.1:	Mineralogical composition from MLA of pre-concentrate (jig, 2 nd cama) from Massangana – Barreiro stream (TB45, sample taken during the field campaign 2017).	45
Fig. 6.2:	Mineralogical composition from MLA of pre-concentrate (jig, 2 nd cama) from Massangana – Taboca stream (TB46, sample taken during the field campaign 2017).	45
Fig. 6.3:	Mineralogical composition from MLA of pre-concentrate (jig, 2 nd cama) from Massangana – Lima stream (TB47, sample taken during the field campaign 2017).	45
Fig. 6.4:	Mineralogical composition from MLA of pre-concentrate (jig, 2 nd cama) from Massangana – B-3 stream (TB48, sample taken during the field campaign 2017).	46
Fig. 6.5:	Mineralogical composition from MLA of pre-concentrate (jig, 2 nd cama) from Bom Futuro (TB53).	46
Fig. 6.6:	Mineralogical composition from MLA of pre-concentrate (jig, 2 nd cama) from Santa Bárbara (TB59).	46
Fig. 6.7:	<>2 mm separated samples.	47
Fig. 6.8:	Sample splitting with riffle splitter: a) 500 mm splitter for samples up to 100 kg, b) 180 mm splitter for samples up to 2 kg.	47
Fig. 6.9:	a) Laboratory equipment for heavy liquid separation, b) Funnel with 200 ml CHBr ₃ and stirrer.	48
Fig. 6.10:	Sample TB55, fraction 250–500 µm (separation determined optically, semi quantitative).	50
Fig. 6.11:	a) Magnetic belt separators (1.1 Tesla), b) Frantz magnetic separators, c) Ring-band magnetic separators (TU Bergakademie Freiberg, Institute for Processing Machines).	51
Fig. 6.12:	Magnetic susceptibilities of selected minerals in a Frantz Isodynamic Separator with a side tilt of 15–25° and a forward tilt of 15–25° (from STENDAL & THEOBALD 1994).	52
Fig. 6.13:	Measuring station handheld XRF spectrometer S1 TITAN Model 800 – BRUKER.	54
Fig. 6.14:	Radiation detector used a) Local dose rate meter 6150AD 6/E with calibratable scintillator probe 6150AD-b/E, b) LB 124 Scint contamination monitor for α and β-γ measurement.	55
Fig. 6.15:	a) to c) Volume-related radiation measurement of the sample in a Petri dish (38 cm ³) under shielding the ambient dose rate (red steel box), d) and e) Mass-related radiation measurement at larger masses/volumes of sample TB45-48, 250–500 µm, HF1, paramagnetic fraction.	55

Fig. 6.16: Results of density separation with bromoform.	61
Fig. 6.17: Processing scheme for the production of mineral concentrates.	64
Fig. 6.18: Percentages of the sieve fractions and sieve curves of the <2 mm fraction.	65
Fig. 6.19: Element content of sample TB45-48 dependent on grain size fraction.	66
Fig. 6.20: Element recovery of sample TB45-48 dependent on grain size fraction.	66
Fig. 6.21: Element content of sample TB53 dependent on grain size fraction.	67
Fig. 6.22: Element recovery of sample TB53 dependent on grain size fraction.	67
Fig. 6.23: Element content of sample TB55 dependent on grain size fraction.	68
Fig. 6.24: Element recovery of sample TB55 dependent on grain size fraction.	68
Fig. 6.25: Element content of sample TB59 dependent on grain size fraction.	68
Fig. 6.26: Element recovery of sample TB59 dependent on grain size fraction.	69
Fig. 6.27: Element contents and recovery of density separation by shaking table, sample TB45-48, 250–500 μm grain size fraction.	70
Fig. 6.28: Element contents and recovery of density separation by shaking table, sample TB45-48, 500–710 μm grain size fraction.	70
Fig. 6.29: Element content and recovery of density separation by shaking table, sample TB45-48, 710–2000 μm grain size fraction.	71
Fig. 6.30: Element/oxide content and recovery of density separation by shaking table, sample TB53, 63–250 μm grain size fraction.	72
Fig. 6.31: Element/oxide content and recovery of density separation by shaking table, sample TB53, 250–500 μm grain size fraction.	72
Fig. 6.32: Element/oxide content and recovery of density separation by shaking table, sample TB53, 500–710 μm grain size fraction.	73
Fig. 6.33: Element/oxide content and recovery of density separation by shaking table, sample TB53, 710–2000 μm grain size fraction.	74
Fig. 6.34: Element/oxide content and recovery of density separation by shaking table, sample TB55, 63–250 μm grain size fraction.	74
Fig. 6.35: Element/oxide content and recovery of density separation by shaking table, sample TB55, 250–500 μm grain size fraction.	75
Fig. 6.36: Element/oxide content and recovery of density separation by shaking table, sample TB55, 500–710 μm grain size fraction.	75
Fig. 6.37: Element/oxide content and recovery of density separation by shaking table, sample TB55, 710–2000 μm grain size fraction.	76
Fig. 6.38: Element/oxide content and recovery of density separation by shaking table, sample TB59, 200–630 μm grain size fraction.	76
Fig. 6.39: Element/oxide content and recovery of density separation by shaking table, sample TB59, 630–2000 μm grain size fraction.	77
Fig. 6.40: Concentrations and recovery in the magnetic fractions of the 63–250 μm particle size fraction – TB45-48.	78
Fig. 6.41: Concentrations and recovery rates in the magnetic fractions HF1 and HF2 of the 250–500 μm grain size fraction – TB45-48.	78
Fig. 6.42: Concentrations and recovery rates in the magnetic fractions HF1 and HF2 of the 500–710 μm grain size fraction – TB45-48.	79
Fig. 6.43: Concentrations and recovery rates in the magnetic fractions HF1 and HF2 of the 710–2000 μm grain size fraction – TB45-48.	80
Fig. 6.44: Concentrations of the oxides after separation of the paramagnetic fraction by a Frantz magnetic separator.	81

Fig. 6.45: Recovery of the oxides after separation of the paramagnetic fraction by a Frantz magnetic separator.	81
Fig. 6.46: Concentrations and recovery rates in the magnetic fractions of the 63–250 and 250–500 μm grain size fractions – TB53.	82
Fig. 6.47: Concentrations and recovery rates in the magnetic fractions of the 500–710 and 710–2000 μm grain size fractions – TB53.	82
Fig. 6.48: Concentrations and recovery rates in the magnetic fractions of the 63–250 μm grain size fraction – TB55.	83
Fig. 6.49: Concentrations and recovery rates in the magnetic fractions of the 250–500 μm grain size fraction – TB55.	83
Fig. 6.50: Concentrations and recovery rates in the magnetic fractions of the 500–710 μm grain size fraction – TB55.	83
Fig. 6.51: Concentrations and recovery rates in the magnetic fractions of the 710–2000 μm grain size fraction – TB55.	84
Fig. 6.52: Concentrations and recovery rates in the magnetic fractions of the 200–630 μm grain size fraction.	84
Fig. 6.53: Concentrations and recovery rates in the magnetic fractions of the 630–2000 μm grain size fraction.	84
Fig. 6.54: Forecasting model for the grinding time.	85
Fig. 6.55: Mass pulls of trial and correction tests.	85
Fig. 6.56: Component recovery of the trial test concentrate.	86
Fig. 6.57: Cumulative element recovery dynamics for the correction test.	86
Fig. 6.58: Monazite grade-recovery plot, correction test.	87
Fig. 6.59: Principal component analysis of flotation products.	87
Fig. 6.60: Variations and changes in the local dose rate during processing.	89
Fig. 6.61: Comparison of the measured a) Dose rate/alpha radiation, b) Alpha /beta + gamma radiation, c) Dose rate/Th content and d) Dose rate/Ce, REE contents in sample TB45-48.	90
Fig. 6.62: a) Mass-dependent local dose rate on HM1 and HM2 concentrates of sample TB45-48, b) Separation of the local dose rate by magnetic separation at 0.47 Tesla into a monazite concentrate and an ilmenite concentrate.	91
Fig. 6.63: Mass-dependent local dose rate in monazite concentrates.	91
Fig. 6.64: Detailed separation of the ilmenite and monazite concentrate from 250–500 μm , HF1 – distribution of elements, minerals and local dose rate as a function of the field strength on the Frantz magnetic separator – photos (left side) show the typical yellow-orange color of monazite.	92
Fig. 6.65: Variations and changes in the dose rate during processing – sample TB53 – Bom Futuro.	92
Fig. 6.66: Comparison of the measured a) Local dose rate/alpha radiation, b) Alpha/beta + gamma radiation and c) Local dose rate/Th content in sample TB53.	93
Fig. 6.67: Variations and changes in local dose rate during processing – sample TB55 – Cachoeirinha.	93
Fig. 6.68: Comparison of the measured a) Local dose rate/alpha, b) Local dose rate/beta + gamma radiation, c) Local dose rate/Th and d) U levels in sample TB55 – Cachoeirinha.	94
Fig. 6.69: Variations and changes in local dose rate during processing – Sample TB59 – Santa Bárbara.	95

Fig. 6.70: Comparison of the measured a) Local dose rate/alpha, b) Local dose rate/beta + gamma radiation, c) Local dose rate/Th and d) alpha/beta + gamma radiation in sample TB59.	95
Fig. 6.71: Examination of the dose rate by finger dosimeter.	96
Fig. 8.1: Processing scheme for the Massangana pre-concentrates.	103
Fig. 8.2: Processing scheme for the Bom Futuro pre-concentrates.	105
Fig. 8.3: Processing scheme for the Cachoeirinha pre-concentrates.	106
Fig. 8.4: Processing scheme for the Santa Bárbara ores.	107

Tables

Tab. 1.1: Industrial tin producers in Brazil in 2016. Source: DNPM (2017).	15
Tab. 1.2: Hydroelectric energy produced in Rondônia (ANEEL, 2016).	16
Tab. 4.1: Overview of the principal features of mining methods and mineral processing at the visited mining operations.	30
Tab. 6.1: Samples and locations from the field campaign Rondônia 2017.	44
Tab. 6.2: Density ranges, average densities of heavy minerals, and separation quotients of mineral combinations.	49
Tab. 6.3: Magnetic susceptibilities of different minerals and the relation to the field strengths (in Tesla).	51
Tab. 6.4: Analyzed oxides/elements and detection limits of Code 8 – REE assay + Code 8 – XRF Nb, Zr, Ta.	53
Tab. 6.5: Quantification of XRD diffractograms Rietveld analysis in mass percent.	57
Tab. 6.6: Mineral phases and their visual estimates of relative abundance.	59
Tab. 6.7: Sample Massangana – TB45-48 – Chemical composition of heavy and light fraction (bromoform separation 2.89 g/cm ³).	62
Tab. 6.8: Sample Bom Futuro – TB53 – Chemical composition of heavy and light fraction (bromoform separation 2.89 g/cm ³).	62
Tab. 6.9: Sample Cachoeirinha – TB55 – Chemical composition of heavy and light fraction (bromoform separation 2.89 g/cm ³).	63
Tab. 6.10: Sample Santa Bárbara – TB59 – Chemical composition of heavy and light fraction (bromoform separation 2.89 g/cm ³).	63
Tab. 6.11: Mass fractions and total masses of <>2 mm fractions of samples TB45-48 (Massangana).	64
Tab. 6.12: Mass fractions and total masses of <>2 mm fractions of samples TB45-48 (total), TB53, TB55 and TB59.	64
Tab. 6.13: Grain size composition of the samples, determined by dry sieving by sieving machine (1 kg sample).	65
Tab. 6.14: Single-grain measurements of Th and U bearing minerals by SEM-EDX (Erz & Stein).	89
Tab. 6.15: Concentrations and recovery rates of Th and U in different particle size ranges.	96
Tab. 7.1: Prices for the elements/oxides for calculation of economic feasibility.	97
Tab. 7.2: Particle-size dependent element oxide concentrations and amounts of valuable substances with economic relevance in 1 t of pre-concentrate.	97

Tab. 7.3:	Recovery and concentration of element oxides after magnetic separation as a function of the separated particle size and density fractions in HF1 + HF2.	98
Tab. 7.4:	Economic evaluation of the pre-concentrate regarding Nb ₂ O ₅ , Ta ₂ O ₅ , Sn and TiO ₂ amounts per ton of pre-concentrate in <2000 μm fraction (100%).	98
Tab. 7.5:	Grain-size related economic evaluation of all concentrates (based on 1 t of pre-concentrate).	98
Tab. 7.6:	Particle-size dependent element oxide concentrations and amounts of valuable substances with economic relevance in 1 t of pre-concentrate.	99
Tab. 7.7:	Recovery and concentration of element oxides after magnetic separation as a function of the separated particle size and density fractions in HF1 + HF2.	99
Tab. 7.8:	Economic evaluation of the pre-concentrate with regard to the Sn amount per ton of pre-concentrate in the <2000 μm fraction (100%).	100
Tab. 7.9:	Tin recovery and revenues at different grain sizes (the amounts were calculated from the diamagnetic fractions of HF1 + HF2 – Tab. 6.8).	100
Tab. 7.10:	Particle-size dependent element oxide concentrations and amounts of valuable substances with economic relevance in 1 t of pre-concentrate.	100
Tab. 7.11:	Recovery and concentration of element oxides after magnetic separation as a function of the separated particle size and density fractions in HF1 + HF2.	101
Tab. 7.12:	Economic evaluation of the pre-concentrate regarding Nb ₂ O ₅ , Ta ₂ O ₅ and Sn amounts per ton of pre-concentrate in the <2000 μm fraction (100%).	101
Tab. 7.13:	Particle-size dependent element oxide concentrations and amounts of economic raw materials in 1 t of ore.	102
Tab. 7.14:	Economic evaluation of the ore regarding Nb ₂ O ₅ , Ta ₂ O ₅ , Sn and TiO ₂ amounts per ton of ore in the <2000 μm fraction (100%).	102

1 Introduction

In the present technical report, we provide information on four tin-tantalum deposits within the Rondônia Tin Province (RTP): These are the Mas-sangana and Bom Futuro garimpos, as well as the Cachoeirinha and Santa Bárbara mines.

The types of exploited ores, tailings and concentrates from these mining operations are studied, and their geological, mineralogical and geochemical features are characterized. The aim is to develop enhanced processing methods to optimize the recovery of cassiterite, columbite and subordinate by-products (e.g. ilmenite, monazite, topaz), and thus to increase the economic output of marketable mineral concentrates.

1.1 Historical background

The first discovery of cassiterite in Rondônia occurred in 1952, in a rubber plantation in the area around the Machadinho River. After some mineralogical studies, the area was claimed for mineral exploration in 1953 (LOBATO et al. 1966). Around 1955, there was a tin rush in Rondônia, when new supergene deposits were discovered around the granite massifs of Pedra Branca and Caritianas (BUCH et al. 2017). Afterwards, between 1957 and 1961, new discoveries were made of the mineral deposits of Santa Bárbara, Jacundá, Mas-sangana and Candeias (WAGHORN 1974). The São Lourenço deposit, 180 km W of Porto Velho, was discovered in 1961.

In the 1960's, Rondônia was responsible for more than 50% of the tin produced in Brazil. The artisanal miners ("garimpeiros") historically only mined high Sn content deposits with 4 to 5 kg SnO₂/m³, whereas other deposits, e.g. in Malaysia, are mined at grades of about 1 kg SnO₂/m³.

In 1969, the Brazilian Government initiated a programme to assess and organize the mining of cassiterite in Rondônia. In 1970, the RTP was created by federal decree. At the same time, the government invited and encouraged mining companies to operate the tin deposits.

Industrial production

In the Oriente Novo deposit (eastern part of Rondônia), the Billiton Group started the first mechanized mine with modern equipment: The Igarapé Preto mine (MT) came into operation in 1970, and Santa Bárbara in 1971 (WAGHORN 1974).

Until 1974, Brazil dependent on tin imports to supply its growing domestic market. However, due to the constant development of the national tin mining industry, the country gradually diminished this dependency (BUCH et al. 2017). From 1975 on, it not only reached self-sufficiency, it also began to supply the world market and became the world's main producer of tin in 1988. With the commissioning of the Pitinga mine in 1983, in the municipality of Presidente Figueiredo – AM, Rondônia lost its position as the largest national cassiterite producer.

The discovery of Bom Futuro

In the middle of 1987, loggers harvesting wood near the Santa Cruz River municipality of Ariquemes, discovered a large amount of cassiterite (Bom Futuro Garimpo). The information was passed to the company MS Mineração Ltda., which immediately acquired the area for research. The garimpos (artisanal mines) became attractive to former employees of mining companies, to farmers in the region and even to local entrepreneurs who saw artisanal mining as a way to expand their profits. The mining activity and the consequent commercialization of the ore directly violated the legislation (DALL'IGNA 1996).

As a form of legalization of the artisanal mining activity, in order to guarantee the mining rights of MS Mineração Ltda., and avoid environmental damage, DNPM created Ordinance 226 (dated 19 September 1988, Ord. 226/1988) determining that all commercialization of the cassiterite produced in the Bom Futuro Garimpo was undertaken by MS Mineração Ltda., which in turn would pass on a percentage to each business group legally established and operating in Rondônia (DALL'IGNA 1996).

The creation of the Brazilian Tin Company

In order to solve the problems of the Bom Futuro Garimpo, the Brazilian Tin Company SA (EBESA) was created in June 1990, bringing together the largest cassiterite producing groups in Rondônia (BUCH et al. 2017). A protocol of intent was signed in 1992 between the artisanal miner's cooperatives and EBESA to jointly operationalize the garimpos. EBESA estimated that from 1987 to 1995, the production was from 80,000 to 100,000 tons of Sn contained in concentrates. This production level highlights the Bom Futuro deposit's economic importance and the need to exploit the deposit rationally (DALL'IGNA 1996).

Current situation

In 2001, there was a total transfer of operational activities from the Bom Futuro mine to Cooperativa dos Garimpeiros de Santa Cruz Ltda. (COOPER-SANTA), which assumed responsibility for mining production and environmental protection. COOPERSANTA is part of the Cooperativa Metalúrgica de Rondônia Ltda. (COOPERMETAL) group, a cooperative organization focused on tin mining, and which originated in the agreement for the development of mining in the Bom Futuro mine area (Renato Muzzollon, personal communication). In 2005, the mineral rights were fully transferred to COOPERSANTA, which integrates the most important cassiterite producers in the region.

In December 2016, the TSX-listed Meridian Mining S.E. agreed to acquire a right to explore a 492.57 ha tailing reprocessing area, a 2,000 ha central area including the Bom Futuro mine, and earn up to an 80% interest in an 18,000 ha non-explored area in Ariquemes from the Brazil-based investor group comprising COOPERSANTA and COOPERMETAL. With announced total resources and reserves of 61 million t of ore, grading approximately 0.6% Sn, Bom Futuro today is the largest tin deposit in the RTP (SNL 2018).

According to the Brazilian Mineral Yearbook of 2017 (DNPM, 2018), the main tin producing companies are: COOPERSANTA, COOPERMETAL, Estanho de Rondônia SA (ERSA), Cooperativa Mineradora dos Garimpeiros de Ariquemes Ltda., Cooperativa dos Garimpeiros do Estado de Rondônia Ltda. (COOGER), Cooperativa Estanífera de Mineradores of Amazônia Legal Ltda. (CEMAL),

and Metalmig Mineração Indústria e Comércio Ltda., as well as the Cooperativa dos Garimpeiros de Mutum Paraná.

1.2 Structure of the garimpos and investigated mines

Garimpos are artisanal mines which are usually registered in the National Mining Agency (ANM). Garimpos commonly operate under the regime of a cooperative of artisanal miners. The mineral rights of the deposits belong to the cooperatives, while the garimpeiros carry out the mining operations. The industrial mining right is an allowance given to a company to exploit mineral resources with stricter laws – especially regarding environmental issues. Garimpeiros can hire other independent garimpeiros in order to increase the ore production or provide a greater budget to improve the mining and mineral processing. The company can also allow garimpeiros to mine on the company's concession.

COOPERSANTA owns the mineral rights in Bom Futuro, and CEMAL holds the mining license in Massangana. The mining permits for Cachoeirinha belong to Metalmig S.A., and the Santa Bárbara claim is licensed to ERSa, a holding of Companhia Siderúrgica Nacional (CSN). All the fieldwork conducted by the geologists from CPRM-BGR/DERA was done with the support and knowledge of those entities.

The four sites are situated in the middle-north portion of Rondônia (Fig. 1.1). All are relatively easy to access and connected to federal road BR-364.

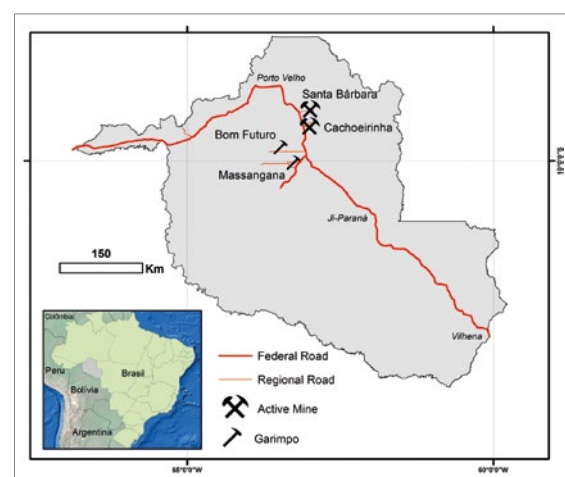


Fig. 1.1: Location of the selected deposits in the state of Rondônia.

1.3 Economic background

According to USGS Mineral Commodity Summaries (USGS 2018), Brazil with 700,000 t has the world's third largest tin reserves, after China (1.1 million t) and Indonesia (800,000 t). According to DNPM (2017), the primary tin production (mine production) in Brazil was 15,393 t Sn (Sn content in concentrate) in 2016. Amazonas was the leading state with 7,100 t Sn (Pitinga), followed by Rondônia with 5,736 t Sn and Pará with 2,215 t Sn. Mato Grosso holds the 4th position with about 193 t Sn, followed by Minas Gerais (143 t Sn) and São Paulo (5.5 t Sn).

Rondônia also produces a significant quantity of niobium, and a relatively small amount of manganese. In 2016, the state produced 463 t of Nb and 29,923 t of Mn (in t content). According to DNPM (2017), Mineração Taboca S.A. (a holding of the Peruvian Minsur) accounts for 47.5% of Brazilian tin production in its Pitinga deposit (Tab. 1.1). In Rondônia, the tin production is led by COOPERMETAL, with 12.07% of Brazilian tin production. Other producers contribute less than 10% of the total tin production (Tab. 1.1).

Compared to other Brazilian states, the mineral production of Rondônia is still not significant regarding the value generated by the Brazilian mining sector. In 2017, the Brazilian mining sector produced mineral raw materials worth approximately US\$ 32 billion. The value of metals produced in Rondônia

was around US\$ 170 million or only 0.53% of the total in 2017. The most significant states for metal production in Brazil are Minas Gerais and Pará which together account for 85% of the total value of mineral commodities in the country.

1.4 Infrastructure

The following chapter describes the infrastructural situation in Rondônia, in terms of energy supply and transport routes to the road and to water.

1.4.1 Energy supply

According to the Brazilian National Agency for Electric Energy (ANEEL, 2016), the state of Rondônia has a installed power generation of 7,500 MW produced by 89 enterprises (Tab. 1.2). The energy produced in Rondônia is equivalent to 5% of all the electric power generated in Brazil. In coming years, 184,718 kW will be added to the energy production by 14 new power plants currently under construction.

The main energy source is hydroelectric plants, followed by thermoelectric plants. Among the hydroelectric plants, four are large scale power plants and correspond to 89.5% of all the energy produced in the state of Rondônia (ANEEL, 2016). However, most of this energy is fed into the Brazilian power grid and shared by the other states.

Tab. 1.1: Industrial tin producers in Brazil in 2016. Source: DNPM (2017).

Company/Cooperative	State	Participation (%)
Mineração Taboca S.A.	AM	47.47
Coopermetal Coop Metalurgica de Rondônia Ltda.	RO	14.07
Cooperativa dos Garimpeiros do Estado de Rondônia – COOGER – Ltda	PA, RO	11.85
Cooperativa dos Garimpeiros de Campo Novo de Rondônia	RO	9.71
Coop. Mineradora dos Garimpeiros de Ariquemes Ltda.	PA, RO	9.20
Estanho de Rondônia S.A.	RO	2.69
Metalmig Mineração Indústria E Comércio Ltda.	PA, RO	1.74
Cooperativa de Mineração dos Garimpeiros de São Félix do Xingu – COOMIX	PA	1.85
Cooperativa Estanífera De Mineradores Da Amazônia Legal Ltda.	RO	1.42

States: AM: Amazonas, RO: Rondônia, PA: Pará

Tab. 1.2: Hydroelectric energy produced in Rondônia (ANEEL, 2016).

Power Plants	Quantity	Power (kW)	%
Hydroelectric	30	6,820,731	91.6
Thermoelectric	58	625,548	8.4
Photovoltaic	1	20	0
Total	89	7,446,299	100

1.4.2 Logistics and transportation

The access to Rondônia and its deposits is relatively good. The state of Rondônia is served by three national airports in the cities of Ji-Paraná, Cacoal and Vilhena, and one international airport in the state capital Porto Velho.

The road network in Rondônia is quite dense and well-developed. It comprises 2,151 km of federal roads, 5,565 km of state roads, and 39,668 km of municipal roads, resulting in a total of 47,385 km of roads. Of the 2,151 km of federal roads, 1,624 km are paved roads and 527 km are unpaved.

The BR-364 is the main and only road by which the tin production is supplied to the consumers in Brazil. The cassiterite concentrates from Rondônia are transported in haulage trucks on this road to Cuiabá (about 1,000 km away from the deposits). Afterwards, the concentrates are transported up to Minas Gerais, Rio de Janeiro and São Paulo through Goiás and Mato Grosso do Sul states.

1.4.3 Waterway transportation

When shipped abroad, the cassiterite concentrate and the refined tin are transported to the harbor of Porto Velho. From Porto Velho, the tin is transported in containers for 2,221 km to the port of Santana in the state of Amapá. From there, the Rondônian tin is shipped to its main clients around the world.

2 Brazilian mining & environmental code with respect to the Rondônia Tin Province (RTP)

In Brazil, the Federal Government is responsible for supervising the mineral resources and the mining industry. The Brazilian Mining Code (BMC) is regulated by Decree nº 227 of 28 February 1967. This regulation has been updated by several amendments, the most extensive being Law nº 9.314 of 1996. Against this background, the RTP deposits are being exploited on the basis of mining concessions and artisanal mining permits. ERSA is an example of a mining operation developed as a mining concession, whereas CEMAL is an example of an artisanal mining permit.

The main difference between a mining concession and an artisanal mining permit concerns the stages involved in developing a project, which are discussed in detail below.

Artisanal mining permit

As mentioned in the previous chapter, the creation of the RTP prohibited the activity of artisanal miners in the province. With the reform of the Brazilian Constitution, the artisanal mining of minerals developed by associations and cooperatives became legal again. The artisanal mining activities are regulated by Law nº 7.805/89 and Decree nº 98.812/90. In 1996, the permit for artisanal mining (garimpo) was created, and was conditional on the approval of the Minister for Mines and Energy.

The artisanal mining permit can be granted to an individual (garimpeiro) or to a cooperative (association of garimpeiros). The individual artisanal miner can claim an area up to 50 ha, and a cooperative can claim a permit for areas up to 1,000 ha. The Brazilian law does not define a limit for claimed areas, so it is therefore common for several areas to be claimed by the same subject.

Currently, the tin deposits of Rondônia are in a state of transformation. After the boom years, the artisanal mining cooperatives realized the need to improve their cassiterite processing. Therefore, technical mining and processing techniques are being implemented again in order to maintain the competitiveness of the products.

Authorization and concession regimes

The BMC contains different set of rules for companies and individuals that want to claim an area for mineral exploration and mining. To claim an area, the agent can be a native Brazilian, an entrepreneur or a local company. The first step to claim an area is to submit a search permit request to the National Agency for Mining (ANM) through a qualified geologist or mining engineer.

The maximum size of the claimed area regarding tin (and other metallic substances) is 2,000 ha. Areas of interest 150 km or less from an international border also need authorization by the National Security Council. After the approval of the prospecting permit, there is a deadline of 3 years to conclude the exploration project. This three year term can be extended beyond 3 years if it was not possible to complete the exploration program. In addition, the mineral exploration must not be suspended for more than 3 months.

After the exploration program is concluded, a report must be submitted to ANM, and in the event of approval, the interested agent can submit a Mining Application. At this stage, only companies can apply. The Mining Application requires the detailed information on building all the mine infrastructure, and feasibility studies. For the feasibility studies, the company must include a plan to manage and control the environmental impact caused by the mining operation, and also gain a permit from the State Environmental Agency of the state where the area is located. If the Mining Application is approved, the company can submit a Mining Concession Application to ANM. This is the last stage to open a mine. It is important to highlight that the company does not need to own the land in the area of interest. However, the owner must be compensated for the impact caused by mining on his land.

3 Geology and mineralogy of the RTP

This chapter shows the geological situation of the RTP, the characteristics of the sedimentation of the Sn and Ta rich formations and their mineralogical composition.

3.1 Geological framework

The RTP is situated in the basement rocks of the southwestern part of the Amazonian craton (AC, Fig. 3.1). The AC is separated into the northern block (Guayana Shield) and the southern block (Brazilian Shield) by the Amazonian Basin, a sinistral transcurrent fault system that is attributed to the Jurassic period, when the Gondwana continent broke up.

The RTP is located in the Rio Negro-Juruena Province (1,800–1,550 Ma, BETTENCOURT et al. 2016). Tin mineralization has been responsible for the production of about 300,000 tons of Sn content in concentrate until 2017. Cassiterite is mainly mined from alluvial sources since the first discovery of the occurrences in 1952. Several Sn,

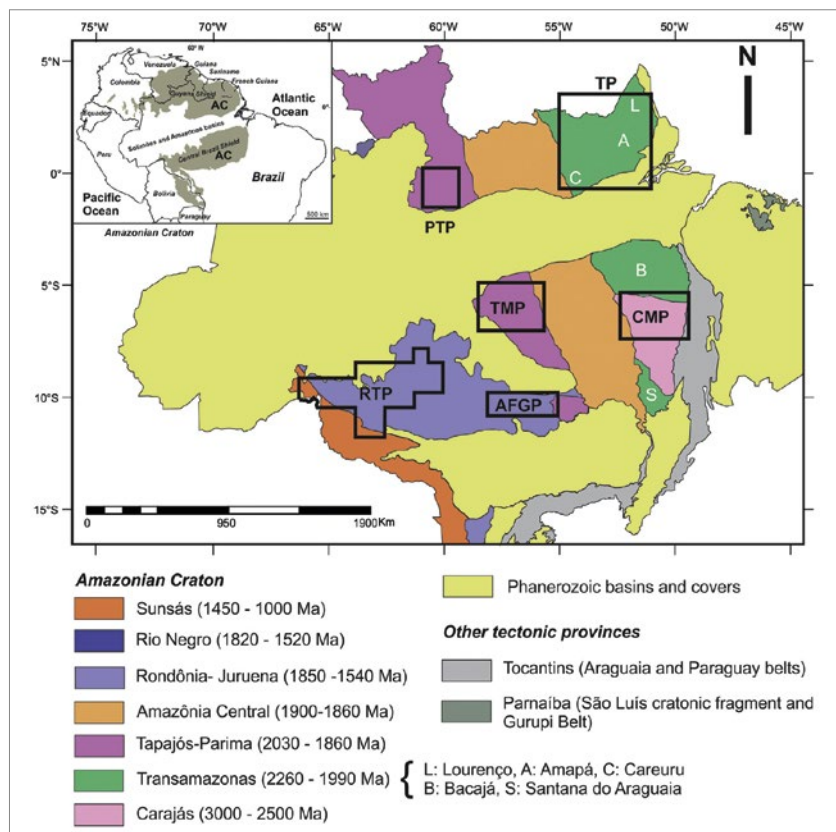
Ta and Nb deposits are known and exploited in the RTP, mainly south and southeast of the capital Porto Velho, near Ariquemes, as well as west of Porto Velho (see figure 1.1). Besides Sn, Ta and Nb, there are also recoverable resources of W and topaz in some mining districts.

The four deposits selected for further investigations and processing testworks – Cachoeirinha, Santa Bárbara, Bom Futuro and Massangana – are essentially primary and secondary cassiterite deposits. The exploited ores are mainly derived from the secondary alluvial and colluvial deposits.

The RTP is composed of Palaeoproterozoic to Mesoproterozoic metamorphic rocks which were intruded by several events of Rapakivi magmatism between 1600 Ma and 970 Ma (BETTENCOURT et al. 1999, BETTENCOURT et al. 2005). The primary Sn deposits (W-Ta-Nb) are closely associated with late-stage peraluminous, partly porphyritic alkali-feldspar granites (BETTENCOURT et al. 1999, BETTENCOURT et al. 2005).

Primary ore is associated with greisen related to the magmatism of the Rondônia intrusive suites (SOUZA 2003, ROMANINI 1982, FRANK 1990,

Fig. 3.1: Mineral provinces of the Amazonian Craton, according to SANTOS (2003) and VASQUEZ et al. (2008). Mineral Provinces: CMP: Carajas Mineral Province, TMP: Tapajós Mineral Province, AFGP: Alta Floresta Gold Province, TP: Transamazonas Province, PTP: Pitinga Tin Province, RTP: Rondônia Tin Province.



SPARRENBARGER 2003). The Rondônia suite is an ensemble of granitic bodies distributed in the middle-north of the state, and rocks of this suite occur in the deposits at Cachoeirinha, Bom Futuro and Massangana (BUCH et al. 2017). The Santa Clara Intrusive Suite occurs more at the northern part of Rondônia state and is related to the greisen hosting the primary tin ore in the Santa Bárbara deposit (Santa Bárbara Hill).

Secondary ores, the main focus of this study, are the most important ore type and are mined in all the studied deposits. PAYOLLA et al. (1984) assert that the supergene tin mineralizations are associated with two sedimentary sequences. These sequences are a product of a depositional system related to arid to semi-arid conditions associated with the Illinoian and Wisconsinian glaciations (BETTENCOURT, et al. 1988). Both sequences are enriched with cassiterite.

The earliest sequence, defined as “Depositional Sequence I” is associated with fluvial systems that are different from the current drainage system. According to BETTENCOURT et al. (1988), this sequence from the bottom to the top is arranged as follows:

- Conglomerates: Conglomerates with a thickness up to 6 meters, rich in sub-rounded quartz. In the areas where the granulation is sandy, there is tabular crossbedding. These areas are related to the most fluvial areas.
- Plastic clay: Layers of 0.5 meters in thickness covering the rudaceous sediments.
- Kaolinitic sandy clays: These layers cover the walls of the thalweg and tend to cover the aforementioned layers.
- Arkosic sands and lacustrine clays: These sediments tend to occur in interbeds. As BETTENCOURT et al. (1988) state, these sediments form coalescent fans towards the hills (bajada deposits). The argillaceous layers tend to form in the most distal regions, having also coarse-grained sand and lithic fragments, which suggests a reworking of the aforementioned deposits. The schematic profile of Depositional Sequence I is shown in figure 3.2 below.

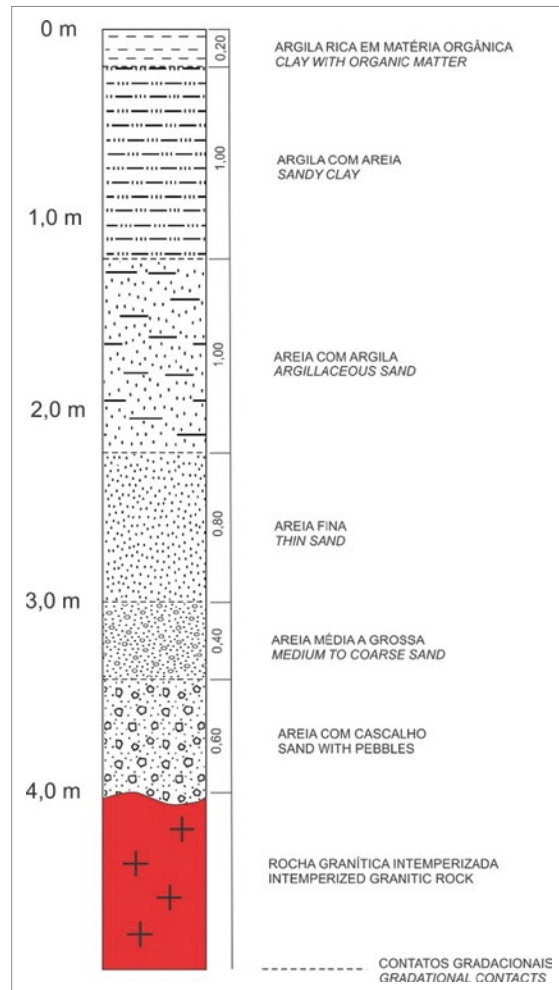
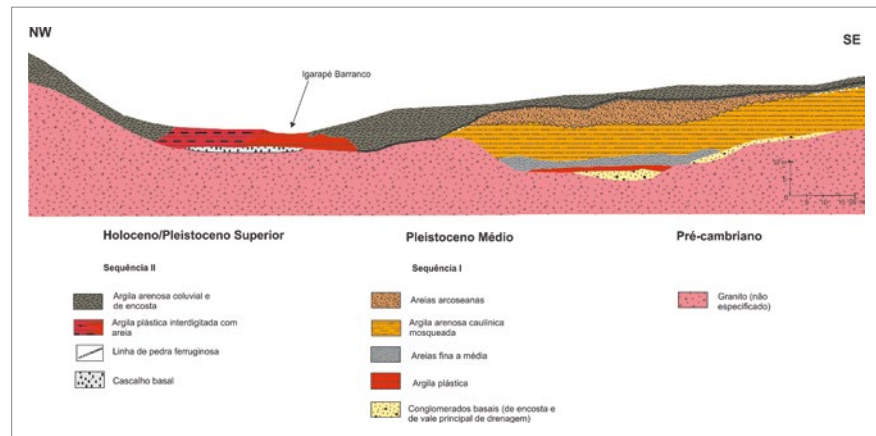


Fig. 3.2: Schematic stratigraphy of the alluvial cassiterite deposits. These deposits are of Pleistocene-Holocene age and are related to Depositional Sequence I (BETTENCOURT et al. 1988). Adapted from VEIGA 1988.

Depositional Sequence I ends with a conglomerate. Depositional Sequence II covers this sequence and is associated with the current thalweg (BETTENCOURT et al. 1988). Depositional Sequence II is composed of two layers:

- Sediments filling the current thalweg: According to BETTENCOURT et al. 1988, these layers were the major reserves exploited for cassiterite. The layers are up to 2 m thick and composed of poorly sorted pebbles, with angular clasts and more rarely, lithic fragments of granites and even greisen. On the top, there are plastic clay layers interbedded with coarse-grained sand.

Fig. 3.3: Stratigraphic section in the Barranco Stream (Oriente Novo Mine) exemplifying the setting of Depositional Sequences I and II (adapted from BETTENCOURT et al. 1988).



- Colluvial sediments: This layer is composed of sandy clay with a mottled appearance, and occurs more specifically on the hillsides.

The scheme used by PAYOLLA et al. (1984) and BETTENCOURT et al. (1988) to describe this sequence is shown in figure 3.3.

3.2 Geology and mineralogy of the investigated deposits

3.2.1 Massangana garimpo

The Massangana garimpo comprises several cassiterite deposits formed in the domain of the Massangana Granitic Complex, which comprises four successive magmatic episodes (ROMANINI 1982). The earliest episode is the Massangana phase, followed successively by the Bom Jardim, São Domingos and Taboca episodes. The lithotypes of the Massangana phase are of calc-alkaline affinity and made up of coarse-grained granitic, porphyritic rocks with ovoid and tabular megacrystals of K-feldspar (ROMANINI 1982). The later igneous episodes, Bom Jardim and São Domingos, are represented by fine-grained to coarse-grained biotite granites with rare K-feldspar (DARDENNE & SCHOBENHAUS 2001). The youngest Taboca episode is represented by hornblende-syenites and quartz-syenites that intrude the granites of the Bom Jardim phase (ROMANINI 1982).

The primary cassiterite ore is related to the Bom Jardim and São Domingos igneous episodes (DARDENNE & SCHOBENHAUS 2001). According to these authors, the cassiterite occurs in quartz

veins, greisen and pegmatites. Wolframite, beryl, topaz and columbite-tantalite are subordinate components.

However, the main ore from Massangana is in the alluvial deposits along the slopes of topographically elevated granite hills. In places where the greisenized cupola is preserved, it is still possible to extract primary cassiterite.

Primary deposits

The Massangana Granitic Complex is formed by two amalgamated granitic batholiths of circular shape. According to ISOTTA et al. (1978), the circular shape is a ring fracture system related to the late magmatic stage of the Bom Jardim episode. There are two systems of fractures (N40-50W and N50-70E) that host quartz veins and pegmatites, which are both mineralized with cassiterite. ROMANINI (1982) declares that the primary mineralization is associated with the cooling fractures in the initial magmatic phases, into which the late magmatism phases intruded.

In the locality of Pau Baixo, an exogreisen is mineralized with cassiterite. Here, rocks of the Jamari Complex were greisenized and silicified. Horizontal quartz veins show that the foliation of the country rocks had minor or no influence on the hosting of the ore. This may indicate that the mineralization is influenced by some subsurface granitic body (Figs. 3.2 and 3.3).

In the region known as Cafezal, a greisenized granite cupola is preserved, where the garimpeiros extract cassiterite and a small amount of amazonite.

Secondary deposits

The secondary deposits of the Massangana Garimpo occur in the thalweg of the drainage systems that cut the batholith and the surrounding areas. The typical alluvial model of Massangana is found in the plains of Pau Baixo. Here, there is reddish brown sediment composed essentially of clay and fine sand. Clasts with coarser granulation often occur, but not larger than pebbles. Identified minerals in the field are mainly quartz and iron oxides, and less frequently cassiterite.

The São Domingos locality at the margin of the Massangana River is an alluvial deposit with gravels grading from coarse sand to pebbles, which represents a flood plain of this river. However, hard rock is found at the bottom under the gravel deposits. The material is composed of coarse-grained feldspars and quartz. Coarse-grained sand with topaz is also found at this locality. Cassiterite is the only ore mineral.

3.2.2 Bom Futuro garimpo

The Bom Futuro garimpo is the most extensively studied deposit among the investigated sites in this report. About 90% of the ore exploited in the Bom Futuro garimpo originated from secondary deposits and tailings. Nowadays, the extracted ore is both secondary and primary, but the aim of the garimpeiros is to increasingly mine the primary ore (chief geologist Renato Muzzollon, personal communication).

Primary deposits

The Bom Futuro deposit comprises a plutonic-volcanic system that intrudes the country rocks of the Jamari Complex. The name Bom Futuro is derived from the volcanic system of the same name. The plutonic system ("Palanqueta") occurs in the north-eastern part of the deposit (Souza 2003, Fig. 3.4).

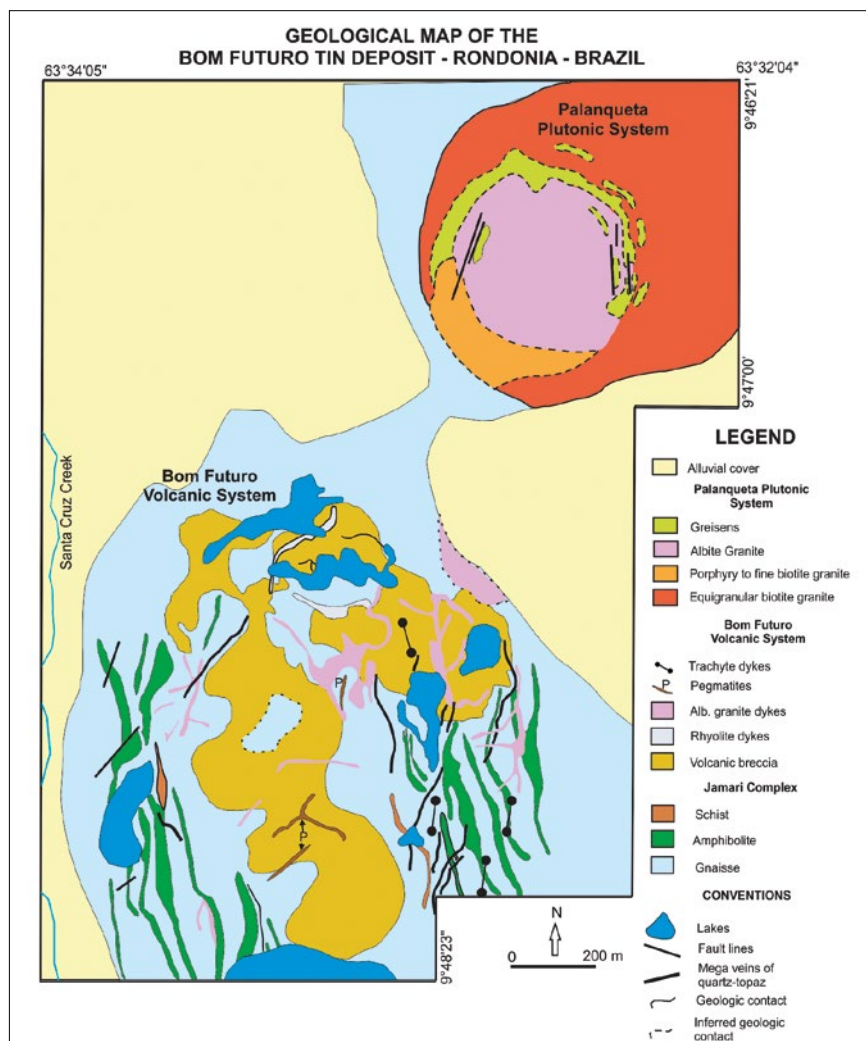


Fig. 3.4:
Geological map of Bom Futuro. Adapted from SOUZA (2003) and BETTENCOURT et al. (1995).

According to SOUZA (2003), the country rocks are gneisses and schists with a NNW-SSE trend and a dip of 50°. The country rocks are cut by dykes of albite-granite, rhyolite, trachytes, pegmatites and quartz-topaz veins related to the volcanic system (Fig. 3.4).

BETTENCOURT et al. (1995) state that the Bom Futuro system is composed of volcanic breccias, rhyolite dykes and albite granites with subordinate pegmatites (Fig. 3.5). In the Palanqueta system, there are greisen, albite granites and biotite granites.

Secondary deposits

The Bom Futuro deposit is an impressive exposure of palaeoalluvial ore. The sedimentary cassiterite deposits are in the northwest and southeast regions of Bom Futuro (SOUZA 2003). Layers of conglomerate interbedded with massive silty, massive argillaceous and white plastic clay layers (Fig. 3.6) are visible. Cassiterite is concentrated in conglomeratic layers, which are composed of pebbles of angular quartz, and a red matrix of coarse-grained quartz. This layer was sampled for further investigations.

The interbedded layers of clay and silt contained fractions of fine to medium-grained quartz and correlate with Depositional Sequence I.

At this locality, the sedimentary system that generated Depositional Sequence I produced repeated layers with lateral variations, which explains the erratic occurrence of supergene tin ores. The thicknesses of the sedimentary layers are variable and can reach 40 meters (BETTENCOURT et al. 1995).

The sedimentary cassiterite deposits are in the northwest and southeast regions of Bom Futuro (SOUZA 2003). In the northwest, alluvial sediments predominate. The deposits are characterized by alluvial fans in a braided river system (SOUZA 2003). In these deposits, there are argillaceous layers interbedded with sandy and conglomeratic seams (Fig. 3.6). SOUZA (2003) describes the conglomeratic seams as the main cassiterite host. In addition to cassiterite, there are topaz, quartz, lithic fragments (greisen and granites) and laterite fragments. The grain size of the cassiterite in these layers does not exceed 5 mm.



Fig. 3.5: Hard rocks (primary ore) in the Bom Futuro Garimpo with greisen, pegmatite and quartz veins.

In the southeast of the Bom Futuro Deposit, the assemblage of the argillaceous, sandy and conglomeratic strata is associated with kaolinite banks. The thickness of these unconsolidated sediments reaches up to 47 meters (QUADROS et al. 2001). However, new field evidence of paleochannels in

deeper layers suggest a greater thickness (Renato Muzzollon, personal communication). The paleochannels are under a thick cover of tailings and clay that are re-processed from time to time by independent artisanal miners.

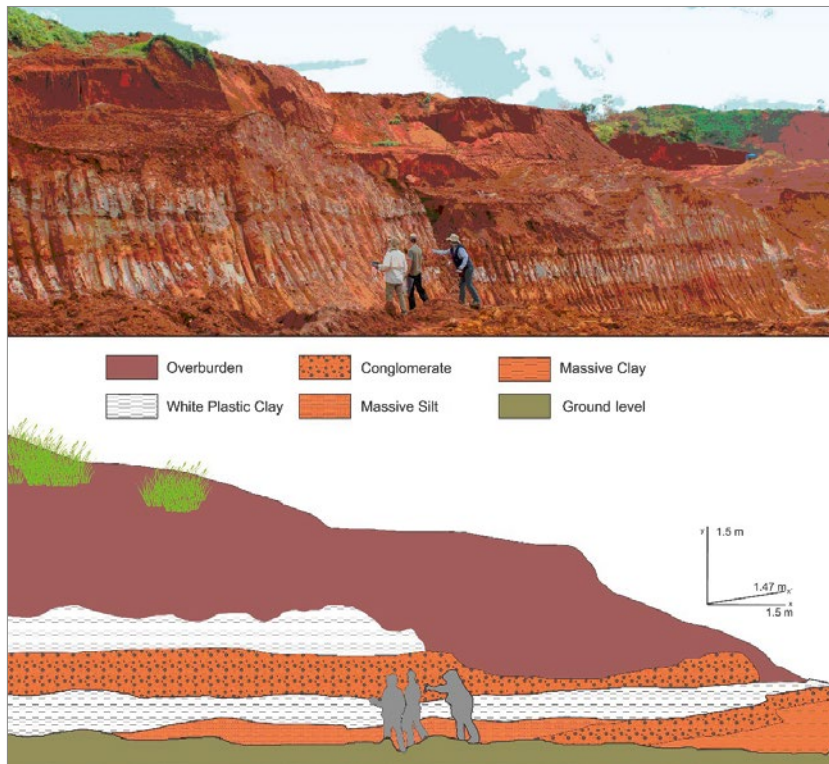


Fig. 3.6: Outcrop of sedimentary layers from Depositional Sequence I in the Bom Futuro deposit. A regular repetition of mineralized layers is observed associated with interbedding between conglomeratic and silt-argillaceous layers.

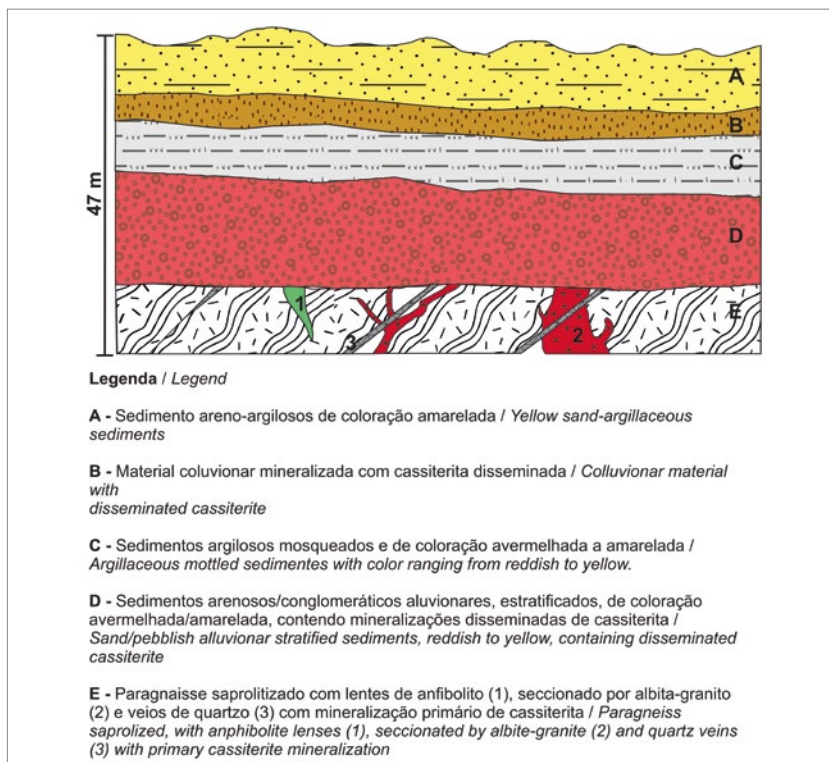


Fig. 3.7: Cross-section of the strata in the southeast region of Bom Futuro. The layers B and C are secondary cassiterite ore. Level E of the section contains primary cassiterite ore. Adapted from QUADROS et al. (2003).

3.2.3 Santa Bárbara and Cachoeirinha mines

Primary deposits

The Santa Bárbara and Cachoeirinha deposits occur in two different granitic massifs. The Cachoeirinha deposit overlies the Caritianas massif, and the Santa Bárbara deposit is located above the Santa Bárbara granite. CARVALHO (1988) describes

a mineralization related to albite-granites and greisen with a N-S strike trend with 50°E dip.

According to FRANK (1990), there are two systems of mica-greisen veins in the Santa Bárbara deposit. The former is coarse-grained and with a preferential N-S strike and dipping between 55–65°W. The youngest formation is a fine-grained greisen system with a N-S strike trend and a 45°W dip. The mineralized veins of sub-centimeter-sized cassiterite occur subparallel to these systems.

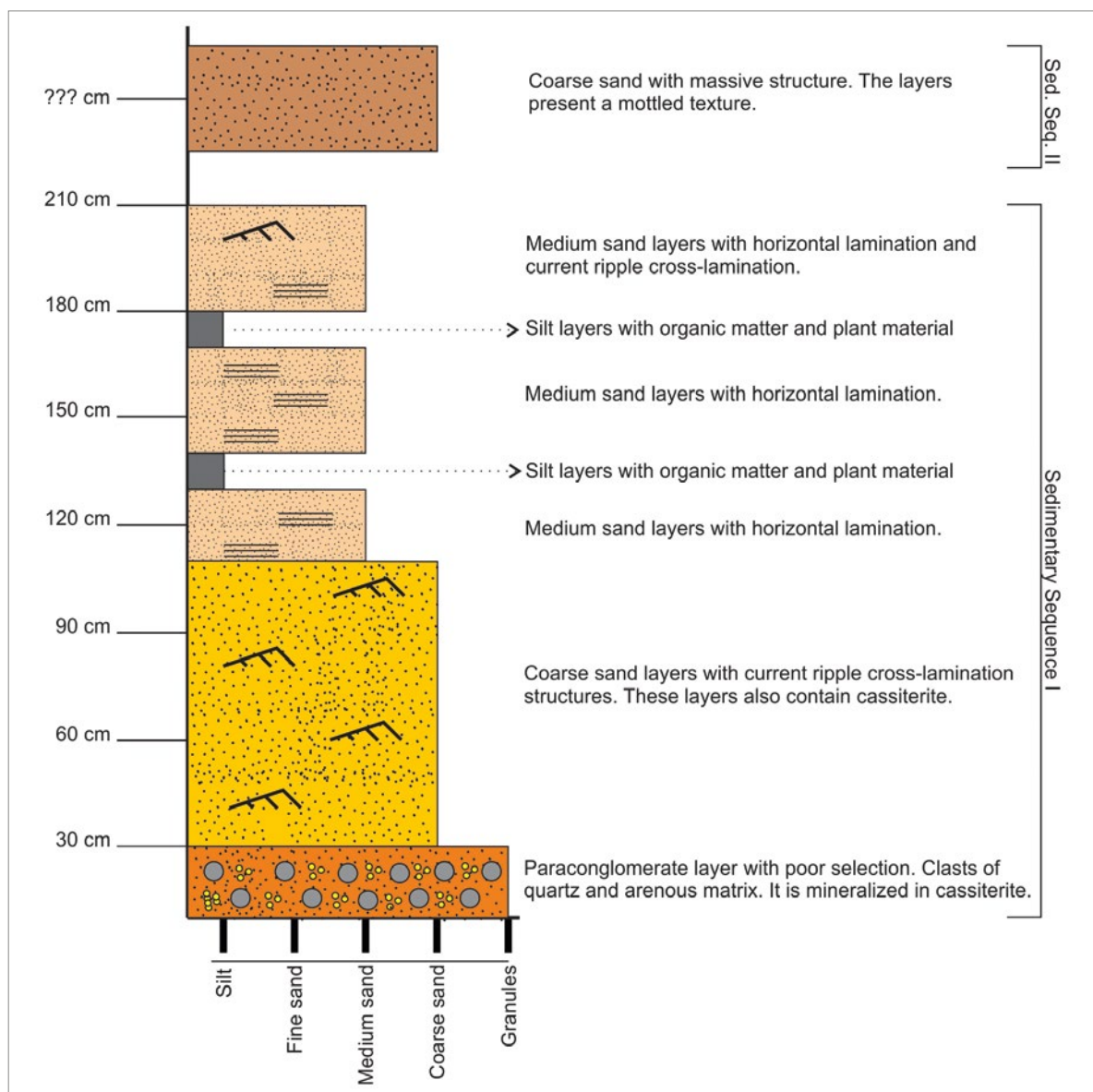


Fig. 3.8: Profile of supergene cassiterite ore in the Cachoeirinha deposit. A decrease in the granulometry of the sedimentary sequence is observed. An important feature is the repetition of silt layers with organic matter and medium-grained sand layers. At the top of the profile, there is a layer of coarse sand with a mottled texture, belonging to Sedimentary Sequence II.

SPARREBERGER (2003) also reported the existence of a stockwork system in the Santa Bárbara area. This system is composed of topaz-siderophyllite-quartz greisen and is set in strongly dipping planes with three general strikes: N-S strike trend with 15 to 45°E dip. Additionally, the author describes a vein system composed of greisen and quartz with strikes ranging from a N-S strike trend with a 45°W dip and a 30–40°E dip, and a N-S strike trend with up to 50–60°E dip, as well as a subsystem of mineralized quartz veins with N-S strikes dipping between 60–80°E.

In the Cachoeirinha deposit, BETTENCOURT & PINHO (1990) mentioned the existence of mica-quartz greisen veins with a general N-S strike trend with 30 to 45°E dip. There are also subordinate bodies of microgranites and aplites with meter-sized dimensions parallel to the greisen veins. There are also aplite and pegmatite dykes of centimeter to meter size with a N-S strike trend with 40°E dip and 75°W dip (OLIVEIRA 2012).

Secondary deposits

Despite the fact that these deposits are located on different granitic massifs, it is considered the same

sedimentary system in this study. In the Cachoeirinha deposit, the mining activities exposed an entire profile of Depositional Sequence I, especially of the lower sedimentary layers of the sequence (Fig. 3.8). At the bottom of the sequence is a conglomerate composed of pebbles and granules of quartz, which is covered by a layer of coarse sand with current ripple cross-laminations. The conglomerate and the coarse sand layers are enriched with cassiterite. Medium-grained sand with horizontal lamination occurs above this conglomerate.

At the top of the supergene deposits, a 1–2 m thick layer of coarse sand with a mottled texture (Fig. 3.9) is also mined for cassiterite and columbite. Using the same interpretation of Bettencourt et al. (1988), this coarse-sand layer belongs to Depositional Sequence II.

In the Santa Bárbara deposit, the white plastic clay layer (Depositional Sequence I) reached around 10 meters in thickness in Igarapé Taboca (Fig. 3.10). At the bottom of this formation, there is a sequence with a medium-coarse sand layer with grains of angular quartz, a massive clay layer, and a medium-grained sand layer, all of them with a thickness of around 1 m. Both sand layers are enriched with cassiterite (Figs. 3.10, 3.11).



Fig. 3.9: Coarse-grained sand related to Depositional Sequence II in Cachoeirinha. Note the massive structure and mottled texture.

No clear interbedding of the layers could be observed within the Santa Bárbara deposit. However, it is considered that Depositional Sequence I is also a major source of cassiterite ore in Santa Bárbara.

The conglomerate and the coarse-grained sand layers of Depositional Sequence I and the coarse-grained sand of Depositional Sequence II are shown in figure 3.11. Cassiterite is contained here in varying amounts in a matrix of fine-medium grained sand and angular to rounded grains of quartz (Fig. 3.11 right).



Fig. 3.10: Mining site in the Santa Bárbara deposit, where an overburden of massive mottled clay covers mineralized sand layers.



Fig. 3.11: Outcrop of Depositional Sequence I in the Cachoeirinha deposit: Conglomerate (left) and coarse-grained sand (right).

4 Methodology and overview of common methods of mining and mineral processing

For the optimization of the mineral processing it is essential to know which methods traditionally carried out, also in order to identify possible weak points of these techniques. Therefore, the following chapter shows the used methods of mineral processing in the investigated mines and cooperatives.

4.1 Methodology of sampling and analytics

To gain an insight into the different ores and processed products, mainly samples of secondary ores (placer and tailings), but also of primary ores (greisen and pegmatites), as well as concentrates from the processing plants were collected at each site. During the first fieldwork campaign in November/December 2016, eight Sn-Ta mines and deposits in Rondônia, mainly near the city of Ariquemes, but also in São Lourenço (approx. 180 km W of Porto Velho), were sampled and investigated with geochemical and mineralogical methods (all collected samples are listed in Appendix 1).

Seventy nine samples were geochemically analyzed by X-ray fluorescence (XRF) and 19 of them were selected for analysis by inductively coupled plasma-mass spectrometry (ICP-MS). Another 10 samples were analyzed by laser ablation-inductively coupled plasma-mass spectrometry (LA-ICP-MS) to determine their REE contents. Mineralogical analysis by MLA (scanning electron microscopy with Mineral Liberation Analysis software) was carried out on 32 samples.

According to the results of these investigations, and regarding the given resource situation, four mines and cooperatives near the city of Ariquemes were selected for further investigations and processing testing: These were the Massangana and Bom Futuro garimpos, as well as the Santa Bárbara and Cachoeirinha opencast mines. These four sites are examined in detail in this report. The following mineralogical, geochemical and economic aspects were looked at:

- Economic contents of Sn and Ta within the secondary ores (according to XRF and ICP-MS results)
- Significant resource situation in all four selected deposits
- Different ore types (placers, tailings and hard rocks) in Bom Futuro
- Relatively high contents of U-Th bearing minerals in Massangana and Bom Futuro
- Low radioactivity in Cachoeirinha ores
- Relatively low degree of intergrowth of the ore minerals in all four deposits (according to MLA results) within the secondary ores
- Suitable infrastructure for transport, energy and accessibility for all four mining operations

During the second fieldwork campaign in May 2017, extensive sampling was carried out to take “larger-sized” bulk samples of pre-concentrates, as well as placers and tailings, totaling approximately 80 kg for each of the four selected mine sites.

The collected samples were dried, divided into aliquots and then shipped to BGR in Hannover, Germany. The mineral concentrate samples were analyzed by XRF. The list of sampled material with the respective location, analysis, characteristics and type is found in the Appendix of this report.

4.2 Common mining methods

The mining methods in the mentioned garimpos are similar. Before mining, the garimpeiros assess the ore content by using a pan concentrator (Fig. 4.1-a). If the layers contain enough cassiterite (about 1%), they start to flush water onto the targeted layers (Fig. 4.1-b).

The use of hydraulic jets is the most popular and well-established technique for the secondary ore (Figs. 4.1-b, 4.1-c). For primary ore, mining is either manual with shovels and picks, and more effectively, with heavy machines like backhoes, shovel loaders and dump trucks (Fig. 4.1-d). The use of explosives in Bom Futuro is common.



Fig. 4.1: a) Garimpeiros checking if the layer contains enough cassiterite to be mined, b) Mining operation with an hydraulic jet in Massangana, c) Mining of alluvium near the Massangana River, in Garimpo Massangana, d) Use of heavy machines to mine in Garimpo Bom Futuro.

The hydraulic jets are powered by diesel engines, normally taken from pickups and trucks. These engines propel the jet of water in the monitor and pump the pulp produced by the water jet to the nearby pre-concentration jigs. The most common jigs are of Yuba and Pan American types. The hydraulic jets are also used to rework tailings.

In Massangana, the most common method is an hydraulic jet to loosen the alluvium and tailings. The primary ore in Massangana is consolidated and therefore mostly mined by hand.

The mineral processing plants are usually some distance away from the mining operations. The garimpeiros transport the pre-concentrate obtained from the jigs near the mine to the plants or they carry the dry ore to the plants with trucks.

4.3 Common methods of mineral processing

The traditional mineral processing methods are very similar among the garimpos. The main differences in mineral processing depend on the different types of ore to be processed (primary, secondary or tailings). An overview of the processing techniques and also of the mining methods performed at the investigated sites is given in table 4.1. Processing methods for each plant in the selected mining operations are described in Chapter 6.

The most common processing machine in the garimpos and in the mines is the jig (Yuba and Pan American types). The jigs are attached to mobile structures and positioned near the min-



Fig. 4.2: a) Jigs outputting clay as tailings in the first gravity concentration, b) and c) Jigs separating the cassiterite and the first and second cama (basin under the jig), d) Shaking table separating the very fine cassiterite.

ing operations (Fig. 4.2-a). The most common jig consists of two trapezoidal chambers. However, the garimpeiros have also combined Pan American jigs with up to 8 trapezoidal chambers (Fig. 4.2-b). The diaphragm of the jig is moved by electric motors (Fig. 4.2-c) with diesel power generators. The jigs are known as “resumidores”, and each trapezoidal chamber is called a “cama”. The best quality pre-concentrate is produced in the 1st cama, whereas the 2nd cama is characterized by a lower cassiterite content.

The pulp is pumped to the first jig in the mining operation. If the good quality output of the 1st cama does not contain monazite or ilmenite, it is sold to the cooperatives. The material of the 2nd cama normally contains a large amount of gangue minerals, and therefore must be jigged again. The second

jigging is called “2nd resumidor”. After the second jig, the output (1st cama) material can be considered finished and is saleable. The material from the 2nd cama must be processed again. The pre-concentrate produced in this way is usually processed in spiral separators, on shaking tables (Figs. 4.2-d, 4.3-c), and the fine fraction is treated afterwards in magnetic separators (Fig. 4.3-d). These successive processes are made in permanent facilities at some distance from the mining operations. The different mineral processing steps are shown and described in Chapter 5.

In Bom Futuro, the initial processing of primary ore is carried out using crushers with four crushing phases. After crushing, the ore is milled (Fig. 4.3-a), jigged, and the tailings from the jigging is sent to the spiral concentrator (Model Humphrey, Fig. 4.3-b).

Tab. 4.1: Overview of the principal features of mining methods and mineral processing at the visited mining operations.

Item	Sub item	BFG	MG	CM	SBM
Type of exploited material	Alluvium	X	X	X	
	Paleoalluvium	X	X	X	X
	Endogreisen	X	X	X	X
	Exogreisen	X	X		X
	Tailings	X	X	X	
Exploitation methods	Manual	X	X		
	Hydraulic Jet	X	X	X	
	Mechanized	X			
	Explosives	X			
Mineral processing	Grinding	X			
	Jigging	X	X	X	
	Shaking Table	X	X	X	
	Hydrocyclone	X			X
	Spiral Concentrator	X		X	X
	Magnetic Separation	X	X	X	X
Final products	Pre-concentrate			X	X
	Concentrate	X	X		
	By-products	X	X	X	X

BFG: Bom Futuro garimpo, MG: Massangana garimpo, CM: Cachoeirinha mine, SBM: Santa Bárbara mine.

The cross-belt magnetic separator is used to separate magnetic minerals and to produce concentrates rich in columbite, monazite or ilmenite (Fig. 4.3-d). In the CEMAL processing plant, the first separated minerals are ilmenite and magnetite (ferromagnetic fraction). In the second output, only ilmenite is separated, and in the third output, columbite is taken from the ore (paramagnetic and diamagnetic fraction). However, the garimpeiros also separate columbite from cassiterite in induced roll magnetic separators.

The shaking table is used for the fine-fraction of the pre-concentrates (Fig. 4.3-c) obtained from the jigs. Normally the cassiterite is separated and the resulting tailings contain monazite with quartz and fine clays. This material is normally discharged.

The cassiterite-rich pre-concentrate from the spiral concentrators is very fine grained: Apparently with grain sizes less than 400 µm. However, the tailings output from this machine was not verified.

4.4 Products from mineral processing

Beyond cassiterite concentrate production, there is also the metallurgy of tin. Until 2012, CEMAL in association with the Cooperativa dos Fundidores de Cassiterita (CFC) produced tin in its facilities in Ariquemes. Since the end of CFC operations, CEMAL has only sold the cassiterite concentrate (Fig. 4.4) produced in its facilities.

Cassiterite concentrates from mines as São Lourenço are usually sold to companies in Ariquemes, such as White Solder Ltda. and MELT S.A. Cassiterite produced by COOPERSANTA in Bom Futuro is reduced in the vicinity, by the partner cooperative COOPERMETAL.

Further processing plants for cassiterite concentrate are in the states of São Paulo and Minas Gerais. When the cassiterite is exported, the main destination is Malaysia, followed by Bolivia.

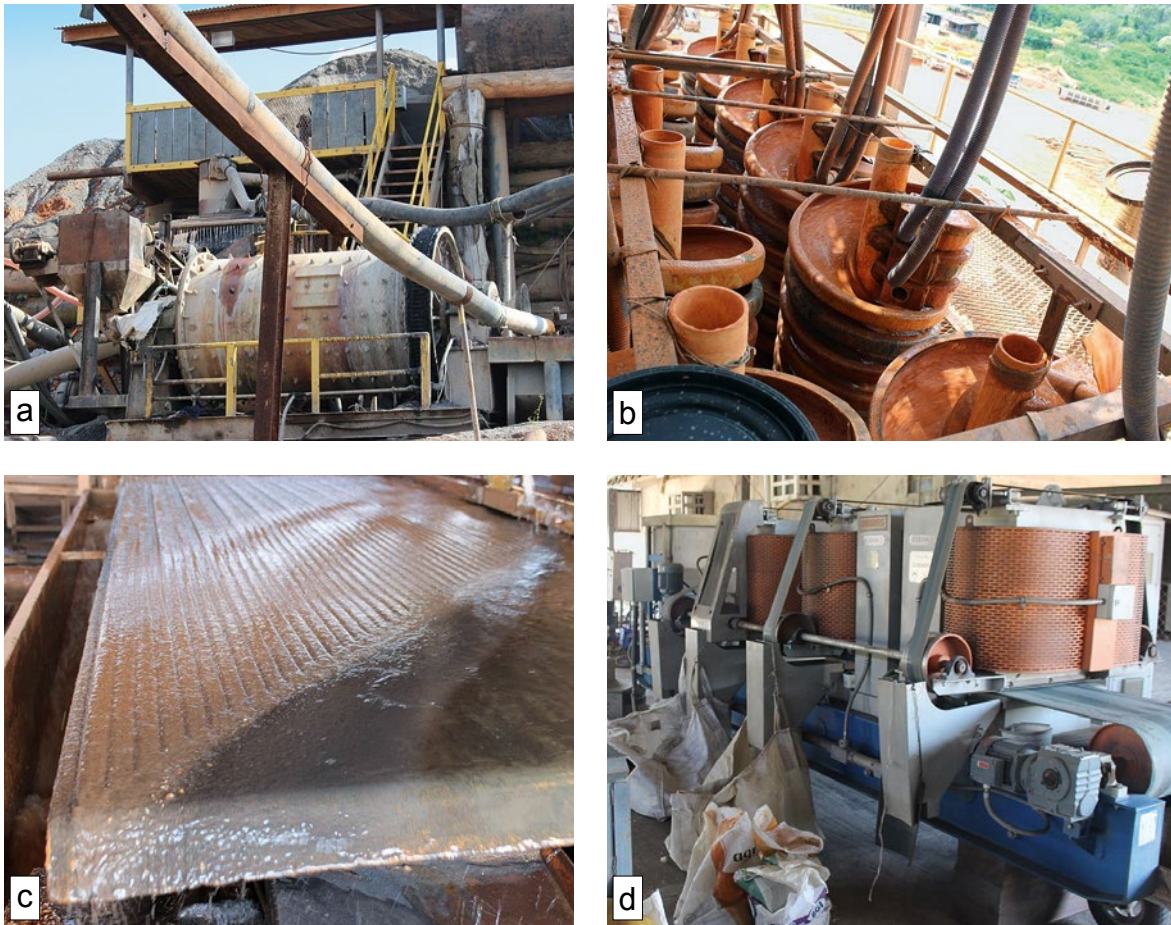


Fig. 4.3: a) Milling of the ores (primary and secondary) in Bom Futuro, b) Spiral separation of the sieved ore in Santa Bárbara, c) Shaking table separating ore minerals from silicates in Massangana (CEMAL plant), d) Magnetic cross belt separator to produce ilmenite, columbite, monazite and cassiterite at the CEMAL plant.



Fig. 4.4: Final cassiterite concentrate product after magnetic separation at the CEMAL plant.

COOPERMETAL sells the refined tin in two forms. There is the 2° line tin (Fig. 4.5-a) with a tin content between 10 to 15%. This product is sold for its high

Pb content with Sn as a by-product. The 1° line tin is the refined tin with an Sn grade of >99.85% (Fig. 4.5-b). This refined tin is sold in 25 kg ingots.



Fig. 4.5: a) Alloy with Sn grades between 10 to 15%. This product is sold for its high Pb content, making the Sn just a by-product, b) Ingots of high quality Sn that match the LME standard.

5 Detailed mineralogical investigations and individual mineral processing methods of the four selected mine sites

As described in Chapter 4.3, the mineral processing of cassiterite ore is predominantly by gravitational methods, and secondarily by magnetic methods. The main differences in mineral processing reflect the different types of ore to be processed: Primary ore (hard rock), secondary ore or tailings with some residual Sn.

Not only in the sampled deposits, but also in other deposits, the most common machinery is the jig system. To increase jigging efficiency, integrated systems are installed to produce concentrates with the highest Sn content. Output concentrates of these jigging processes are processed in different ways, commonly by magnetic separation and spiral concentrators.

Given the difference in methodology used in each sampled deposit, the team needed to adopt the sampling approach. Therefore, it is not possible to compare the efficiencies of mineral processing from these areas. However, we consider that our sampling provides an insight into the best mineral processing in each sampled deposit.

5.1 Massangana cooperative (CEMAL)

Mineral processing

The Massangana deposit is mined under the garimpeiro cooperative allowance. Therefore, the garimpeiros develop their own methods for mineral processing. Only the refinement of the concentrates is developed by the cooperative. Thus, the garimpeiros usually use mobile jigs in the mining areas, while the CEMAL processing plant performs further mineral processing with shaking tables and magnetic separators.

In Massangana, the secondary ore and tailings ore are the predominant source of cassiterite. Therefore, samples of tailings, as well as concentrates from shaking tables and from the magnetic separator have been investigated. Primary ore mining

is very artisanal in Massangana and also involves the mining of gems (topaz and amazonite) which is not discussed in this report.

Tailings ore mineral processing in the Massangana garimpo

In the Massangana area, the main activity is the mining and re-processing of tailings. Samples of the tailings feed ore collected for this study originated from the Pau Baixo stream region (TB06E). The mineral processing starts with a first jigging step. The produced first pre-concentrate from this jigging (TB06B) goes to the shaking table of the CEMAL facilities. The output from the second chamber (2nd cama) of the first jig is forwarded to a second jig where the process is repeated. To represent this output from the second jig chamber, four samples from different localities were collected (TB45, TB46, TB47 and TB48). The second jig produces a pre-concentrate (TB06A) and its tailings are discarded at the mining site (TB06C). The pre-concentrate from the first and second jigs undergoes gravity separation on the shaking table, and the cassiterite pre-concentrate from this process goes to the magnetic separator to produce the final cassiterite concentrate (TB08C). Columbite (TB08A), monazite (TB08B) and ilmenite concentrates are produced as by-products of the magnetic separation. The tailings from the shaking table process were also sampled (TB43). The mineral processing flow in the Massangana CEMAL plant, including the sampling spots, is shown in figure 5.1.

Mineralogical investigations of feed ores and concentrates

Pre-concentrates from the 1st cama of the jigs at Massangana are generally of good quality with high cassiterite grades of about 70% (representative of the percentage in the area according to MLA) and economically interesting contents of columbite-tantalite (~3%), with significant amounts of ilmenite (~20%, Fig 5.2). These pre-concentrates are ready for further processing (e.g. magnetic separation) and can be fairly easily upgraded. In comparison, the pre-concentrates from the 2nd cama are dominated by ilmenite (~70%) and topaz (~18%) with subordinate amounts of zircon (~3%), columbite-tantalite (~2%), monazite (<1%) and

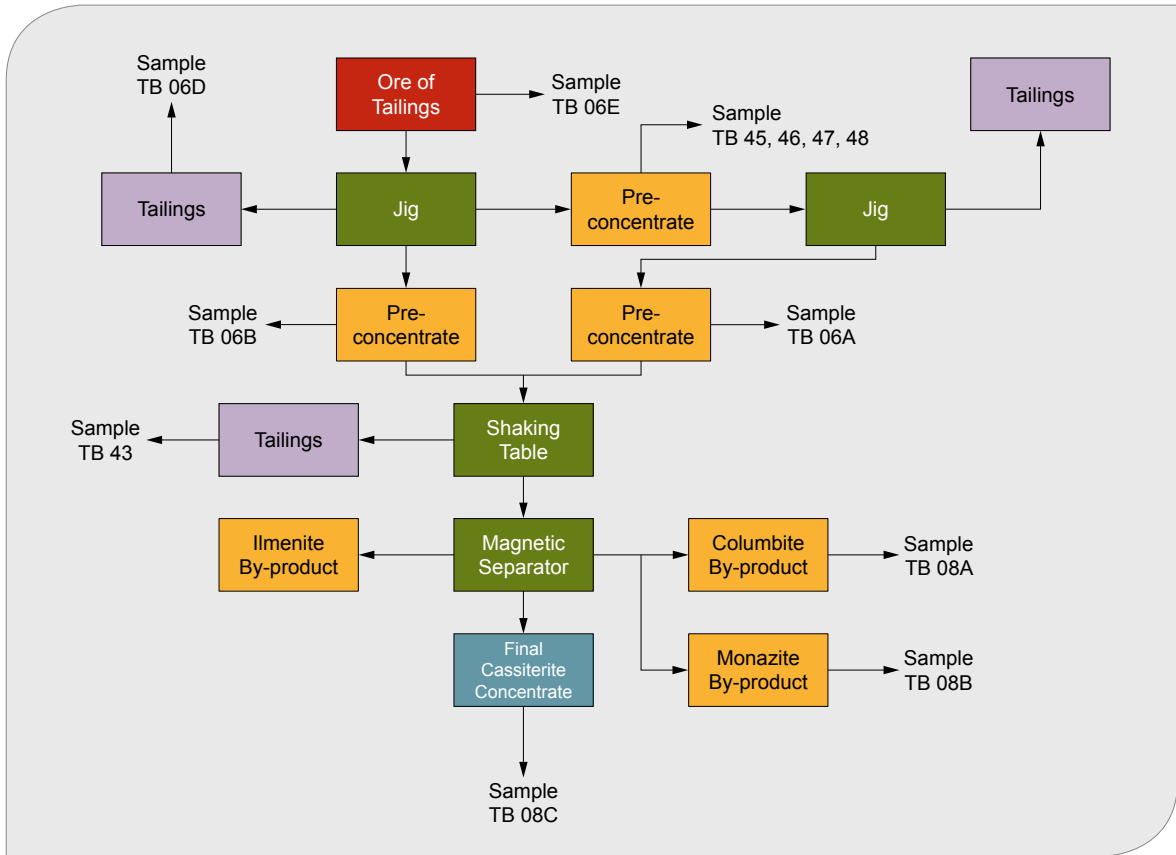


Fig. 5.1: Processing scheme of the Massangana plant with sampling locations.

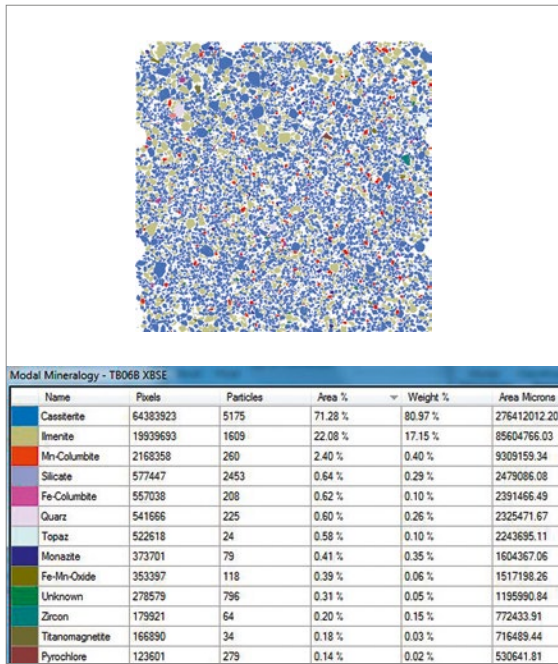


Fig. 5.2: Mineralogical composition from MLA on pre-concentrate from the 1st cama of jigs at Massangana (TB06B, sample taken during campaign in 2016).

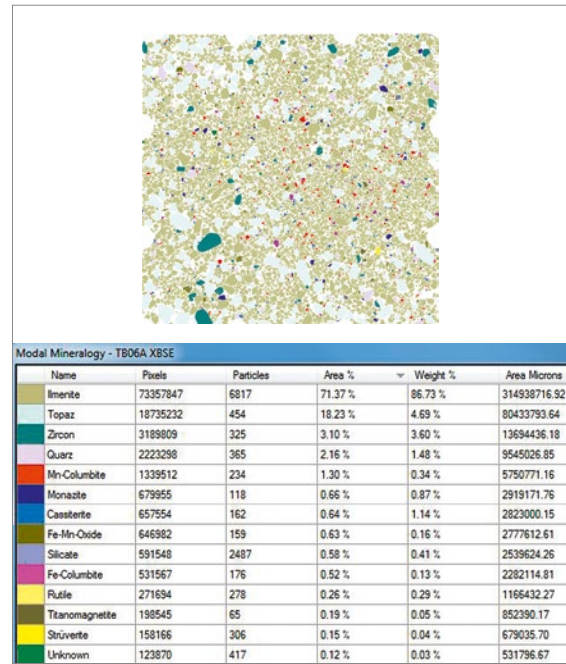


Fig. 5.3: Mineralogical composition from MLA on pre-concentrate from the 2nd cama of jigs at Massangana (TB06A, sample taken during campaign in 2016).

cassiterite (<1%) (Fig. 5.3). These pre-concentrates need to be further processed to achieve a product of higher value. However, elevated monazite contents can be problematic for both pre-concentrates because this mineral can carry high concentrations of Th and U. Therefore, monazite needs to be removed from the final cassiterite concentrate.

Geochemical analysis of pre-concentrates and tailings is used to crosscheck the MLA results, but also to determine whether the processing works well or if economically important elements are lost into the tailings during processing. Tailings from the initial jig process still contain quite high concentrations of Sn, Zr and Nb. In this case, the analyses of the different grain size fractions show high Sn (0.4 wt. %), Zr (0.7 wt. %) and Nb (900 ppm) values in the fines (60–100 µm grain size). This indicates that quite a significant amount of cassiterite, zircon and columbite is lost during jigging. This is one of the main reasons for further processing testing, and will be discussed intensively in Chapter 7. Even the tailings from the shaking tables (Fig. 6.4) show economic concentrations of Sn (0.8 wt. %), Zr (2.2 wt. %), Nb (0.9 wt. %) and Hf (0.8 wt. %).

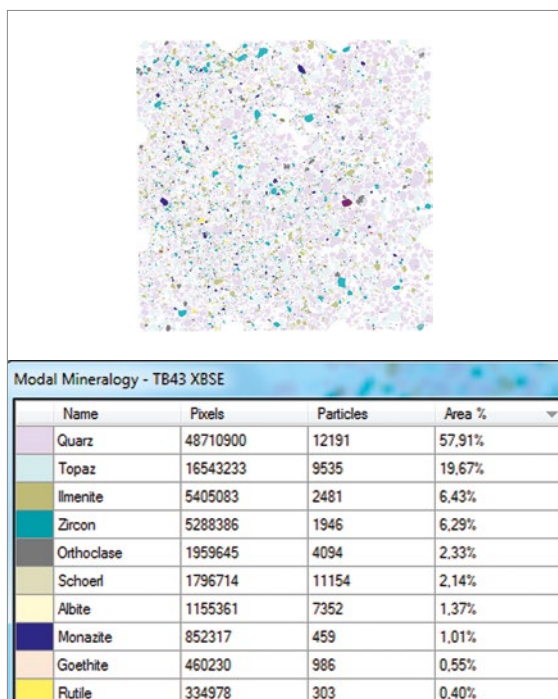


Fig. 5.4: Mineralogical composition from MLA on tailings from the shaking tables of the CEMAL plant in Massangana (TB43, sample taken during field campaign in 2017).

The major Hf bearing mineral is zircon and it is therefore worth considering the production of zircon concentrates as well for Zr and Hf extraction. However, higher radiation levels mainly due to U incorporated within zircon has to be taken into consideration, and therefore needs further investigation.

5.2 Bom Futuro cooperative (COOPERSANTA)

Mineral processing

At Bom Futuro nowadays, tin is extracted at a large scale from the three different types of “ore”. Like the other deposits, the secondary ore and ore from tailings are widely mined. Additionally, since 2014, Bom Futuro developed a processing flow to extract cassiterite from hard rock. In this study, ores and concentrates from all the steps existing at Bom Futuro have been sampled and analyzed.

Secondary ore

Sample TB11 represents the secondary ore mined in Bom Futuro. It consists of a conglomeratic layer at the bottom of a paleoalluvial sequence (more detail, see Ore Geology). The mineral processing of the secondary ore starts with milling and is followed by jigging. The team collected samples from the output of the mill (TB37A and TB37B), and the jig products. The jigging results in two initial concentrates: One is coarse-grained (TB37D) and the other is fine-grained (TB38A). The tailings from the jig process were also collected (TB37C). The pre-concentrates obtained by jigging are forwarded to the gravity spiral and afterwards to the shaking table. Samples of tailings and pre-concentrates from the gravity spiral were collected (TB38B and TB38C respectively). The last mineral processing stage is the shaking table. This process is represented by its tailings (TB38D) and the final cassiterite concentrate (TB38E) outputs. Figure 5.5 represents the simplified flow for the mineral processing in the Bom Futuro garimpo.

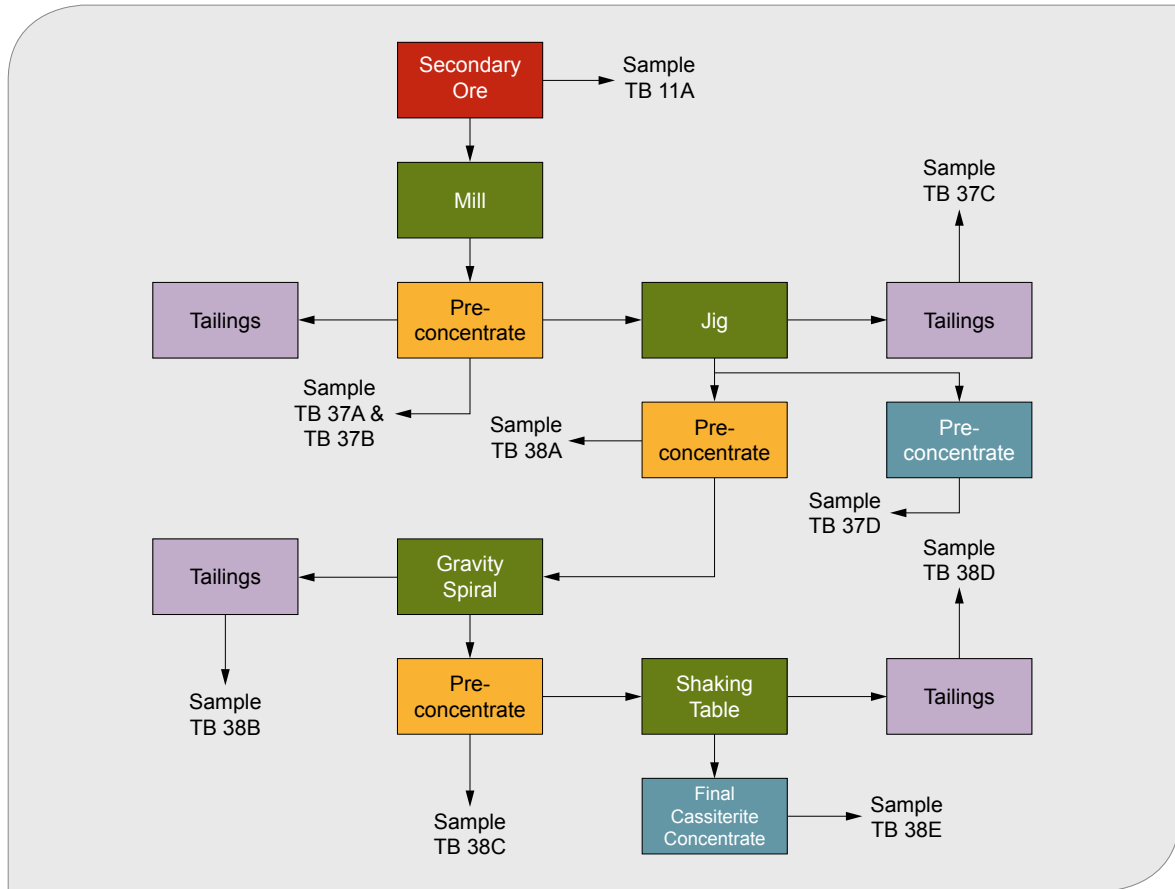


Fig. 5.5: Processing flow chart for placer ore in the Bom Futuro plant with sampling locations.

Tailings ore

Tailings that can still be considered as ore are stockpiled in the Bom Futuro area. A previous study identified around 6% cassiterite in pre-concentrates from stockpiles at Bom Futuro (BUCH et al. 2017). The mining methodology is the same as for secondary ores. However, the cassiterite contents are very variable. Currently, COOPERSANTA has a partnership with Australian Meridian Mining to mine the tailing stockpiles in an economic way.

The sampling of this material is represented by samples TB13A-D. The system is composed of a jig and a shaking table. The tailings ore (TB13A) enters the jig and its pre-concentrate (TB13B) is put on the shaking tables. The final concentrate is the shaking table output, represented by sample TB13D. To verify eventual losses in the jiggling, a sample from the tailings (TB13C) was also collected. Figure 5.6 represents the simplified mineral processing flow for the tailings ore at Bom Futuro, and also shows from which steps the samples were collected.

Primary ore concentrate

At Bom Futuro nowadays, the primary mineralization in the region known as “Serra” is also mined. The mineral processing starts with the crushing and grinding of the ore. Then the ground material is sent to the processing plant for milling, jiggling and gravitational concentration in the spiral concentrator. The best concentrates (~69% weight Sn) are considered as final products. Other concentrates are sent to the magnetic separator. Samples were collected at the output from the mill (TB14A), at the concentrate output from the jig (TB15A), at the concentrate output from the spiral (TB14B), and the tailings output from the jigs (TB14C). The pre-concentrates from the first and second jigs, and also from the gravity spiral, are sent to the magnetic separation and shaking table stages. The pre-concentrate obtained by the magnetic separator (TB15D), and also the final cassiterite concentrate output from the shaking table (TB15E). Figure 5.7 shows the schematic mineral processing flow and where the samples were taken from.

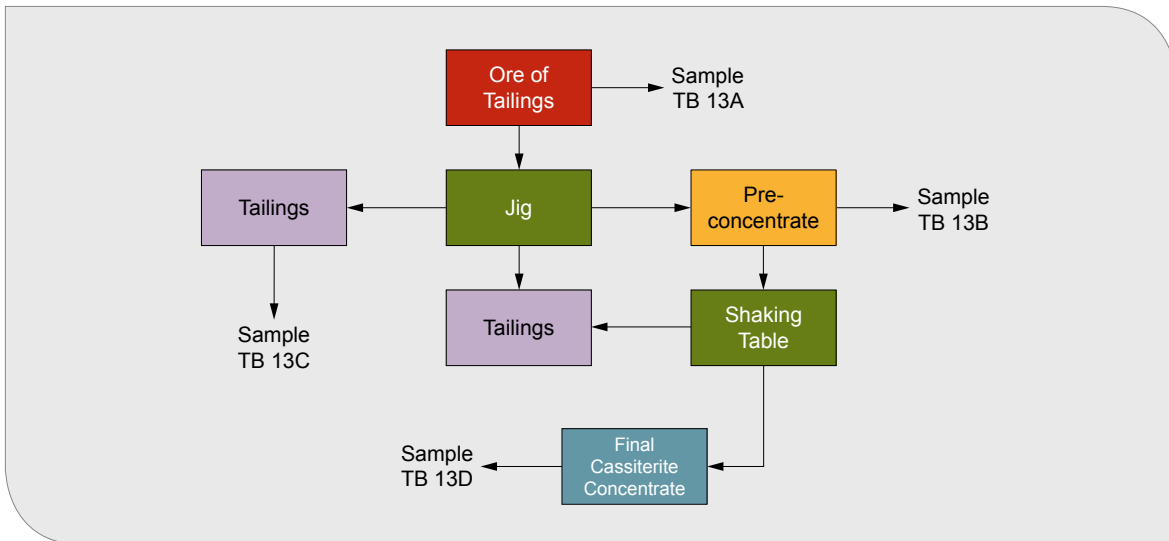


Fig. 5.6: Simplified tailings processing scheme of the Bom Futuro plant with sampling locations.

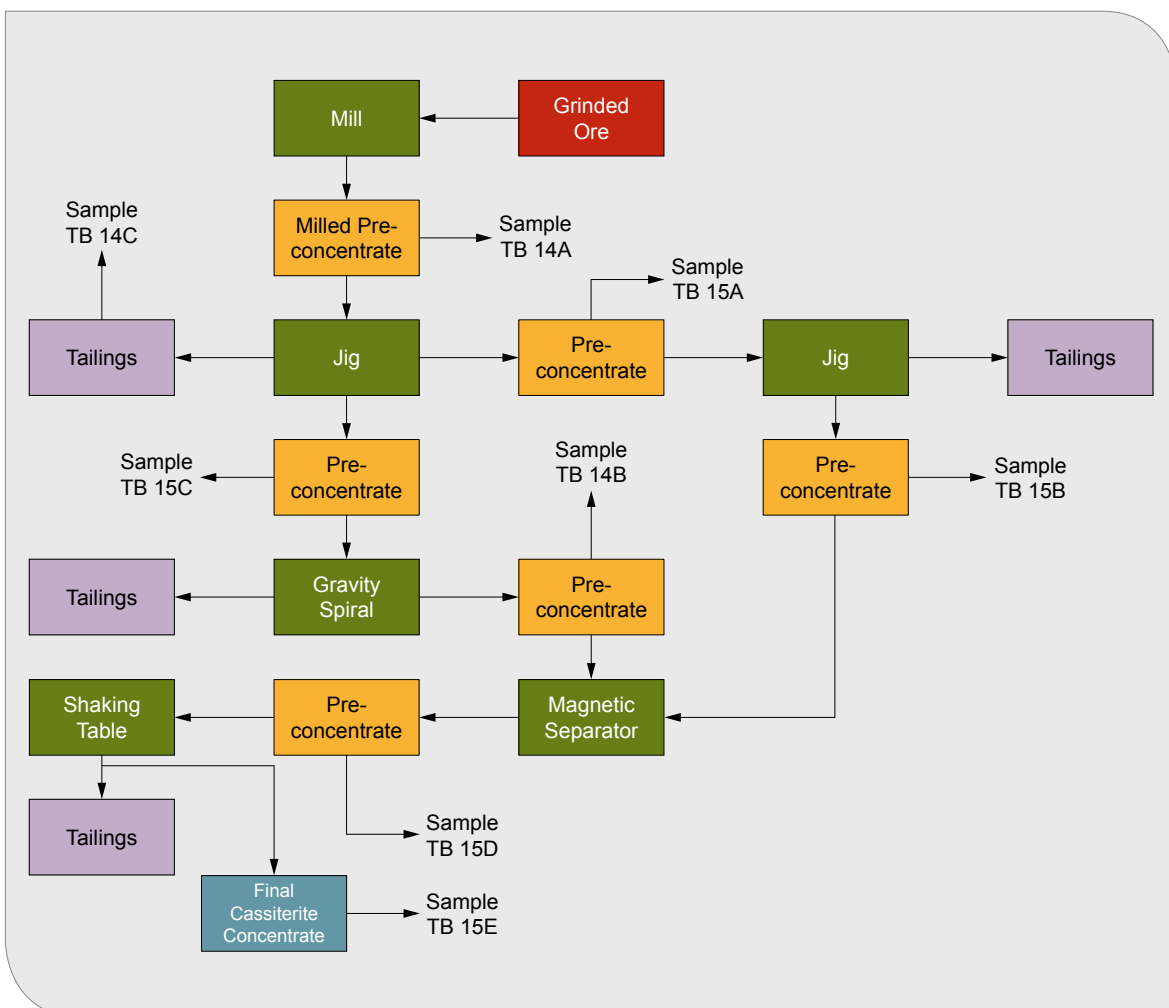


Fig. 5.7: Processing scheme for primary ore of the Bom Futuro plant with sampling locations.

Mineralogical investigations of feed ores and concentrates

Secondary ore (placer and old tailings) at Bom Futuro is initially processed by jigs, and subsequently by shaking tables and spiral separators. The produced pre-concentrates are dominated by ilmenite (~65%), but with moderate cassiterite grades (~13%, Fig. 5.8), and with minor zircon (<2%) and monazite (<1%) contents. Nevertheless, these pre-concentrates need to be further upgraded. These pre-concentrates can be fairly easily upgraded by magnetic separation, at least to remove ilmenite. In these pre-concentrates the increased monazite contents also need to be taken into consideration.

Primary ore from the hard rock mining operations at Bom Futuro need initial crushing and milling. After milling, the primary ore is processed in jigs and the fine-grained material then goes to the spirals. The concentrates contain high cassiterite grades (up to 60%) with subordinate ilmenite (~20%) and topaz (~7%, Fig. 5.9). Ilmenite can be easily removed by

magnetic separation. In contrast to secondary ore, the pre-concentrates from primary ore are characterized by the presence of sulfides (<4%, Fig. 5.9), interestingly the monazite contents are relatively low (~0.1%).

A coarse-grained and fine-grained cassiterite concentrate is obtained by processing the primary ore at Bom Futuro (Fig. 5.9, 5.10). The coarse-grained cassiterite concentrate displays intergrowth of cassiterite grains >1 mm, in particular with topaz, fluorite and sulfides (Fig. 5.11, left), which may considerably complicate further processing. In contrast, fine-grained material from the same ore shows almost no signs of intergrowth (Fig. 5.11 right). The evaluation of the MLA data of these two samples shows that <70% cassiterite from the coarse-grained concentrate is liberated compared to a higher liberation grade of >80% cassiterite from the fine-grained concentrate (Fig. 5.12). That also means that >30% cassiterite from the coarse-grained concentrate is intergrown with at least one phase, but in the fine-grained concentrate <20% cassiterite is intergrown. Hence, the grain size is a

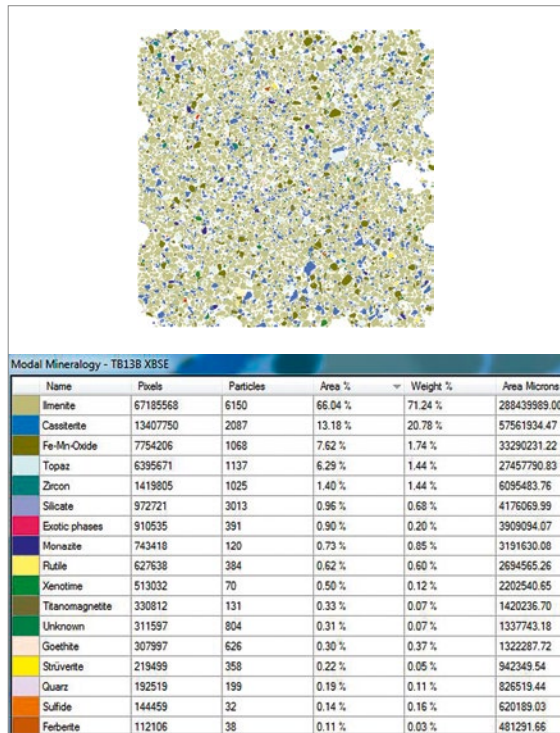


Fig. 5.8: Mineralogical composition from MLA on pre-concentrate from secondary ore at Bom Futuro (TB13B, sample taken during field campaign in 2016).

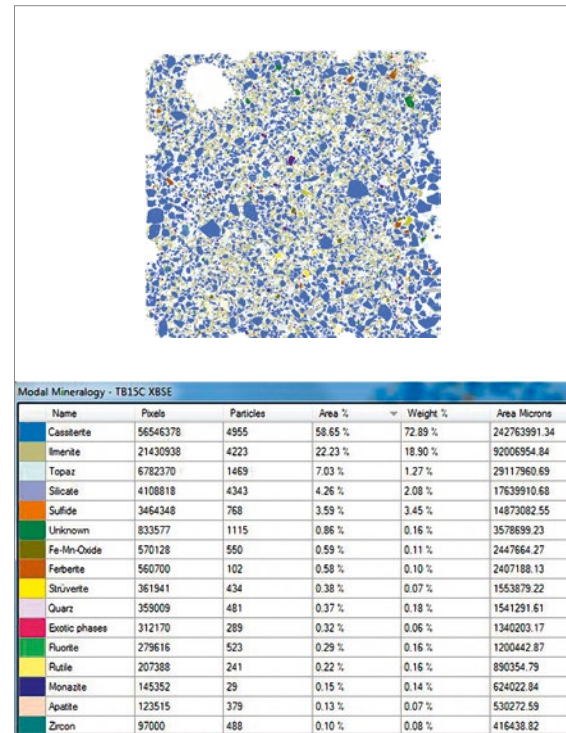


Fig. 5.9: Mineralogical composition from MLA on pre-concentrate from primary ore at Bom Futuro (TB15C, sample taken during field campaign in 2016).

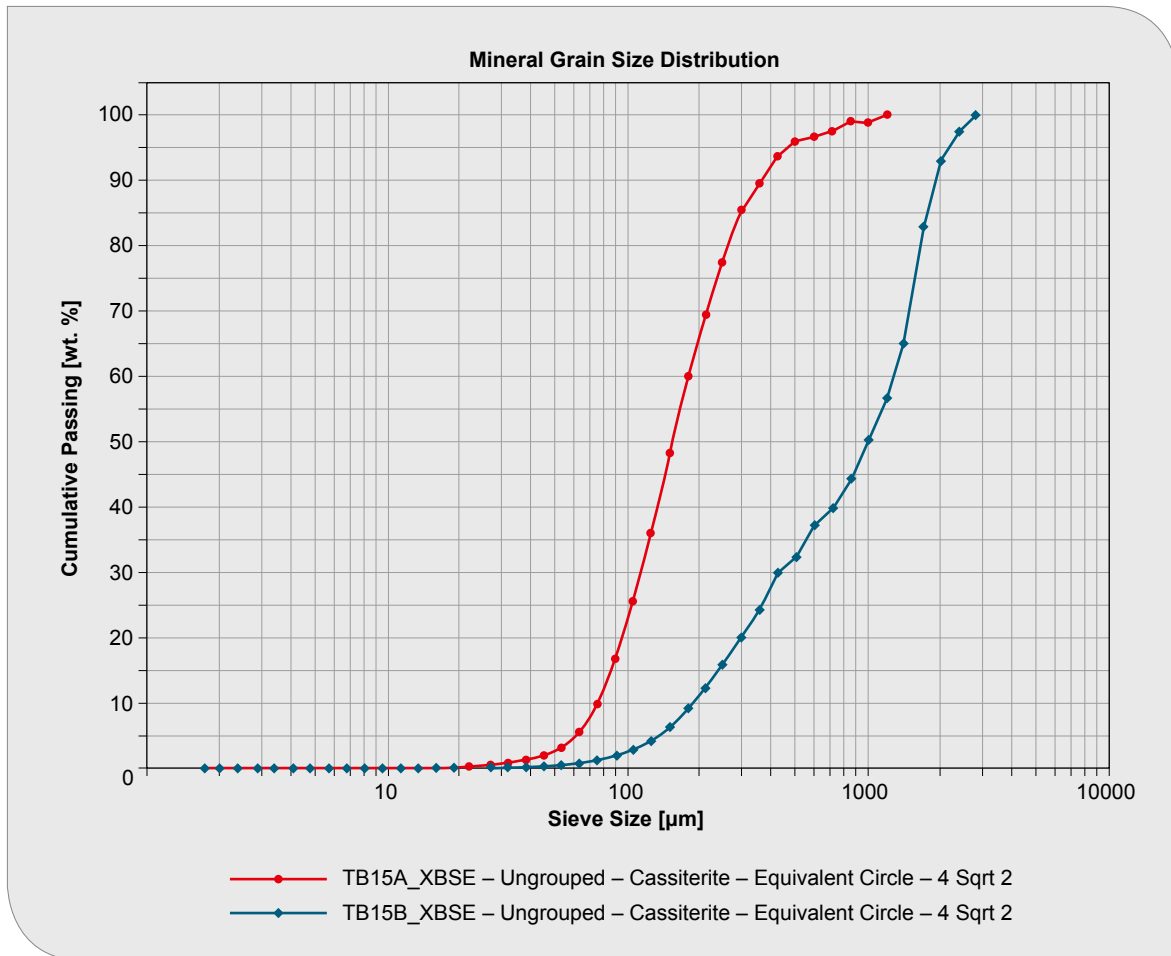


Fig. 5.10: Particle size distribution for coarse-grained (blue line, TB15A) and fine-grained (red line, TB15B) cassiterite concentrate from Bom Futuro.

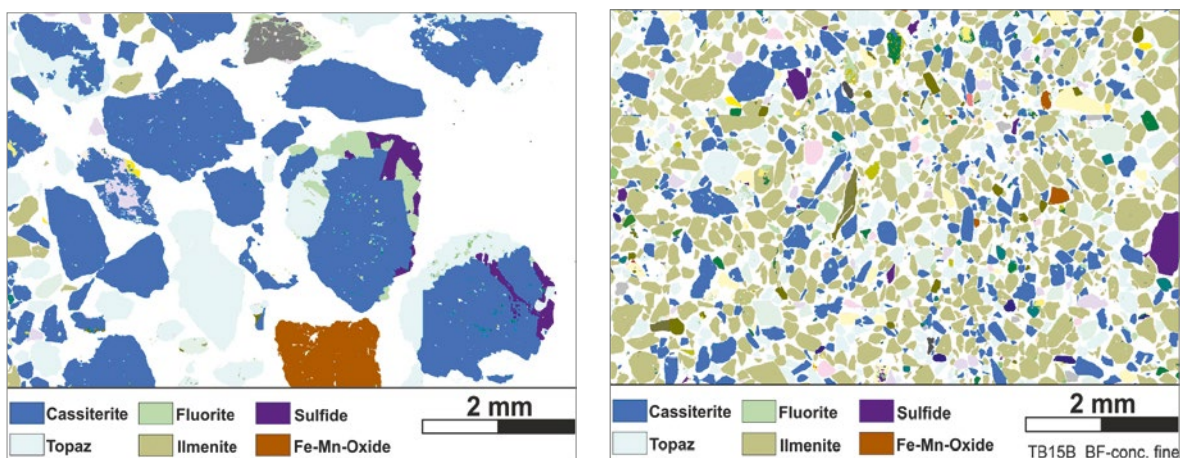


Fig. 5.11: Details from MLA on coarse-grained and fine-grained concentrate from primary ore at Bom Futuro: Coarse-grained ore material with intergrowth features (left, TB15A) and fine-grained ore material (right, TB15B).

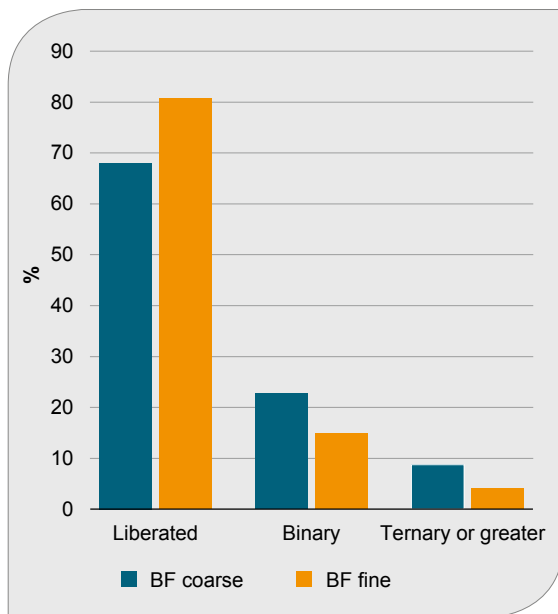


Fig. 5.12: Mineral liberation from MLA for coarse-grained and fine-grained concentrate from primary ore at Bom Futuro.

crucial factor for the efficient processing of the ores, and crushing of the coarse-grained concentrate should be considered. Therefore, special attention to the grain size will be paid when developing enhanced processing methods (see Chapter 6).

Geochemical analysis of the mined horizon of the northwestern placer deposit shows that the cassiterite-hosting conglomeratic layer contains about 800 ppm tin. Geochemical analyses of tailings show that there is at least some loss of cassiterite (0.1 wt. % Sn) into the tailings during processing. Compared to Massangana, the concentrations of Hf in pre-concentrates and tailings from Bom Futuro are rather low, consequently, the zircon from Bom Futuro most likely has low Hf concentrations.

5.3 Santa Bárbara mine (ERSA)

Mineral processing

The Santa Bárbara deposit is historically one of the most prominent cassiterite producers in Rondônia. Samples were collected from tailings stockpiles at the Santa Bárbara Hill (TB01A/B, TB02) and Taboquinha (TB03) locations. The secondary

ore belongs to Depositional Sequence I (for more details see Chapter 3.2), and the mineralized sand layer is represented by samples TB04A and TB04B.

The mineral processing plant of the Santa Bárbara mine is different from the others because of the lack of jigs. The secondary ore goes to a system of sieves and a mill to homogenize the grain size of the ore. After sieving, the ore enters a system of conjugated gravity spirals (TB05A and TB59) that produce a final pre-concentrate rich in cassiterite (TB05C and TB58) and tailings with predominantly quartz and often cassiterite (TB05D). The pre-concentrate is transported to ERSA's facilities in Ariquemes for further mineral processing. ERSA utilizes three magnetic separation steps to obtain cassiterite concentrates. The first step produces ilmenite as a by-product. The second and third steps produce a very pure cassiterite concentrate and columbite concentrates as by-products. Unfortunately, none of these concentrates could be sampled.

ERSA produces metallic tin from its concentrates in the same facilities. The company provided some slag samples for further investigations (TB49 and TB50). According to the information provided by the company, the slags are reprocessed to obtain the residual tin. Figure 5.13 shows the mineral processing flow at Santa Bárbara, as well as the sample locations.

Mineralogical investigations of feed ores and concentrates

Pre-concentrates from the spiral separator are the final product from the processing plant at Santa Bárbara. These pre-concentrates contain cassiterite grades of approximately 13%. Apart from that they are dominated by zircon (~25%), topaz (~25%) and ilmenite (~13%), but also contain significant amounts of columbite-tantalite (~9%, Figure 5.14). Therefore, further processing, e.g. magnetic separation is required. Monazite contents of around 1% are problematic due to high U and Th concentrations. Geochemical analysis of the tailings from the spiral separator (sample TB5B) shows very low concentrations of tin (~100 ppm Sn) and other valuable elements, which indicates that the spirals effectively separate cassiterite and other ore minerals from gangue.

The old tailings from former mining and processing at Santa Bárbara still contain economically significant tin grades (up to 0.5 wt. %), plus Nb (up to 800 ppm), Ta (up to 130 ppm) and also Zr (up to 0.3 wt. %), W (up to 230 ppm), and Hf (130 ppm) concentrations. Moreover, these high grades are found in the coarse-grained fraction, re-processing of these tailing materials is feasible.

5.4 Cachoeirinha mine (METALMIG)

Mineral processing and smelting

The mined ore in Cachoeirinha originated from the paleoalluvium of the sedimentary sequences (PAYOLLA et al. 1983). The sampled ore consists of a sedimentary sequence associated with a braided river system with samples of fluvial facies (TB18A-F) and an alluvial-fan-like sand (TB56).

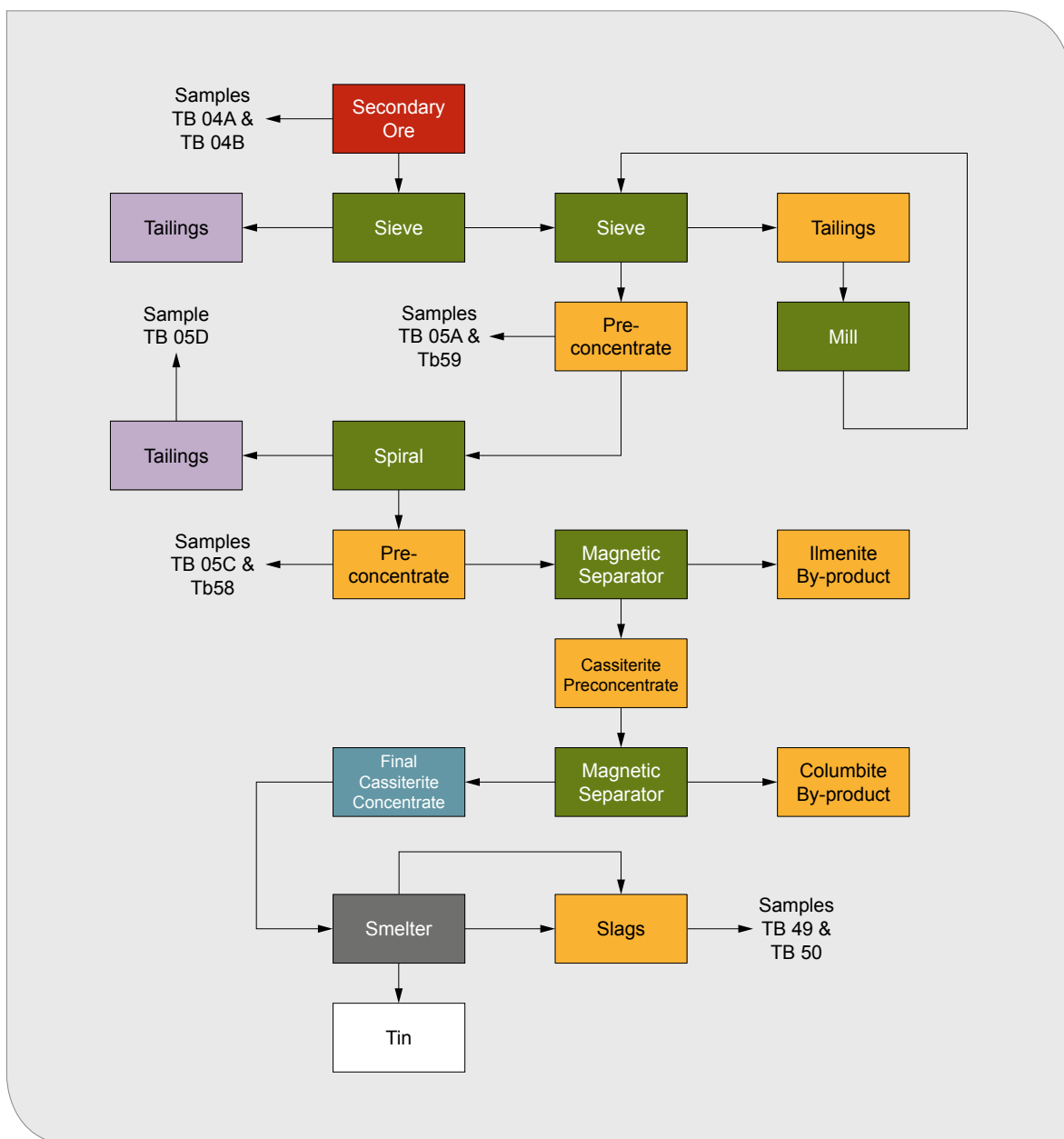


Fig. 5.13: Simplified mineral processing scheme of the Santa Bárbara plant with sampling locations, the cassiterite concentrate is refined to metallic tin (99.85% Sn) in the ERSA-CSN smelter at Ariquemes.

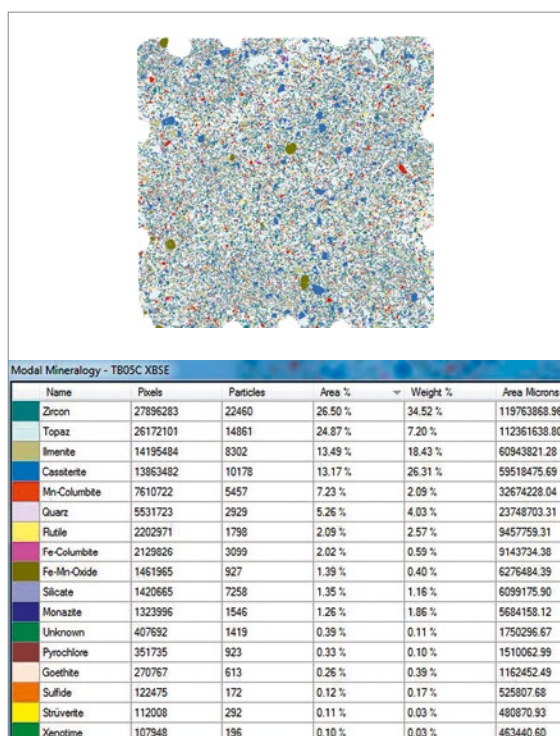


Fig. 5.14: Mineralogical composition from MLA of pre-concentrate from the spiral separator at the Santa Bárbara plant (sample TB05C, taken during the field campaign 2016).

The ore is processed by a conjugated twin-jig system that generates a pre-concentrate. This pre-concentrate (TB55) is processed again in a smaller jig that produces the final pre-concentrate of the Cachoeirinha mine (TB09E).

The pre-concentrate is transported to Ariquemes where further mineral processing stages are done in the METALMIG facilities. METALMIG owns the mineral rights of the Cachoeirinha mine. The pre-concentrate is processed in two different magnetic separators. The first is a roll magnetic separator that removes the ilmenite (TB09F) from the cassiterite pre-concentrate (TB09G). This cassiterite pre-concentrate passes through another magnetic separator that removes the columbite in the form of a saleable by-product (TB09K). The final cassiterite concentrate (TB09H) is delivered to the smelter for the tin metallurgy. The smelter produces not only tin, but also slag. This slag is processed again in the company's facilities to recover some lost tin. The slag processing starts

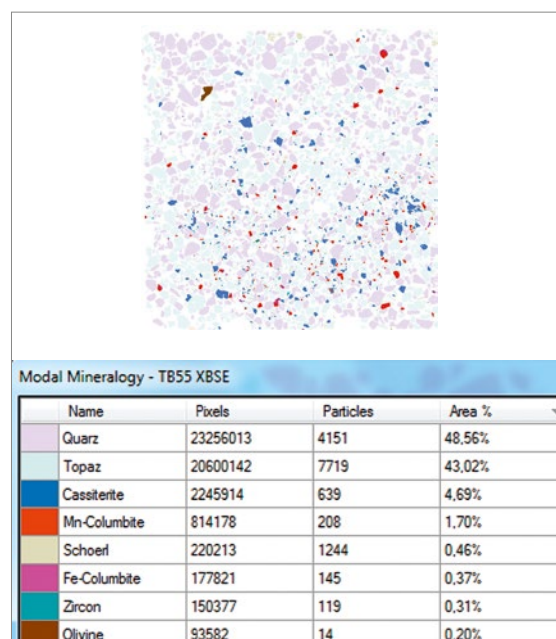


Fig. 5.15: Mineralogical composition from MLA of pre-concentrate (jig, 2nd cama) from Cachoeirinha (TB55, sample taken during the field campaign 2017).

with crushing and subsequent jigging, and finally the fine-grained material is processed on shaking tables. The coarse-grained pre-concentrate from the jig (TB09B), the fine-grained pre-concentrate before the shaking table (TB09A), and the tailings from the shaking table (TB09C) have been sampled. The mineral processing in the Cachoeirinha deposit and the further processing stages in the METALMIG facilities is similar to those at the Santa Bárbara deposit and ERSA (see Fig. 5.13).

Mineralogical investigations of feed ores and concentrates

During the first field campaign in 2016, only the placer material was sampled. The samples were analyzed geochemically. This analysis indicated very high grades of the relevant economic elements of around 1.1 wt. % Sn, 1 wt. % Nb, and 0.14 wt. % Ta within a conglomeratic layer in the sequence, which also shows relatively low Th (≤ 100 ppm) and

U (≤ 20 ppm) values. Such promising high grades of valuable metals accompanied by the low radioactivity of the ores led to the decision to further investigate the deposit during the second field campaign in 2017. Pre-concentrates obtained from the jigs in the 2017 field campaign are dominated by topaz (40%), and reveal high concentrations of cassiterite (up to 5%) and columbite of around 2% from MLA studies (Fig. 5.15). Enhancement of the processing technique is very feasible because currently some cassiterite (about 0.1 wt. % Sn) and columbite (650 ppm Nb) is lost into the tailings.

6 Mineral processing tests

This extensive chapter presents and describes the methods used for ore mineral separation, and discusses their results with regard to their feasibility, their challenges and their economic effectiveness. The processing tests and some of the geochemical analytics were done at G.E.O.S. Ingenieurgesellschaft GmbH by Dr. Frank Haubrich, and the mineralogical investigations by MLA were carried out at BGR.

The presented investigations and processing tests for the enrichment of raw materials refer to:

- Achievable concentrations/recovery – ore treatment tests
- Causes and reduction of radioactivity – concentrates (U-Th contents of minerals)

Basically, the work was focused on the enrichment of niobium, tantalum and tin. In addition, other raw material elements were considered, such as zirconium and REE, which could be obtained as by-products.

For sample characterization, the following analytical investigations and processing tests were carried out:

Analytically:

Particle size:

- Sieve analysis

Mineralogy:

- Polished thin sections on heavy and light fractions
- Optical microscopy + SEM-EDX on single grains
- Mineral Liberation Analysis – MLA
- XRD (HF 200–630 µm)

Geochemistry:

- Quantitative (Actlabs/Canada)
- Semi-quantitative handheld-XRF (BRUKER S1-TITAN 800)

Radiation:

- Local dose rate, alpha, beta + gamma radiation

Following processing tests:

Density separation:

- Shaking table

Magnetic separation:

- Magnetic roll separator, Frantz magnetic separator

Flotation:

- Separation of Th-U bearing minerals

6.1 Origin of the samples

The starting material for the processing tests at G.E.O.S. were the pre-concentrates taken from the 2nd cama of jigs from the four deposits (Tab. 6.1).

Tab. 6.1: Samples and locations from the field campaign Rondônia 2017.

ID-No.	Locality	Facility	Description
TB45	Massangana	Barreiro stream	Pre-concentrate
TB46	Massangana	Taboca stream	Pre-concentrate
TB47	Massangana	Lima stream	Pre-concentrate
TB48	Massangana	B-3 stream	Pre-concentrate
TB53	Bom Futuro	Planta Gilberto	Pre-concentrate
TB55	Cachoeirinha	Planta	Pre-concentrate
TB59	Santa Bárbara	Planta	Ore

The four individual pre-concentrates sampled at Massangana (TB45 to TB48, Fig. 6.1 to 6.4) were blended into a single bulk sample as the amount of the individual pre-concentrates was too low for separate processing tests. The <2 mm fractions of the four samples were blended into one total sample, as all individual pre-concentrate substreams at Massangana are processed in the CEMAL plant.

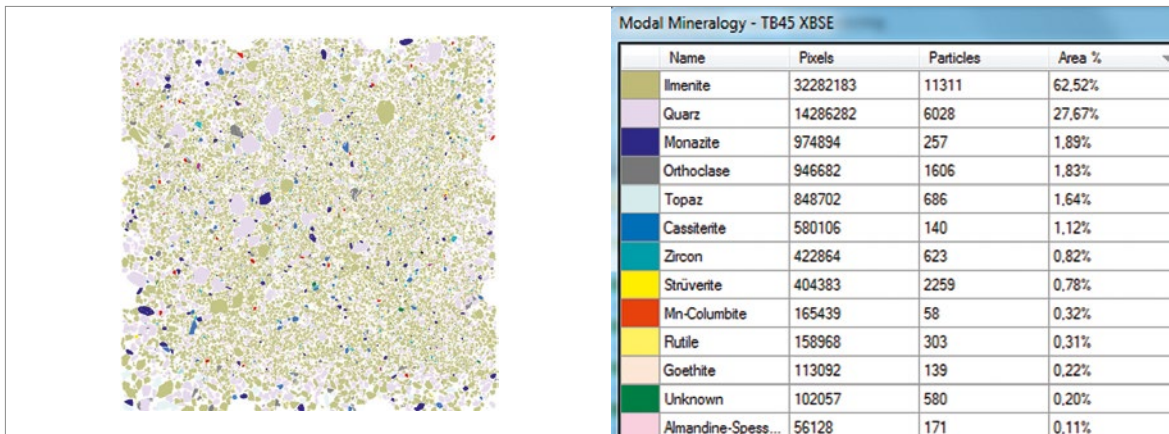


Fig. 6.1: Mineralogical composition from MLA of pre-concentrate (jig, 2nd cama) from Massangana – Barreiro stream (TB45, sample taken during the field campaign 2017).

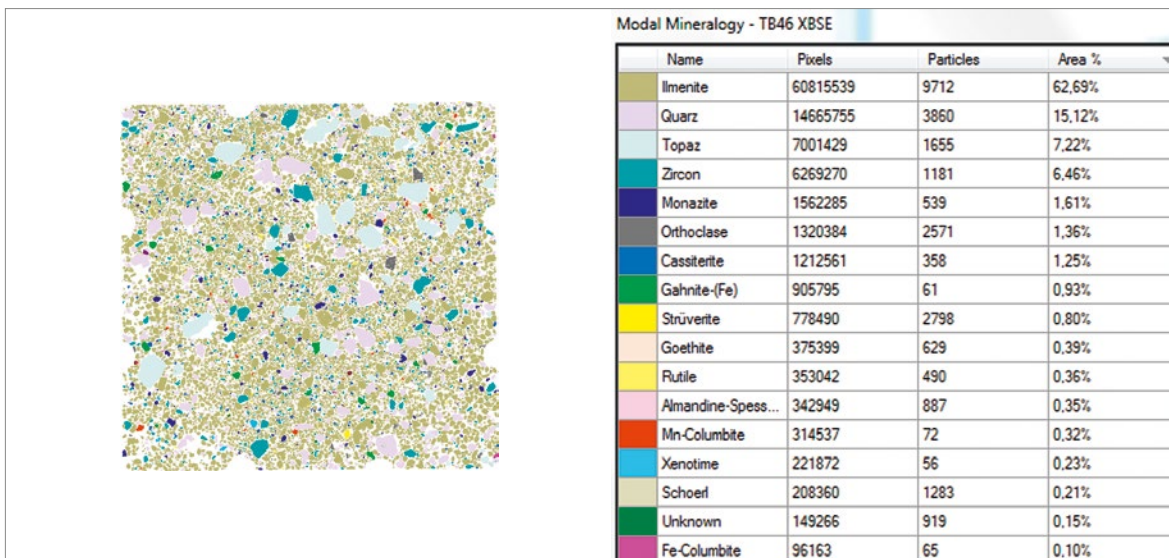


Fig. 6.2: Mineralogical composition from MLA of pre-concentrate (jig, 2nd cama) from Massangana – Taboca stream (TB46, sample taken during the field campaign 2017).

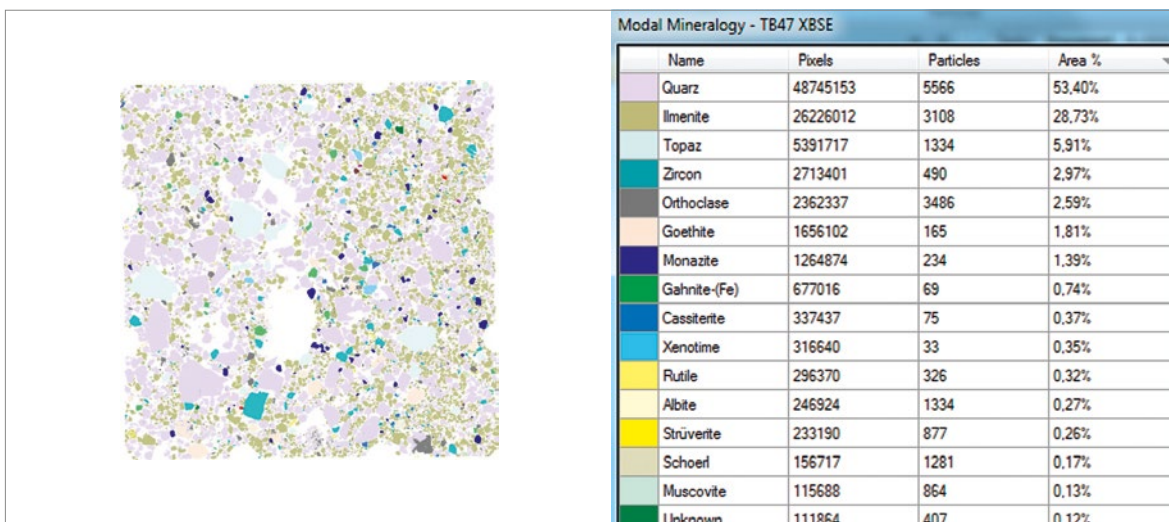


Fig. 6.3: Mineralogical composition from MLA of pre-concentrate (jig, 2nd cama) from Massangana – Lima stream (TB47, sample taken during the field campaign 2017).

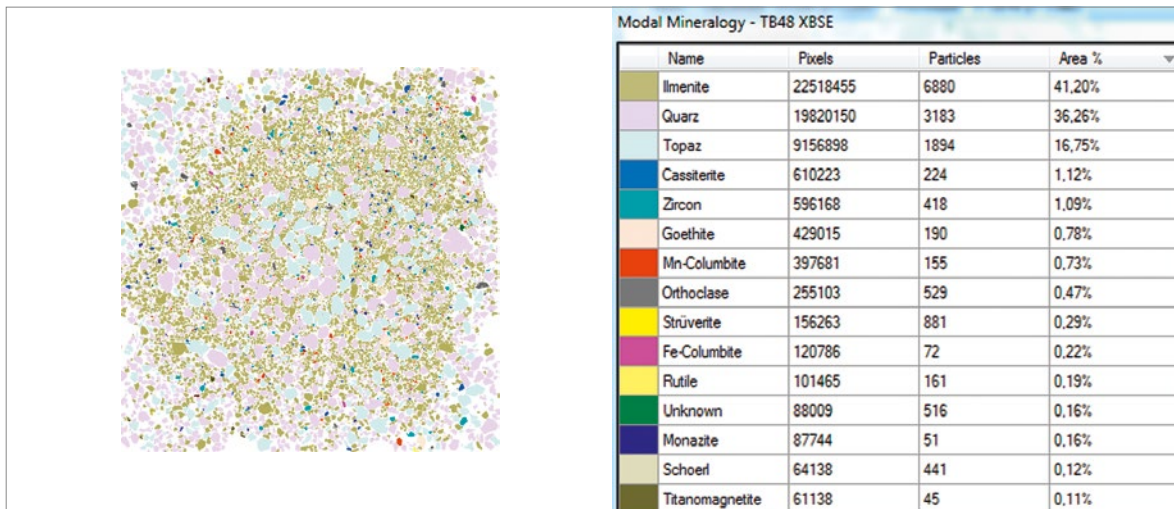


Fig. 6.4: Mineralogical composition from MLA of pre-concentrate (jig, 2nd cama) from Massangana – B-3 stream (TB48, sample taken during the field campaign 2017).

The sample from Cachoeirinha is already referred to above (Fig. 5.14), and the pre-concentrate from Bom Futuro (TB53, Fig. 6.5) was taken from the 2nd cama of jigs at the Gilberto plant. Material from Santa Bárbara (TB59, Fig. 6.6) was taken as a bulk sample without pre-enrichment. The sample was

taken after processing by the ball mill and before the spiral separator. However, the sieve analysis showed that no milling was done. A large proportion of the 2 to 5 mm fraction could be separated (18.5%).

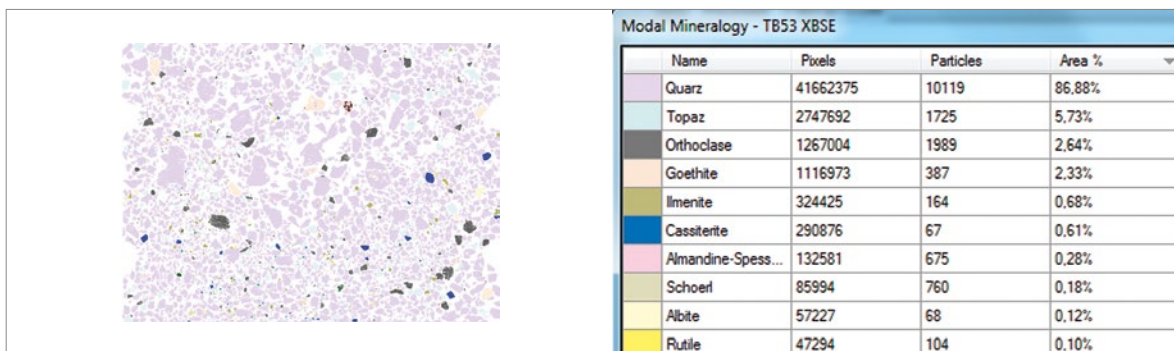


Fig. 6.5: Mineralogical composition from MLA of pre-concentrate (jig, 2nd cama) from Bom Futuro (TB53).

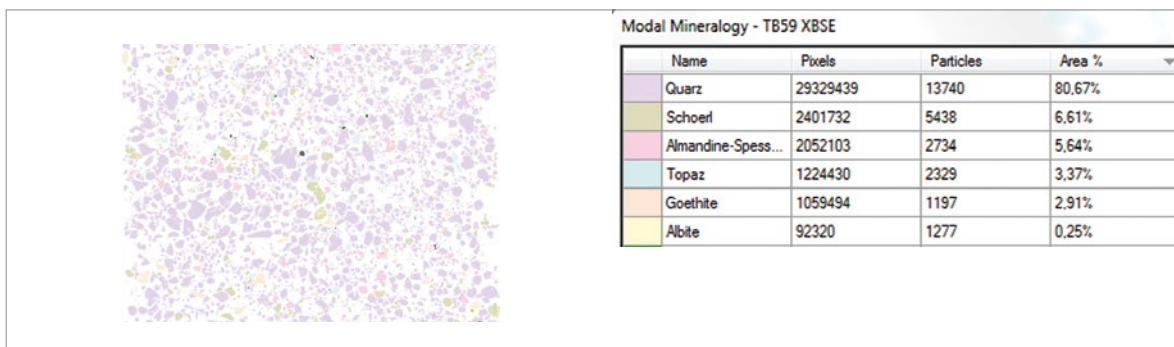


Fig. 6.6: Mineralogical composition from MLA of pre-concentrate (jig, 2nd cama) from Santa Bárbara (TB59).

6.2 Sample preparation

6.2.1 Screening and sample splitting

All samples were separated with a screening machine (400 mm diameter) in $< > 2$ mm (Fig. 6.7). From the 4 subsamples of Massangana TB45 to TB48 (17 kg each), the > 2 mm fractions were separated and separately analyzed. The < 2 mm fractions from Massangana were combined to form a mixed sample. All the following investigations and evaluations refer to the < 2 mm particle size fraction.



Fig. 6.7: $< > 2$ mm separated samples.

Partial samples were separated from each of the < 2 mm fractions by using a riffle splitter (Fig. 6.8):

1. 1 kg subsample
2. 10 kg sample
3. Main sample (approx. 11–45 kg)



Fig. 6.8: Sample splitting with riffle splitter: a) 500 mm splitter for samples up to 100 kg, b) 180 mm splitter for samples up to 2 kg.

1 kg subsample – separation in 100 μ m grain size grades

A 1 kg sample was taken from the total sample by means of a riffle splitter and separated by a sieving machine (FRITSCH) in the following 100 μ m fractions: < 63 , 63–100, 100–200, 200–300, 300–400, 400–500, 500–630, 630–800, 800–2000 μ m.

The narrow separation was chosen with the aim of examining whether the valuable substances Nb/Ta and Sn (Ce, Zr) or elements Th and U, preferably accumulate in certain particle size ranges. Together with the mass fractions, determination is then possible of which fractions contain most of the valuable substances/elements.

10 kg subsample – separation into 3 particle size classes

For initial investigations, a 10 kg sample was separated into the particle fractions: < 63 , 63–200, 200–630 and 630–2000 μ m. Part of the grain size fractions is used for density separation with bromoform.

Main sample – separation into 4 particle size classes

Due to partially unfavorable enrichment parameters by using the shaking table in the 10 kg variant, the four particle size fractions 63–250, 250–500, 500–710 and 710–2000 μ m were selected from the remaining samples (11 kg to 45 kg) with the aim of achieving a better separation of the minerals

based on density differences by using the shaking table.

Samples TB45-48, TB53 and TB55 were sieved dry. TB59 at first had to be deagglomerated wet due to strong agglomeration, and was then sieved wet. TB59 was further separated into <20 and 20–63 μm fractions after deagglomeration.

6.2.2 Density separation by heavy liquids (bromoform)

The density separation using bromoform was performed to obtain an exact separation of heavy and light minerals at a density of 2.89 g/cm^3 (Fig. 6.9).

Approximately 150–250 g of the dry sample was placed in a separation funnel with about 200 ml CHBr_3 and stirred. As a result, all particles with a density of $>2.89\text{ g/cm}^3$ sank, while particles with a density of $<2.89\text{ g/cm}^3$ floated. The fractions were collected on filter paper, washed with ethanol, dried and prepared for analysis.

Both the heavy and light fractions were obtained from particle sizes 63–200, 200–630 and 630–2000 μm . The chemical composition of the resulting 24 sub-fractions was determined by the certified laboratory Actlabs/Canada.

6.3 Pre-processing tests

6.3.1 Density separation by shaking table

The enrichment of heavy minerals through density separation by using shaking tables is a method which was already described in Agricola (1556). Although the systems have been further developed and mechanized since, the physical fundamentals and the basic structure remained the same since then. The efficiency and quality of mineral separation by shaking tables is dependent on the relative density differences of the minerals, and on the relative differences of the given grain size range.



Fig. 6.9: a) Laboratory equipment for heavy liquid separation, b) Funnel with 200 ml CHBr_3 and stirrer.

The separation success is based on the law of simultaneity, which states that a small heavy grain sinks in a liquid with the same speed as a large light grain. Applied to the shaking table, this means that a heavy, small grain will take the same path as a large, light grain. Consequently, no separation of heavy and light fractions can take place if the selected grain size range is too broad.

To assess the separability of mineral mixtures, the following equation can be used:

Separation quotient (S_Q) by shaking table (according to TREPTOW 1925 and FISCHER 1920):

$$S_Q = \frac{x-1}{y-1}$$

x = Heavier mineral
y = Lighter mineral

The larger the separation quotient, the better the separation success. If $S_Q > 2.5$, separation is possible in all grain size ranges (TREPTOW 1925 and FISCHER 1920).

Table 6.2 shows various heavy mineral combinations tested for their separability (from each other) based on specific density differences.

The separation quotient for the combination of cassiterite/topaz indicates that good separation effi-

ciency can be achieved even with larger particle size differences. The combinations of cassiterite/ilmenite, cassiterite/columbite, and cassiterite/zircon enabled separation effects between the minerals, but mixtures still remain. The combinations ilmenite/zirconium, columbite/ilmenite and columbite/monazite barely allowed any separation. In these combinations, separation has to be carried out by other physical processes, e.g. magnetic separation or electrostatic separation.

The separation of heavy minerals from quartz was successful over almost the entire grain size range.

The enrichment of heavy minerals by means of a shaking table works increasingly better, the smaller the differences in the particle size fraction. Therefore, samples TB45-TB48, TB53 and TB55 were separated into four particle size ranges: 63–250, 250–500, 500–710 and 710–2000 μm . Sample TB59 was separated only into two particle size ranges, 200–630 and 630–2000 μm . According to experience, the largest grain size of a grain size band should not be more than 2.5 to 3.5 times bigger than the smallest grain size.

Heavy minerals were enriched on a laboratory shaking table of the Russian "TRUD" type (Fig. 6.10) with a stroke length of 16 mm and a stroke rate of 220 min^{-1} .

Tab. 6.2: Density ranges, average densities of heavy minerals, and separation quotients of mineral combinations.

Mineral	Analyzed oxide/element	Average density	Density range	Mineral combinations	Separation quotient
		[g/cm ³]			
Cassiterite	SnO ₂	6.7	6.3–7.2	Cassiterite/Topaz	2.24
Columbite	Nb ₂ O ₅ /Ta ₂ O ₅	5.5	5.1–8.2	Cassiterite/Ilmenite	1.50
Ilmenite	TiO ₂ /Fe ₂ O ₃	4.8	4.5–5.0	Cassiterite/Columbite	1.27
Zircon	ZrO ₂	4.7	4.6–4.8	Cassiterite/Zircon	1.54
Monazite	Ce/La (Th)	5.0	4.6–5.4	Ilmenite/Zircon	1.03
Topaz	Al ₂ O ₃ /SiO ₂	3.6	3.5–3.6	Columbite/Ilmenite	1.18
Quartz	SiO ₂	2.7	2.65	Columbite/Monazite	1.13

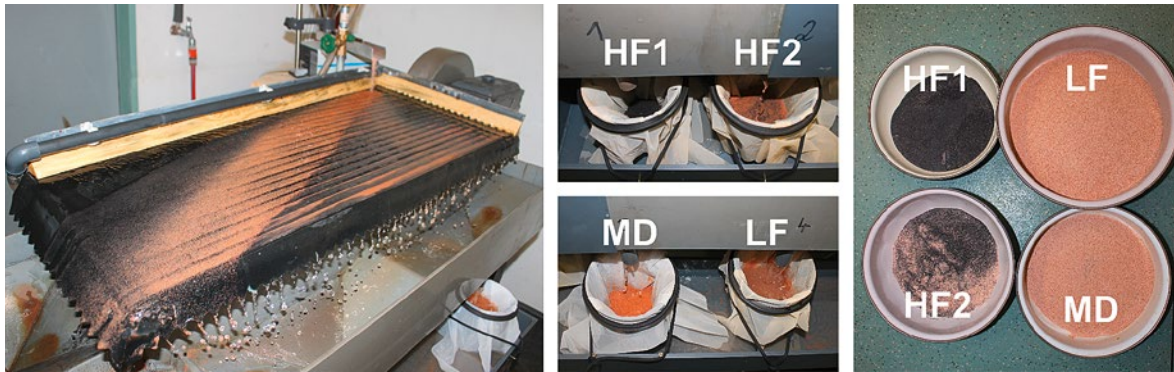


Fig. 6.10: Sample TB55, fraction 250–500 μm (separation determined optically, semi quantitative).

Four fractions were separated per sample and particle size range:

- **HF1** – Heavy fraction 1 – heavy mineral concentrate
- **HF2** – Heavy fraction 2 – heavy mineral concentrate + light fraction
- **MD** – Middlings – “Traces” of heavy mineral concentrate
- **LF** – Light fraction – light fraction – without heavy minerals

The verification of the success of density separation was carried out optically based on the different mineral colorations (Fig. 6.10).

6.3.2 Magnetic separation

The magnetic separation of the minerals is based on different magnetic properties. The physical parameter for the separation properties is the magnetic susceptibility χ in $10^{-6} \text{ cm}^3/\text{g}$, which is a physical quantity indicating the magnetizability of matter in an external magnetic field. In general, ferromagnetic, paramagnetic and diamagnetic minerals are distinguished.

Ferromagnetic minerals can be magnetic themselves, but are more magnetized by an external magnetic field and drawn towards the stronger magnetic field. They are able to retain the magnetization after removal of the magnetic field. Typical ferromagnetic minerals are: magnetite, pyrrhotite, (ilmenite, maghemite).

Paramagnetic minerals are not magnetic themselves, but they can be magnetized by an external magnetic field by being drawn into the magnetic field. Typical paramagnetic minerals are: ilmenite, ilmenorutile, leucoxene, monazite (Nd), columbite (Fe), garnet, biotite, tourmaline, tungstenite.

Diamagnetic minerals cannot be magnetized by a magnetic field. They are forced out of the magnetic field. Typical diamagnetic minerals are cassiterite, pyrite, rutile, zircon, topaz, and apatite.

The following table 6.3 gives an overview of the magnetic susceptibilities of different minerals and their relationship with the determined field strengths (in Tesla).

The following magnetic separators were used for mineral separation (Fig. 6.11):

1. NdBF_e permanent handheld magnets with field strengths 0.37 T and 0.47 T (small throughput)
2. Magnetic belt (roll) separator (permanent magnet NdBF_e magnetic roller with 1.1 Tesla) (high throughput, but fixed field strength)
3. Ring band magnetic separator (electromagnet – variation of the magnetic field strength by changing the current intensity) (average throughput)
4. Frantz magnetic separator (electromagnet – variation of the magnetic field strength by changing the current intensity, inclination and angle of the magnetic groove) (low throughput of approx. 100 g/h, very precise graduation of the magnetic parameters possible).

Tab. 6.3: Magnetic susceptibilities of different minerals and the relation to the field strengths (in Tesla).

Magnetic type	Mineral	Magnetic susceptibility (χ)		Separated at (Tesla)
		Range χ (10^{-6} cm ³ /g)		
Ferromagnetic	Magnetite	20000	80000	< 0.1 T
Paramagnetic	Ilmenite	200	1500	< 0.37 T
	Columbite	no data	no data	0.37–1.1 T
	Monazite	120	250	0.37–1.1 T
	Rutile (black-brown)	2		< 1.1 T
Diamagnetic	Zircon, Rutile (red)	-0.17	0.73	> 1.1 T
	Cassiterite	-2.3	-0.08	> 1.1 T
	Topaz	-0.42		> 1.1 T

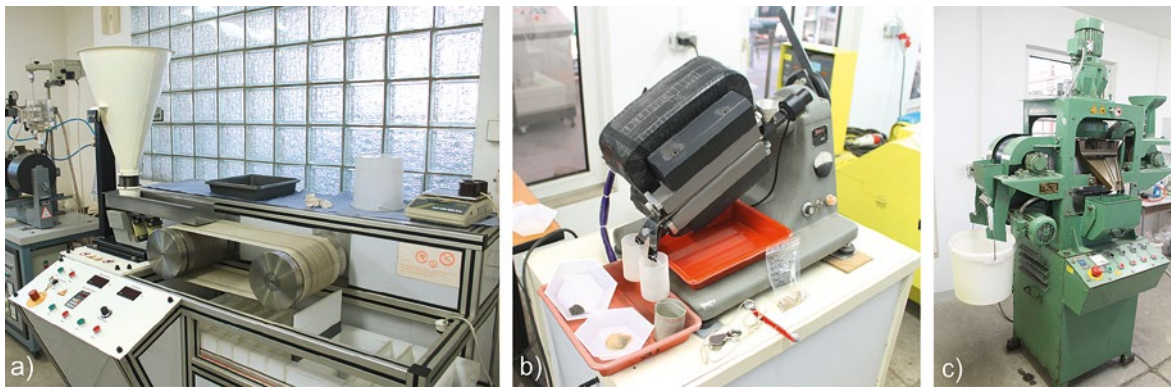


Fig. 6.11: a) Magnetic belt separators (1.1 Tesla), b) Frantz magnetic separators, c) Ring-band magnetic separators (TU Bergakademie Freiberg, Institute for Processing Machines).

In the course of the treatment experiments, the proportion of the ferromagnetic fraction was found to be very low (<0.02%). In contrast, some very high levels of strongly paramagnetic minerals such as ilmenite were obtained. The recovery of a ferromagnetic fraction was therefore left out. Instead, the HF1 and HF2 (partial MD) fractions were split into a paramagnetic (<1.1 Tesla-Para) and a diamagnetic (>1.1 Tesla-Dia) fraction by using the magnetic band separator at 1.1 Tesla.

The paramagnetic fraction of Massangana sample TB45-48 contained up to 95% ilmenite, which entirely prevented a strong enrichment of e.g. columbite. Here a very fine magnetic separation

was carried out by means of a Frantz magnetic separator.

Figure 6.12 gives an overview of the parameters needed to separate minerals using Frantz magnetic separators:

The main parameters include the longitudinal/lateral inclination, and the current strength, which represents the variable magnetic field. It can only be partially converted into the field strength (Tesla, Gauss). These parameters are therefore also used for comparability in the international literature on Frantz magnetic separators.

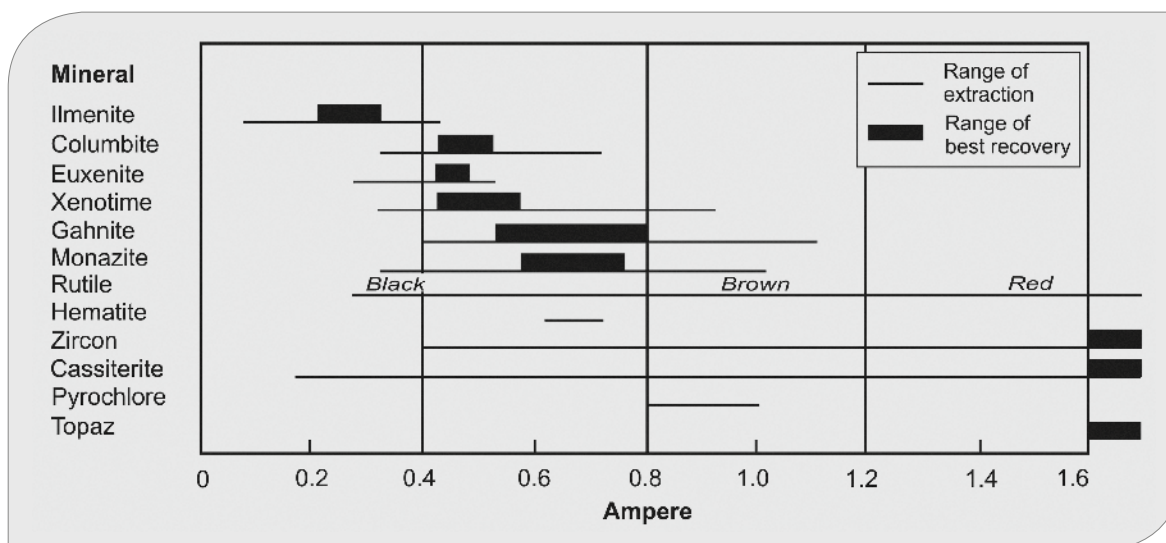


Fig. 6.12: Magnetic susceptibilities of selected minerals in a Frantz Isodynamic Separator with a side tilt of 15–25° and a forward tilt of 15–25° (from STENDAL & THEOBALD 1994).

6.3.3 Flotation tests

Flotation tests were performed with one sample (TB45-48, 250–500 µm, MD) to investigate whether monazite is removable. The monazite contains the majority of thorium and uranium, which greatly increases the radioactivity of the concentrates. Hence, the monazite should be removed as completely as possible. These tests are described in Chapter 6.8.5.

6.4 Mineralogical methods

6.4.1 XRD analysis

Heavy mineral fractions of 200–630 µm screenings were analyzed by qualitative and quantitative X-ray diffraction. XRD was performed at the X-ray laboratory of the Institute of Mineralogy of the TU Bergakademie Freiberg, Germany, with a modified URD-65 diffractometer using Co-K_α irradiation. The XRD preparations were laterally sifted into the cuvette. The program ANALYZE (GEIT) was used for identification of mineralogical phases and evaluation of their quantitative proportions.

6.4.2 Polished grain thin sections

Each of the 24 subsamples resulting from bromoform heavy liquid separation were submitted for

the preparation of thin sections. The polished grain thin sections were prepared by Dettmar Dissection Technology GmbH & Co. KG Bochum, Germany.

6.4.3 Polarization microscopy

The polished grain thin sections were studied using a research-grade JENAVERT (Carl Zeiss, Jena) reflected polarizing light microscope at magnifications between 50 and 500 times (Appendix 10). Photographic images were made via the ocular tube using a CASIO EX-S12. Image sizes are calibrated by precision scales at different magnifications. Supplementary transmitted polarizing light microscopy was conducted using an AMPLIVAL microscope (Carl Zeiss, Jena).

6.4.4 Scanning electron microscopy and EDX analysis

Scanning electron microscopy and EDX analysis was applied for clarification of ambiguous polarized light findings, to study mineral intergrowth patterns, and for qualitative to semi-quantitative determination of the major and trace element composition of important minerals. The work was conducted at the TU Bergakademie Freiberg using a JEOL JCM-5700 SEM equipped with a Bruker-EDX system at the Institute of Geology, and with a FEI XL 30 ESEM-FEK SEM equipped with a nitrogen-cooled

Ametec-EDX detector at the Institute of Ceramic, Glass and Construction Materials.

6.4.5 Mineral liberation analysis – MLA

Mineral liberation analysis was used for the automated detection of mineralogy (SEM-MLA). For this a MLA 650F Quanta FEG ESEM (from FEI) was used at BGR, Hannover. It used a 25 kV excitation voltage under high vacuum. The element spectrum was detected by means of two silicon drift detectors (XFlash Detector 5030) from Bruker Nano. The evaluation of the EDX spectra was carried out quantitatively fully automatically by means of special MLA software (mineral liberation analysis).

6.5 Geochemical methods

The samples were analyzed both by the certified raw materials laboratory Actlabs/Canada and by in-house handheld XRF. The 24 light and heavy mineral fractions separated by bromoform treatment were analyzed at Actlabs/Canada. The certified results were partially used as standard measurements to calibrate the handheld XRF. For the complete element spectrum, see Appendices 3 and 4.

6.5.1 Actlabs/Canada

Actlabs/Canada offers special packages for raw material analysis which cover a variety of elements. For analysis of the samples, the following packages were selected:

“Code 8 – REE Assay” and “Code 8 – XRF Nb, Zr, Ta for higher PO₄ content”. The analyzed elements are listed in table 6.4.

Note: Code 8 – REE Assay – Rare Earth Element-Niobium-Zirconium-Yttrium-Tantalum-Uranium-Thorium-Beryllium-Phosphate-Tin Assay ICP-OES and ICP-MS Package. The analysis requires a lithium metaborate/tetraborate fusion with subsequent analysis by ICP-OES and ICP-MS.

6.5.2 Analysis by handheld XRF

Approximately 400 measurements were performed using a handheld XRF S1 TITAN Model 800 from BRUKER (Fig. 6.13). About 10 g of sample was ground to <100 μm in an analytical mill (RETSCH MM2), homogenized and transferred to sample cups (BRUKER). The sample cups were covered with a prolene membrane (4 μm thickness). The analysis was carried out in the “Geochemical calibration” mode by using a special “G.E.O.S. Calibration mode”. The total measuring time was

Tab. 6.4: Analyzed oxides/elements and detection limits of Code 8 – REE assay + Code 8 – XRF Nb, Zr, Ta.

Oxide	[%]	Element		Element		Element		Element	
			[ppm]		[ppm]		[ppm]		[ppm]
Al ₂ O ₃	0.01	Ag	0.5	Hf	0.2	Th	0.1	Nd	0.1
CaO	0.01	As	5	In	0.2	Tl	0.1	Sm	0.1
Fe ₂ O ₃	0.01	Ba	3	Mo	2	U	0.1	Eu	0.05
K ₂ O	0.01	Be	1	Nb	1	V	5	Gd	0.1
MgO	0.01	Bi	0.4	Pb	5	W	1	Tb	0.1
MnO	0.001	Co	1	Rb	2	Y	2	Dy	0.1
Na ₂ O	0.01	Cr	20	Sb	0.5	Zn	30	Ho	0.1
P ₂ O ₅	0.01	Cs	0.5	Sc	1	Zr	4	Er	0.1
SiO ₂	0.01	Cu	10	Sn	1	La	0.1	Tm	0.05
TiO ₂	0.001	Ga	1	Sr	2	Ce	0.1	Yb	0.1
LOI	0.001	Ge	1	Ta	0.1	Pr	0.05	Lu	0.04

2 minutes, of which 60 seconds were used for heavy element analysis and 60 seconds for light element analysis. All measurements were subjected to a plausibility check, whereby the analyzed elements were controlled in the “Spectrum mode”. The handheld XRF S1 TITAN Model 800 uses a spot size of 8 mm, a FAST SDD® detector with a <math><145\text{ eV}</math> resolution, and an Rh target X-ray tube (4 W, 6–50 kV, 4.5–195 $\mu\text{A}</math>).$

The experience gained with standards showed that, depending on the element, the analysis results using handheld XRF can generally deviate significantly from certified analysis. Nevertheless the data can be used to produce guide values. It was empirically shown that the concentrations for Ce and P were 50% too low in some cases. Larger deviations were expected especially at higher concentrations, since the device was not calibrated for these ranges. The contents of Nb, Ta and Ti are sufficiently accurate ($\pm 10\%$). Nevertheless, the handheld XRF analysis is an excellent and fast method to monitor the accumulation and/or depletion of minerals and/or elements between process steps without the need for costly analysis.

It is very important to note that the handheld XRF analysis can never replace certified analysis, although the relative differences between the processing steps was well represented.

For financial reasons, it was decided not to perform each analysis precisely (certified). Therefore, the presented analyses are to be regarded as indicative.

6.6 Radiation analytics

6.6.1 Radiation measurement equipment

It is known that uranium and thorium bearing heavy minerals were present in the samples. Therefore, radiation measurements were carried out. Naturally it was assumed that increasing radiation exposure has to be expected with increasing enrichment of the elements/heavy minerals.

The dose rate (reported in nSv/h) and the alpha and beta + gamma radiation (given in pulses/sec-



Fig. 6.13: Measuring station handheld XRF spectrometer S1 TITAN Model 800 – BRUKER.

ond) were measured to determine the local radiation exposure.

The local dose rate reflects the total radiation from the sample, including the environment. The alpha, beta and gamma rays respectively reflect the helium nuclei, electrons and photons emitted by the radioactive minerals, which are mainly derived from the decay of thorium and uranium and their decay products.

The local dose rate was measured with the dose rate meter 6150AD 6/E with calibratable scintillator probe 6150AD-b/E (Fig. 6.14-a), display/measuring range: 1 nSv/h – 99.99 μ Sv/h, energy range: 20 keV – 7 MeV (automess – Automation und Messtechnik GmbH).

The alpha and beta + gamma radiation was simultaneously measured by the instrument LB 124 Scint-300 Contamination Monitor for α and β - γ measurement (Fig. 6.14-b, Berthold Technologies GmbH & Co. KG).

The measurements were carried out in cooperation with the company WISUTEC, which has the experience and certification for the proper handling of radioactive materials.

6.6.2 Radiation measurement

To determine the radiation, a Petri dish with a volume of 38 cm³ was filled with the sample to the edge, and the mass was determined (Fig. 6.15).

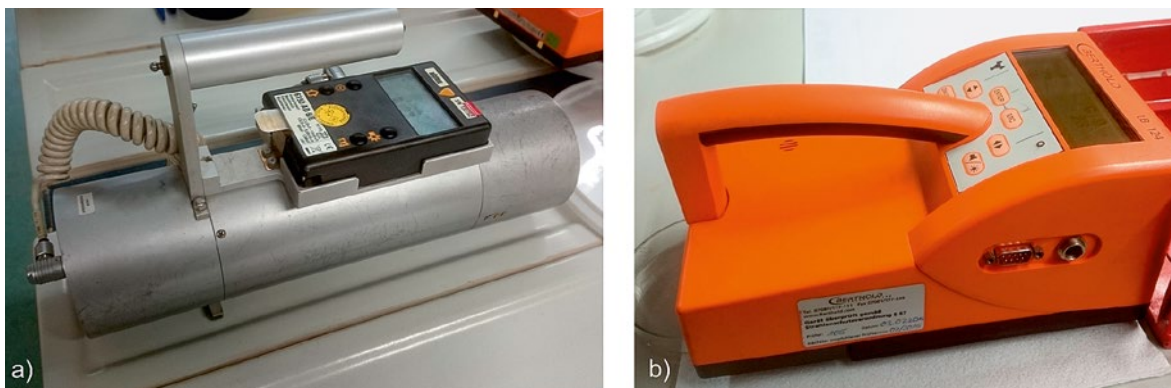


Fig. 6.14: Radiation detector used a) Local dose rate meter 6150AD 6/E with calibratable scintillator probe 6150AD-b/E, b) LB 124 Scint contamination monitor for α and β - γ measurement.

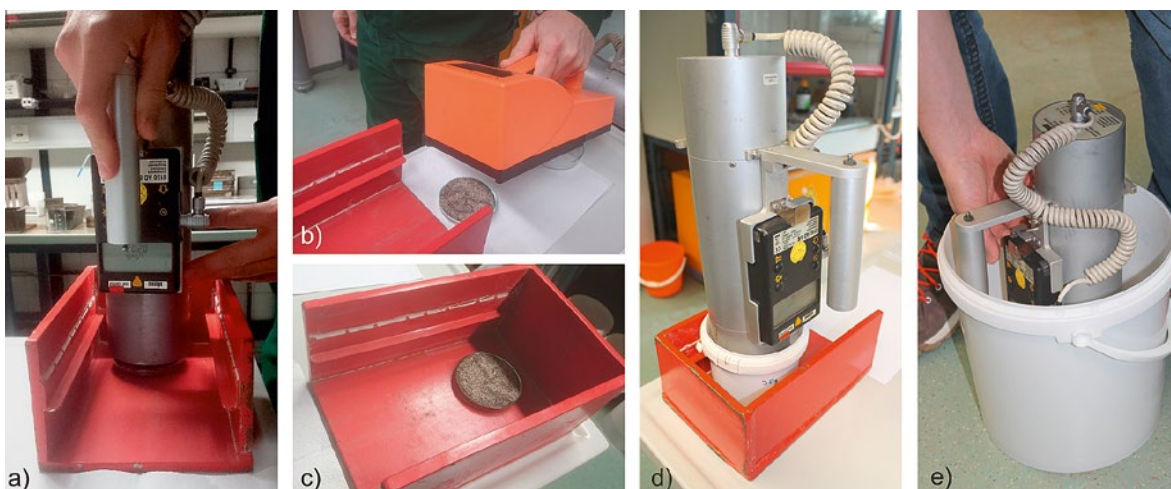


Fig. 6.15: a) to c) Volume-related radiation measurement of the sample in a Petri dish (38 cm³) under shielding the ambient dose rate (red steel box), d) and e) Mass-related radiation measurement at larger masses/volumes of sample TB45-48, 250–500 μ m, HF1, paramagnetic fraction.

The local dose rate was measured under shielding (red steel box).

Background values for the local dose rate are:

- local dose rate background under shielding = 107–115 nSv/h
- local dose rate background without shielding = 140–144 nSv/h (depending on location)

The alpha and beta + gamma radiation was measured without shielding on the same sample.

From almost all sample fractions, about 100 to 150 g of each was taken as a retained (reference) sample for possible further analysis and for determination of the radiation exposure.

The increase in local dose rate with increasing mass was tested by placing variable sample amounts into a plastic bucket followed by mounting the meter (Fig. 6.15-d,e) and then doing the measurement. As a result, the increase in local dose rate up to a mass of 7.3 kg sample material could be determined. The mass-dependent radiation for larger sample quantities was simulated using this setup.

6.7 Ore analytics (geochemistry, mineralogy)

6.7.1 Mineralogy – EDX, XRD, MLA

The feasibility of processing methods yielding saleable ore concentrates primarily depends on the mineralogical-geochemical composition of the ores. The samples were studied accordingly by complex mineralogical methods.

The parent material of mineralogical studies is heavy and light mineral fractions resulting from bromoform heavy liquid separation of screenings outlined in Chapter 4. Polished thin sections were prepared from each of the resulting 24 mineral fractions and studied by polarizing light microscopy and mineral liberation analysis (MLA). Numerous selected mineral grains were studied by SEM-EDX. Polarizing light microscopy and SEM-EDX aimed at assessing the representative mineral composition and mineral intergrowth relationships relevant for ore processing. The mineralogical

work was focused on ore minerals and properties of critical importance in processing (e.g. grain size distribution or intergrowth) and the identification and characterization of any radioactive minerals present.

Mineralogical-geochemical identified mineral phases

The subsamples resulting from screening and heavy liquid separation of the four parent samples display similar basic mineral compositions, but also distinct peculiarities. The light mineral fractions are predominantly composed of quartz and minor feldspar as expected. The heavy mineral fractions are dominated by ore minerals, topaz, and partly by goethite-kaolinite intergrowths.

In a first step, the dominant minerals were identified by polarizing light microscopy. The optical identification was verified on selected specimens by SEM-EDX, that also yielded identification of optically ambiguous minerals. Rare and optically inconspicuous minerals were identified under the SEM by BSE imaging and characterized by EDX (Appendix 10). Table 6 lists all mineral phases identified (some occur in single thin sections only).

EDX revealed the presence of rather pure mineral phases, but also varieties of the same minerals show partly significant chemical inhomogeneities and enrichments in trace elements. This applies especially to rutile, cassiterite, and zircon. The presence of foreign constituents appears to be independent of mineral exsolutions and inclusions of foreign minerals in the micrometer range and larger. Cassiterite and rutile partly display significant enrichment in Fe, Nb, Ta, and W, and minor enrichment in Ca, Al, and Si. Zircon partly reveals significant diadochy of Zr by Hf, and enrichments in Al, Ca, Sc, Fe, and Th, and minor Y, Yb, and Mn. The tantalum content of columbite grains varies significantly with columbite mainly poor in Ta, Mn, and Ti. Some columbite shows traces of Sc and/or W, and Sn.

Ilmenite represents one of the most abundant ore minerals in samples TB45 and TB53. It usually contains some Mn and rarely several 1000 ppm of Nb, Ta, or W and Sn. There are various intergrowths and transformations of ilmenite including rutile aggregates, oriented exsolutions of hema-

tite, and solid solutions of the systems $\text{TiO}_2\text{-Fe}_2\text{O}_3$ (pseudorutile) und $\text{TiO}_2\text{-FeNb}_2\text{O}_6$ (ilmenorutile).

X-ray diffraction analysis – XRD

Qualitative XRD diffractograms of the four heavy mineral fractions of screenings 200–630 μm were compared with diffractograms of the ASTM database. The results are summarized in table 6.5, and XRD diagrams are shown in Appendix 12. The best matches between XRD patterns and the ASTM database partly show some chemical peculiarities.

Table 6.5 shows the results of quantitative evaluation of the XRD diffractograms by the Rietveld method based on structural models. The Rietveld analysis shows that the minerals listed are present in mass percentages of down to 0.1 %. Other phases identified are irrelevant for mass balancing.

Note that XRD analysis only applies to crystalline components. X-ray amorphous and metamict components are ignored. Rietveld quantification is highly dependent on the assumed grain size of XRD preparations. When differing grain size distri-

butions are present in the milled XRD preparations, errors of more than 10 % are possible. The values in table 6.7 are rounded to the nearest whole percent accordingly.

Radioactive minerals

The SEM-EDX work identified carrier minerals of U and Th as sources of radioactivity in the studied samples. Important radioactive minerals are monazite and zircon. Accessory or trace carriers of U and Th are represented by xenotime, fluocerite, calkinsite, euxenite, and pyrochlore phases.

The majority of radioactive mineral grains exhibit Th/U ratios >1 according to EDX measurements, and minerals with ratios <1 are rare. Monazite grains usually contain ≤ 1 at. % (atomic percent) Th that rarely reach up to 2.5 at. % Th, and mostly ≤ 0.3 at. % U attaining up to 2.9 at. % U in rare cases. Zircon grains commonly contain ≤ 0.6 at. % Th and ≤ 0.2 at. % U, with rarely up to 1.8 at. % Th and 3.1 at. % U. The corresponding mass percentage of these elements in monazite and zircon is many times higher than the atomic percentage.

Tab. 6.5: Quantification of XRD diffractograms Rietveld analysis in mass percent.

Mineral	TB 45-48	TB 53	TB 55	TB 59
	Mass percent	Mass percent	Mass percent	Mass percent
Ilmenite	62	7		1
Columbite-Fe	1	1	5	1
Cassiterite	3	8	8	0
Rutile		3		
Anatase		2		1
Pseudorutile	20	12		1
Hematite	3	3		8
Monazite-Ce	3			
Zircon	2	3		1
Topaz	3	50	82	36
Quartz	3	2	1	5
Goethite		2		18
Kaolinite-1A		4	4	28
Biotite-1M		3		

It is important to note that none of the grains of columbite, cassiterite or ilmenite studied by EDX revealed U or Th. This appears to be favorable for separation of radioactive minerals from ore minerals.

Mineralogical characterization of heavy and light mineral fractions

The mineralogical characterization of heavy and light mineral fractions produced from screenings is based on reflected and transmitted polarizing light microscopy of the polished thin sections prepared from each of the density fractions. SEM-EDX work served as verification of optical mineral identification, and identification of rare and optically inconspicuous minerals. The degree of primary mineral intergrowth is generally low even in the coarse fractions. However, epigenetic agglomerates and concretions may result in the carry-over of barren minerals in concentrates during processing.

An important aspect for processing is the significant incorporation of Fe in cassiterite and zircon that may result in paramagnetic behavior of these minerals. The same applies to oxidic iron phases in altered ilmenite that might be otherwise diamagnetic. Table 6.6 shows a summary of the observed minerals and mineral associations and their relative abundances. It is noted that the abundances represent visual estimates that are semi-quantitative at best.

Massangana – TB45-48

Light mineral fractions (Thin sections # 01 to # 03)

The light mineral fractions are predominantly composed of quartz, minor mica and feldspar with the latter mostly represented by strongly corroded microcline. Carry-overs of isolated zircon and ilmenite grains are sporadic. Zircon and ilmenite and other minerals such as monazite, magnetite, and sulfides are locally intergrown with quartz, feldspar, and mica.

Fine-grained scaly aggregates of kaolinite are abundant and partly impregnated by goethite. The kaolinite-goethite aggregates partly form encrustations on other minerals and often contain fragments of various primary minerals.

Heavy mineral fractions (Thin sections # 04 to # 06)

The dominant heavy mineral is ilmenite, with increasing relative abundance in finer screenings. The ilmenite appears partly fresh and partly altered along irregular streaks or oriented zones to transitional Ti-Fe phases of the pseudorutile series, and hematite sometimes to Ti oxides anatase and rutile. Next abundant but distinctly subordinate are quartz and topaz. The relative abundance of topaz increases in coarser screenings.

Minor components are monazite, cassiterite, zircon, and columbite, all with variable chemical compositions. Columbite is usually poor in Ta, Mn, and Ti but sporadically enriched in Ta and W. Zircon is both poor in trace elements and enriched in Ca, Al, Hf, and Th, partly also F. Iron bearing zircon is absent.

Cassiterite is rarely enriched in iron. It occurs both pure and enriched in Nb, sometimes with minor Ta and W. Exsolutions of Ta-Ti bearing columbite are abundant among cassiterite grains.

Monazite is represented by Ce-La-Nd varieties with significant Th and minor U. Partially altered euxenite with a predominance of U over Th is present but rare. Spinel of the gahnite-hercynite series is a characteristic trace mineral. Trace sulfides form inclusions in zircon and ilmenite, in particular pyrite. Single grains are sometimes encrusted by kaolinite-goethite (see Appendix 4). The distribution and characteristics of minerals in the thin sections is given in Appendix 10.

Bom Futuro – TB53

Light mineral fractions (Thin sections # 07 to # 09)

The light mineral fractions are predominantly composed of quartz. The proportion of kaolinite and kaolinite-goethite-hematite agglomerates decreases in finer screenings. The agglomerates partly cement quartz grains in the coarse screenings. Collomorphic crusts of manganese oxides occur on some grains. K-feldspar and phengitic mica are minor.

The fine and middle screenings contain zircon and rare monazite. Columbite is absent and cassiterite very rare. Sporadic ilmenite is usually accompanied by pseudorutile and Ti oxides. Quartz grains

Tab. 6.6: Mineral phases and their visual estimates of relative abundance.

Sample Mineral phase	TB 45 L			TB 45 S			TB 53 L			TB 53 S			TB 55 L			TB 55 S			TB 59 L			TB 59 S			
	01	02	03	04	05	06	07	08	09	10	11	12	13	14	15	16	17	18	19	20	21	22	23	24	
Barren minerals																									
Quartz	X	X	X	x	x	x	X	X	X	x	x	x	X	X	X	x	x	x	X	X	X	x	x	x	
K-feldspar	x	x	x						x	x					x										
Albite/Plagioclase		x																							
Topaz				x	x	x		x		X	X	X		x		X	X	X				X	X	X	
Muscovite							x	x	x				x		x										
Biotite-Phengite	x	x	x				x	x	x	x	x	x		x	x						x				
Kaolinite	x	x	x				X	x	x	x	x	x	X	X	X	x	x	x	X	X	X	X	X	X	
Goethite	x	x	x				x	x	x	x	x	x				x	x	x	x	x	x	X	X	X	
Al-Si-Fe-O-Aggreg.	x	x	x				X	x	x	x	x	X	X	X	x				X	X	X	X	X	X	
Hematite				x	x	x	x	x	x	x	x		x	x	x	x	x	x	x	x	x	X	X	X	
Manganomelane							x	x	x																
Ore minerals																									
Ilmenite	x	x	x	X	X	X		x	x	X	X	X		x								x	x	x	
Pseudorutile	x	x	x	X	X	X	x	x	x	X	X	X		x		x	x	x		x			x	x	
Rutile/Anatase pure	x	x	x	x	x	x	x	x	x	x	x	x				x				x					
Rutile-Nb-W-Ta				x	x	x	x	x	x	x	x	x	x	x	x	x	x	x	x	x	x	x	x	x	
Cassiterite pure				x	x	x				x	x	x			x	x	x	x						x	
Cass.-Nb-Ta-W				x	x	x			x	x	X	X	x	x		x	x	x	x		x	x	x	x	
Columbite				x	x	x				x	x	x				x	x	x					x	x	
Columbite-Ta-W-Sc				x	x	x							x			x	x	x	x				x	x	x
Zircon pure	x	x	x	x	x	x	x	x	x	x	x	x		x		x	x			x	x	x	x	x	
Zircon-Th-Sc-Fe				x	x	x				x	x	x	x	x		x	x		x	x	x	x	x	x	
Monazite	x	x	x	x	x	x		x		x	x	x		x						x					
Accessories																									
Xenotime								x	x													x	x		
Euxenite						x																			
Bastnaesite/Calkinsite	x																							x	
OH-/Pb-Pyrochlore						x																			
Ixiolite														x											
Goyazite								x			x														
Florencite																						x			
Fluocerite/Yttrifluorite																		x		x					
Spinel					x	x																			
Baryte									x																
Titanite									x																
Pyrite	x	x		x	x																		x		
Pyrrhotite									x														x		
Sphalerite											x														
Chalcopyrite				x																			x		
Galena																							x		
Fe-Co Gersdorffite									x																

X = Major component 100-5%, x = Minor component 5-1%, x = Accessory <1%

sometimes contain inclusions of zircon, xenotime or sulfides.

Heavy mineral fractions (Thin sections # 10 to # 12)

The heavy mineral fractions are predominantly composed of topaz. Roundish fine-grained scaly aggregates of kaolinite and kaolinite-goethite-hematite and collomorphic hydrohematite and goethite are present particularly in fine screenings and partly derived from the weathering of sulfides. These epigenetic aggregates cement quartz and partly topaz in the coarse fractions, and form crusts on other mineral grains. Common are also phenitic mica and biotite, and more rarely, corroded feldspar and porous topaz.

The dominant ore minerals are ilmenite and its alteration products and cassiterite. Zircon and monazite are subordinate and more abundant in finer screenings. In contrast, columbite appears to be more abundant in coarser screenings. It usually contains Fe and Ta. Zircon occurs enriched in Th, Sc, and F. The Th and U contents of monazite vary. Cassiterite shows varying but moderate enrichments in Nb, Ta and W, and often contains exsolutions of Fe-Nb-Ta bearing rutile. Coarser intergrowths with rutile and anatase are also present.

Intergrowths of ore and barren minerals are more important in the coarse fraction as expected. They comprise primary intergrowths and secondary kaolinite-goethite agglomerates (see Appendix 4). The distribution of minerals in the thin sections is given in Appendix 8.

Cachoeirinha – TB55

Light mineral fractions (Thin sections # 13 to # 15)

The fine screening is dominated by bulbous aggregates of kaolinite and kaolinite-goethite and subordinate quartz. The latter becomes dominant in coarser fractions. Fine-grained aggregates of hematite and hydrohematite are also present. These epigenetic aggregations form crusts and coatings on quartz and ore minerals, particularly in the coarse fraction. Feldspar, mica, and topaz are sporadic.

Ore minerals are sporadic and occur as isolated carried-over grains in the finest screening only.

They comprise columbite, cassiterite, zircon, and rutile/anatase with single monazite and ixiolite. Zircon is often enriched in Sc and F.

Heavy mineral fractions (Thin sections # 16 to # 18)

The coarse fractions are dominated by topaz, and the fine fraction by cassiterite and columbite that are partly intergrown. The fine fraction also contains significant zircon that is almost absent in coarser fractions. Cassiterite exhibits conspicuous corrosion pits and often contains numerous exsolutions of columbite. It is both pure and significantly enriched in Fe, Nb, and Ta, rarely also in W. The composition of columbite varies between Fe-columbite with minor Mn and Ti, and a solid solution with up to 1/3 tantalite. W and Sc are partly enriched. Ilmenite is absent but its decomposition products pseudorutile-rutile-anatase are present instead. Fine-grained scaly aggregates of kaolinite and kaolinite-goethite partly enclose ore minerals and form crusts on coarser grains (see Appendix 4). The distribution of minerals in the thin sections is given in Appendix 8.

Santa Bárbara – TB59

Light mineral fractions (Thin sections # 19 to # 21)

The light mineral fractions are predominantly composed of quartz and kaolinite-goethite agglomerates with varying contents of hematite. Mica occurs sporadically. Ore minerals are also sporadic and mostly intergrown with barren minerals. Liberated ore mineral grains of rutile, columbite, zircon, and cassiterite are only present in the finest fraction and partly encrusted by kaolinite-goethite.

Heavy mineral fractions (Thin sections # 22 to # 24)

The fractions are dominated by kaolinite-goethite agglomerates and mostly collomorphic hematite. These are apparently most abundant in the coarse fraction. Topaz is subordinate.

The ore minerals columbite, cassiterite, ilmenite and other Ti phases, and the minerals zircon and xenotime are trace components, and partly encrusted or enclosed by kaolinite-goethite agglomerates. The apparently regular Sc and W enrichment in columbite is remarkable. Sulfide

mineral grains are sporadic (see Appendix 4). The distribution of minerals in the thin sections is given in Appendix 8.

Summary of the mineralogical composition of the ores

The mineralogical compositions of the density separation products of the four parent samples display similarities as well as distinct differences. The varying composition of target minerals represents a challenge in processing the ore concentrates, particularly for magnetic separation methods. Agglomerations and crusts of kaolinite and kaolinite-goethite modify the density and surface properties of target minerals. Monazite and zircon are the most predominant carriers of Th and U, and accordingly the predominant radioactive minerals in the sampled placer deposits.

6.7.2 Geochemistry of heavy and light fractions (bromoform separation)

The total element content of the pre-concentrates was determined by the mass fractions of the subsamples, which were produced by separation into heavy and light fractions. This analysis later served

as a basis for the evaluation of the total element contents (Chapter 6).

The bromoform fractions made up more than 99 % of the grain fraction <2 mm, thus representing almost exactly the total sample <2 mm. Only in the case of sample TB59 is the proportion <63 μm greater than 0.2 %.

A visual overview of the heavy and light fractions of the various samples and grain sizes is shown in figure 6.16.

For the evaluation of the analysis, only those elements important for the preparation and enrichment were presented in the following tables.

Massangana – TB45-48

Table 6.7 reveals that the Nb/Ta ratio is ~10 in all 3 grain size ranges of the heavy fraction. This ensures that the mineral composition of the Nb-Ta phases remained the same over the entire grain size range. The total contents of $\text{Nb}_2\text{O}_5 + \text{Ta}_2\text{O}_5$ were 1 % in the <630 μm particle size range, and clearly below 1 % in the coarser range. The SnO_2 contents were between 2 and 3 % in the <630 μm fraction and significantly lower in the coarser fraction. Remarkably, ZrO_2 contents of up to 6 % were

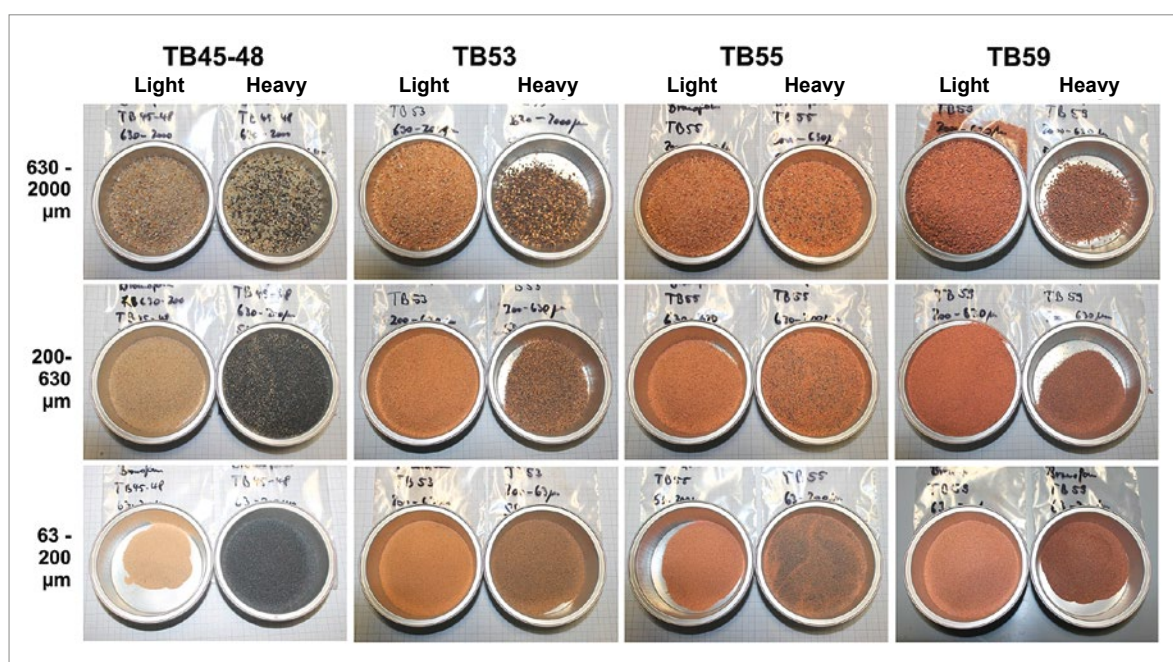


Fig. 6.16: Results of density separation with bromoform.

Tab. 6.7: Sample Massangana – TB45-48 – Chemical composition of heavy and light fraction (bromoform separation 2.89 g/cm³).

Size [µm]	Density fraction	Ta ₂ O ₅	Nb ₂ O ₅	SnO ₂	ZrO ₂	Fe ₂ O ₃	TiO ₂	Ce	Th	U
		%	%	%	%	%	%	ppm	ppm	ppm
63–200	LF	< 0.003	< 0.003	0.001	0.02	0.9	0.10	51	6	2
200–630	LF	< 0.003	< 0.003	0.003	0.04	0.8	0.09	34	6	2
630–2000	LF	< 0.003	0.008	0.001	0.03	0.9	0.12	28	6	2
63–200	HF	0.087	0.934	2.01	4.59	41.1	43.7	4290	917	134
200–630	HF	0.098	1.033	2.77	1.54	42.6	42.9	5330	1320	145
630–2000	HF	0.027	0.273	0.62	5.99	18.1	20.1	6980	1990	371
Total	LF + HF	0.064	0.670	1.741	2.21	29.2	29.7	4426	1133	154

present in the heavy mineral fraction. Unfavorable were high Th contents of up to 0.2%, and moderate U contents of up to 0.037%. Most of the heavy mineral fraction was present in the form of ilmenite as TiO₂ and Fe₂O₃.

Bom Futuro – TB53

Sample TB53 represents pre-enriched material from the jig.

Table 6.8 shows that the Nb/Ta ratio is 1 to 2.5 in all 3 grain size ranges of the heavy fraction. The different ratio in the grain sizes indicates inhomogeneities in the Nb/Ta phases. The total contents of Nb₂O₅ + Ta₂O₅ were also low in the heavy mineral fractions at only 160 ppm. The main raw material was SnO₂ with almost 20% in the middle grain size fraction.

The expected Th and U contents in the SnO₂ enrichment were estimated to be low.

Cachoeirinha – TB55

Sample TB53 represents pre-enriched material from the jig.

The main raw materials in TB55 are Nb₂O₅, Ta₂O₅ and SnO₂. The elements are most concentrated in the smallest particle sizes. The Nb/Ta ratio was constant in all three particle size ranges. This ensures that the mineral composition of the Nb-Ta phases remained the same over the entire particle size range. Thorium and uranium were preferably enriched in the smallest particle size. They seem to have an affinity for ZrO₂ (zirconium).

Tab. 6.8: Sample Bom Futuro – TB53 – Chemical composition of heavy and light fraction (bromoform separation 2.89 g/cm³).

Size [µm]	Density fraction	Ta ₂ O ₅	Nb ₂ O ₅	SnO ₂	ZrO ₂	Fe ₂ O ₃	TiO ₂	Ce	Th	U
		%	%	%	%	%	%	ppm	ppm	ppm
63–200	LF	< 0.003	< 0.003	0.004	0.013	1.49	0.15	31	7	1
200–630	LF	< 0.003	< 0.003	0.004	0.013	1.04	0.09	20	4	1
630–2000	LF	< 0.003	0.003	0.003	0.014	1.00	0.06	23	4	1
63–200	HF	0.05	0.13	7.71	4.38	14.6	16.2	284	182	87
200–630	HF	0.05	0.09	19.56	0.43	11.4	7.4	242	51	23
630–2000	HF	0.04	0.04	9.49	0.07	21.4	1.2	436	39	12
Total	LF + HF	0.010	0.016	2.750	0.111	4.0	1.05	82.9	14	5

Tab. 6.9: Sample Cachoeirinha – TB55 – Chemical composition of heavy and light fraction (bromoform separation 2.89 g/cm³).

Size [μm]	Density fraction	Ta ₂ O ₅	Nb ₂ O ₅	SnO ₂	ZrO ₂	Fe ₂ O ₃	TiO ₂	Ce	Th	U
		%	%	%	%	%	%	ppm	ppm	ppm
63–200	LF	< 0.003	0.02	0.034	0.056	2.41	0.133	694	70	7
200–630	LF	< 0.003	0.007	0.011	0.005	0.94	0.035	118	14	1
630–2000	LF	< 0.003	< 0.003	0.006	0.004	0.68	0.019	59	8	1
63–200	HF	1.373	13.03	32.13	6.126	5.42	1.136	330	777	387
200–630	HF	0.841	8.23	20.96	0.428	3.38	0.420	102	74	68
630–2000	HF	0.179	1.75	19.05	0.017	1.24	0.104	59	11	22
Total	LF + HF	0.337	3.28	12.54	0.321	1.8	0.195	85	52	38

Santa Bárbara – TB59

Sample TB59 is not pre-enriched material from the jig. It was taken between the screening machine and ball mill at the Santa Bárbara processing plant.

The raw material content at Santa Bárbara seemed to be low with only 0.03 % SnO₂ and 0.02 % Nb₂O₅ + Ta₂O₅. However, the sample represented the non-enriched ore.

The contents of Nb₂O₅, Ta₂O₅ and SnO₂ were highest in the smallest fraction. Since this material was not ground, and thus no exposure of the single mineral grains took place, an exact separation into heavy and light minerals was not possible.

6.8 Processing

6.8.1 Processing flow

The enrichment of the raw material elements should be done by sieving, density separation and magnetic separation. The following preparation steps were chosen:

After each processing step, partial samples were obtained, which were further processed in the following steps. The further the processing advances, the more subsamples are created. From each partial sample/fraction, approx. 100–150 g each was taken as a retained sample in order to carry out further investigations.

Tab. 6.10: Sample Santa Bárbara – TB59 – Chemical composition of heavy and light fraction (bromoform separation 2.89 g/cm³).

Size [μm]	Density fraction	Ta ₂ O ₅	Nb ₂ O ₅	SnO ₂	ZrO ₂	Fe ₂ O ₃	TiO ₂	Ce	Th	U
		%	%	%	%	%	%	ppm	ppm	ppm
63–200	LF	0.003	0.021	0.025	0.027	4.05	0.185	108	56	6
200–630	LF	< 0.003	0.016	0.019	0.019	2.31	0.148	97	41	4
630–2000	LF	< 0.003	0.006	0.007	0.013	1.77	0.065	45	23	3
63–200	HF	0.033	0.339	0.475	1.630	25.52	1.431	588	568	95
200–630	HF	0.004	0.050	0.095	0.102	32.78	0.398	589	217	30
630–2000	HF	< 0.003	0.016	0.044	0.040	44.74	0.331	425	233	35
Total	LF + HF	0.002	0.019	0.027	0.051	6.7	0.15	125.2	62	8

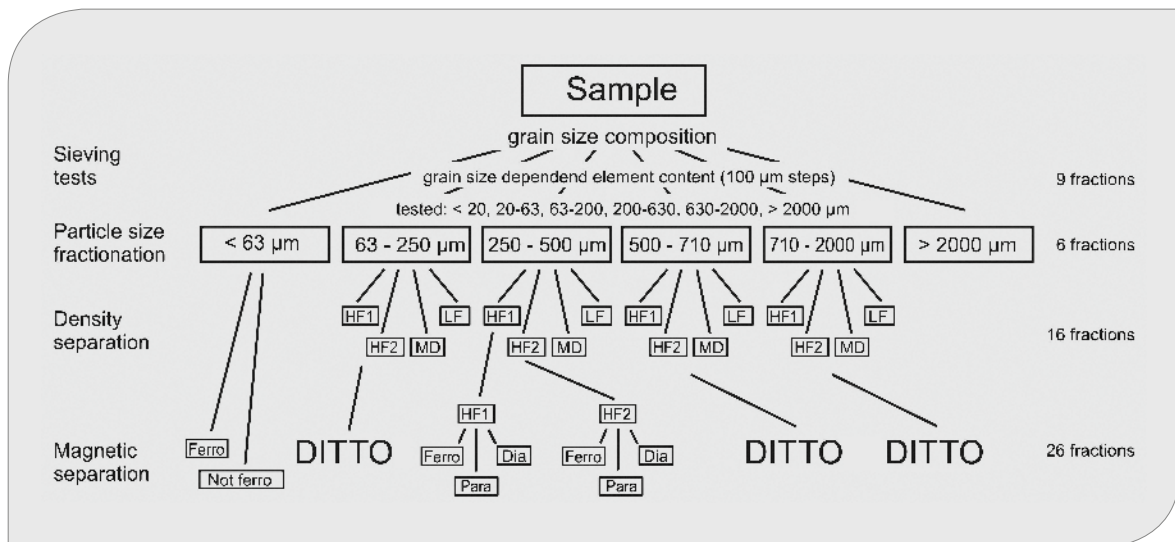


Fig. 6.17: Processing scheme for the production of mineral concentrates. Abbreviations:
HF – heavy fraction, LF – light fraction, MD – middlings, Para – paramagnetic flow, Dia – diamagnetic flow, ferro – ferromagnetic flow, Not ferro – not ferromagnetic.

6.8.2 Sieve analysis

The total samples were separated for comparability in <math><2\text{ mm}</math>. The proportions of the sieve fractions are shown in table 6.11 and 6.12.

Table 6.12 shows that samples TB53 and TB59 contain a very large fraction $>2\text{ mm}$. These frac-

tions are processed separately. The following evaluations refer exclusively to the grain fraction <math><2\text{ mm}</math>, which contains the majority of the samples.

The evaluation of the sieve analysis showed that the mineral grains in samples TB45-TB48, TB53 and TB55 are very well isolated, uncovered and hardly overgrown.

Tab. 6.11: Mass fractions and total masses of <math><2\text{ mm}</math> fractions of samples TB45-48 (Massangana).

Grain size	TB45	TB46	TB47	TB48
	[kg] (%)	[kg] (%)	[kg] (%)	[kg] (%)
< 2.00 mm	16.033 (94.7)	15.188 (89.3)	15.427 (91.9)	16.748 (98.6)
> 2.00 mm	0.895 (5.3)	1.812 (10.7)	1.357 (8.1)	0.24 (1.4)
Total	16.928 (100)	17.009 (100)	16.784 (100)	16.988 (100)

Tab. 6.12: Mass fractions and total masses of <math><2\text{ mm}</math> fractions of samples TB45-48 (total), TB53, TB55 and TB59.

Grain size	TB45-48	TB53	TB55	TB59
	[kg] (%)	[kg] (%)	[kg] (%)	[kg] (%)
< 2.00 mm	63.396 (93.6)	49.912 (92.8)	59.594 (98.4)	16.119 (81.5)
> 2.00 mm	4.304 (6.4)	10.821 (17.8)	1.005 (1.6)	3.692 (18.5)
Total	67.700 (100)	60.733 (100)	60.984 (100)	19.904 (100)

Tab. 6.13: Grain size composition of the samples, determined by dry sieving by sieving machine (1 kg sample).

Grain size	TB45-48	TB53	TB55	TB59
[μm]	[kg] (%)	[kg] (%)	[kg] (%)	[kg] (%)
800–2000	11.51	24.78	41.29	39.87
630–800	6.18	11.03	15.43	10.38
500–630	7.87	14.69	13.06	9.77
400–500	10.17	16.05	9.67	9.38
300–400	22.07	18.02	9.90	11.65
200–300	27.44	11.95	6.99	11.69
100–200	14.02	3.18	3.44	5.95
63–100	0.55	0.24	0.18	1.21
< 63	0.20	0.07	0.05	0.10
Total	100	100	100	100

The grain size composition of the samples in the different increments is shown in table 6.13.

The data from table 6.13 is used as the basis for calculating the output of elements in figures 6.19–6.26.

Element composition – grain size dependent

The reason for the particle size fractionation in 100 μm steps is to determine whether the raw materials Nb/Ta and Sn (Ce, Zr, Ti) or Th and U preferentially accumulate in certain particle size ranges. Together with the mass fractions, this

makes it possible to determine which particle size fractions contain the largest amount of valuable material.

Massangana – TB45-48

Figure 6.19 clearly shows that Nb, Ta, Sn, are in some cases also enriched in Zr in the <400 μm fractions. Zr shows two enrichment zones at the lowest and the largest particle sizes. In the >2 mm fractions, single grains of zircon could be separated. Most of the total sample is determined by Ti and Fe as ilmenite. The concentrations of the elements Ce, La and Th are highest in the coarse grain sizes.

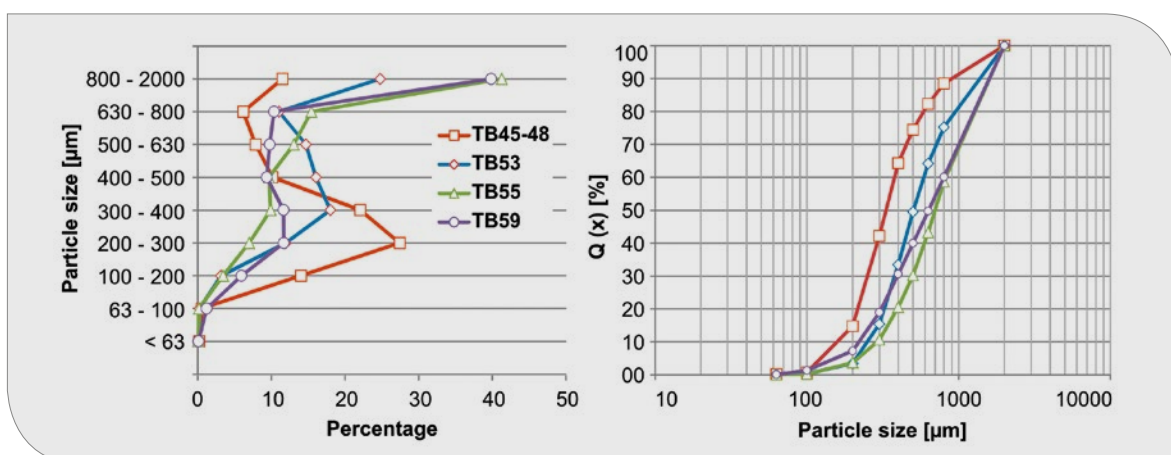


Fig. 6.18: Percentages of the sieve fractions and sieve curves of the <2 mm fraction.

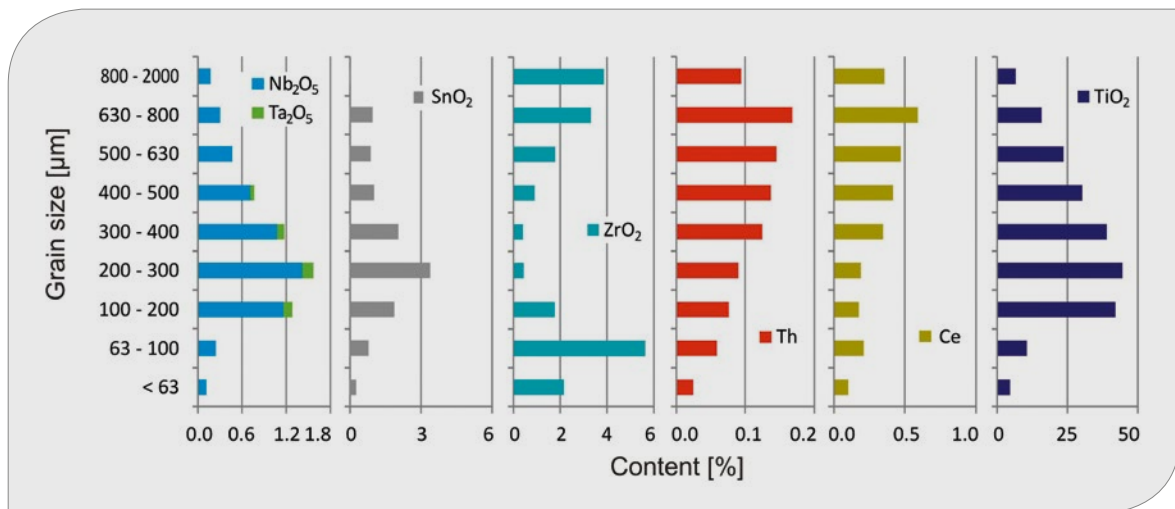


Fig. 6.19: Element content of sample TB45-48 dependent on grain size fraction.

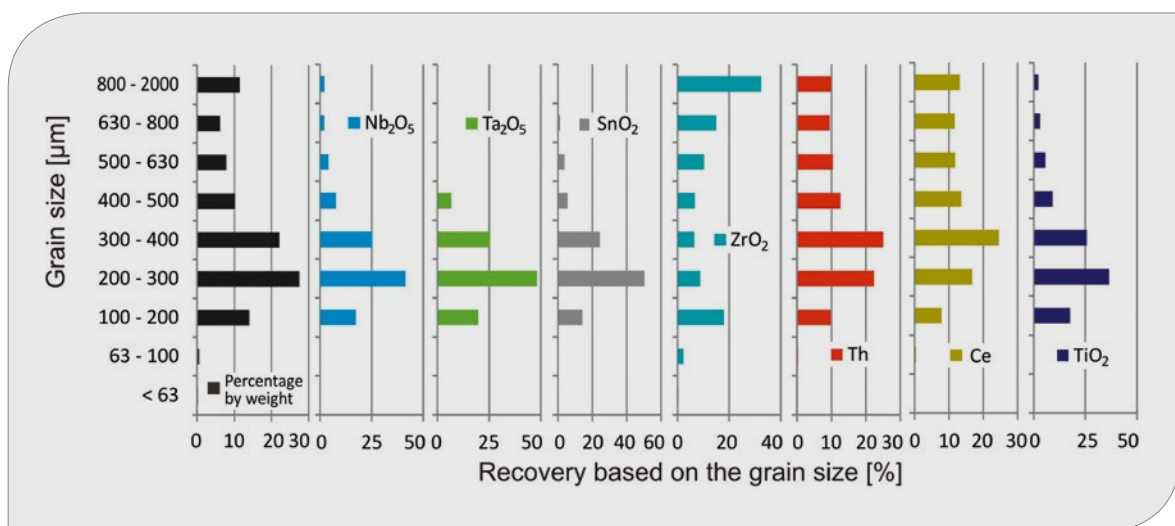


Fig. 6.20: Element recovery of sample TB45-48 dependent on grain size fraction.

With regard to mass recovery (Fig. 6.20), the main raw materials Nb_2O_5 , Ta_2O_5 and SnO_2 are mainly enriched in the 100–500 μm particle size range. The elements Zr, Ce, La and Th are mainly present in the coarser particle sizes.

Bom Futuro – TB53

In sample TB53, SnO_2 (cassiterite) was enriched very successfully by jig to about 3–4%. The distribution of the concentrations is very uniform over the entire particle size range.

The highest concentrations of Nb, Ta, Zr and Th in the small particle size ranges shown in figure 6.21 are negligible in terms of mass. The largest proportions of Nb, Ta and Sn are >100 μm over the entire particle size range.

The largest proportion of Fe, in part also Nb and Sn, are in the granulometry > 800 μm . It is related to the agglomerates of Fe hydroxides, which include the Nb/Ta and Sn mineral phases

In the >2 mm fraction (not shown here), SnO_2 total contents of 1% were detected. Since the >2 mm fraction is 18.5%, considerable amounts of SnO_2 would be lost if the material were not ground.

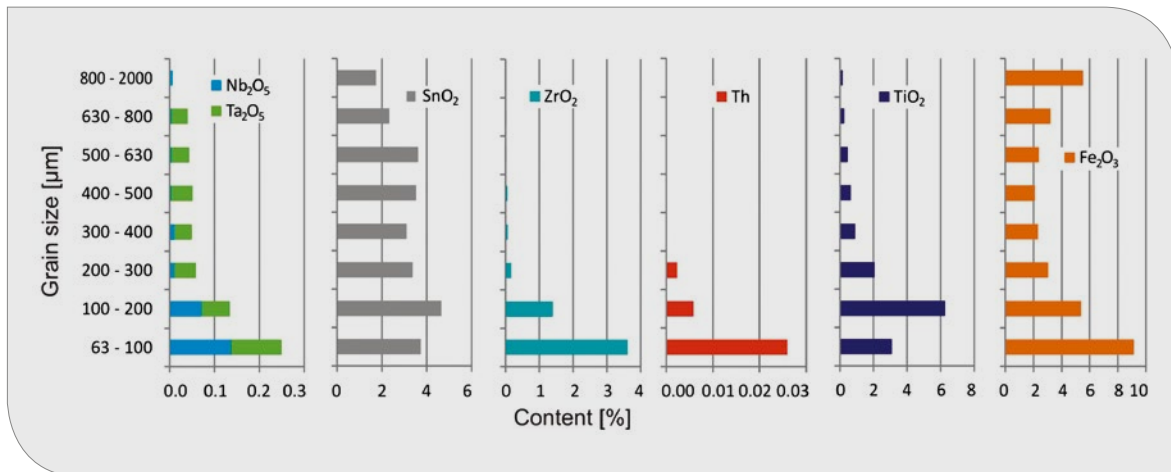


Fig. 6.21: Element content of sample TB53 dependent on grain size fraction.

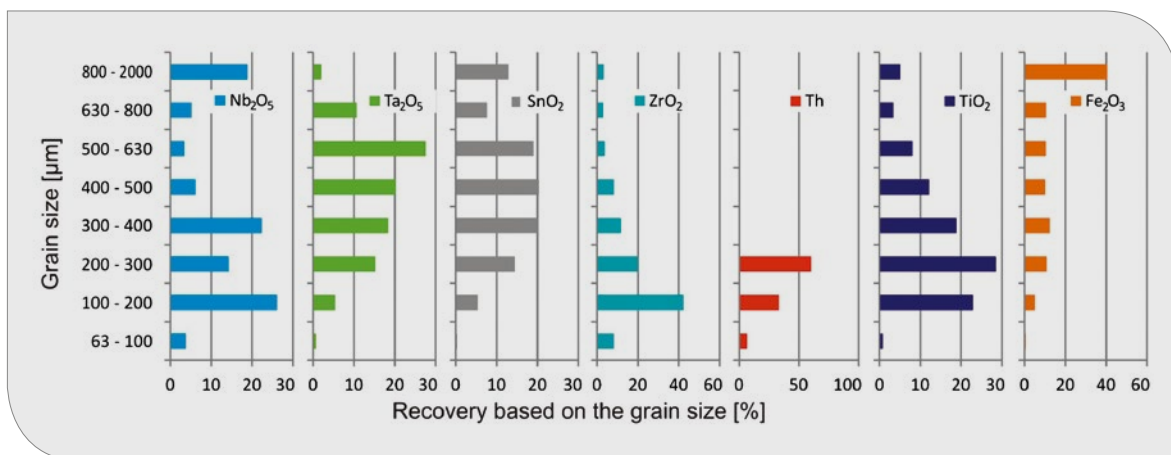


Fig. 6.22: Element recovery of sample TB53 dependent on grain size fraction.

Cachoeirinha – TB55

Sample TB55, like TB45-48 and TB53, was also strongly enriched by the jig. Figure 6.23 clearly shows that SnO_2 is already present in high concentrations distributed over all particle sizes. Especially in the small particle sizes, SnO_2 is enriched up to 30%, and $\text{Nb}_2\text{O}_5 + \text{Ta}_2\text{O}_5$ to 10–15%. The highest concentrations of Nb, Ta, Zr and Th are in the <200 μm particle sizes.

In terms of mass, the highest yield of SnO_2 (40%) is to be expected in the coarse fraction >800 μm . The proportions of Nb and Ta are distributed over the entire particle size range. Higher concentrations of ZrO_2 are expected only in the 100–200 μm

fraction. Th seems to be partially bound to the major Zr mineral zircon (Figs. 6.23, 6.24).

Santa Bárbara – TB59

The concentrations of the valuable elements in St. Bárbara are very low compared to the other samples. This sample is not a pre-concentrate.

The element contents for Nb, Ta and Sn are highest in the smallest fractions. The Ta content is below the detection limit and could not be specified exactly. The majority of Nb, Ta and Sn are present in the <400 μm fraction. Fe is mainly in the form of iron-containing concretions and aggregates of goethite and hematite (Figs. 6.25, 6.26).

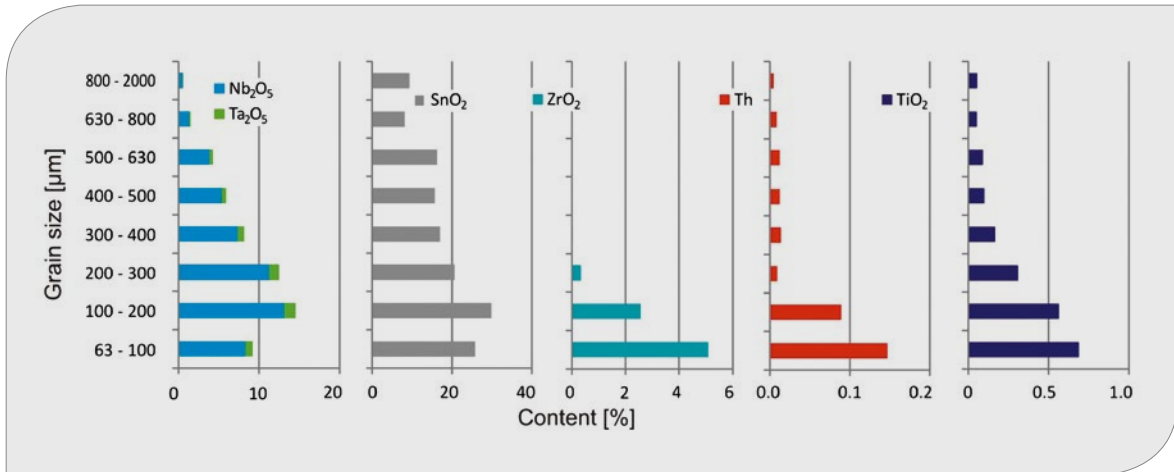


Fig. 6.23: Element content of sample TB55 dependent on grain size fraction.

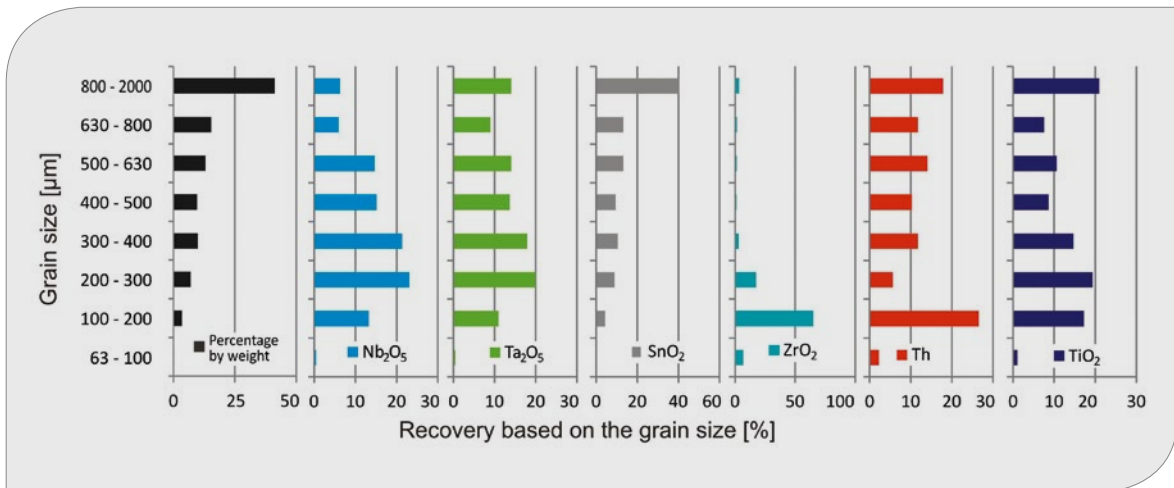


Fig. 6.24: Element recovery of sample TB55 dependent on grain size fraction.

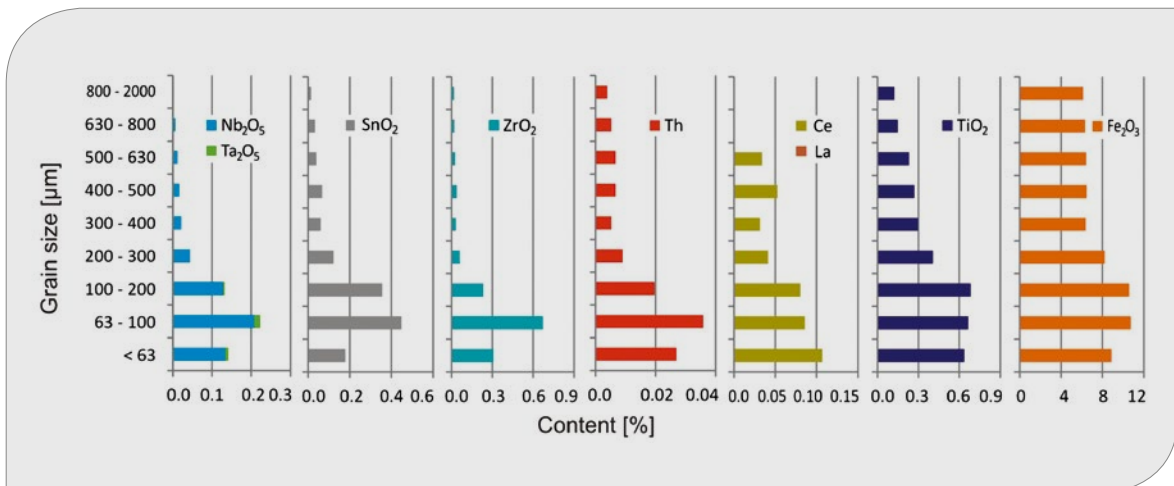


Fig. 6.25: Element content of sample TB59 dependent on grain size fraction.

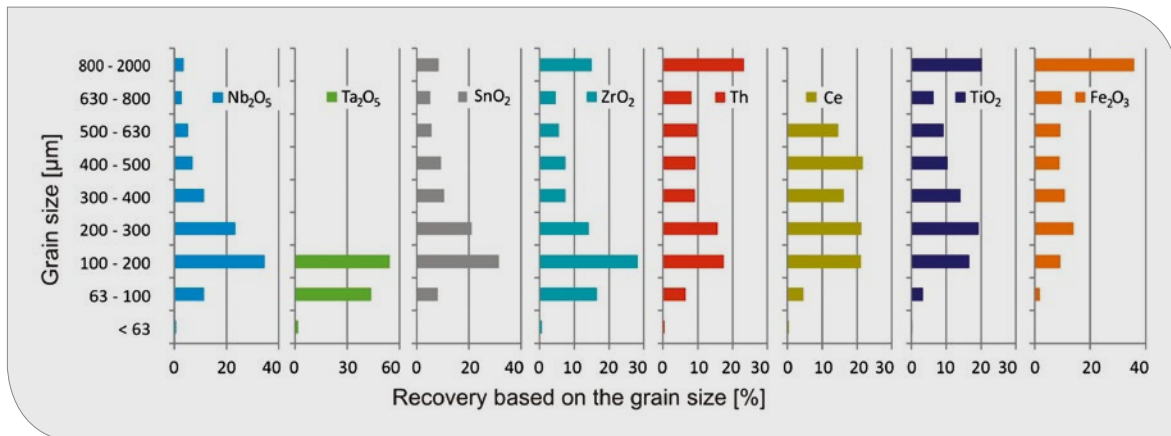


Fig. 6.26: Element recovery of sample TB59 dependent on grain size fraction.

6.8.3 Density separation

The enrichment of heavy minerals took place by using the shaking table. The corresponding parameters were described in Chapter 6.3.1. The success of the density separation was verified optically semi-quantitatively by the different mineral colors.

In the concentration data, the proportions of Al_2O_3 , SiO_2 and Fe_2O_3 were additionally indicated. This data served to evaluate whether the separation into light and heavy fractions took place properly.

The obtained results allowed an assignment to the proven minerals and the analyzed chemical elements. Nb_2O_5 and Ta_2O_5 were mostly bound to the columbite and SnO_2 represents cassiterite. ZrO_2 reflected the presence of zircon. At least in sample TB45-48, almost the entire TiO_2 could be assigned to the ilmenite content. In sample TB53 and TB55, TiO_2 was mainly bound to rutile. The Al_2O_3 content could be explained by the presence of topaz.

The top line of the following graphs shows the initial concentration of the elements/oxides ("Total"). In the course of density separation, the contents in the HF1 and HF2 fractions should increase, whereas the contents in the middlings and light fractions should decrease.

Massangana – TB45-48

The 63–250 µm fraction was not processed by the shaking table, because the high concentration of

heavy minerals hardly allowed separation of the light fraction. The separation of the fraction was carried out afterwards by magnetic separation.

250–500 µm grain size fraction:

The accumulation of heavy minerals in the particle size fraction 250–500 µm is shown in figure 6.27. The sample contained a large amount of ilmenite (>90%), which negatively affected the accumulation of SnO_2 , Nb_2O_5 and Ta_2O_5 . To better assess the separation, an additional heavy mineral fraction HF3 was separated.

The highest concentrations of $\text{Nb}_2\text{O}_5 + \text{Ta}_2\text{O}_5$ (2.8%) and SnO_2 (19%) were achieved in HF1. It was not possible to reach a higher accumulation of columbite and cassiterite by the shaking table, as the large amount of ilmenite prevented further enrichment. Significant increases were observed for the ZrO_2 content in HF3. Monazite (Ce) with corresponding La and Th contents was also concentrated in HF1 and HF2.

The high Al_2O_3 proportions in HF3-LF were based on the content of topaz, which was previously enriched by jig (pre-enrichment). In LF, mainly topaz and quartz were enriched.

Concerning recovery, all heavy minerals were almost completely enriched in HF1 and HF2. However, the total mass can only be reduced by 25% (HF3, MD, LF = 25%). A satisfactory enrichment of 19% was only achieved for SnO_2 . The high ilmenite content prevented higher enrichment.

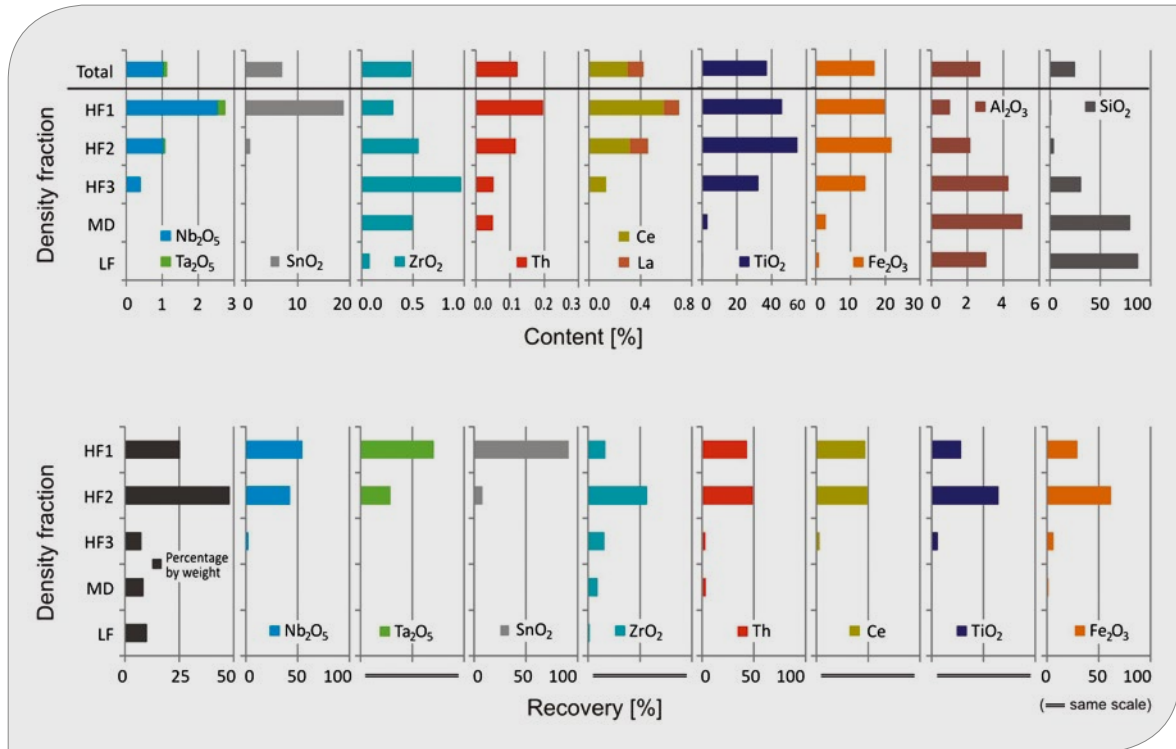


Fig. 6.27: Element contents and recovery of density separation by shaking table, sample TB45-48, 250–500 μm grain size fraction.

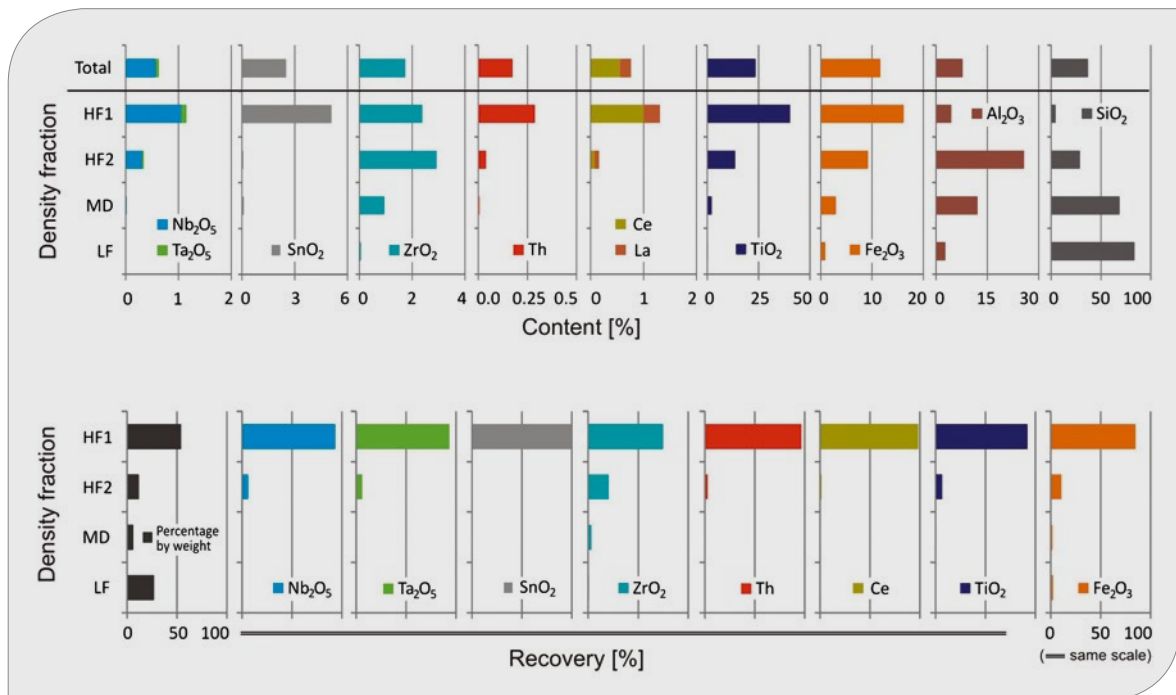


Fig. 6.28: Element contents and recovery of density separation by shaking table, sample TB45-48, 500–710 μm grain size fraction.

500–710 μm grain size fraction:

In fraction 500–710 μm , SnO_2 was only enriched to 5%. Although all SnO_2 entered the HF1 fraction, a higher enrichment was prevented due to very high TiO_2 contents (ilmenite). Nb_2O_5 and Ta_2O_5 were only enriched to 1%. Referring to recovery, all heavy minerals were almost completely concentrated in HF1.

710–2000 μm grain size fraction:

In the 710–2000 μm fraction, only SnO_2 contents of 2.5% as well as Nb_2O_5 and Ta_2O_5 contents of 0.8% each were achievable. ZrO_2 was enriched as zircon up to 6.5%. This fraction contained the highest thorium and cerium contents in comparison to the smaller grain sizes.

Very high aluminum contents are evident in all fractions, indicating high topaz contents. Most of the heavy mineral fraction was made up of ilmenite (TiO_2 content). The 710–2000 μm particle size fraction exhibited relatively small amounts of economically valuable minerals/elements.

Bom Futuro – B53

The Bom Futuro sample mainly comprised cassiterite as an economic mineral. The $\text{Nb}_2\text{O}_5/\text{Ta}_2\text{O}_5$ proportions were shown to be low. Other heavy minerals included rutile, topaz and zircon, as well as small amounts of monazite and xenotime.

63–250 μm grain size fraction:

In the 63–250 μm fraction in HF1, SnO_2 could be enriched up to 42%. Only small amounts were left in the HF2 fraction. The recovery in HF1 is >90%. Although Nb_2O_5 and Ta_2O_5 were enriched in HF1, they only reached very low concentrations of 0.5%. A large proportion of the HF1 fraction was made up of rutile (TiO_2), which also contained Nb_2O_5 , Ta_2O_5 and SnO_2 .

Thorium and uranium were bound to small amounts of zircon, monazite and xenotime. A large part of the HF3 fraction included topaz, which could be observed via the aluminum content.

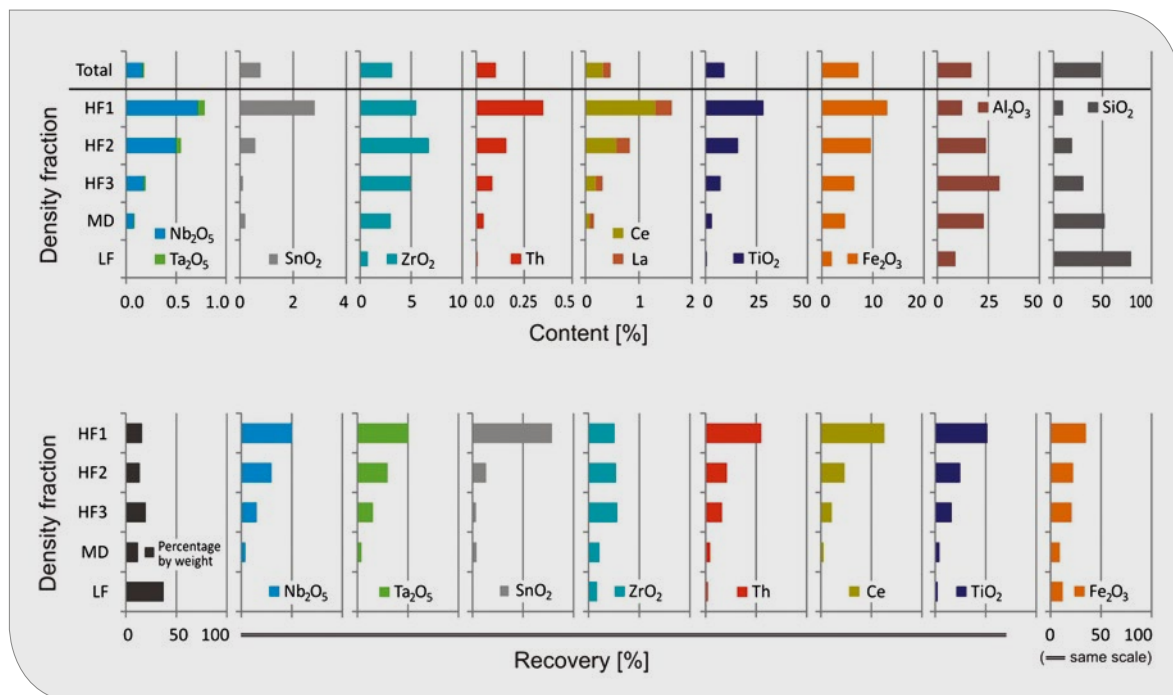


Fig. 6.29: Element content and recovery of density separation by shaking table, sample TB45-48, 710–2000 μm grain size fraction.

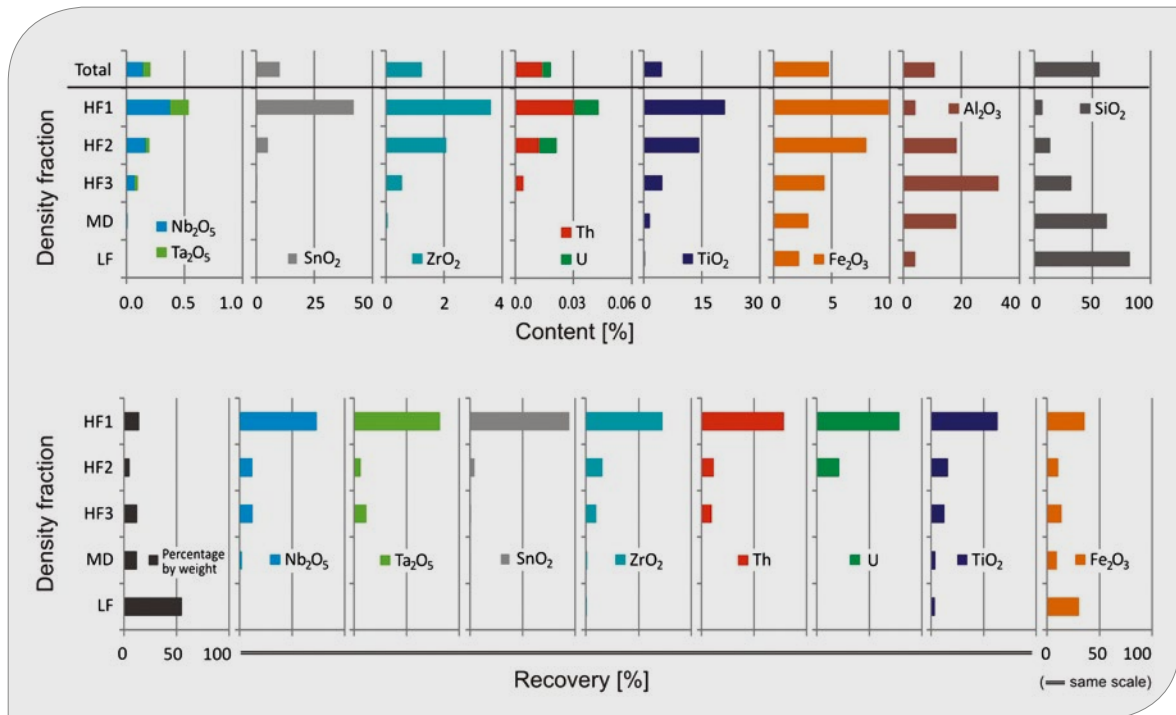


Fig. 6.30: Element/oxide content and recovery of density separation by shaking table, sample TB53, 63–250 μm grain size fraction.

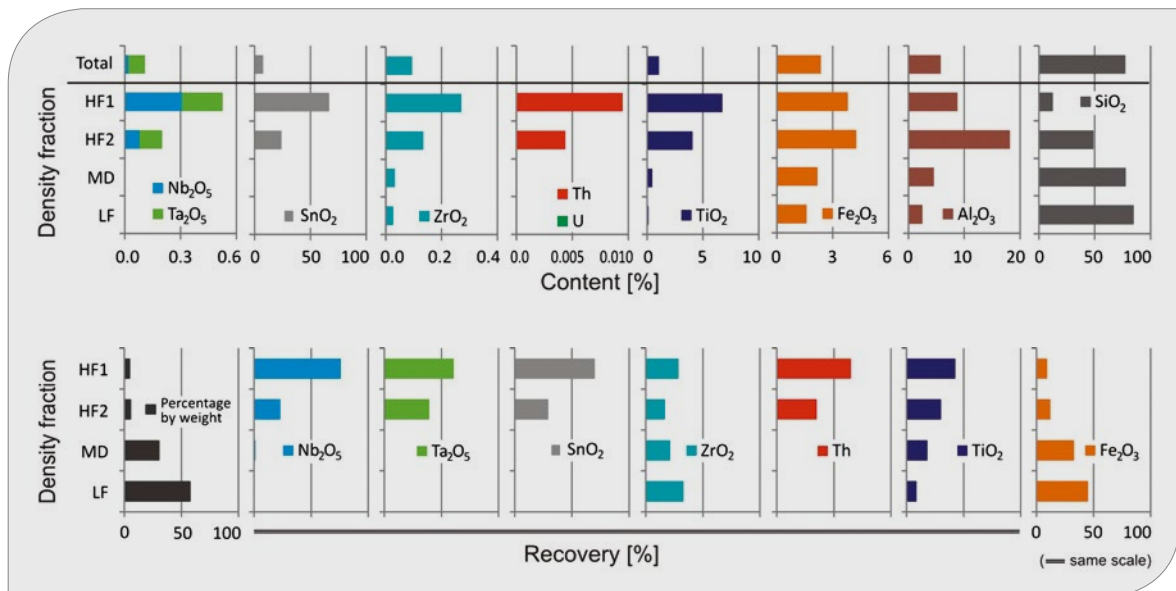


Fig. 6.31: Element/oxide content and recovery of density separation by shaking table, sample TB53, 250–500 μm grain size fraction.

250–500 μm grain size fraction:

With respect to the 250–500 μm fraction, SnO_2 could be enriched to >60% in HF1. An enrichment of 25% was still reached in HF2. The cassiterite concentrate was also diluted by topaz (aluminum

contents). Overall, 100% of the SnO_2 was concentrated in the two heavy mineral fractions with less than 10% mass recovery. Although Nb_2O_5 and Ta_2O_5 were concentrated in HF1 and HF2, they were only enriched to 0.5%.

500–710 μm grain size fraction:

SnO_2 was almost quantitatively enriched to concentrations of up to 70% in HF1 and to 17% in HF2. Nb_2O_5 and Ta_2O_5 together reached only 0.6%, but were completely concentrated in HF1 and HF2. Thorium and uranium were below the detection limit and therefore not shown.

The high aluminum concentration in the HF2 fraction was bound to topaz, which was also enriched in HF1, and diluted the SnO_2 concentrate.

Overall, the valuable elements/oxides were very effectively concentrated, as more than 90% of the light minerals were separated in MD and LF (Fig. 6.32).

710–2000 μm grain size fraction:

In the 710–2000 μm fraction, SnO_2 was quantitatively enriched in the HF1 fraction, however an enrichment of only 24% was achieved. Nb_2O_5 and Ta_2O_5 together reached only 0.25%. A large part of the HF1 fraction was also made up of topaz, which diluted the other concentrates.

In TB55, SnO_2 could be excellently concentrated by means of the shaking table. Nb_2O_5 and Ta_2O_5

could not be enriched. The mineralogical analysis showed that Nb_2O_5 and Ta_2O_5 occurred as inclusions and trace elements in the lattice of the Ti phases (rutile) and formed few independent minerals. Likewise, part of the SnO_2 was bound to the Ti-rich phases (Fig. 6.33).

Cachoeirinha – TB55

The sample material was already a highly enriched pre-concentrate from the jig. The main heavy minerals in sample TB55 were cassiterite, columbite, zircon and topaz. Topaz made up the largest share of the heavy mineral fraction.

63–250 μm grain size fraction:

In the 63–250 μm fraction, cassiterite could be almost completely concentrated to >40% SnO_2 in HF1. Nb_2O_5 and Ta_2O_5 together reached between 16 and 19%, and were almost completely enriched in HF1 and HF2. Zircon was concentrated in HF2 to 7.5% ZrO_2 and, together with small monazite amounts, contained the majority of Th and U. The Th and U contents were highest in the smallest particle size fraction.

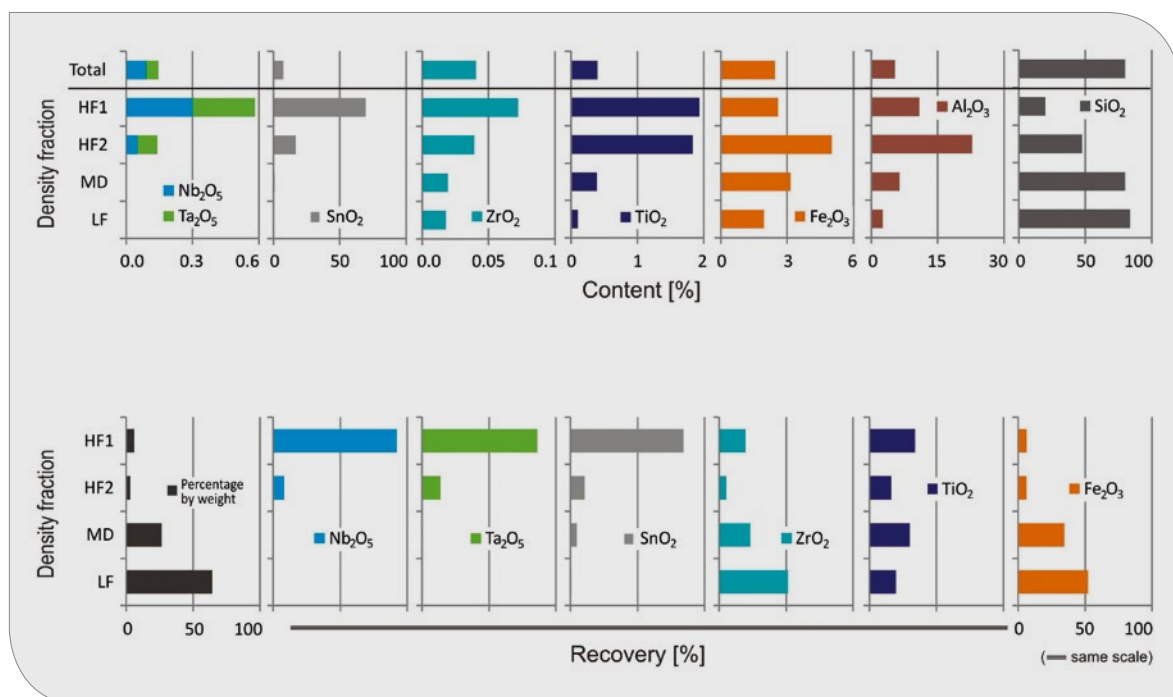


Fig. 6.32: Element/oxide content and recovery of density separation by shaking table, sample TB55, 500–710 μm grain size fraction.

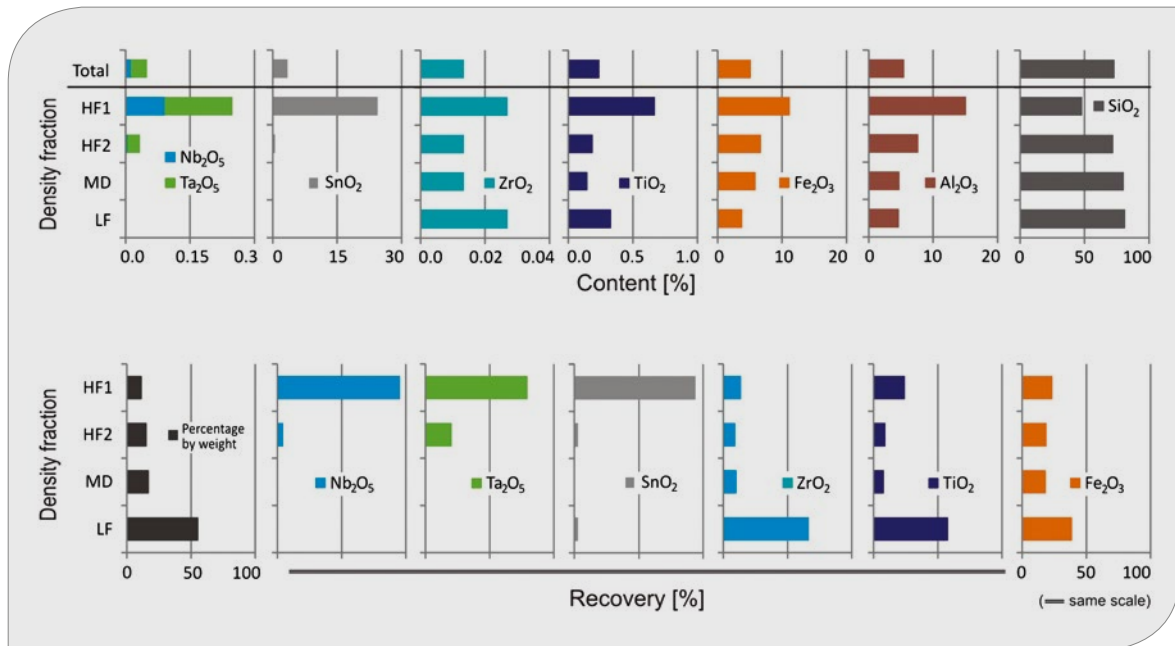


Fig. 6.33: Element/oxide content and recovery of density separation by shaking table, sample TB53, 710–2000 μm grain size fraction.

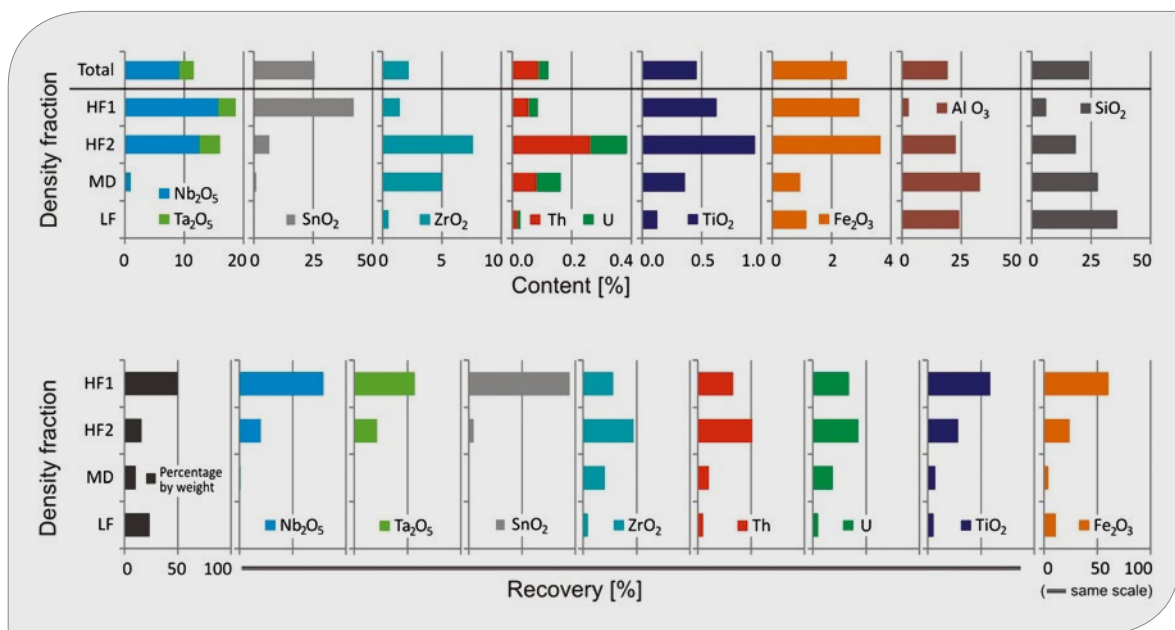


Fig. 6.34: Element/oxide content and recovery of density separation by shaking table, sample TB55, 63–250 μm grain size fraction.

250–500 μm grain size fraction:

In the 250–500 μm fraction, Nb_2O_5 and Ta_2O_5 together could be accumulated to 16–18% with little loss to the middlings. SnO_2 could be concentrated to 30–48% in HF1 and HF2. Likewise, topaz had a diluting effect on the concentrates.

500–710 μm grain size fraction:

Nb_2O_5 and Ta_2O_5 could still be enriched in HF1 and HF2 to 5 to 10% with about 95% recovery. Approximately 5% were lost to the middlings. Cassiterite could be enriched to 27–49%. Likewise, 5% cassiterite was lost to the middlings. These

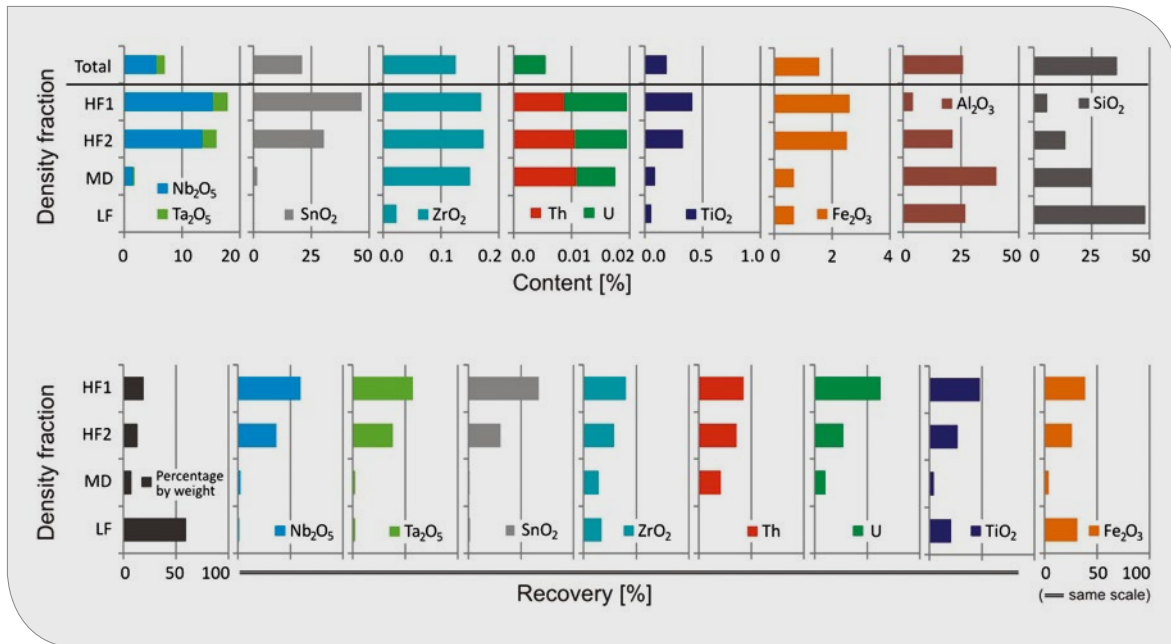


Fig. 6.35: Element/oxide content and recovery of density separation by shaking table, sample TB55, 250–500 μm grain size fraction.

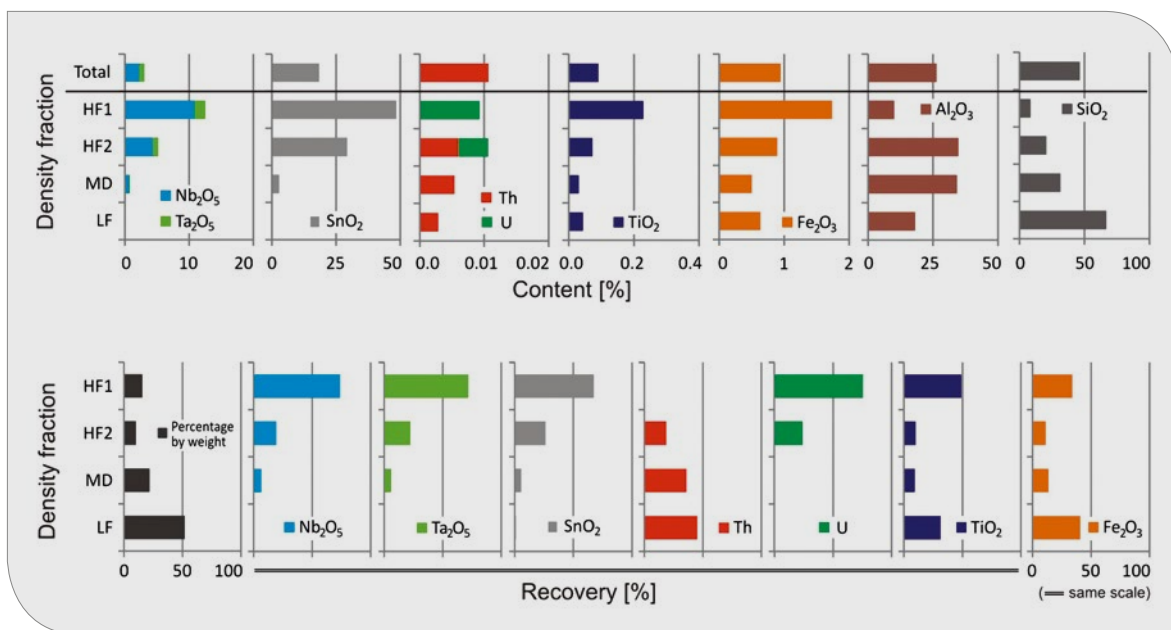


Fig. 6.36: Element/oxide content and recovery of density separation by shaking table, sample TB55, 500–710 μm grain size fraction.

losses were due to the large amount of topaz (aluminum contents in HF2 and MD), which artificially increased the fraction's total density. This hindered the precise separation of cassiterite and columbite. Thorium and uranium were present only in very low concentrations (Fig. 6.36).

710–2000 μm grain size fraction:

SnO_2 reached concentrations of 40–48% in fractions HF1 and HF2. Both fractions had to be further processed to achieve a high recovery. Small amounts of cassiterite and columbite were lost in the MD and LF. Both thorium and uranium were below the detection limit.

TB55 exhibited very high columbite and cassiterite contents. The high topaz content complicated the concentration of columbite and cassiterite in the HF1 fraction. To achieve a high recovery, HF1 and HF2 had to be further processed together. The thorium and uranium contents slightly increased only in the smallest particle size fraction and posed no problem.

Santa Bárbara – TB59

The samples from Santa Bárbara were not pre-concentrates, unlike TB45-48, TB53 and TB55. Only two particle size fractions were processed on the shaking table.

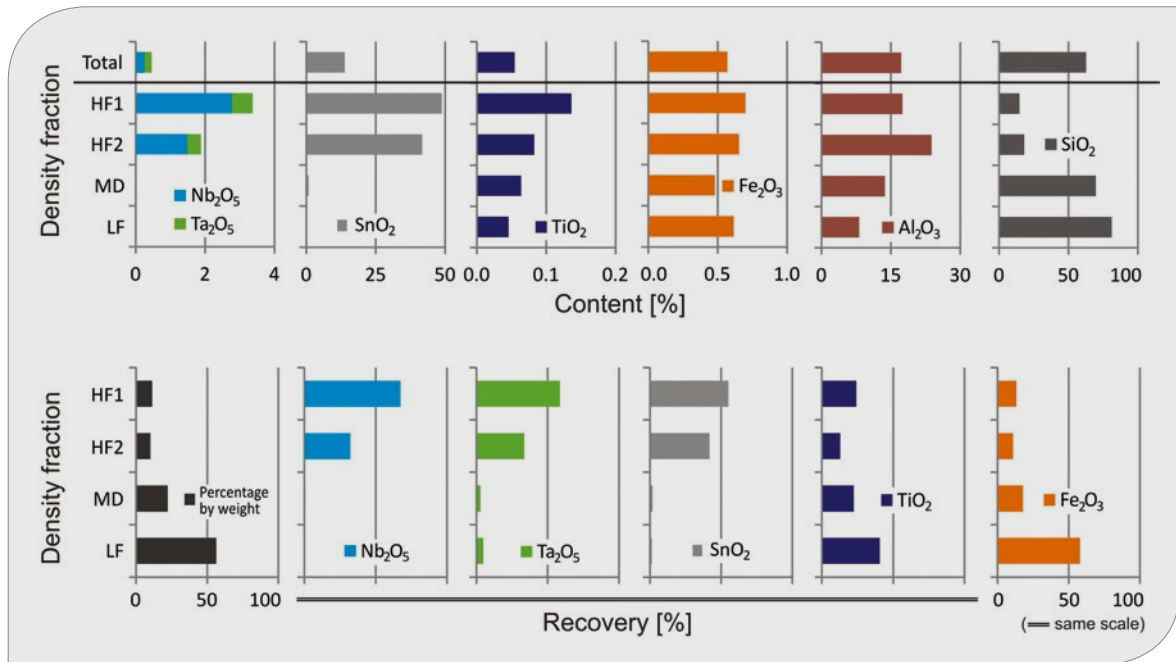


Fig. 6.37: Element/oxide content and recovery of density separation by shaking table, sample TB55, 710–2000 µm grain size fraction.

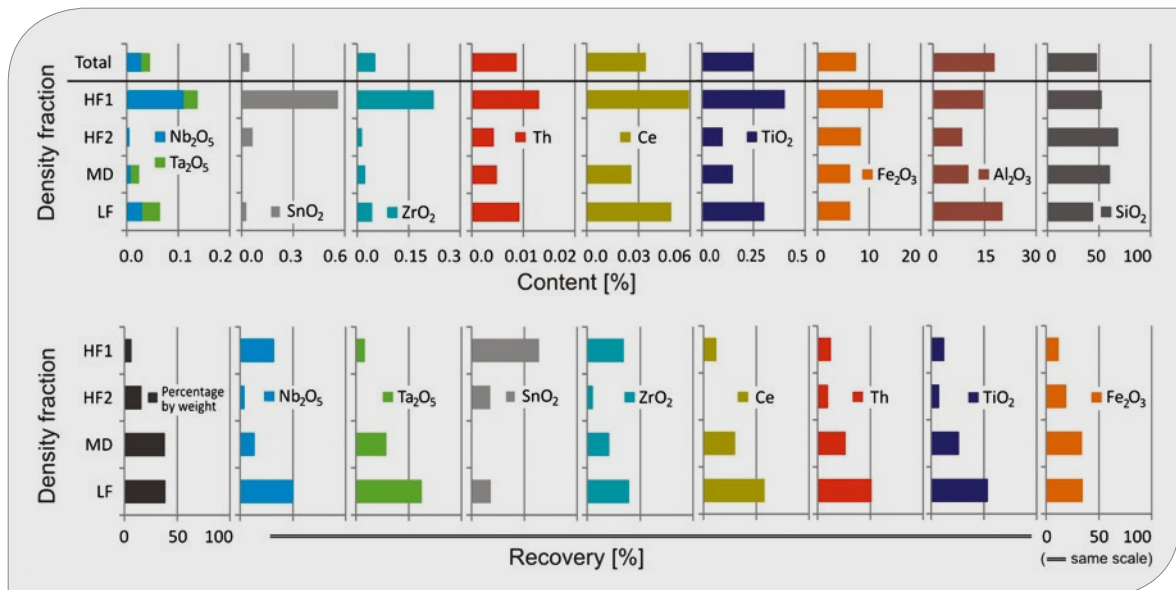


Fig. 6.38: Element/oxide content and recovery of density separation by shaking table, sample TB59, 200–630 µm grain size fraction.

200–630 μm grain size fraction:

The 200–630 μm fraction showed initial enrichments of Nb_2O_5 , Ta_2O_5 and SnO_2 , but was far from offering economic benefits. The recovery results clearly indicated that most of the valuable elements were transferred to the middlings and light fraction. This means that the valuable minerals were too highly intergrown with the light minerals. In contrast to the other samples, no higher concentrations can be achieved in this case.

630–2000 μm grain size fraction:

As in the case of the smaller particle size fraction, no economically utilizable concentrates of Nb_2O_5 , Ta_2O_5 and SnO_2 could be prepared. The recovery results also showed that the majority of the valuable elements were transferred into the light fraction. Analogously, this means that the valuable minerals were too highly intergrown with the light minerals as well.

The enrichment of the valuable minerals columbite and cassiterite from TB59 was not possible, at least in the current state of the sample. If possible, the material has to be ground to a target particle size of $<200 \mu\text{m}$ to enable liberation of the Nb_2O_5 , Ta_2O_5 and SnO_2 bearing mineral phases. Afterwards, enrichment by shaking table can be attempted again.

6.8.4 Magnetic separation

Magnetic separation allows the separation of minerals with different magnetic properties. All HF1 and HF2, and in part also the MD fractions, were split into paramagnetic and diamagnetic fractions. The separation into a paramagnetic and a diamagnetic fraction should enable a further enrichment of the raw materials. The top line of the graphs shows the concentration of elements/oxides from the shaking table (HF1 and HF2).

The evaluation of the magnetic fractions was carried out only for those fractions representing potentially saleable concentrates. For the TB45-48 sample, these concentrates were $\text{Nb}_2\text{O}_5/\text{Ta}_2\text{O}_5$ and SnO_2 , for TB53 it was SnO_2 , and for TB55 it was $\text{Nb}_2\text{O}_5/\text{Ta}_2\text{O}_5$ and SnO_2 . In some of the concentrates, ZrO_2 was enriched up to 25%.

The samples from TB59 could not be enriched to saleable concentrates. The enrichment methods used in the study were not applicable in the material's current state.

Massangana – TB45-48

The 63–250 μm fraction was not enriched further by the shaking table because the heavy mineral

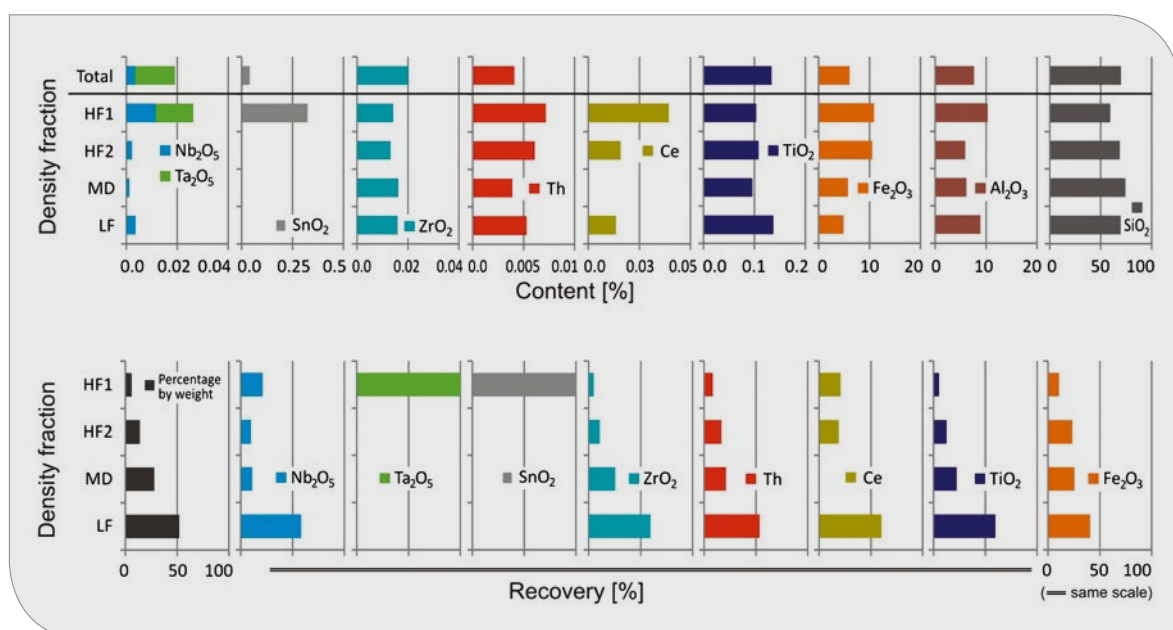


Fig. 6.39: Element/oxide content and recovery of density separation by shaking table, sample TB59, 630–2000 μm grain size fraction.

fractions were too high. The particle size fraction was directly separated into a diamagnetic, a strongly paramagnetic (Para 0), and a weakly paramagnetic fraction (Para 1), by means of a band/roll magnetic separator. In the paramagnetic fractions, Nb_2O_5 and Ta_2O_5 were almost completely enriched as columbite, and TiO_2 as ilmenite. Cassiterite was concentrated to >70% in the diamagnetic fraction.

In HF1 of the 250–500 μm fraction, cassiterite accumulated to 90%. Referring to the SnO_2 amount in the total sample, 37% of the total SnO_2 content was already enriched by this fraction. In the HF2 fraction, only about 8% SnO_2 in concentrate was produced. Cassiterite was also transferred to the paramagnetic fraction with 3.1%. ZrO_2 was concentrated in HF2 of the diamagnetic fraction to 22%.

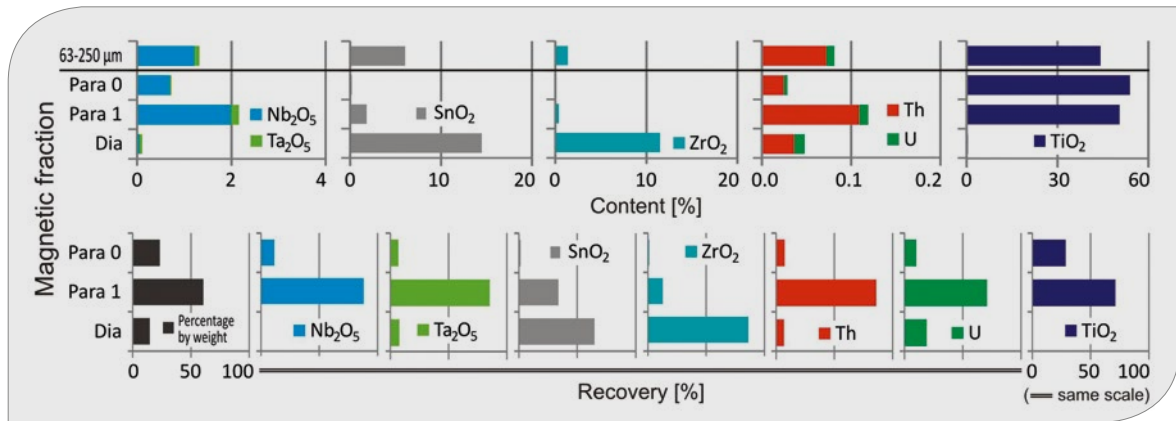


Fig. 6.40: Concentrations and recovery in the magnetic fractions of the 63–250 μm particle size fraction – TB45-48.

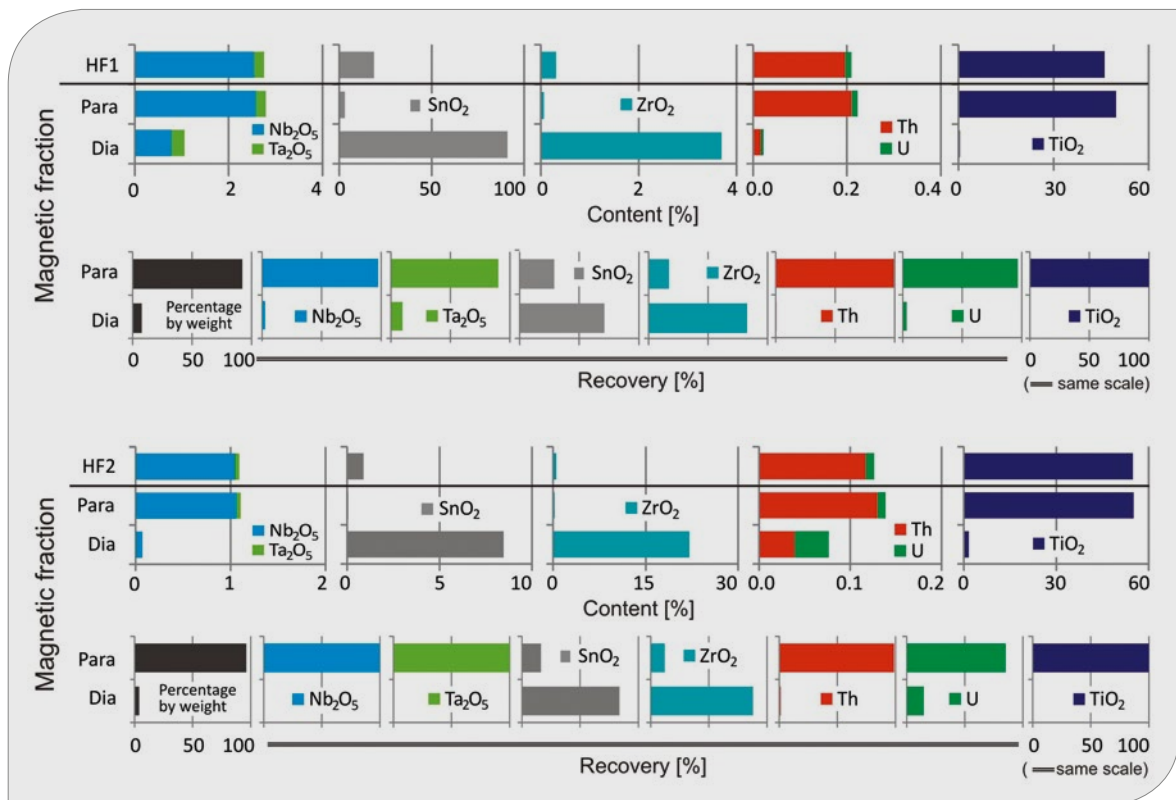


Fig. 6.41: Concentrations and recovery rates in the magnetic fractions HF1 and HF2 of the 250–500 μm grain size fraction – TB45-48.

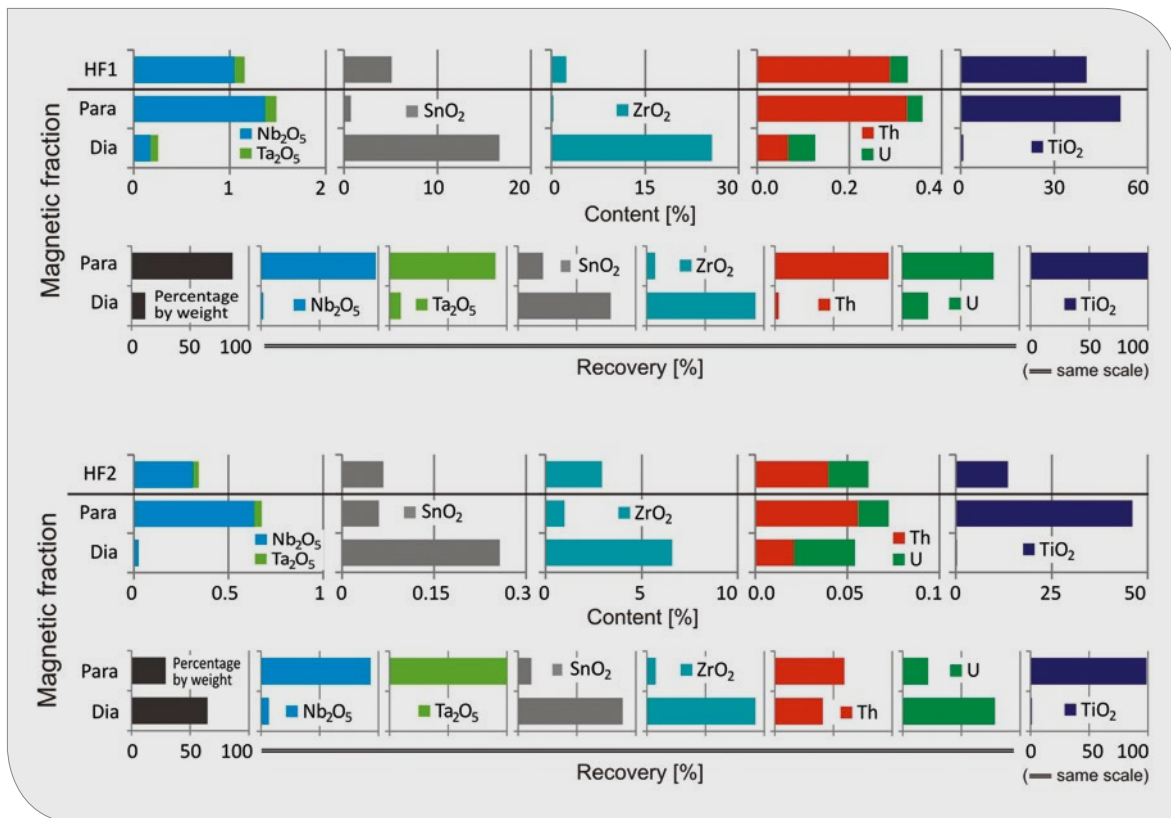


Fig. 6.42: Concentrations and recovery rates in the magnetic fractions HF1 and HF2 of the 500–710 µm grain size fraction – TB45-48.

The paramagnetic fraction was dominated by TiO₂ (ilmenite), but columbite was also present. Almost the total thorium and a large part of the uranium were enriched in the paramagnetic fraction.

In the 500–710 µm grain size fraction, SnO₂ was enriched up to 18%, and ZrO₂ to 25% in HF1 of the diamagnetic fraction. The paramagnetic fraction contained almost the entire amount of Nb₂O₅, Ta₂O₅ and TiO₂.

The contents of Nb₂O₅, Ta₂O₅ and SnO₂ were shown to be low in the coarse fraction. Zircon very strongly accumulated in the diamagnetic fraction, and could provide an economic contribution.

In the >500 µm fractions, the SnO₂ concentrations reached a maximum of only 18% in the diamagnetic fraction. The SnO₂ percentages in the >500 µm fractions were shown to be low. With increasing grain size, thorium and uranium were also enriched. It is estimated that thorium and uranium were mainly bound to monazite, pyrochlore and zircon in the coarser grain fractions.

In all fractions of columbite, a maximum accumulation of only 2.55% Nb₂O₅ and 0.21% Ta₂O₅ could be achieved. This effect is explainable by the dilution of the concentrate by ilmenite. Ilmenite and columbite have almost identical physical properties. Both minerals have a similar density of about 5.0 g/cm³ and are paramagnetic. Among other things, cerium, thorium and uranium contents rise with an increasing concentration of heavy minerals, indicating a growing monazite proportion. Consequently, the radioactivity of the concentrates also increases. Furthermore, cassiterite was enriched in the paramagnetic fraction, which is usually included in the diamagnetic fraction.

Therefore, detailed experiments were carried out to:

1. increase the Nb₂O₅/Ta₂O₅ content
2. separate the paramagnetic cassiterite
3. investigate the fractions to which the Th and U contents are to be attributed

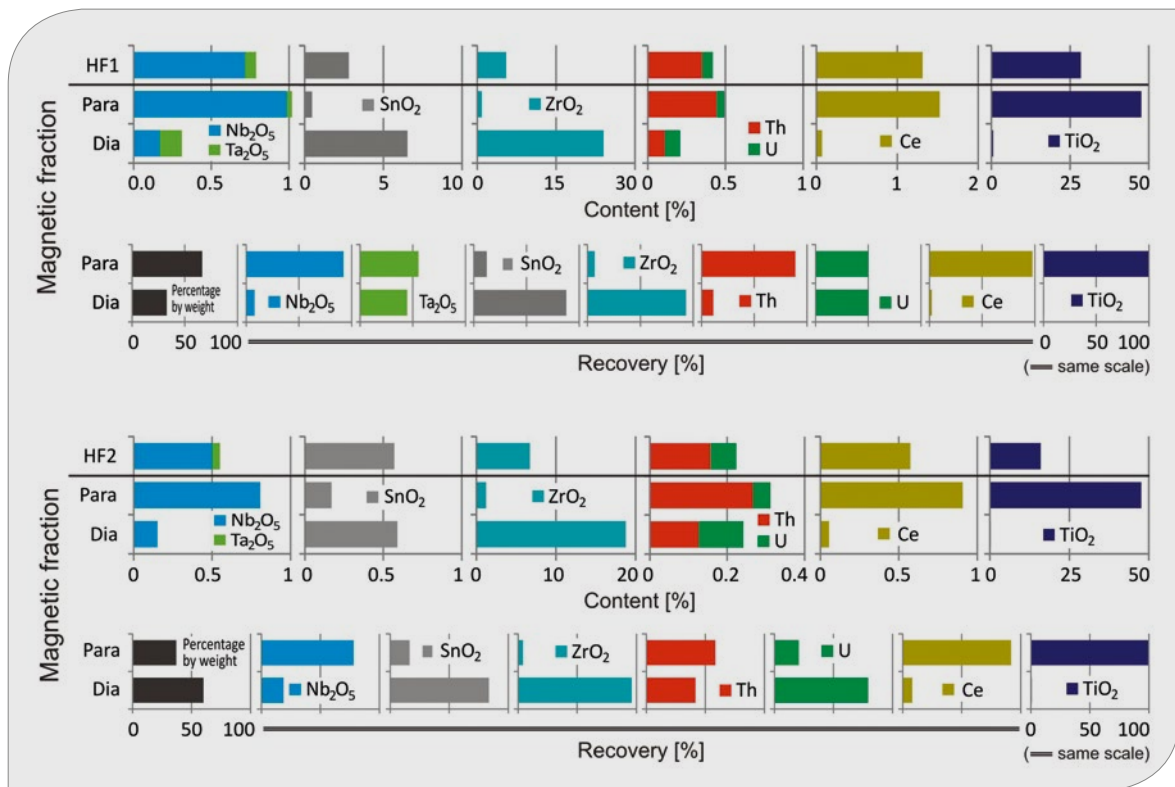


Fig. 6.43: Concentrations and recovery rates in the magnetic fractions HF1 and HF2 of the 710–2000 μm grain size fraction – TB45-48.

For this purpose, the HF1-paramagnetic fraction (250–500 μm particle size) was separated in a first step at 0.47 Tesla into an ilmenite-rich and a columbite-monazite-cassiterite-rich fraction.

In a second step, the two fractions were further separated by using Frantz magnetic separators and very small magnetic steps. The applied settings were described in the methodology section (Chapter 6.3.2).

Separation of the paramagnetic fraction – exemplary by HF1, 250–500 μm

Approximately 1.5 kg of the paramagnetic fraction, HF1, 250–500 μm , was separated into an ilmenite-rich and a monazite-columbite-cassiterite-rich concentrate by using a NdBF_e handheld magnet (0.47 Tesla). The ilmenite-rich concentrate had a mass fraction of about 95.2%.

The results clearly show that ilmenite, columbite and monazite could be separated by means of finely adjusted magnetic separation (Figs. 6.44

and 6.45). Coincidentally, the numerical values of the current intensity scale in Ampere (A) roughly corresponded to the field strength in Tesla, at least concerning the present settings applied at the Frantz magnetic separator.

The following conclusions can be drawn from figures 6.44 and 6.45.

The strongly paramagnetic ilmenite can be almost completely removed at approx. <0.3 A (approx. 0.3 Tesla). TiO₂ is present in the weaker paramagnetic fraction as weathering products of ilmenite in the form of rutile or pseudorutile. In the 0.3 to about 0.6 Tesla range, columbite can be separated achieving concentrations of up to 60% Nb₂O₅ + Ta₂O₅. (Fig. 6.44). The ilmenite fraction also contains columbite, which could not be completely removed by this methodology.

In the 0.6 to approx. 0.9 Tesla range, monazite becomes paramagnetic (Ce/Nd contents) and can be separated. The monazite contains almost the total Th and U of the paramagnetic fraction. This means that removal of the monazite enables the

Th and U contents of the concentrates to be significantly reduced. Consequently, the columbite hardly shows any Th and U. The cassiterite remains in the

fraction as the last mineral and reaches up to 40% SnO₂. The paramagnetic cassiterite can be added to the diamagnetic concentrate to increase the yield.

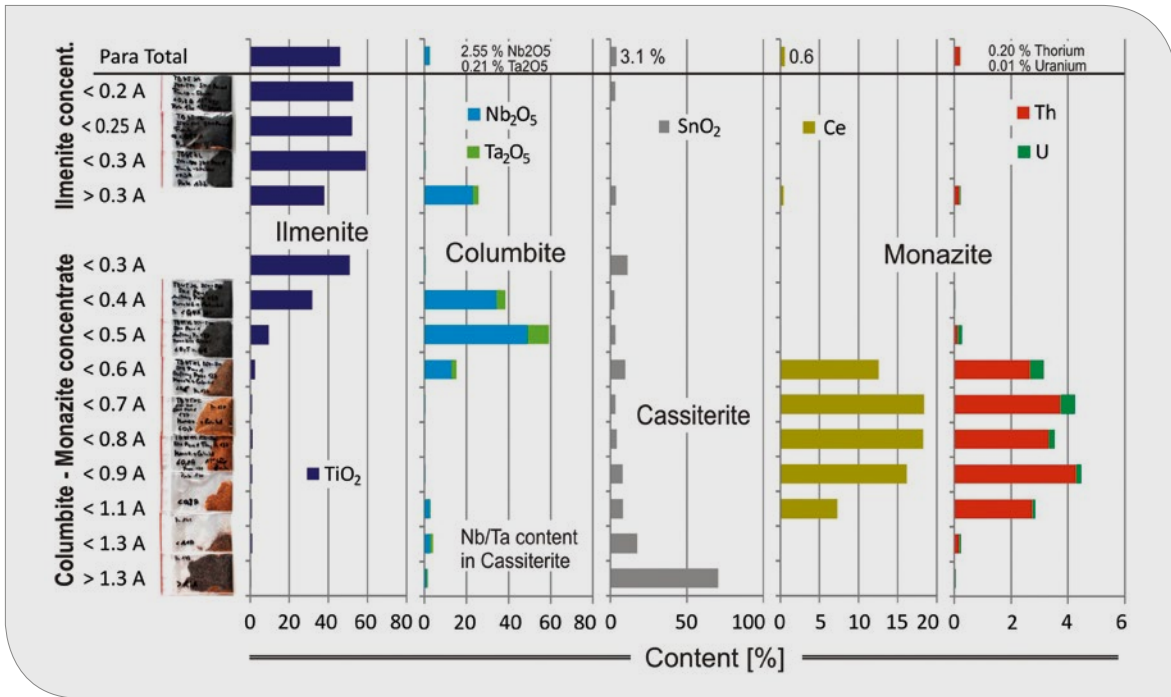


Fig. 6.44: Concentrations of the oxides after separation of the paramagnetic fraction by a Frantz magnetic separator.

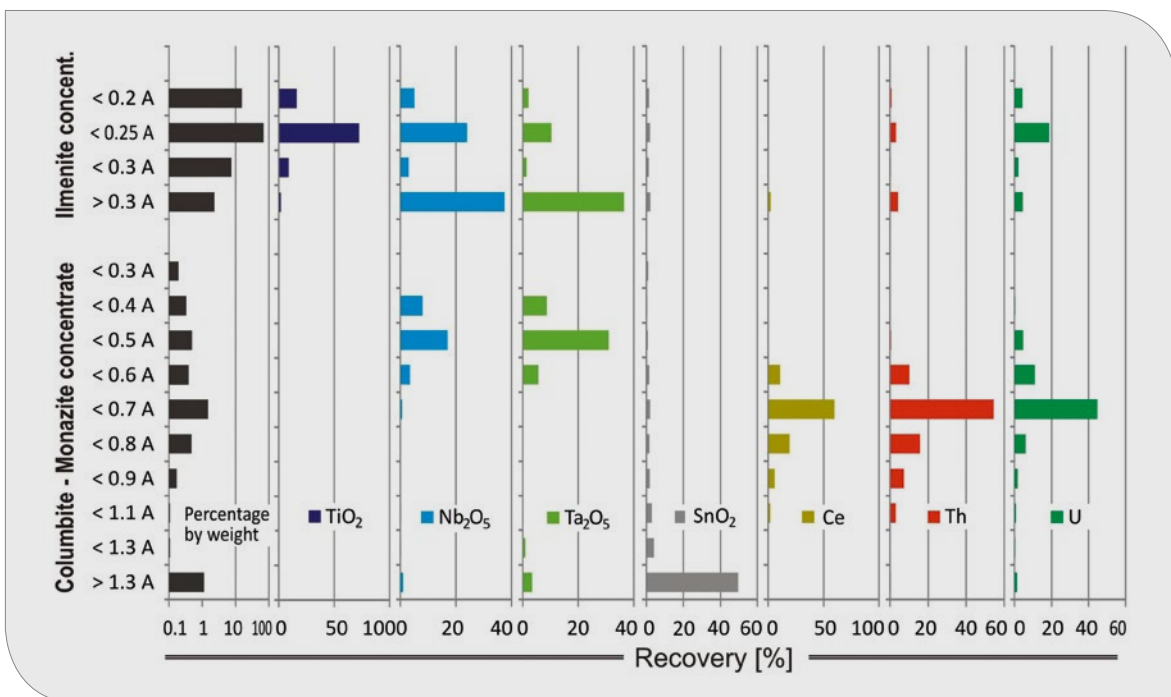


Fig. 6.45: Recovery of the oxides after separation of the paramagnetic fraction by a Frantz magnetic separator.

The precise separation of the small columbite amount (about 1%) from ilmenite (95% of the paramagnetic fraction) still remains a challenge. It was possible to prepare concentrates of about 50% Nb₂O₅ and 10% Ta₂O₅, however, dilution of the concentrates by ilmenite still took place.

Bom Futuro – TB53

63–250 µm/HM1: The SnO₂ concentration could be increased from 42% to 67.2% by magnetic separation at 1.1 Tesla (diamagnetic fraction), but with a loss of SnO₂ into the paramagnetic fraction. The paramagnetic fraction still contained 18.2% SnO₂. Part of the SnO₂ was bound to Fe bearing rutile and pseudorutile, which was enriched in the paramagnetic fraction.

250–500 µm/HM1: The SnO₂ concentration could be increased from 66.8% to 76.3% by magnetic separation at 1.1 Tesla (diamagnetic fraction), but also here a loss of SnO₂ into the paramagnetic fraction occurred. The diamagnetic fraction mainly consisted of cassiterite and topaz.

500–710 µm/HM1: The SnO₂ concentration could only be minimally increased by magnetic separation. A percentage of 11.8% SnO₂ entered the paramagnetic fraction, thus reducing recovery.

710–2000 µm/HM1: The SnO₂ concentration could only be increased from 24.4% to 28.5%, which additionally was associated with a loss of SnO₂ into the paramagnetic fraction (Fig. 6.47).

An optimization of the cassiterite recovery could be possible if the magnetic separator is applied at a magnetic field strength between only 0.8 and 1.0 Tesla. This could possibly prevent cassiterite losses into the paramagnetic fraction. Furthermore, it is doubtful whether magnetic separation at the >500 µm grain size should take place at all: The small increase of the SnO₂ concentration in the diamagnetic fraction was associated with huge SnO₂ losses into the paramagnetic fraction.

Nb₂O₅ and Ta₂O₅ could not be further enriched as independent minerals. The total concentrations were only 0.016 and 0.01% respectively.

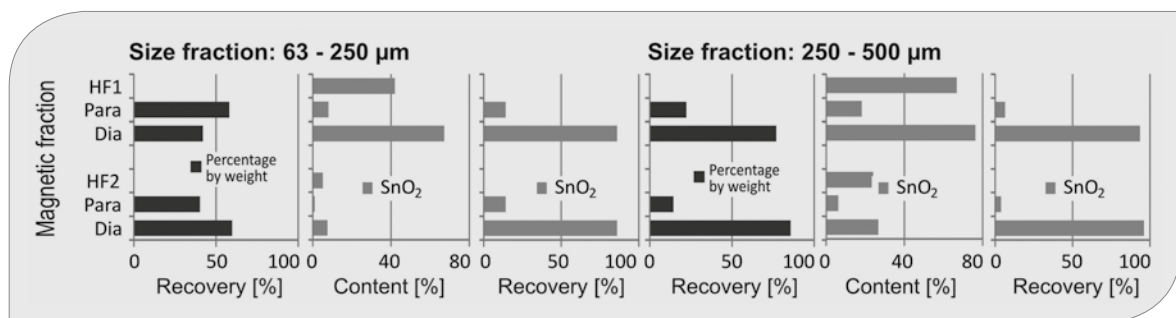


Fig. 6.46: Concentrations and recovery rates in the magnetic fractions of the 63–250 and 250–500 µm grain size fractions – TB53.

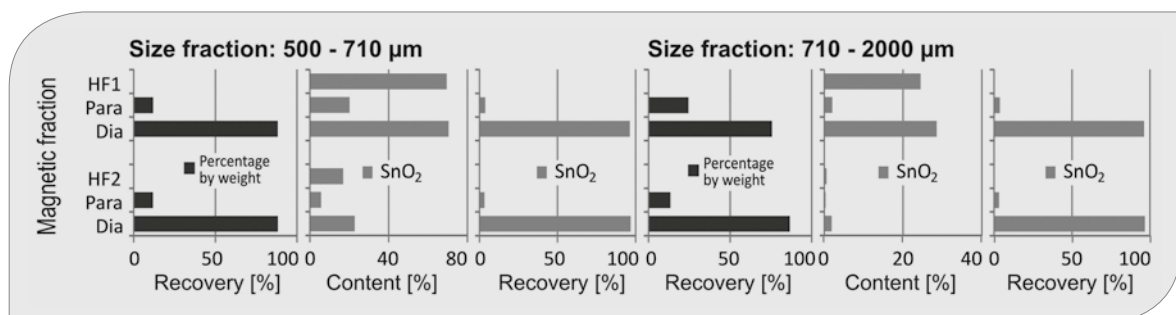


Fig. 6.47: Concentrations and recovery rates in the magnetic fractions of the 500–710 and 710–2000 µm grain size fractions – TB53.

Cachoeirinha – TB55

Sample TB55 not only contained a lot of cassiterite but also columbite, which can be separated very satisfactorily. Experience has shown that the cassiterite is transferred into the diamagnetic fraction, and the columbite into the paramagnetic fraction.

In all diamagnetic fractions of HF1, SnO_2 concentrations of >50% were achieved with a recovery of

>80%. The HF2 fractions likewise contained considerable SnO_2 concentrations, so that HF1 and HF2 together should be considered as a concentrate. Overall, only a small amount of SnO_2 entered the paramagnetic fraction. Columbite was strongly enriched in the paramagnetic fraction. Part of the Nb_2O_5 and Ta_2O_5 were also transferred into the diamagnetic fraction because the cassiterite contains Nb and Ta, either as columbite inclusions or incorporated into the crystal lattice. It is reasonable to

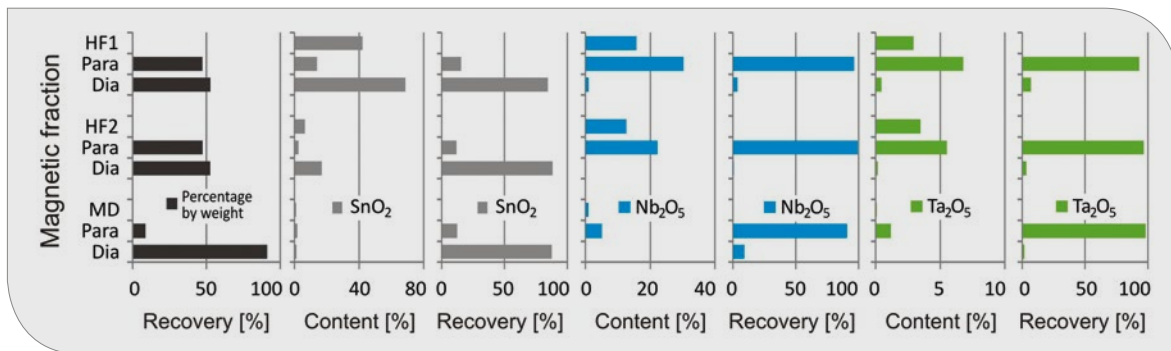


Fig. 6.48: Concentrations and recovery rates in the magnetic fractions of the 63–250 μm grain size fraction – TB55.

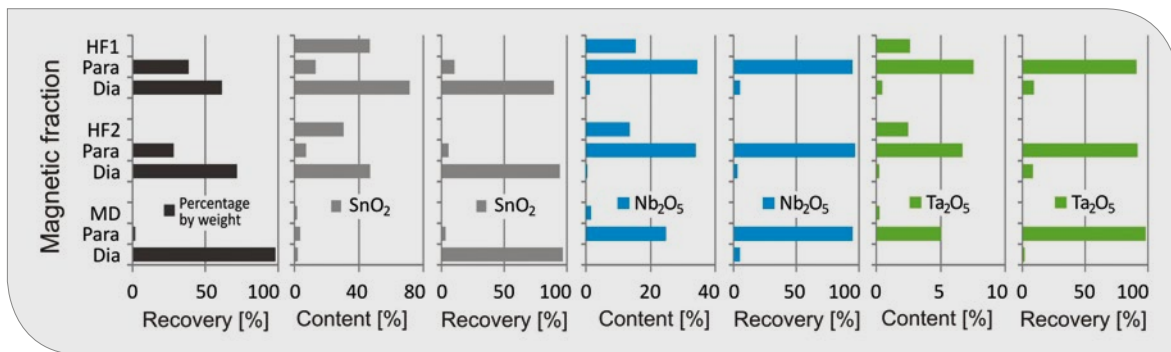


Fig. 6.49: Concentrations and recovery rates in the magnetic fractions of the 250–500 μm grain size fraction – TB55.

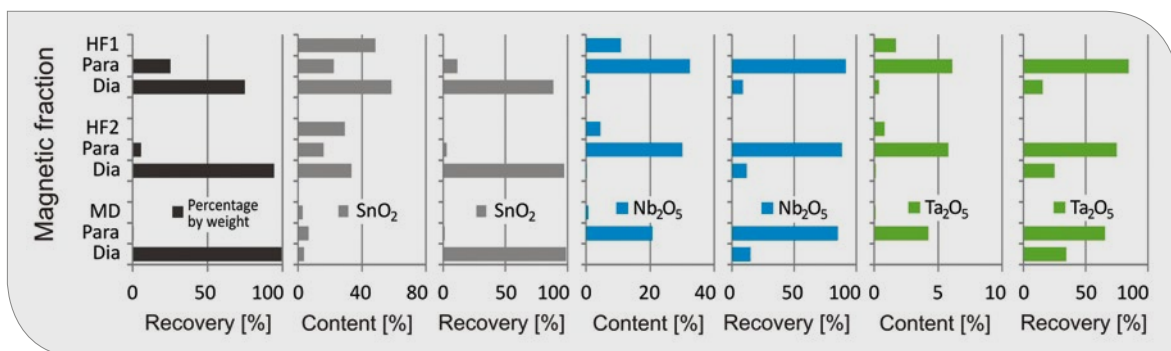


Fig. 6.50: Concentrations and recovery rates in the magnetic fractions of the 500–710 μm grain size fraction – TB55.

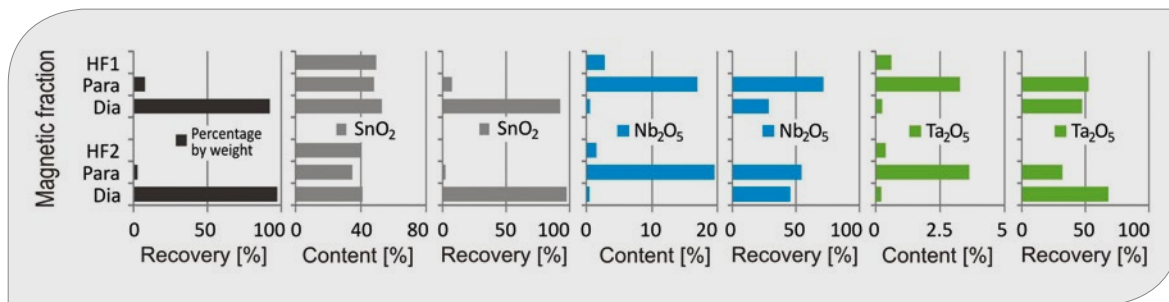


Fig. 6.51: Concentrations and recovery rates in the magnetic fractions of the 710–2000 μm grain size fraction – TB55.

subject the MD fractions to magnetic separation after density separation was conducted, because Nb_2O_5 and Ta_2O_5 could be further enriched from low concentrations (<1 %) to up to 25 %.

Unfortunately, the $\text{Nb}_2\text{O}_5/\text{Ta}_2\text{O}_5$ content in the cassiterite had to be rated as a loss. It is transferred into the slag during tin smelting. The slags could be significantly enriched in $\text{Nb}_2\text{O}_5/\text{Ta}_2\text{O}_5$ and thus be considered as an additional raw material after Sn removal.

Santa Bárbara – TB59

Both $\text{Nb}_2\text{O}_5/\text{Ta}_2\text{O}_5$ and SnO_2 could not be enriched by magnetic separation because the minerals could not be separated. The majority of mineral grains bearing the valuable elements were intergrown with Fe hydroxides and clay minerals. Under the present conditions no saleable concentrate could be produced from the sample material TB59.

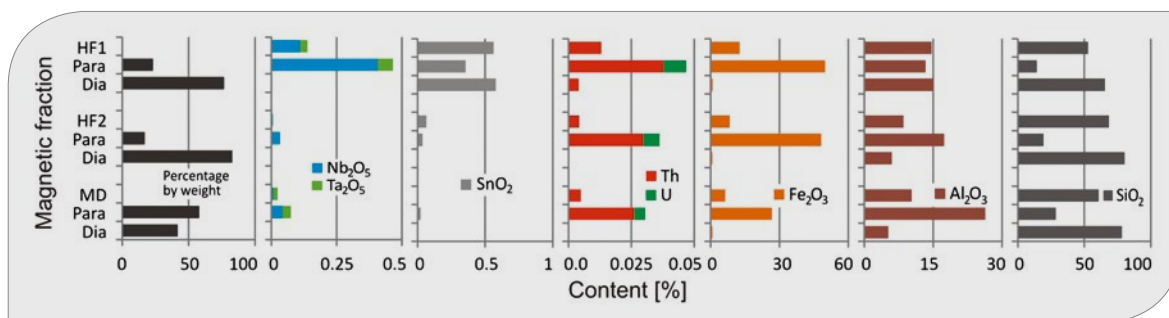


Fig. 6.52: Concentrations and recovery rates in the magnetic fractions of the 200–630 μm grain size fraction.

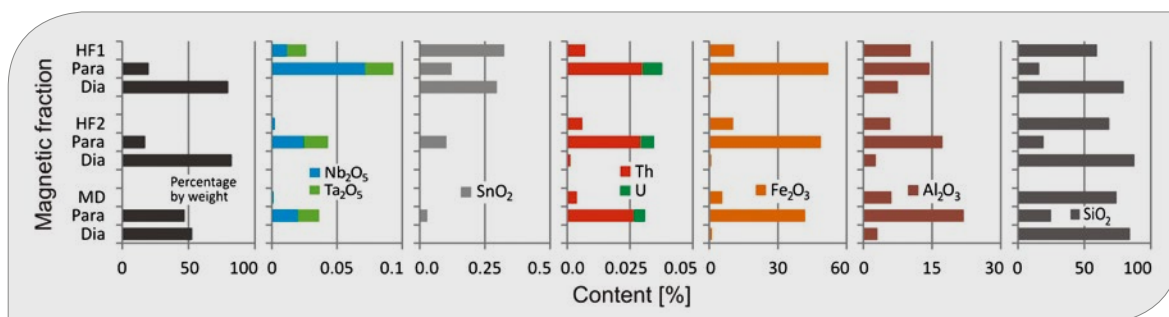


Fig. 6.53: Concentrations and recovery rates in the magnetic fractions of the 630–2000 μm grain size fraction.

6.8.5 Monazite flotation (experimental set-up)

Comminution method and results

A shaking table concentrate of the 250–500 μm size fraction was ground in a rod mill (25 kg rod charge, 50 wt. % solids in pulp). In order to properly prepare the feed for the flotation, the sample was ground in 3 steps with identification of the D80 of the mill discharge after each round. The cumulative comminution times used were: 3, 6, 9 and 13 minutes. Additionally, the material was de-slimed at $-10\ \mu\text{m}$ after each round.

After 3 minutes of comminution, the D80 was at around 250 μm with roughly 5% of the material coarser than 315 μm . The second step of comminution resulted in 5% oversize 200 μm . The estimated D80 was around 170 μm . After 9 minutes of grinding, the D80 was appropriate for the froth flotation test at 120 μm . 13 minutes of comminution provided a D80 of around 70 μm , which implies better mineral liberation. However, the cumulative slime quantity ($<10\ \mu\text{m}$ particles) after 13 minutes of comminution exceeded 20 wt. % of the total feed. It was thus decided to use 10 minutes of comminution, which resulted in a D80 of around 100 μm .

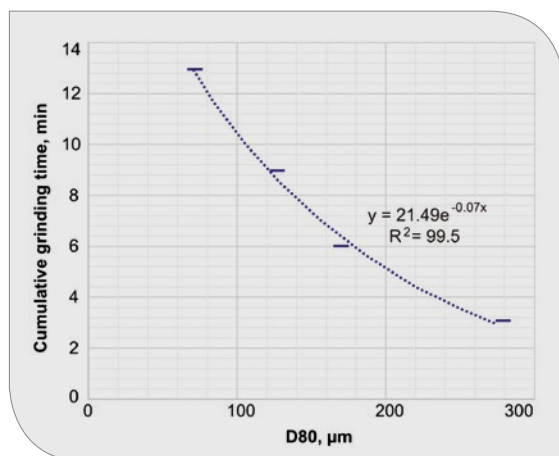


Fig. 6.54: Forecasting model for the grinding time.

Flotation methods and results

Two kinetic tests were performed: With depressant and without. Silica glass (Na_2SiO_3) was used as

the depressing agent at a dosage of 500 g/t. Fatty acids collector (Flotisor FS-2) was applied at a dosage of 300 g/t in a trial test (without depressor), and at 150 g/t in a correction test (with depressor). Even though fatty acids have a frothing action to a certain extent, one drop of frother was utilized in the tests to ensure the froth stability (approx. 25 g/t).

To decrease the entrapment effect and increase froth drainage capacity, the collector was added in 3 steps. The trial test had conditioning steps with 50 g/t, 100 g/t and 150 g/t collector. The correction test with silica glass used 25 g/t, 50 g/t and 75 g/t FS-2. A conditioning time of 10 min was used at each conditioning stage to enable collector attachment.

Concentrates collection was performed during 6 minutes total after each conditioning stage: 1 min, 2 min, and 3 min. As a result of the trial test without depressant, 99 wt. % of a feed sample was collected for 3 concentrates, see figure 6.55. The application of lower collector dosages and depressors during flotation enabled adequate flotation concentrate mass pulls to be achieved.

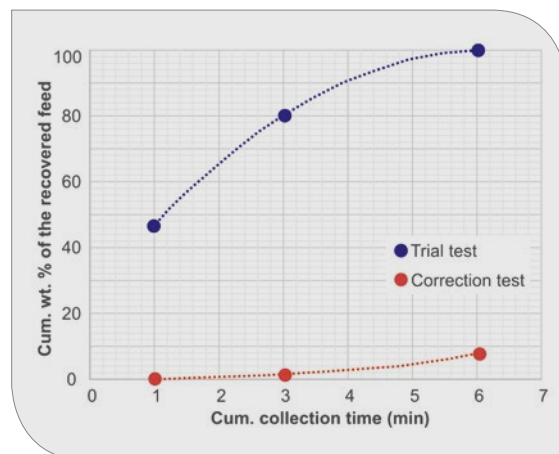


Fig. 6.55: Mass pulls of trial and correction tests.

The results of the analysis of 3 concentrates in a trial test revealed that there is extremely small selectivity between element recovery when the reagent scheme was only based on fatty acids with Flotanol frother. As shown in figure 6.56, the fastest recovery is observed for Ce, which represents monazite, while the slowest kinetics of Zr and Si, characterize zircon floatability.

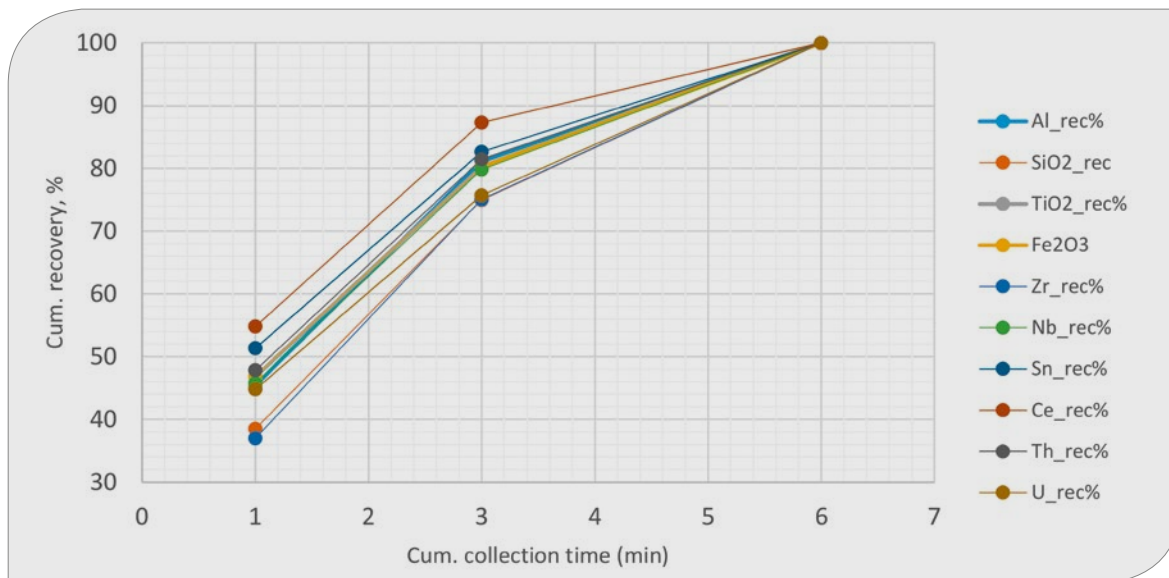


Fig. 6.56: Component recovery of the trial test concentrate.

These results revealed the need for adjustments through collector dosage reduction and depressor usage, which was performed in the correction test. Thus, the application of depressant and reduction of the collector enabled selectivity towards monazite flotation (Ce recovery) to be achieved, as shown in figure 6.57.

It is also notable that the depressant effect of silica glass significantly reduces after approx. 23 minutes

of flotation. It is expressed through an increase in the slope of the recovery lines for all analyzed elements (Fig. 6.57).

By performing element-to-mineral conversion with stoichiometric mineral formulas, a rough value for mineral grades and corresponding recovery rates were obtained. For example, the grade-recovery plot for monazite recovery in a correction kinetic test was obtained (Fig. 6.58).

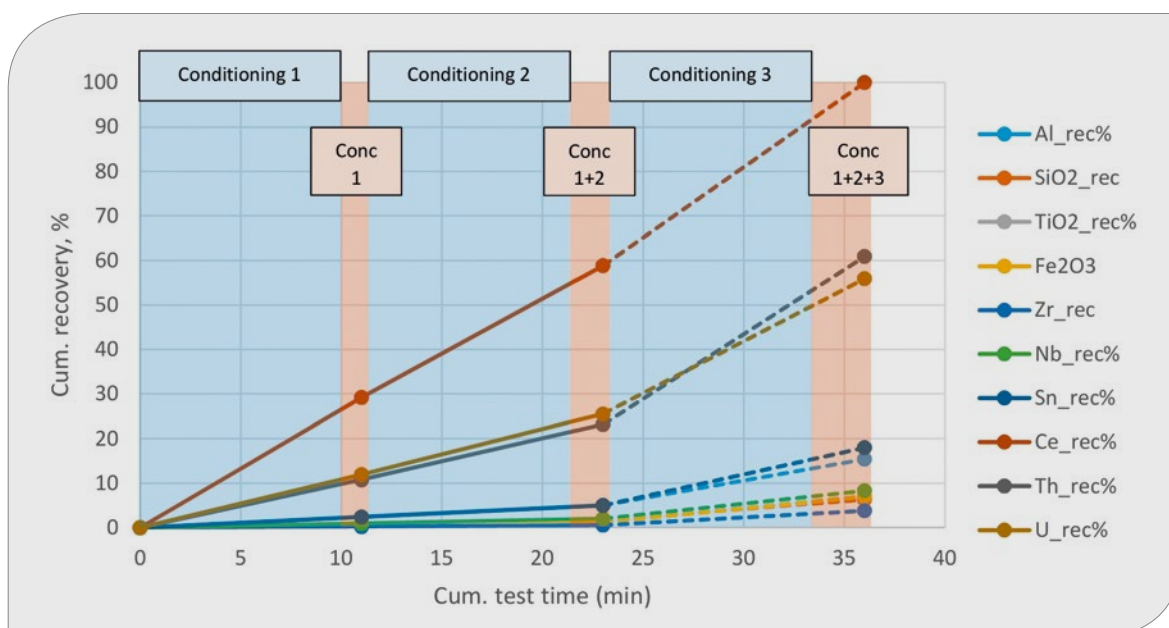


Fig. 6.57: Cumulative element recovery dynamics for the correction test.

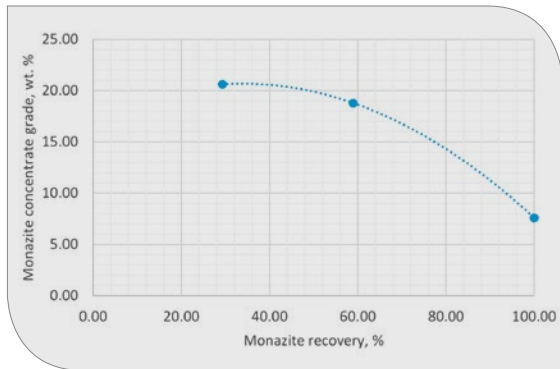


Fig. 6.58: Monazite grade-recovery plot, correction test.

Principal component analysis (Fig. 6.59) of the results revealed a strong correlation between Ce, P_2O_5 , Y, La, Th and U grades in the samples, which indicates their affiliation to one phase: Monazite. There are also correlations between Ca and Si contents, which could be attributed to the presence of garnet in the samples. Tantalum content according to the analysis is correlated to zircon. Fe, Mn and Ti are components that constitute ilmenite composition in the sample. Hf vector length and an angle of less than 45 degrees of the Zr vector indicates an incorporation of the element Hf within the mineral zircon. The close proximity of zircon and ilmenite-composing elements on the circular

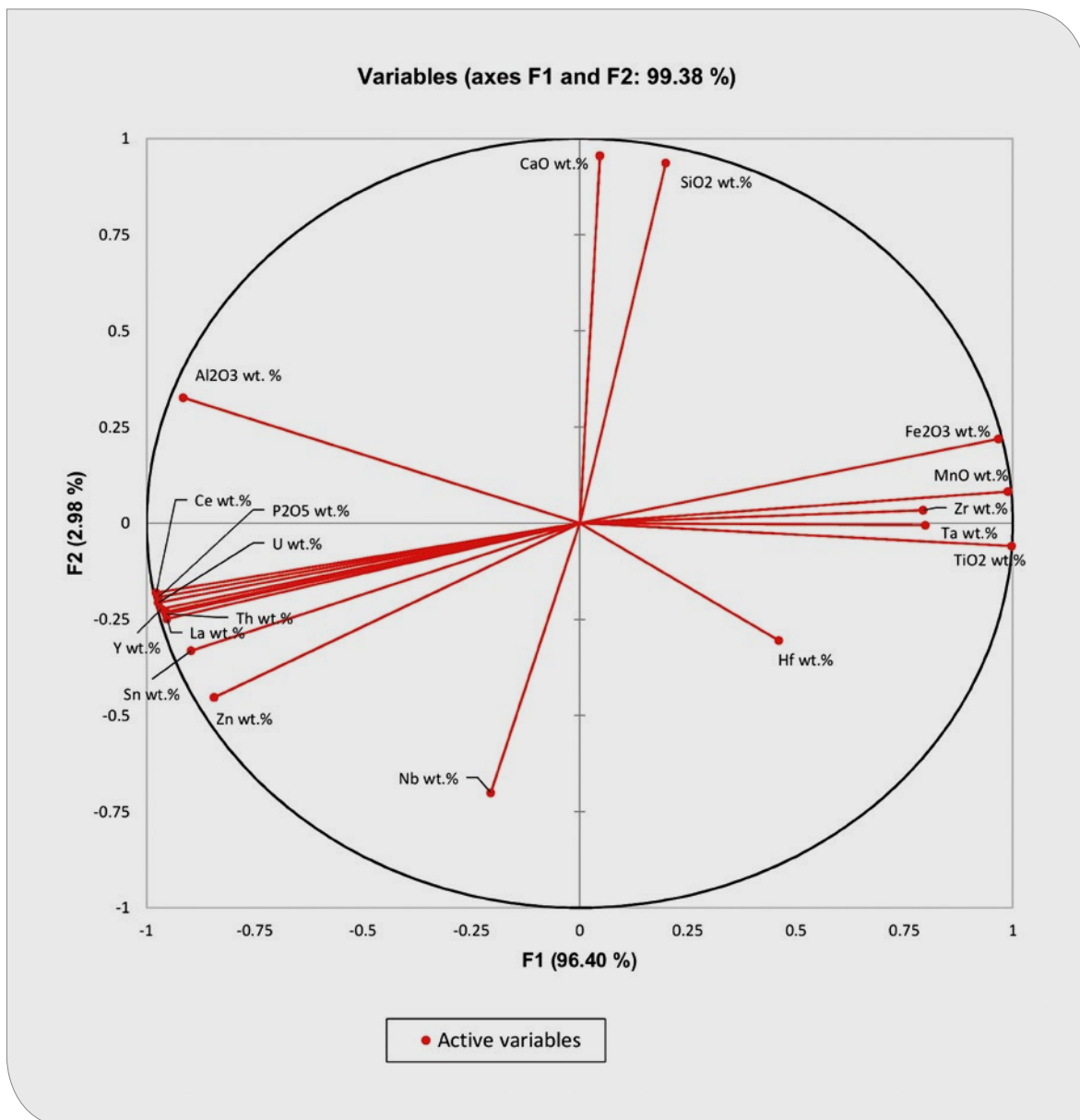


Fig. 6.59: Principal component analysis of flotation products.

PCA plot confirms the fact that these minerals possess similar floatabilities and that their separation in neutral-alkali milieu is hard to achieve with a fatty acid collector.

Discussion of the flotation tests

A reagent scheme with 150 g/t fatty acids (FS-2) and 500 g/t silica glass showed adequate mass pulls for the flotation. The collector dosage could be reduced even more. Depressor agent was effective for selective monazite recovery. Further optimization of the reagent dosages is needed: This will involve a matrix of experiments (9 tests with variable reagent dosages) to allow the results to be modelled. Other reagent schemes should be also tested to find the most feasible solution.

All tests were performed at a natural pH (weak alkali). The influence of pH on the flotation performance should be studied further. The application of different pH levels may help to optimize the reagent scheme and improve the flotation selectivity.

Even though U and Th seem to be strongly correlated to the Ce and P_2O_5 values (which indicates their association with monazite), the PCA results do not fully explain why around 40% Th and around 45% U were not recovered within the monazite concentrate (which contained 100% Ce and 100% P_2O_5 by distribution). Further testing would improve the statistical significance of the principal component analysis, check the measurement and sampling errors, and discover what share of radioactive elements are associated with monazite, and if there are some other phases with radioactive compounds.

Element to mineral conversion is based on a stoichiometric formula, which makes mineral grade results uncertain. Increasing the number of tests could help generate a rough estimation of the element coefficients in the minerals, and establish mineral formulas in the ore. This could make mineral recovery rates and mineral grades more reliable. Dealing with minerals rather than elements makes it possible to perform simulations. This enables more comprehensive analysis, and furthers the improvement of process performance.

6.8.6 Radiation measurements and separation of radioactive minerals

Results and recommendations of different separation methods

Both the total and the SEM-EDX analysis showed that a significant amount of Th and U can occur as accompanying elements in various minerals. Mainly monazite, zircon, xenotime, bastnaesite and pyrochlore were identified as Th and U bearing minerals. The different content of the minerals and their respective Th and U concentrations produce radioactive radiation, which can be detected as dose rates and as alpha, beta and gamma radiation. Because these minerals mainly accumulate in the heavy mineral concentrates, the Th and U contents also increase in these fractions. The local dose rate and alpha, beta and gamma radiation increase with increasing concentrations of heavy minerals.

In heavy mineral concentrates, the following Th and U bearing minerals were identified (Tab. 6.14).

Massangana – TB45-48

Both in the fine and in the coarser particle size ranges, increases in the local dose rate, and the alpha, beta and gamma radiation occurred as a result of heavy mineral accumulations. Local dose rate increases were observed especially in the >500 μm fractions (Fig. 6.60).

In TB45-48, monazite and zircon occurred as Th and U bearing minerals. Th and U bearing Nb-rich phases (like pyrochlore) occur especially in the coarse fraction. No Th and U was detected in fine-grained columbite. However, monazite was analyzed containing up to 2.3% Th in the 500–710 μm fraction. The main radioactive mineral is monazite.

The comparison of Th contents and dose rates showed very good correlation (Fig. 6.61c). It was possible to determine the Th content with sufficient accuracy by means of the local dose rate. Because the main Th bearing mineral in the <500 μm particle size fraction is monazite, it is thus also possible to determine the Ce or REE contents to a certain extent (Fig. 6.61d).

Samples with different concentration grades had to be precisely analyzed by means of the local dose rate to calibrate the monazite, and thus also the Th contents, in the concentrates. Furthermore, the measurement always had to take place under the same conditions with the same volume and

the same measuring device. Under these conditions, the monazite/REE content, and thus also the Th-content, could be determined via the local dose rate.

Tab. 6.14: Single-grain measurements of Th and U bearing minerals by SEM-EDX (Erz & Stein).

Grain size	Mineral	TB45-48	TB53	TB55	TB59
63–200	Monazite	up to 1.0 at% Th, 0.2 at% U	up to 0.4 at% Th, 2.9 at% U		
	Zircon			up to 0.3 at% Th, 0.1 at% U	up to 1.4 at% Th, 0.2 at% U
	Xenotime				
200–630	Monazite	up to 2.3 at% Th	up to 0.8 at% Th, 0.2% U	up to 0.8 at% Th, 0.1 at% U	up to 0.6 at% Th
	Zircon	up to 0.3 at% Th	up to 1.8 at% Th		up to 1.0 at% Th, 0.2% U
	Xenotime		up to 0.25 at% U		up to 0.6 at% Th, 0.12 at% U
630–2000	Monazite	up to 1.2 at% Th		up to 0.5 at% Th	
	Zircon				up to 1.6 at% Th
	Xenotime		up to 0.3 at% Th, 0.95 at% U		
	Bastnaesite				up to 0.4 at% Th
	Nb-Y phase (Pyrochlor?)	up to 0.6 at% Th, 0.5 at% U			

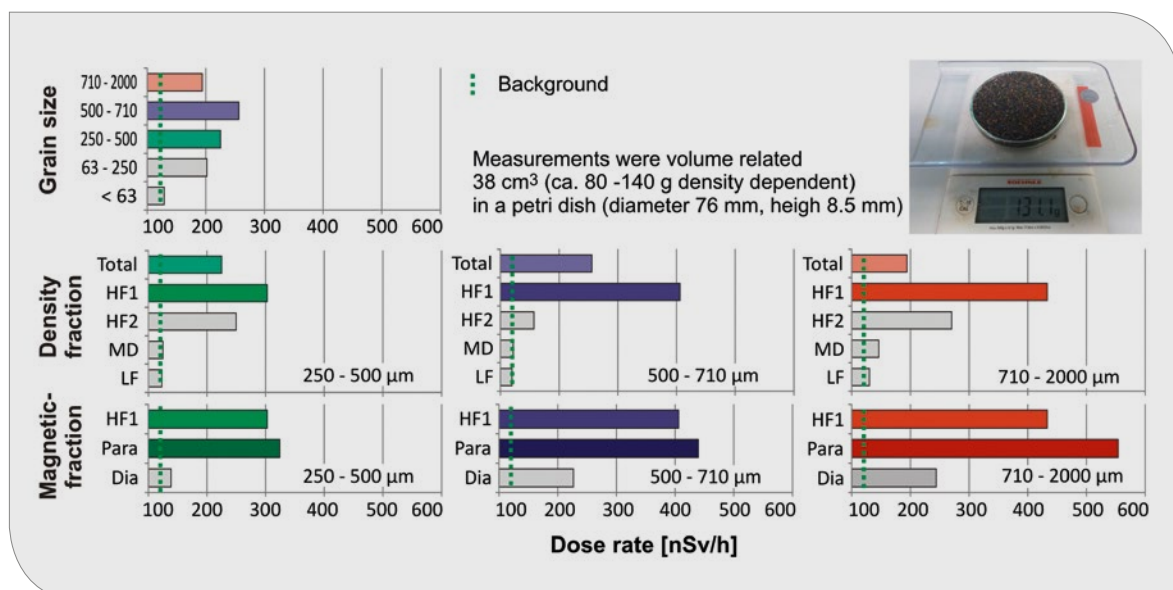


Fig. 6.60: Variations and changes in the local dose rate during processing.

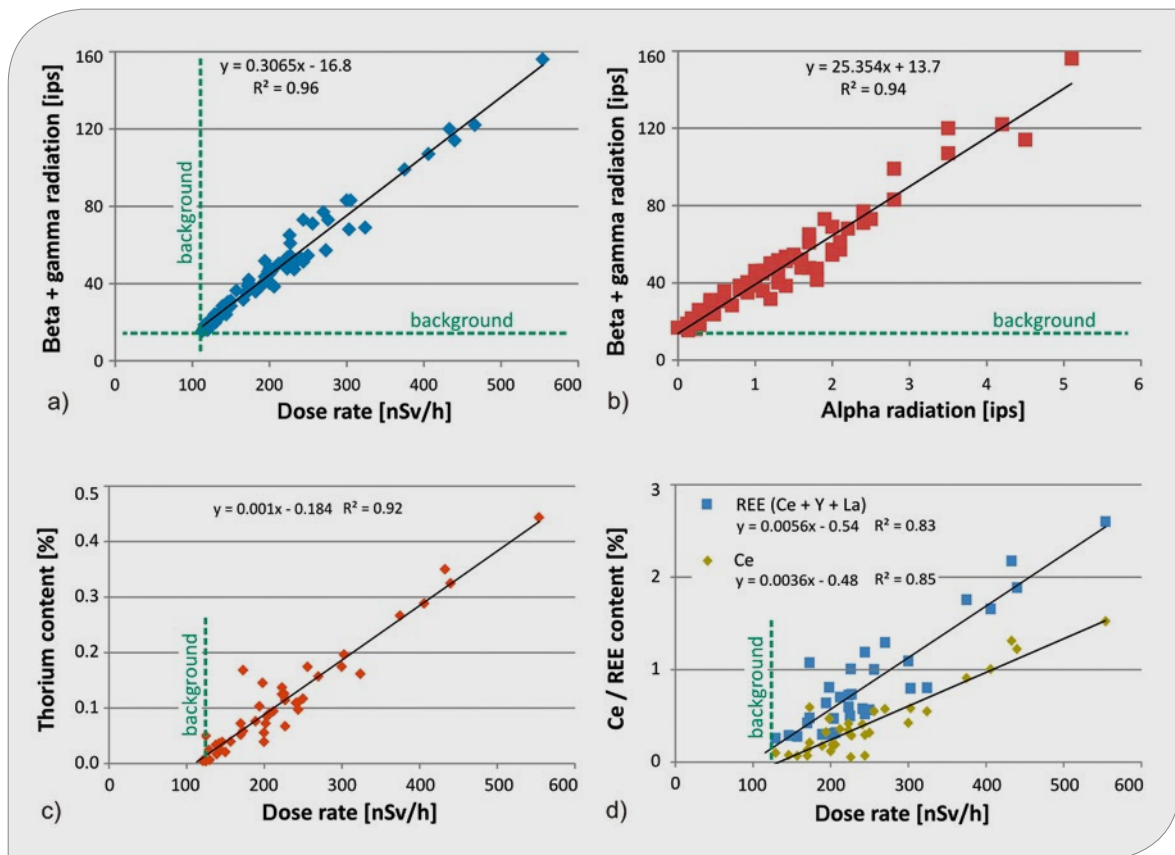


Fig. 6.61: Comparison of the measured a) Dose rate/alpha radiation, b) Alpha/beta + gamma radiation, c) Dose rate/Th content and d) Dose rate/Ce, REE contents in sample TB45-48.

Under the present conditions, the following function could be derived for the Th content of the samples at a given dose rate:

$$\text{Th content} = 0.01 * \text{Local dose rate} - 0.1084 \quad (\text{Equation 1})$$

The present equation takes into account the ambient/environmental background value, and has to be validated or re-determined according to local conditions.

A detailed determination of the local dose rate on the 250–500 μm , HF1/HF2 and 500–710 μm fractions, revealed for HF1 that there is a logarithmic increase of the local dose rate as a function of the mass (Fig. 6.62a). It was observed that the 500–710 μm fraction exhibited a local dose rate almost twice as high as the 250–500 μm fraction. According to Equation 1, it can be anticipated that this grain size fraction contains considerably higher Th contents.

The paramagnetic concentrates of the 250–500 μm , HM1 and HM2 particle size fractions were separated by means of an NdBF₆ paramagnet (0.47 Tesla) into a monazite-columbite (cassiterite) concentrate and an ilmenite-rich concentrate (Fig. 6.62b). The ilmenite-rich concentrate barely showed any increased local dose rate. Almost the entire radiation strength was attributable to the monazite concentrate.

The monazite concentrate was not available as pure monazite. It contained, among other things, almost the complete columbite and Fe bearing cassiterite. Clarification is required to determine which of the minerals are responsible for the increased radiation exposure.

By using a Frantz magnetic separator, the ilmenite and monazite concentrates were separated from 250–500 μm , HF1 in very small steps. This allowed a further separation of the individual minerals. It was very clear from the results that no increase

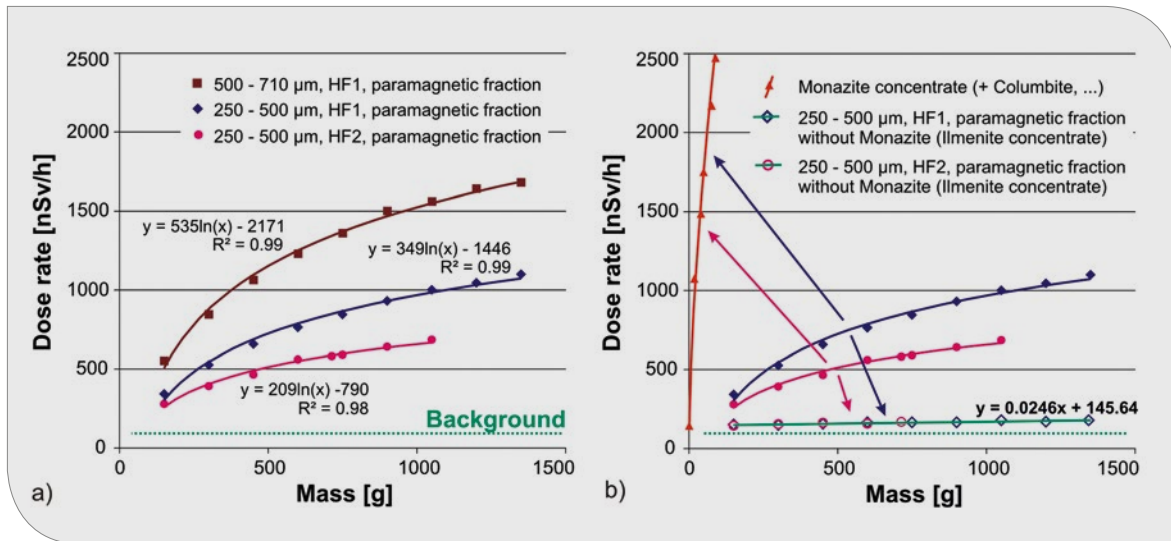


Fig. 6.62: a) Mass-dependent local dose rate on HM1 and HM2 concentrates of sample TB45-48, b) Separation of the local dose rate by magnetic separation at 0.47 Tesla into a monazite concentrate and an ilmenite concentrate.

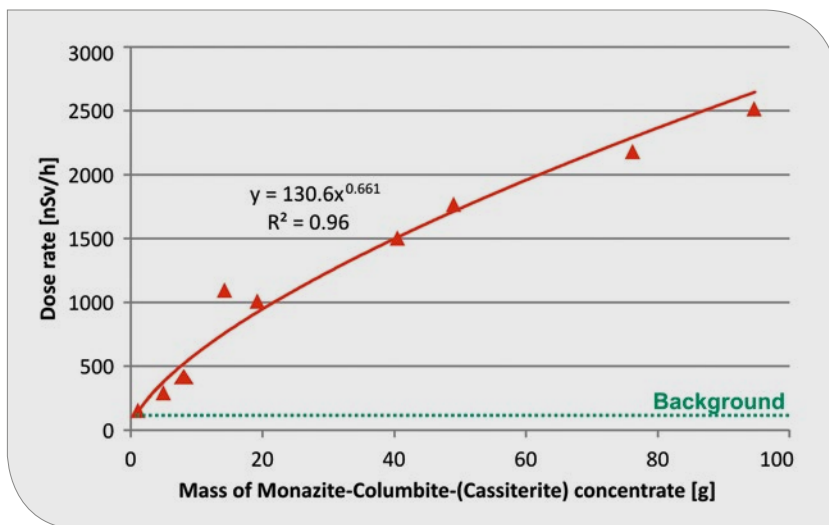


Fig. 6.63: Mass-dependent local dose rate in monazite concentrates.

in local dose rate occurred in the <0.5 A fractions. The local dose rate and thus also the radiation only increased very strongly with elevated levels of Ce, Th and U. The Th and U contents together reached concentrations of more than 4 %.

Furthermore, it was estimated that the columbite can be strongly concentrated by magnetic separation (60 % $\text{Nb}_2\text{O}_5/\text{Ta}_2\text{O}_5$) and that this has no immediate relation to higher Th and U levels causing an elevated local dose rate or radiation. This means that almost the entire radiation is related to the monazite. Thus, it is up to the skill of the processing engineer to produce highly enriched concentrates

from the low-concentrated $\text{Nb}_2\text{O}_5/\text{Ta}_2\text{O}_5$ fractions, which at the same time exhibit hardly any radiation.

Bom Futuro – TB53

In sample TB53, monazite, zircon and xenotime occurred as Th and U bearing minerals. There is a dependency on the local dose rate and on alpha, beta + gamma radiation, but this was not as pronounced as in TB 45-48. This was due to the considerably lower Th contents as shown in figure 6.66.

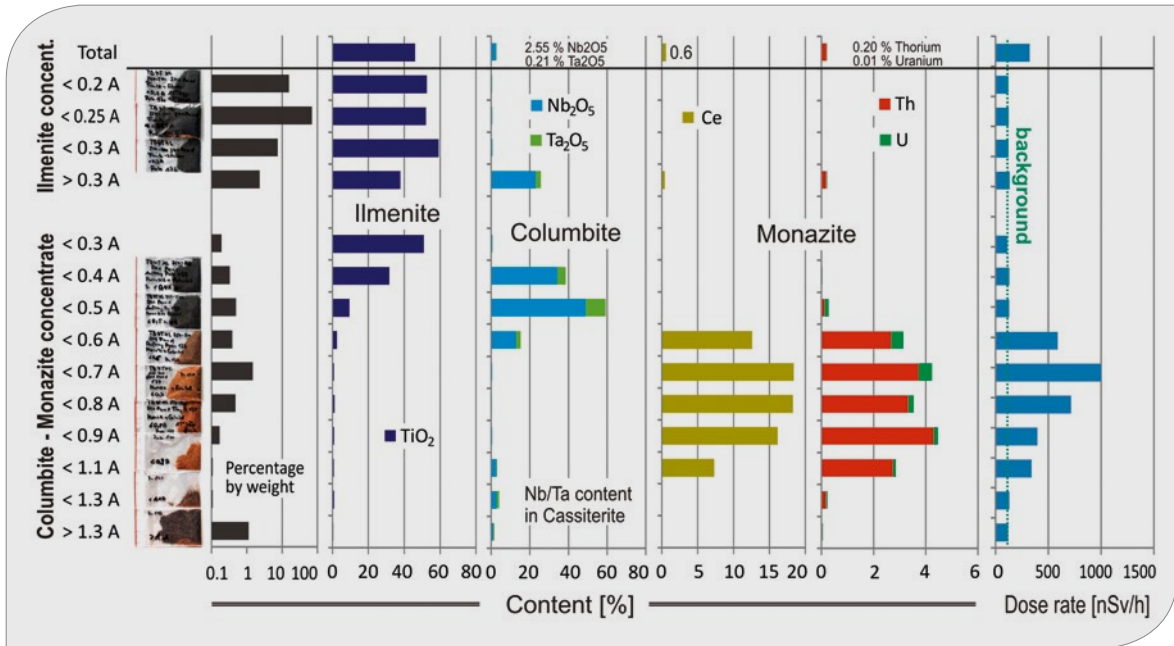


Fig. 6.64: Detailed separation of the ilmenite and monazite concentrate from 250–500 μm, HF1 – distribution of elements, minerals and local dose rate as a function of the field strength on the Frantz magnetic separator – photos (left side) show the typical yellow-orange color of monazite.

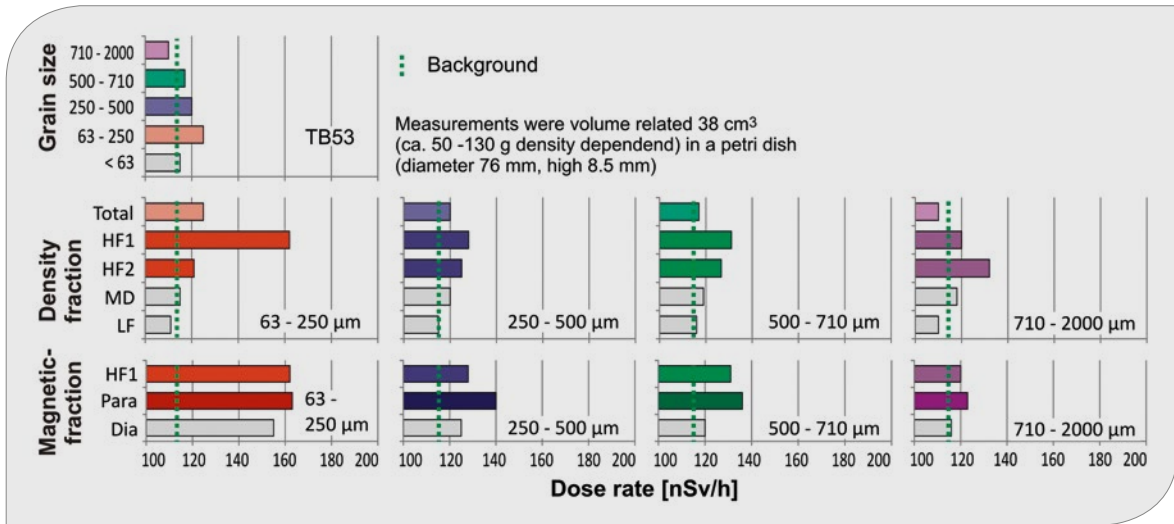


Fig. 6.65: Variations and changes in the dose rate during processing – sample TB53 – Bom Futuro.

A small increase in the local dose rate occurred in the fine-grained fraction in both the paramagnetic and diamagnetic fractions. The local dose rate increase in the paramagnetic fraction was due to small amounts of xenotime and monazite. The monazite can contain up to 2.9% U and 0.4% Th. In the diamagnetic fraction, U and Th can be bound to zircon.

It was not possible to compare the local dose rate and uranium content because most U levels were below the detection limit. In conclusion, the increase in the local dose rate during the concentration of valuable minerals was estimated to be low.

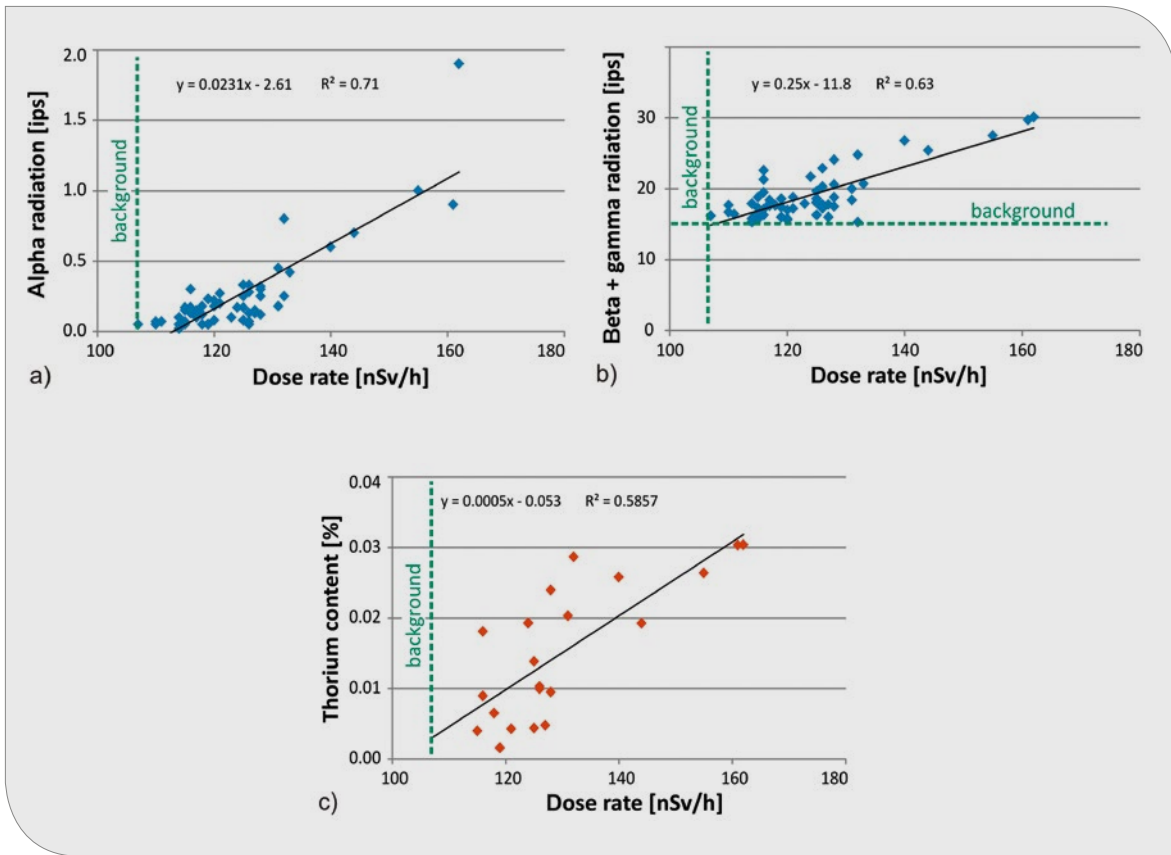


Fig. 6.66: Comparison of the measured a) Local dose rate/alpha radiation, b) Alpha/beta + gamma radiation and c) Local dose rate/Th content in sample TB53.

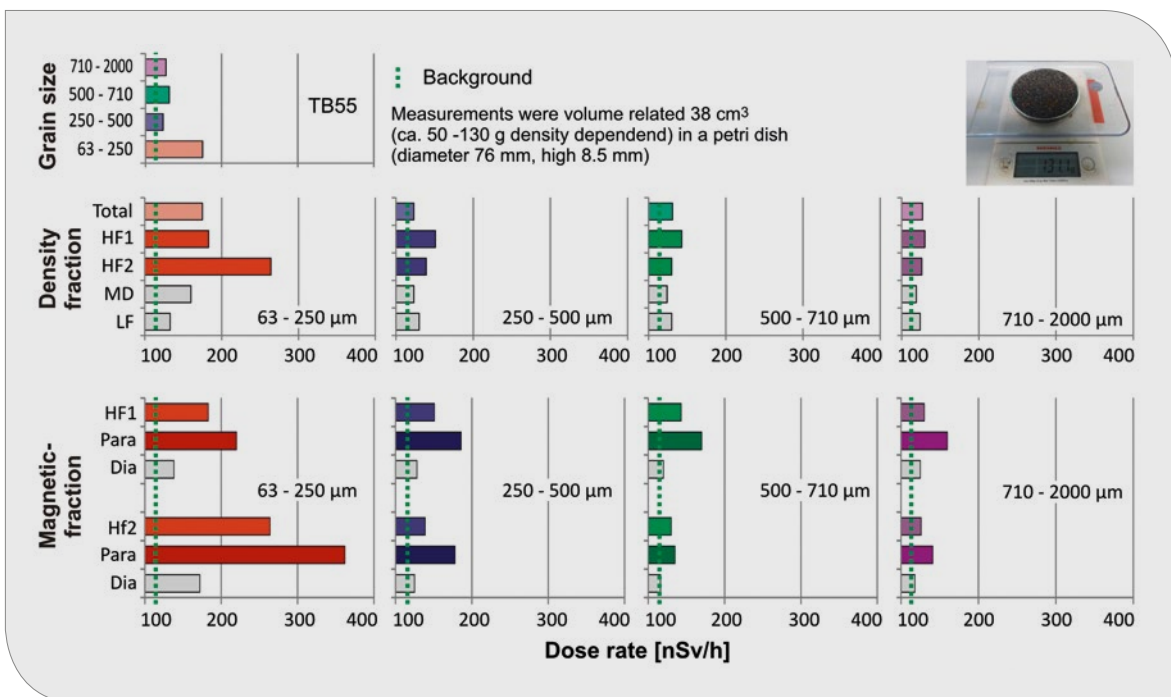


Fig. 6.67: Variations and changes in local dose rate during processing – sample TB55 – Cachoeirinha.

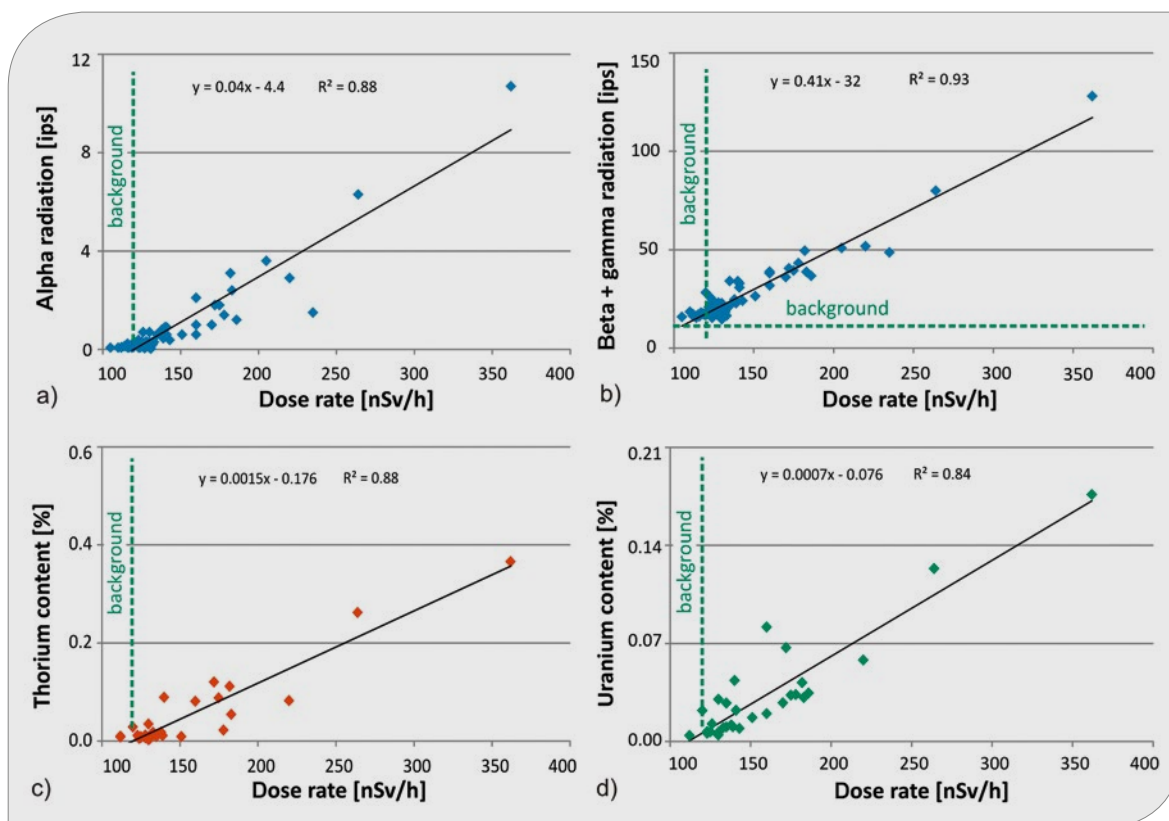


Fig. 6.68: Comparison of the measured a) Local dose rate/alpha, b) Local dose rate/beta + gamma radiation, c) Local dose rate/Th and d) U levels in sample TB55 – Cachoeirinha.

Cachoeirinha – TB55

In TB55, the Th and U contents were moderate. Only zircon with Th and U was detected in the smallest particle size fraction. In the coarser fractions, monazite was found as a Th and U bearing mineral. The highest local dose rate was found in the paramagnetic 63–250 μm , HF2 fraction, which correlated with high ZrO_2 levels (11% ZrO_2). The zircon contained 1.5% Fe and entered the paramagnetic fraction.

There is a clear correlation between local dose rate and Th/U contents. However, the total radiation was estimated to be low even for a high accumulation of valuable elements.

Santa Bárbara – TB59

Sample TB59 could not be enriched due to the insufficient degree of liberation of the minerals. Nevertheless, the local dose rate and alpha, beta + gamma radiation and Th contents were compared.

Apart from a slight correlation of the alpha/beta + gamma radiation, no further conclusions could be drawn (Fig. 6.69).

It was not possible to compare the local dose rate and uranium content because most U levels were below the detection limit. Although TB59 also contained Th and U bearing minerals (Tab. 6.14) such as monazite, zircon, xenotime and bastnaesite, these did not affect the local dose rate because the concentrations were too low.

The previous dose rate measurements were carried out on masses up to about 150 g. Even with masses of 2.8 kg, the measured increase in the local dose rate was only from 121 to 150 nSv/h.

Table 6.15 shows the concentrations and the recovery rates of Th and U in the samples in relation to different particle size ranges. Remarkably, the Th concentration in the paramagnetic fractions in TB45–48 increased to 0.24% during enrichment of the total sample. TB59 was not listed here.

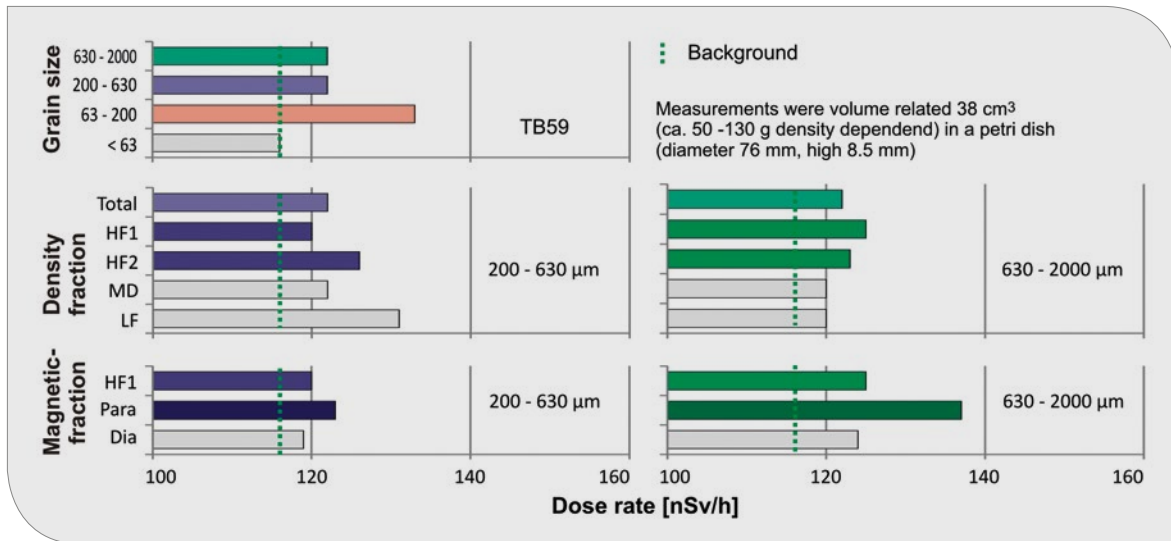


Fig. 6.69: Variations and changes in local dose rate during processing – Sample TB59 – Santa Bárbara.

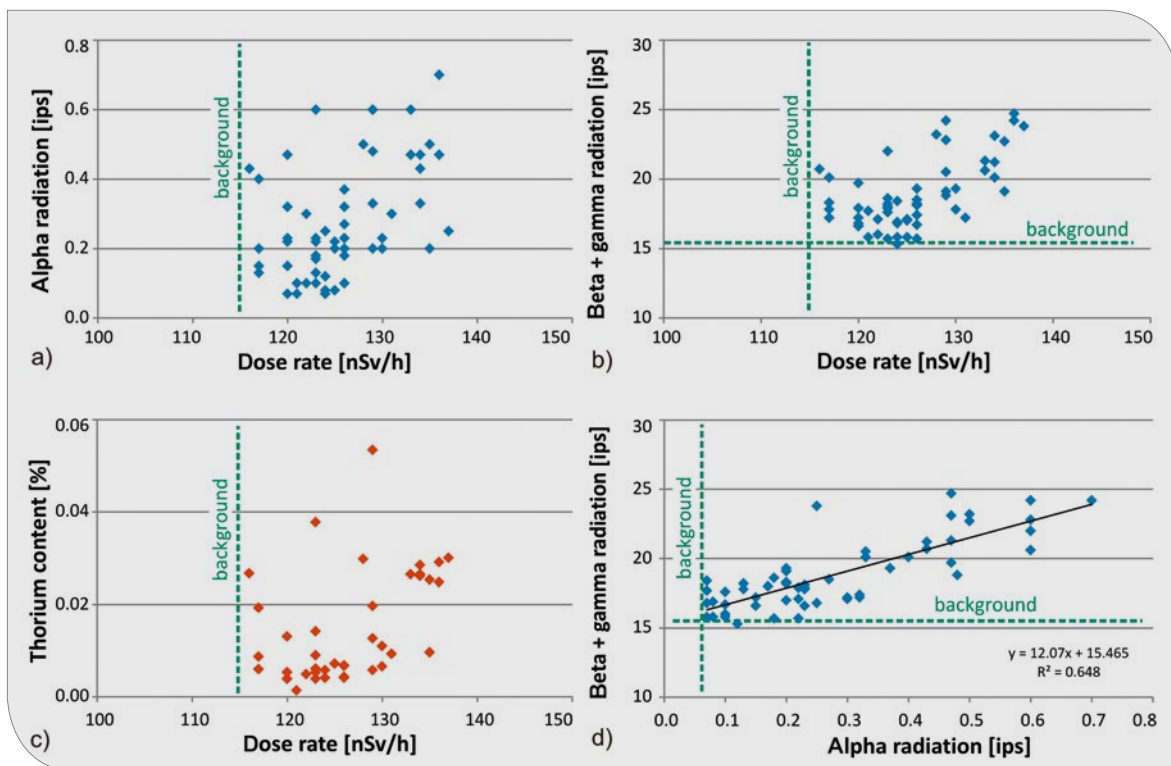


Fig. 6.70: Comparison of the measured a) Local dose rate/alpha, b) Local dose rate/beta + gamma radiation, c) Local dose rate/Th and d) alpha/beta + gamma radiation in sample TB59.

Precautions in handling Th and U bearing substances

EU hazard class 7 – Handling of radioactive substances, stipulates limits of <400 ppm Th, and

<100 ppm U. High levels of thorium and uranium were only found in the Massangana – TB45-48 deposit. The Th and U contents were mainly due to monazite, which was enriched in the paramagnetic heavy mineral fraction. It is necessary to separate

Tab. 6.15: Concentrations and recovery rates of Th and U in different particle size ranges.

Grain size [µm]	Density fraction	Magn. frac.	TB45-48				TB53				TB55			
			Th		U		Th		U		Th		U	
			rec.	con.	rec.	con.	rec.	con.	rec.	con.	rec.	con.	rec.	con.
			[%]		[%]		[%]		[%]		[%]		[%]	
< 500	HF1+HF2	Para	52.8	0.120	27.0	0.017	26.6	0.027	5.8	0.007	47.9	0.232	45.3	0.087
< 500	HF1+HF2	Dia	1.5	0.035	4.1	0.023	11.0	0.020	8.8	0.011	16.1	0.074	11.2	0.040
< 710	HF1+HF2	Para	71.8	0.173	38.8	0.017	29.4	0.027	6.5	0.007	48.1	0.231	49.5	0.082
< 710	HF1+HF2	Dia	2.4	0.042	9.4	0.037	11.7	0.019	10.2	0.010	17.0	0.070	12.6	0.036
< 2000	HF1+HF2	Para	84.8	0.208	48.3	0.023	37.6	0.023	10.6	0.006	48.2	0.230	51.3	0.080
< 2000	HF1+HF2	Dia	5.8	0.088	27.3	0.085	15.5	0.014	16.7	0.007	19.1	0.063	15.8	0.029
< 2000	HF1	Para	60.5	0.244	33.7	0.026	27.0	0.024	7.2	0.007	19.0	0.079	30.6	0.044
< 2000	HF1	Dia	3.1	0.072	11.8	0.071	10.4	0.020	8.5	0.008	4.9	0.005	6.7	0.007

rec.: recovery, con.: concentration

the monazite when the processing for columbite recovery. Special care is necessary when enriching the monazite, as the Th content in pure monazite can reach up to 4 %.

Thorium is both an α -emitter and a γ -emitter and this type of radiation is dangerous for inhalation and ingestion. Thorium bearing dusts are radiotoxic because of their respirability (deeply inhalable into the lungs) and can cause cancer.

When handling substances containing thorium, such as monazite, employees must not exceed a radiation dose of 1000 μ Sv/year (1 mSv/a). This can be monitored by the employees wearing so-called "finger ring dosimeters" (Fig. 6.71), which record the dose rate over a long period of time.

There is no "danger limit" for the local dose rate. Appropriate measures to reduce exposure have to be followed (restricting the duration of exposure/exposure time, increasing the distance, working with shielding).

The main problem with handling Th bearing substances is possible inhalation into the lungs. Inhalation of Th and U bearing monazite should be strictly avoided, as it may cause lung cancer. Therefore, the enrichment or separation of the monazite by magnetic separation should not be conducted under dry conditions.



Fig. 6.71: Examination of the dose rate by finger dosimeter (thermoluminescence detector made of lithium fluoride– 1.0 mSv to 10.0 Sv) – HARSHAW BTKD (2001).

The very good correlation of the dose rate with the thorium content (Fig. 6.61c) can be used as a simple means of monitoring the contamination of ilmenite, columbite or cassiterite concentrates with Th/monazite. For this purpose, a radiation detector is necessary (e.g. radiation detector PCE-RAM 10, price net: € 295). For calibration of the device, certified analysis of the chemical elements Th, U, Ce, La, Y, Nd, Zr (low, medium, high levels of monazite) would have to be carried out on a sufficient number of Th-U bearing samples. In addition, it would be necessary to have a defined sample volume (about 50 cm³), which is used to check that the same amount of sample material is used each time.

7 Economic approach and evaluation

All of the raw materials considered: Nb₂O₅, Ta₂O₅, SnO₂ and TiO₂ were enriched in the heavy fractions. The raw materials were present in different particle size and magnetic fractions. Only the heavy mineral fractions HF1 and HF2 were considered to determine the recovery.

The economic evaluation of pre-concentrates was conducted on the basis of certified chemical analysis by Actlabs/Canada (Section 5.1.3 – Analysis of heavy and light fractions – bromoform separations).

The prices for Nb₂O₅, Ta₂O₅, SnO₂ (Sn) and TiO₂ refer to the stock market prices of the following sources as at 24.07.2018:

London Metal Exchange – LME:

<https://www.lme.com/en-GB/Metals/Non-ferrous/Tin#tabIndex=0>

<https://minerals.usgs.gov/minerals/pubs/.../myb1-2013-niobi.pdf>

<https://www.metalary.com/niobium-price/>

<https://www.metalary.com/tantalum-price/>

<https://www.metalary.com/tin-price/>

<https://minerals.usgs.gov/minerals/pubs/mcs/2015/mcs2015.pdf>

<http://www.asianmetal.com>
(Sn, Nb₂O₅, Ta₂O₅, TiO₂)

The following prices in US\$/kg were used as a basis assuming that the given minimum concentrations for the produced concentrates were met:

In the following economic evaluation the values for Nb₂O₅ and Ta₂O₅ are calculated from the official market price and downscaled according to the actual content. Metal contents within the pre-concentrates below 0.5% of Nb₂O₅ and Ta₂O₅ are not considered due to economic reasons.

7.1 Massangana

1 t of pre-concentrate (bulk sample TB48-48) includes the following valuable substances:

Nb₂O₅ and Ta₂O₅ were almost completely enriched in the paramagnetic fraction. Nb₂O₅ and Ta₂O₅

Tab. 7.1: Prices for the elements/oxides for calculation of economic feasibility.

Mineral	Element/Oxide	[US\$/kg]	Source
Cassiterite	Sn	16.90	min 20% Sn, asianmetal.com
Columbite	Nb2O5	36.00	min 50% Nb ₂ O ₅ , 5% Ta ₂ O ₅ , asianmetal.com
Columbite	Ta2O5	211.00	min 30% Ta ₂ O ₅ , 15% Nb ₂ O ₅ , asianmetal.com
Ilmenite	TiO2	0.175	min 50% TiO ₂ , min 30% Fe, In port asianmetal.com

Tab. 7.2: Particle-size dependent element oxide concentrations and amounts of valuable substances with economic relevance in 1 t of pre-concentrate.

Grain size [µm]	TB45	Ta ₂ O ₅		Nb ₂ O ₅		SnO ₂		TiO ₂	
	[%]	[%]	[kg/t]	[%]	[kg/t]	[%]	[kg/t]	[%]	[kg/t]
63–200	7.5	0.077	0.767	0.821	8.21	1.764	17.6	38.4	384.5
200–630	64.7	0.082	0.822	0.865	8.65	2.317	23.2	35.9	359.2
630–2000	27.6	0.018	0.181	0.180	1.80	0.401	4.0	13.1	130.8
< 2000		0.064	0.639	0.670	6.70	1.741	17.4	29.7	297.2

Tab. 7.3: Recovery and concentration of element oxides after magnetic separation as a function of the separated particle size and density fractions in HF1 + HF2.

Grain size [μm]	Density fraction	Magn. frac.	Mass rec. [%]	TiO ₂		Ta ₂ O ₅		Nb ₂ O ₅		SnO ₂	
				rec.	con.	rec.	con.	rec.	con.	rec.	con.
< 500	HF1+HF2	Para	49.7	79.5	52.80	81.2	3.6	83.2	25.3	8.9	1.7
< 500	HF1+HF2	Dia	4.7	0.1	0.99	1.5	0.061	1.0	0.63	76.8	62.1
< 710	HF1+HF2	Para	56.0	89.3	52.58	89.4	2.6	92.1	22.4	10.8	1.6
< 710	HF1+HF2	Dia	6.7	0.1	0.90	1.8	0.052	1.2	0.55	83.9	57.2
< 2000	HF1+HF2	Para	59.5	94.3	52.32	91.4	2.2	95.5	21.3	11.3	1.5
< 2000	HF1+HF2	Dia	9.5	0.2	0.81	2.1	0.041	1.7	0.43	87.7	54.5

rec.: recovery, con.: concentration

together could be concentrated to about 29% with a recovery of 80–90%. The concentrations can be increased if the ilmenite is completely separated.

SnO₂ could be enriched in the diamagnetic fraction up to nearly 90%, but with only about 37% recovery if only the HF1 fraction (<500 μm) is used. From the total sample <2000 μm , 66% of the SnO₂ (recovery) was obtained with a concentration of about 57% in the diamagnetic fraction of the HM1

fraction. By removing the Sn from the paramagnetic fraction, the recovery increased to 87.7% at a concentration of 54.5% SnO₂. In addition to cassiterite, ZrO₂ accumulated in zircon up to 25% in the diamagnetic fraction (not shown).

Table 7.4: Economic evaluation of the pre-concentrate regarding Nb₂O₅, Ta₂O₅, Sn and TiO₂ amounts per ton of pre-concentrate in <2000 μm fraction (100%).

Tab. 7.4: Economic evaluation of the pre-concentrate regarding Nb₂O₅, Ta₂O₅, Sn and TiO₂ amounts per ton of pre-concentrate in <2000 μm fraction (100%).

Mineral	Element	Mass [kg/t]	Price [US\$/kg]	Total value [US\$/t (100%)]
Cassiterite	Sn	13.7	16.90	231.50
Columbite	Nb ₂ O ₅	6.7	36.00	241.20
Columbite	Ta ₂ O ₅	0.6	211.00	n.c.
Ilmenite	TiO ₂	297.2	0.18	53.50
Total				526.20

n.c.: not considered

Tab. 7.5: Grain-size related economic evaluation of all concentrates (based on 1 t of pre-concentrate).

Grain size [μm]	Total value recovery [\$/t]	Loss [\$/t]	Loss [%]
< 2000	509.90 (100%)		
< 500	404.90	105.0	20.6
< 710	445.90	64.0	12.6
< 2000	464.40	45.6	8.9

Further economically recoverable elements were zirconium in zircon and Rare Earth Elements – REE in monazite. The ZrO_2 content in the diamagnetic fraction increased up to 25 % (mainly in grain sizes $>500 \mu m$) and was present in addition to cassiterite. Cassiterite could be separated from zircon using electrostatic methods/processes. This enables strong increases in the cassiterite and zircon concentrations.

The Rare Earth Elements in monazite reached levels of $>22 \%$ (Ce, Nd, La, and Y). The monazite as the carrier of the radioactivity (Th and U contents) should be removed from the concentrates as completely as possible – feasible by magnetic separation. Consideration should be given to whether the monazite could/should be dumped due to its radioactivity or whether it would be suitable as a raw material for the production of REE metals.

7.2 Bom Futuro

1 t of pre-concentrate (bulk sample TB53) includes the following valuable substances:

Most of the paramagnetic fraction consisted of TiO_2 and Fe_2O_3 bearing phases. Rutile and ilmenorutile, together leucocoxene, occurred as a TiO_2 phase (about 40 % TiO_2). Initially diamagnetic rutile (TiO_2) entered the paramagnetic fraction because it contained Fe contents of up to 1.5%. In addition, the Ti phases contained Nb, Ta and Sn in low concentrations. No Nb_2O_5/Ta_2O_5 concentrate could be recovered from sample TB53 as the contents were too low and no substantial enrichment took place. The Nb_2O_5/Ta_2O_5 contents essentially were not attributable to independent mineral phases but were contained as trace elements and finest inclusions in the Ti and Fe phases.

Tab. 7.6: Particle-size dependent element oxide concentrations and amounts of valuable substances with economic relevance in 1 t of pre-concentrate.

Grain size [μm]	Mass share [%]	Ta_2O_5		Nb_2O_5		SnO_2		TiO_2	
		[%]	[kg/t]	[%]	[kg/t]	[%]	[kg/t]	[%]	[kg/t]
63–200	2.2	0.027	0.268	0.079	0.79	4.487	44.9	9.5	95.1
200–630	52.7	0.011	0.106	0.018	0.18	3.388	33.9	1.4	13.6
630–2000	44.9	0.009	0.085	0.011	0.11	1.929	19.3	0.3	2.8
< 2000		0.010	0.100	0.016	0.16	2.750	27.5	1.0	10.5

Tab. 7.7: Recovery and concentration of element oxides after magnetic separation as a function of the separated particle size and density fractions in HF1 + HF2.

Grain size [μm]	Density fraction	Magn. frac.	Mass rec. [%]	TiO_2		ZrO_2		Nb_2O_5		Ta_2O_5		SnO_2	
				rec.	con.	rec.	con.	rec.	con.	rec.	con.	rec.	con.
< 500	HF1+HF2	Para	1.6	62.8	43.2	11.8	1.10	33.5	0.46	7.2	0.12	3.8	13.1
< 500	HF1+HF2	Dia	4.2	2.7	0.9	58.0	6.44	29.3	0.21	28.8	0.22	49.5	61.3
< 710	HF1+HF2	Para	1.8	66.5	41.9	11.9	1.09	38.2	0.47	9.2	0.15	4.6	14.0
< 710	HF1+HF2	Dia	5.8	3.2	0.8	59.0	6.33	42.1	0.21	41.0	0.22	69.7	62.0
< 2000	HF1+HF2	Para	3.5	69.4	40.2	12.4	1.05	43.4	0.42	13.4	0.13	5.1	12.8
< 2000	HF1+HF2	Dia	13.2	6.0	0.6	61.5	6.07	51.6	0.18	61.0	0.20	92.3	53.2
< 2000	HF1	Para	2.2	50.1	41.6	9.8	1.12	34.4	0.45	10.9	0.14	4.4	13.9
< 2000	HF1	Dia	6.0	2.8	0.7	46.6	6.91	43.5	0.21	49.1	0.23	74.0	60.8

rec.: recovery, con.: concentration

SnO₂ could be enriched to about 60 % with a recovery of up to 92 % in the diamagnetic fraction (total fraction <2 mm). The paramagnetic fraction may also contain up to 14 % SnO₂. In addition, the cassiterite may contain up to 0.2 % Nb.

The pre-concentrate mainly contained tin as a valuable element which yields a theoretical revenue as presented in the following table:

The proportions of Nb₂O₅, Ta₂O₅ and TiO₂ were not taken into consideration as the required concentrations were not reached. For calculation of the possible recovery, only the diamagnetic fraction was considered, since it exhibited the required SnO₂ concentration.

7.3 Cachoeirinha

1 t of pre-concentrate (bulk sample TB55) includes the following valuable substances:

In the paramagnetic fraction, Nb₂O₅ and Ta₂O₅ were strongly enriched as Fe columbite. The columbite contained Sn as a trace element, which partially explained the SnO₂ content in the paramagnetic fraction.

In the diamagnetic fraction, mainly cassiterite was enriched. It was possible to produce concentrates with 70 % SnO₂ at a recovery of about 88 %. Part of the cassiterite was also transferred to the paramagnetic fraction because it contains up to 1.5 % Fe.

Tab. 7.8: Economic evaluation of the pre-concentrate with regard to the Sn amount per ton of pre-concentrate in the <2000 µm fraction (100 %).

Mineral	Element	Mass [kg/t]	Price [US\$/kg Sn]	Total value [US\$/t] (100 %)
Cassiterite	Sn	21.6	16.90	365.04
Total				365.04

Tab. 7.9: Tin recovery and revenues at different grain sizes (the amounts were calculated from the diamagnetic fractions of HF1 + HF2 – Tab. 6.8).

Grain size [µm]	Sn [kg recovery]	Recovery [%]	Concentrate [%] SnO ₂	Total value [\$/t]	Loss [\$/t]
< 2000	21.6 (100 %)	100.0		386.60	
< 500	10.7	49.5	61.6	191.40	195.30
< 710	15.1	69.7	62.0	269.50	117.20
< 2000	19.9	92.3	53.3	356.90	29.80

Tab. 7.10: Particle-size dependent element oxide concentrations and amounts of valuable substances with economic relevance in 1 t of pre-concentrate.

Grain size [µm]	Mass share [%]	Ta ₂ O ₅		Nb ₂ O ₅		SnO ₂		TiO ₂	
		[%]	[kg/t]	[%]	[kg/t]	[%]	[kg/t]	[%]	[kg/t]
63–200	3.3	1.284	12.84	12.189	121.9	30.06	300.6	1.1	10.7
200–630	35.2	0.688	6.88	6.726	67.3	17.13	171.3	0.3	3.5
630–2000	61.4	0.085	0.85	0.827	8.3	8.98	89.8	0.1	0.6
63–2000		0.337	3.37	3.282	32.8	12.55	125.4	0.195	1.951

Tab. 7.11: Recovery and concentration of element oxides after magnetic separation as a function of the separated particle size and density fractions in HF1 + HF2.

Grain size [μm]	Density fraction	Magn. frac.	Mass rec. [%]	TiO ₂		ZrO ₂		Nb ₂ O ₅		Ta ₂ O ₅		SnO ₂	
				rec.	con.	rec.	con.	rec.	con.	rec.	con.	rec.	con.
< 500	HF1+HF2	Para	4.9	43.3	1.30	38.1	7.45	73.1	46.1	69.3	8.52	4.3	15.81
< 500	HF1+HF2	Dia	7.7	9.0	0.18	34.3	6.01	3.0	1.44	5.9	0.50	36.3	80.5
< 710	HF1+HF2	Para	5.8	47.9	1.24	38.4	7.41	86.9	46.0	80.6	8.37	5.9	18.94
< 710	HF1+HF2	Dia	12.0	11.9	0.17	36.1	5.71	4.4	1.39	8.1	0.47	52.4	75.5
< 2000	HF1+HF2	Para	6.4	50.0	1.21	38.6	7.36	91.4	45.0	84.4	8.18	7.9	29.45
< 2000	HF1+HF2	Dia	21.7	20.7	0.15	37.3	5.54	6.7	1.17	12.7	0.40	88.6	69.5
< 2000	HF1	Para	4.7	34.3	1.13	15.3	1.99	68.0	45.6	63.2	8.38	6.8	30.91
< 2000	HF1	Dia	12.1	13.8	0.17	15.2	1.15	5.0	1.37	8.9	0.47	58.3	78.6

rec.: recovery, con.: concentration

Tab. 7.12: Economic evaluation of the pre-concentrate regarding Nb₂O₅, Ta₂O₅ and Sn amounts per ton of pre-concentrate in the <2000 μm fraction (100%).

Mineral	Element	Mass [kg/t]	Price [US\$/kg Sn]	Total value [US\$/t] (100%)
Cassiterite	Sn	40.7	16.90	687.80
Columbite	Nb ₂ O ₅	20	36.00	720.00
Columbite	Ta ₂ O ₅	3.37	211.00	711.07
Total				2118.87

Among other things, the cassiterite also contained Nb and Ta, which may explain the Nb₂O₅/Ta₂O₅ contents in the diamagnetic fraction.

ZrO₂ was present as zirconium in both the paramagnetic and the diamagnetic fraction with up to 7% each. It was preferably found in the 63–250 μm particle size range and the HF2 fraction with up to 30% in the paramagnetic fraction (but only very low recovery – no economic value/benefit).

Zircon could be recovered as a by-product. Zircon was contained in the diamagnetic fraction together with cassiterite. The separation of cassiterite and zircon can be accomplished by electrostatic methods. It should also be investigated whether the zircon in the paramagnetic fraction can be separated from columbite by magnetic separation. This could strongly increase the columbite and zircon contents.

7.4 Santa Bárbara

1 ton of ore (bulk sample TB59) includes the following valuable substances:

For sample TB59, no economic enrichment could be achieved by using the applied methodology. In the current state of the sample material, SnO₂ was enriched to only 1.6%. The material was almost completely present in the agglomerated state without any exposure of valuable minerals. Before carrying out further investigations on the enrichment of valuable elements, the material has to be ground to a minimum of 200 μm .

Tab. 7.13: Particle-size dependent element oxide concentrations and amounts of economic raw materials in 1 t of ore.

Grain size [μm]	Mass share [%]	Ta_2O_5		Nb_2O_5		SnO_2		TiO_2	
		[%]	[kg/t]	[%]	[kg/t]	[%]	[kg/t]	[%]	[kg/t]
63–200	4.7	0.015	0.147	0.145	1.45	0.200	2.004	0.7	6.710
200–630	37.3	0.002	0.019	0.021	0.21	0.030	0.303	0.2	1.840
630–2000	57.5	0.002	0.015	0.007	0.07	0.011	0.113	0.1	0.925
63–2000		0.002	0.023	0.019	0.19	0.027	0.273	0.154	1.537

Tab. 7.14: Economic evaluation of the ore regarding Nb_2O_5 , Ta_2O_5 , Sn and TiO_2 amounts per ton of ore in the <2000 μm fraction (100%).

Mineral	Element	Mass [kg/t]	Price [US\$/kg]	Total value [US\$/t]
Cassiterite	Sn	0.215	16.90	3.63
Columbite	Nb_2O_5	0.190	36.00	6.84
Columbite	Ta_2O_5	0.023	211.00	4.85
Ilmenite	TiO_2	1.537	0.17	0.28
Total				15.60

8 Summary and recommendations

The investigated samples from the plants at Massangana, Bom Futuro and Cachoeirinha are to be considered as economically very interesting pre-concentrates. The valuable minerals are almost completely liberated in the particle size range <2 mm and can be successfully concentrated by density separation and magnetic separation. Sample TB59 has to be ground and concentrated in several stages in order to produce saleable concentrates.

In general, it is proposed to carry out a first grain separation at 2 mm for samples from the Massangana (TB45-48), Bom Futuro (TB53) and Cachoeirinha (TB55) sites. The coarse components >2 mm have only a low potential for valuable

substance. A second grain separation should take place at $630 \mu\text{m}$ because a good concentration of heavy minerals by shaking table takes place only in a narrow grain band range.

8.1 Massangana

The valuable components in the pre-concentrates (bulk sample TB45-48) are SnO_2 (cassiterite) and $\text{Nb}_2\text{O}_5/\text{Ta}_2\text{O}_5$ (columbite). In addition, ilmenite (TiO_2) and topaz are included as main components, and zircon (ZrO_2) and monazite (REE) as minor components.

The following scheme is proposed to process the raw material from the Massangana deposit (Fig. 8.1):

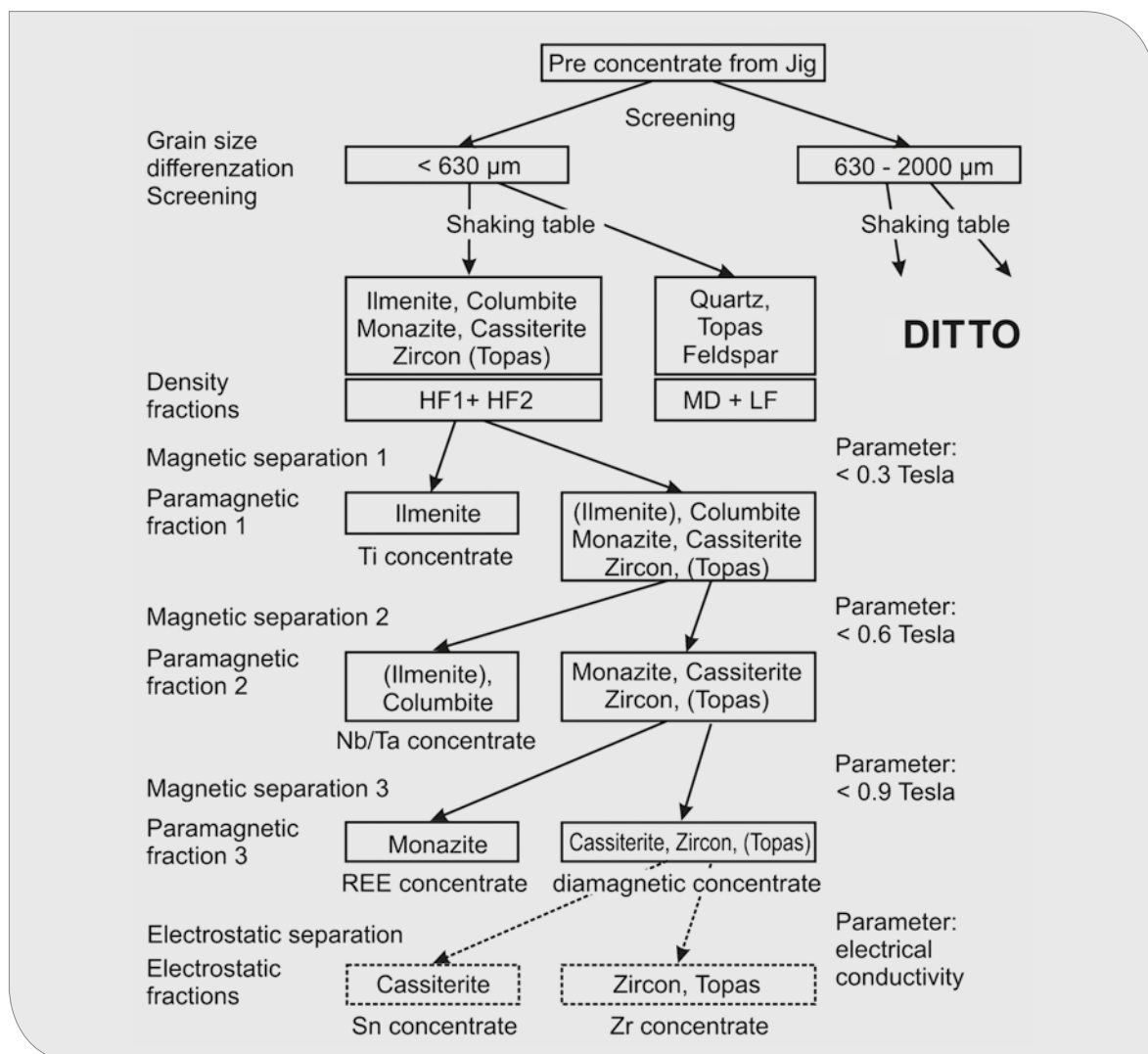


Fig. 8.1: Processing scheme for the Massangana pre-concentrates.

The pre-concentrates are strongly diluted by the >630 µm coarse fraction, which only contains small amounts of valuable compounds. The >630 µm fraction contains relatively small cassiterite amounts and hardly any columbite (possibly pyrochlore). But the fraction contains a lot of topaz, zircon and monazite. The latter is the main carrier of radioactivity as it includes Th and U.

In general, the application of the entire <2 mm grain size range to the shaking table is not recommended. To achieve a favorable concentration of the heavy minerals cassiterite and columbite, a narrower grain size band is necessary. For Mas-sangana, the <630 µm and >630 µm fractions/grain size bands are proposed. The <630 µm fraction contains the bulk of the cassiterite and columbite. A lot of ilmenite and some monazite are also concentrated in this fraction.

By finely graded magnetic separation, ilmenite, columbite and monazite can be separated and concentrated. In a first step, the ilmenite is separated as paramagnetic fraction 1 at low magnetic field strengths (about 0.25 to 0.3 Tesla). During ilmenite separation, care has to be taken to ensure that as little columbite as possible is included. If possible, the ilmenite should be separated twice through the magnetic separator to release columbite residuals. The ilmenite is highly concentrated and is saleable as TiO₂ raw material. The remaining concentrate contains the major part of the columbite, monazite, cassiterite and zircon.

The columbite can be separated as paramagnetic fraction 2 by carrying out a second magnetic separation between 0.3–0.6 Tesla. It is possible to produce concentrates of up to 50 % Nb₂O₅/Ta₂O₅, corresponding to a columbite content of about 65 % Fe (Mn) columbite. The by-product minerals are ilmenite (and weathering products of the ilmenite) and possibly monazite.

In a third magnetic separation step at 0.6 to 0.9 Tesla, the monazite can be separated as paramagnetic fraction 3. Care should be taken to separate the monazite as completely as possible, since it is the carrier of the radioactivity.

The residual fraction contains the bulk of the cassiterite, zircon and topaz. The separation of cassiterite from zircon and topaz takes place by electrostatic separation.

By applying a narrow grain size band, it would be possible to separate topaz and zircon from the cassiterite of the diamagnetic fraction in order to increase the cassiterite content (the separation of light zircon and topaz from the dark colored cassiterite is optically verifiable).

Zircon could be collected as an additional raw material from the coarse fraction >630 µm. In the diamagnetic fractions, ZrO₂ concentrates of 23–25 % were produced, corresponding to 34–37 % zircon. The remaining part of the concentrate is formed by some SnO₂ and especially topaz. The present work was focused on finding a way to separate zircon and topaz, which however could not be accomplished within the project.

The following concentrates could be produced:

- **Cassiterite:** up to 90 % SnO₂ but only 36 % recovery (diamagnetic fraction)
- **Cassiterite:** up to 65 % SnO₂ at 81 % recovery (diamagnetic + paramagnetic fraction)
- **Columbite:** 30 % Nb₂O₅, 5.7 % Ta₂O₅ (65–80 % recovery in paramagnetic fraction)
- **Ilmenite** (+ pseudorutile): >50 % TiO₂ (>90 % recovery in paramagnetic fraction)
- **Zircon:** up to 25 % ZrO₂, but higher radiation exposure due to Th/U (diamagnetic fraction)
- **Monazite:** up to 25 % REE, but high radiation exposure due to Th/U (paramagnetic fraction)

The radioactivity of the concentrates can be reduced by:

- Separation of the particle size fraction >630 µm
- Separation of the monazite by magnetic separation

Utilization of the valuable compounds:

- Ilmenite (sale)
- Columbite (Ilmenite) (sale)
- Monazite (disposal or eventually REE commodity)
- Cassiterite (zircon/topaz content) (sale)

A separation of cassiterite from zircon/topaz can be carried out by electrostatic methods.

8.2 Bom Futuro

The pre-concentrates at Bom Futuro (bulk sample TB53) are already well enriched in cassiterite. High contents of topaz and rutile are present. The valu-

able component is SnO_2 (cassiterite). Columbite is present, but mainly intergrown with cassiterite, and cannot be separated.

The following scheme is proposed for the processing of raw materials from the Bom Futuro deposit:

Paramagnetic rutile (Fe-bearing) can be separated by magnetic separation. Pure rutile is transferred to the diamagnetic fraction together with topaz and cassiterite.

The >2 mm portion of sample TB53 accounts for approximately 18%. This fraction still contained 0.5 to 1% SnO_2 representing 5–8% of the total SnO_2 .

The coarse fraction would have to be ground to <200 μm to recover this SnO_2 content. Subsequently, an enrichment of the cassiterite via the shaking table would be possible.

For good raw material recovery, HF1 and HF2 have to be processed together. This procedure enables a higher recovery, however, at lower SnO_2 concentrations.

Magnetic separation (if necessary) should take place at field strengths lower than 1.1 Tesla to avoid carrying over the cassiterite into the paramagnetic fraction.

The separation of cassiterite and topaz can be accomplished by electrostatic methods.

The following concentrates could be produced:

- **Cassiterite:** Concentrates of 60% SnO_2 can be achieved with a recovery of up to 92% (total <2 mm).

Utilization of the valuable compounds:

- Cassiterite (sale)

The radioactivity of the concentrates is considered to be low.

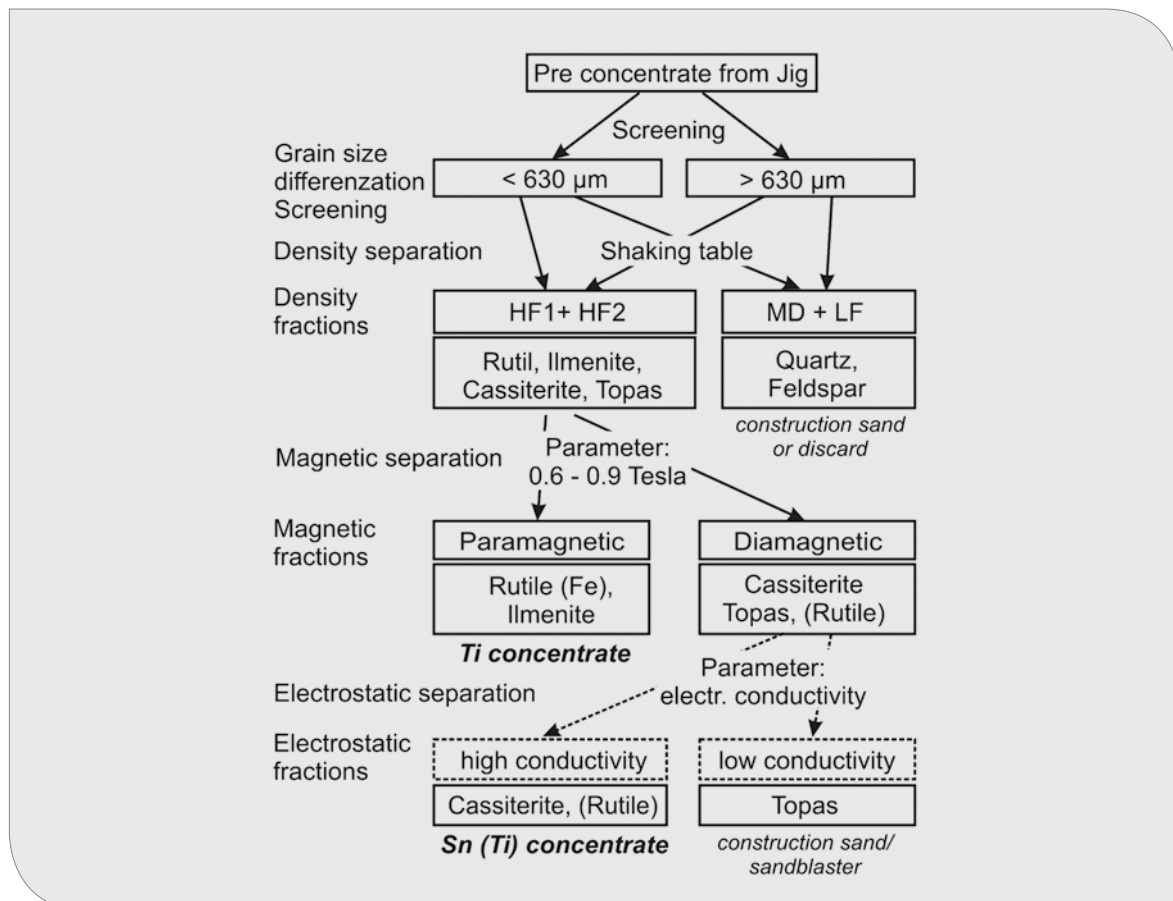


Fig. 8.2: Processing scheme for the Bom Futuro pre-concentrates.

8.3 Cachoeirinha

The main heavy minerals in bulk sample TB55 from Cachoeirinha are cassiterite, columbite, topaz and zircon. Topaz has the largest share in the heavy mineral fraction. Zircon is only enriched in the <200 μm small grain size range.

TB55 shows very high columbite and cassiterite contents. High levels of topaz hinder a better columbite and cassiterite enrichment in the HF1 fraction. To achieve a high recovery, the HF1 and HF2 fractions have to be further processed together. The thorium and uranium contents are slightly increased only in the smallest particle size fraction and pose no problem.

In all diamagnetic fractions of HF1, SnO_2 concentrations of >50% are achieved with a recovery of >80%.

Columbite is separated and enriched in the paramagnetic fraction, cassiterite in the diamagnetic fraction. In the diamagnetic fraction, small amounts

of Nb/Ta are separated, which are present as trace elements or intergrowths in cassiterite. Likewise, it is reasonable to individually separate the MD fractions once again by magnetic separation, as such a procedure very effectively enables the separation of residual Nb/Ta.

The following concentrates could be produced:

- **Cassiterite:** up to 80% SnO_2 with only 58% recovery (only HF1 in diamagnetic fraction)
- **Cassiterite:** up to 70% SnO_2 with 88% recovery (HF1 + HF2 in diamagnetic fractions <2000 μm)
- **Columbite:** 45% Nb_2O_5 , 8% Ta_2O_5 (84–91% recovery in paramagnetic fraction)
- **Zircon:** up to 7% ZrO_2 (diamagnetic fraction)

Utilization of the valuable compounds:

- Cassiterite (sale)
- Columbite (sale)

The following scheme is proposed for the processing of raw materials from the Cachoeirinha deposit (Fig. 8.3):

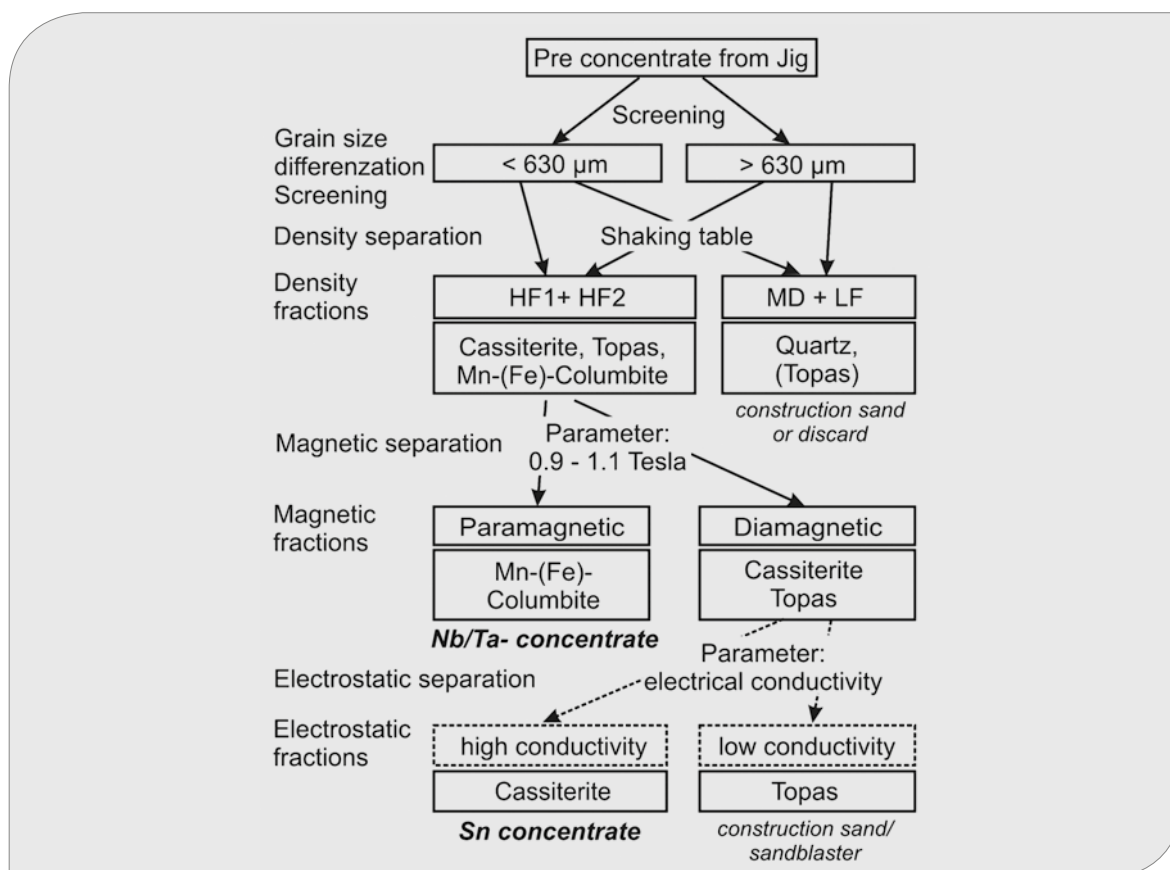


Fig. 8.3: Processing scheme for the Cachoeirinha pre-concentrates.

The radioactivity of the concentrates is considered to be low.

8.4 Santa Bárbara

For the Santa Bárbara deposit, no economic enrichment in bulk sample TB59 of SnO_2 and $\text{Nb}_2\text{O}_5/\text{Ta}_2\text{O}_5$ in bulk sample TB59 could be accomplished with the present material. The reasons for this are the coarse grain size and/or a strong intergrowth of the valuable minerals with Fe- hydroxides and clay minerals. In the 63–200 μm fraction, almost all valuable minerals, such as cassiterite, columbite and zircon, are available as free grains, almost without intergrowths (MLA-data). The total contents of 0.2% SnO_2 in the <200 μm fraction are promising, however, this grain size accounts for only 4.7% of the total material. Overall, only 4.4 g

SnO_2 were included in the 16.1 kg sample material with a particle size <2 mm. Such a small amount is difficult to concentrate.

The SnO_2 contents are promising, but the material has to be ground first to <200(300) μm (according to the client, the ore is ground, but the sample was taken before the grinding process through the ball mill). Subsequently, concentration can be carried out by using a spiral separator, shaking table and magnetic separator.

No concentrates could be produced so far because the content of valuable compounds was too low.

The following scheme is proposed for the processing of raw materials from the Santa Bárbara deposit (Fig. 8.4):

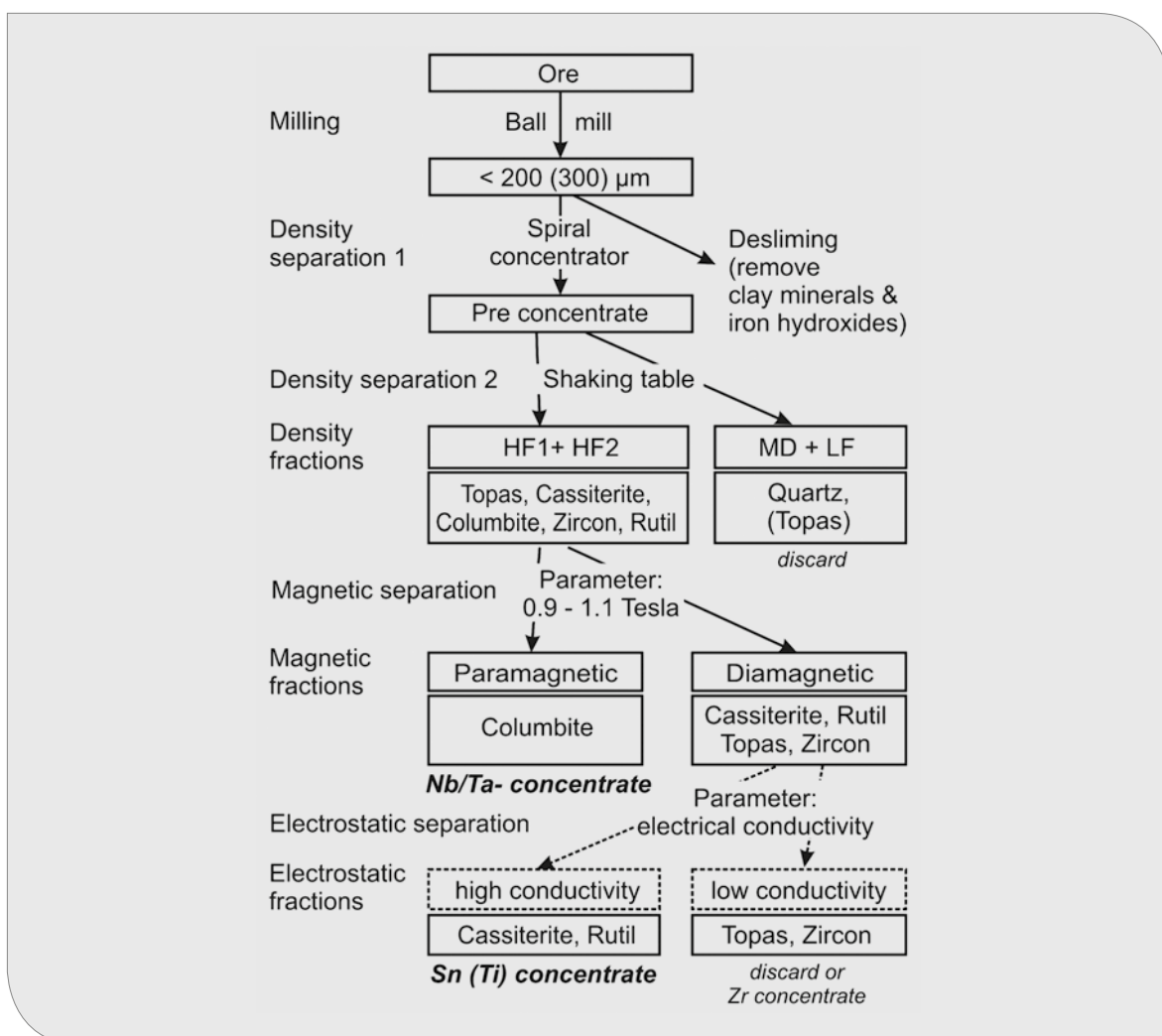
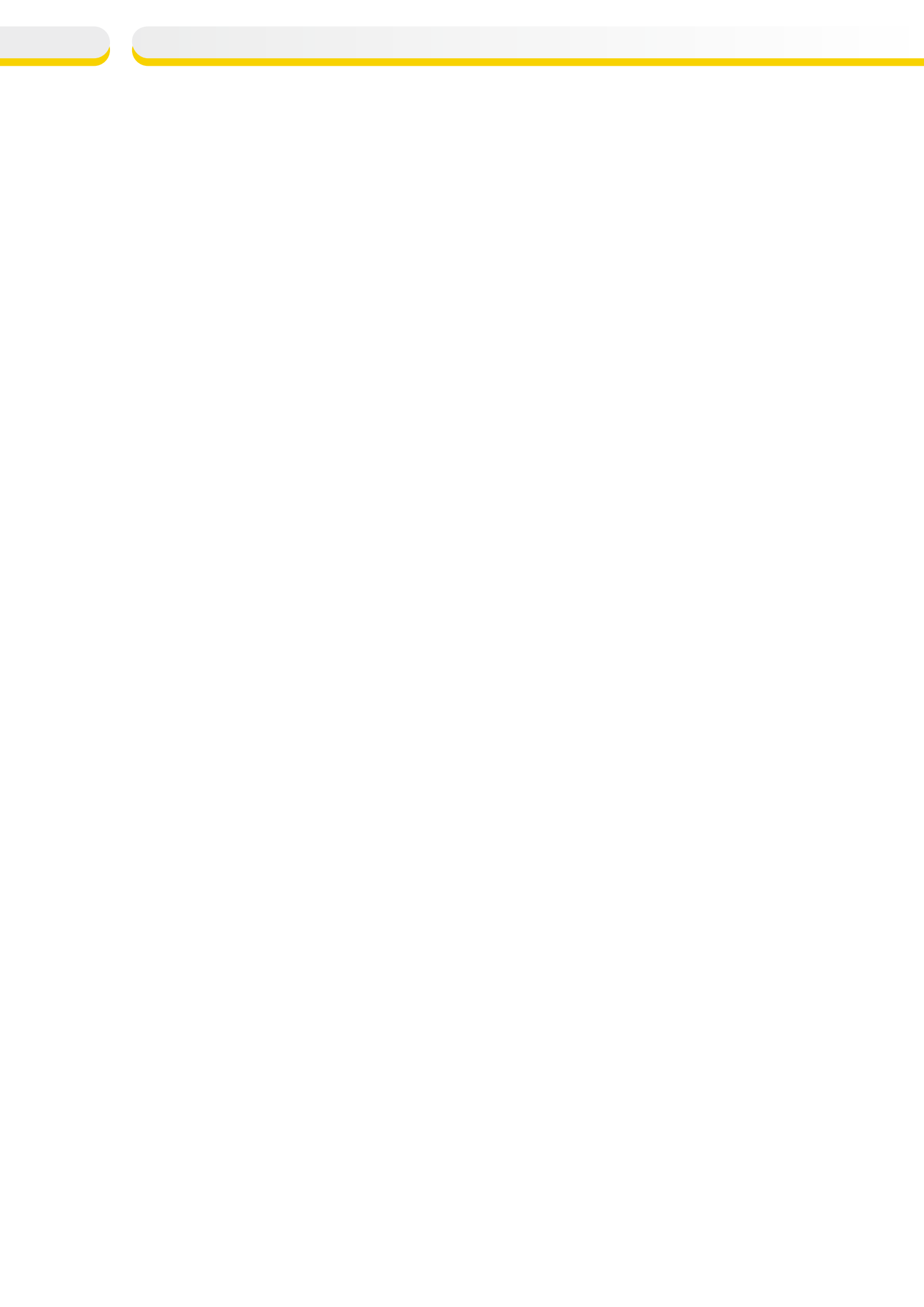


Fig. 8.4: Processing scheme for the Santa Bárbara ores.

9 References

- AGRICOLA, G. (1556): *De re metallica libri XII (Vom Bergkwerck XII Bücher) – Zwölf Bücher vom Berg- und Hüttenwesen.*
- ANEEL (2016): Banco de informações de geração de energia. Available in: <http://www2.aneel.gov.br/aplicacoes/ResumoEstadual/CapacidadeEstado.cfm?cmbEstados=RO:ROND%D4NIA>. Accessed in July 2018.
- BETTENCOURT, J. S., MUZZOLON, R., PAYOLLA, B. L. & Pinho, O. G., DALL'IGNA, L. G. (1988): Os depósitos estaníferos da região central de Rondônia. In: J. S. Bettencourt, R. Muzzolon, B. L. Payolla, R. Dall'Agnol, O. G. de Pinho. (Org.). *Principais depósitos minerais do Brasil.: DNPM-CVRD 1988*, v. 3, p. 213–241.
- BETTENCOURT, J. S. (1988): Os Depósitos estaníferos da região central de Rondônia. In: Schobbenhaus, C., Coelho, C. E. S. (Coords.). *Principais depósitos minerais do Brasil: metais básicos não-ferrosos, ouro e alumínio.* Brasília: DNPM/CVRD, v. 3, p. 213–241.
- BETTENCOURT, J. S. (1992): Pesquisas geológica, metalogenética e mineral no Craton Amazônico (Sistematização crítica de parte da obra no período compreendido entre 1980 e 1992). 1992. 163 p. Tese (Livre Docente)-Instituto de Geociências, Universidade de São Paulo, São Paulo, 1992.
- BETTENCOURT, J. S., TOSDAL, R. M., LEITE Jr., W. B. & PAYOLLA, B. L. (1999): Mesoproterozoic rapakivi granites of the Rondônia Tin Province, southwestern border of the Amazonian Craton, Brazil-I. Reconnaissance U-Pb geochronology and regional implications. *Precambrian Research*, v. 95, p. 41–67, 1999.
- BETTENCOURT, J. S. et al. (2005): Sn-polymetallic greisen-type deposits associated with late-stage rapakivi granites, Brazil: fluid inclusion and stable isotope characteristics. *Lithos*, 80:363–386.
- BUCH et al. (2017): Áreas de Relevante Interesse Mineral – Reavaliação da Província Estanífera de Rondônia. Informe de Recursos Minerais. Porto Velho: CPRM.
- CARVALHO, R. T. (1988): Depósitos de cassiterita de Santa Bárbara, Jacundá e Alto Candeias, Rondônia. In: Schobbenhaus, C., Coelho, C. E. S. (Coords.). *Principais depósitos minerais do Brasil: metais básicos não-ferrosos, ouro e alumínio.* Brasília: DNPM/CVRD, 1988. p. 243–253. v. 3, cap. 20.
- DALL'IGNA, L. G. (1996): A Mineração e o Garimpo de Cassiterita em Rondônia. *A Terra em Revista*, Belo Horizonte, v. Ano II, n. Número I, p. 56–61.
- DARDENNE, M. A. & SCHOBENHAUS, C. (2001): *Meta-logênese do Brasil.* 1. ed. Brasília: Universidade de Brasília. v. 01. 349 p.
- DEPARTAMENTO NACIONAL DE PRODUÇÃO MINERAL – DNPM (2018): *Anuário Mineral Brasileiro, Principais substâncias metálicas 2017, ano base 2016.* 43 p.
- DRZYMALA, J. (2018): Mineral processing – lab exercise. Magnetic separation. Wroclaw University of Science and Technology, Department of Mineral and Waste Processing.
- FRANK, R. E. (1990): Geologia, petrologia e mineralizações estaníferas do Complexo Graníticos de Santa Bárbara, Rondônia, Brasil, 244 p. Dissertação (Mestrado em Geologia)-Instituto de Geociências, Universidade Federal do Rio de Janeiro, Rio de Janeiro, 1990.
- FISCHER, H. (1920): *Technologie des Scheidens, Mischens und Zerkleinerns.* Springer Verlag Heidelberg. ISBN 978-3-662-33436-2, DOI 10.1007/978-3-662-33833-9.
- ISOTTA, C. A. L., CARNEIRO, J. M., KATO, H. T. & BARROS, R. J. L. (1978): Projeto Província Estanífera de Rondônia. Porto Velho. DNPM/CPRM. Vols. 1–3. (Relatório final).
- HARSHAW, BTKD (2001): <https://www.yumpu.com/de/document/view/15674720/technisches-datenblatt-fur-das-beta-fingerringdosimeter>.
- ISOTTA et al. (1978): Projeto Província Estanífera de Rondônia: relatório final. Porto Velho: CPRM, 1978 16 v. v.1
- LEITE JUNIOR, W. B. (2002): A suite intrusiva Santa Clara (RO) e a mineralização primária polimetálica

- (Sn, W, Nb, Ta, Zn, Cu e Pb) associada. 302 p. Tese (Doutorado em Recursos Minerais e Hidrogeologia)-Instituto de Geociências, Universidade de São Paulo, São Paulo, 2002.
- LOBATO et al. (1966): Pesquisa de cassiterita no Território Federal de Rondônia: relatório final. Rio de Janeiro: DNPM-DFPM, 1966. 209 p. (Boletim. 125).
- MCCLENAGHAN, M. B. (2014): Overview of common processing methods for recovery of indicator minerals from sediment and bedrock in mineral exploration. *Geochemistry: Exploration, Environment, Analysis*, Vol. 11 2011, pp. 265–278. DOI 10.1144/1467-7873/10-IM-025.
- PAYOLLA, B. L. (1984): Estratigrafia preliminar e ambientes de deposição dos depósitos estaníferos secundários nos distritos de Cachoeirinha, Monte Negro e Oriente Novo, Estado de Rondônia, Brasil. In: Bettencourt, J. S. (ed.): SYMPOSIUM AMAZONICO, 2, abr. 1984, Parte I, Manaus. Anais. Manaus: DNPM, 1984. p. 359–373.
- QUADROS, M. L. do E. S., AMORIM, J. L. & CORDEIRO, A. V. (2001): Considerações sobre a geologia e as mineralizações de cassiterita do garimpo de Bom Futuro, município de Ariquemes, Estado de Rondônia. Relatório de Viagem. CPRM. Porto Velho.
- SANTOS, J.O.S. (2003): Three distinctive collisional orogenies in the Southwestern Amazon craton: constraints from U-Pb geochronology. In: South American Symposium on Isotope Geology, 4, 24–27 Aug. 2003, Salvador. Papers, Salvador: CBPM, p. 282–285.
- SNL (2018): SNL Metals & Mining, a group within S&P Global Market Intelligence; fee based database; Charlottesville, USA.
- SOUSA, V. S. (2003): Evolução magmática e Modelo Metalogenético do sistema Vulcano-Plutônico Bom Futuro. Doutorado em Geologia. Universidade de Brasília.
- SPARREBERGER, I. (2003): Evolução da mineralização primária estanífera associada ao maciço granítico Santa Bárbara, Rondônia. 252 p. Tese (Doutorado em Recursos Minerais e Hidrogeologia) – Instituto de Geociências, Universidade de São Paulo, São Paulo, 2003.
- STENDAL, H. & THEOBALD, P. K. (1994): Heavy-mineral concentrates in geochemical exploration. In: Hale, M. & Plant, J.A. (eds) *Drainage Geochemistry, Handbook of Exploration Geochemistry*, 6, 185–225.
- ROMANINI, S.J. (1982): Geologia e geoquímica do complexo granitóide de Massangana e sua relação com as mineralizações de estanho. Dissertação de Mestrado em Geociências. Câmara de Ensino de Pós-Graduação e Pesquisa, Universidade Federal da Bahia, Salvador.
- TREPTOW, E. (1925): Grundzüge der Bergbaukunde einschliesslich Aufbereitung und Brikettieren: II. Band. Springer Fachmedien 1925 Wiesbaden GmbH. ISBN 978-3-7091-5043-6.
- USGS (2018): USGS Minerals Information – Mineral Commodity Summaries Tin: <https://minerals.usgs.gov/minerals/pubs/commodity/tin/>
- VASQUEZ, M. L., MACAMBIRA, M. J. B. & ARMSTRONG, R. A. (2008): Zircon geochronology of granitoids from western Bacajá domain, southeastern Amazonian craton, Brazil: Neoproterozoic to Orosirian evolution. *Precambrian Research* v. 161, p. 279–302.
- VEIGA A.T.C. (1988): As minas de estanho de Igarapé Preto – Amazonas, Massangana-Rondônia e São Francisco-Mato Grosso, Província Estanífera de Rondônia. In: Schobbenhaus, C., Coelho, C. E. S. (Coords.). *Principais depósitos minerais do Brasil: metais básicos não-ferrosos, ouro e alumínio*. Brasília: DNPM/CVRD, v. 3, Cap. 21, p. 255–260.
- WAGHORN, J.G. (1974): The geology Rondônia, western Brazil, with special reference to the tin-bearing granite complexes and placer deposits. 140 p. Doctorate Dissertation – London: Faculty of Science of the University of London.



10 Appendix

Appendix 1: List of collected samples	112
Appendix 2: Element content – grain size dependent	116
Appendix 3: Element content – heavy/light fractions of Bromoform separations	119
Appendix 4: Mineralogical composition of the different grain size fractions	122
Appendix 5: Massangana – concentrations/recovery of elements	126
Appendix 6: Bom Futuro – concentrations/recovery of elements	129
Appendix 7: Cachoeirinha – concentrations/recovery of elements	132
Appendix 8: Santa Barbara – concentrations/recovery of elements	135
Appendix 9: Radiation measurements	138
Appendix 10: Optical microscopy and SEM-BSE of polished thin sections	144
Appendix 11: Mineral Liberation Analysis – MLA	149

Appendix 1

List of collected samples (entire list of all samples collected in two field campaigns)

Tab. 1A: List of collected samples.

Sample		Local	Type of Material	Details	Analysis
TB 1	A	Santa Bárbara Hill	Tailings	Gray tailings with more clay and ilmenite	XRF
	B		Tailings	Coarse grained tailings	XRF
TB 2		Santa Bárbara Hill	Tailings	Clayish tailings. Distal area in the same tailing deposit from the samples TB1	XRF
TB 3		Taboquinha	Tailings	Region of Output from the samples of Taboquinha I	XRF
TB 4	A	Taboca Stream	Secondary Ore	White clayish sand layer. Correlated to the Seq I	XRF
	B		Secondary Ore	Red Clayish sand layer covering the previous layer	XRF
TB 5	A	Santa Bárbara Processing Plant	Pre-concentrate	Input feed of the spirals	XRF
	B		Tailings	Tailing output of the spirals	XRF
	C		Concentrate	Output of spirals	MLA
	D		Tailings	Output of spirals of lower Sn concentrat.	XRF
TB 6	A	Pau Baixo Stream	Concentrate	Second jig's output (for magnetic sep.)	MLA
	B		Concentrate	First jig's output	MLA
	C		Tailings	Tailing output of the second jig	XRF
	D		Tailings	Tailing output of the first jig	XRF
	E		Secondary Ore	Ore input	XRF
TB 8	A	CEMAL Processing Plant	Concentrate	Columbite concentrate	MLA
	B		Concentrate	Monazite concentrate	MLA
	C		Concentrate	Cassiterite concentrate	MLA
	D		Tailings	Shaking table's tailings	XRF
	E		Concentrate	Cassiterite + tailings	MLA
TB 9	A	Metalmig	Slag	Feed the shaking table, after crushed and jigged	XRF
	B		Slag	Crushed and jigged slag	SEM
	C		Slag	Tailing from the concentration of the sample TB9A	–
	D		Slag	Metallic slag from the bottom of the metallurgy	–
	E		Concentrate	Preconcentrate of 1 st jigging process	XRF
	F		Concentrate	Ilmenite concentrate after the magnetic separator	MLA
	G		Concentrate	Cassiterite and sand after the magnetic separator	MLA
	H		Concentrate	Final cassiterite concentrate (smelter feed)	MLA
	I		Concentrate	Cassiterite and columbite from the Oriente Novo area	MLA
	J		Concentrate	Cassiterite after columbite separation	MLA
	K		Concentrate	Columbite concentrate	MLA
	L		Slag	Retained filter powder material	XRF

Sample	Local	Type of Material	Details	Analysis	
TB 10	Bom Futuro	Primary Ore	Primary Ore from the Sector 1	–	
TB 11	A	Palleo alluvium	Sedimentary Ore	Conglomeratic layer	XRF
	B		Sedimentary Ore	Ferruginous crust	XRF
TB 13	A	Bom Futuro G. Kubotani's Processing Plant	Ore of Tailing	Input feeding the jigg	XRF
	B		Concentrate	Output of the jigg	MLA
	C		Tailings	Tailing of the jigg	XRF
	D		Concentrate	Output of the shaking table	XRF
TB 14	A	Separator „Paulo Amâncio“	Concentrate	Preconcentrate from the mill	MLA
	B		Concentrate	Concentrate after the spiral	MLA
	C		Tailings	Output of the system	XRF
TB 15	A	Magnetic Separador „Paulo Amâncio“	Concentrate	Coarse grained concentrate	MLA
	B		Concentrate	Fine grained concentrate with cassiterite and ilmenite	MLA
	C		Concentrate	1 st jigging concentrate	MLA
	D		Tailings	Tailings from the 1 st jigging concentrate	XRF
	E		Concentrate	Shaking Table concentrate (input – TB14B)	MLA
TB 16	A	Manteiga Stream	Primary Ore	Primary Ore of W	–
	B		Primary Ore	Zinnwaldit	–
	C		Primary Ore	Sulfide ore	–
	D		Clast	Limonite scattered on the ground	–
	E		Clast	Magnetite scattered on the ground	–
	F		Clast	Wolframite crystals	–
	G		Mineral	Molybdenite and Zinnwaldit	–
TB 17	Manteiga Stream	Tailings	Tailings stockpile	XRF	
TB 18	A	Cachoeirinha	Secondary Ore	Sand layer with crossed structures	XRF
	B			Sand layer with parallel lamination and turfaceous material	XRF
	C			Fine grained sand, above the turfaceous layer.	XRF
	D			Clay layer under the TB 18A layer.	XRF
	E			Clay layer above the TB 18C layer.	XRF
	F			Conglomeratic layer under the TB 18D layer	XRF
TB 19	A	Cachoeirinha – Processing Plant	Tailings	Tailing from the 1 st jigging process	XRF
	B		Concentrate	Topaz found in the jigging process	–
	C		Concentrate	Topaz and dark minerals	–
TB 21	A	Tailings „Virgens“ Macisa	Tailings	Tailings composed of sand layers	XRF
	B		Tailings	Tailings composed of sand and clay	XRF
TB 22	A	Macisa	Tailings	Arenous tailings	XRF
	B		Secondary Ore	Clayish bedding under tailings	XRF

Sample	Local	Type of Material	Details	Analysis	
TB 23	A	Macisa	Tailings stockpile disposed along the Macisa Stream	0–0,4 m	XRF
	B			0,40–1,5 m	XRF
	C			1,5–2,3 m	XRF
	D			2,3–3,20 m	XRF
	E			3,20–3,7 m	XRF
	F			3,7–4,1 m	XRF
	G			4,7–5 m	XRF
TB 24	A	Pascana Stream Macisa Sector	Mined Tailings	Tailing without clay	XRF
	B		Gross Tailings	Gross tailing	XRF
	C		Final Tailings	Output of 2 nd jig	XRF
	D		Concentrate	2 nd Jig, 1 st output	MLA
	E		Concentrate	2 nd Jig, 2 nd output	MLA
	F		First Tailing	Output of 1 st Jig	XRF
TB 25	A	Isaac Hill	Primary ore	Country rock with quartz vein	–
	B			Mineralized quartz vein	–
TB 26	Isaac Hill Foothills	Mineralized Granite	Weathered mineralized granite	–	
TB 27	A	Zé Andrade Processing Plant	Secondary Ore, Alluvium	Mined ore	XRF
	B		Tailings	Outlet of 2 nd jig system	XRF
	C		Tailings	Outlet of 1 st jig system	XRF
	D		Concentrate	2 nd Jig, 2 nd output	MLA
	E		Concentrate	2 nd Jig, 1 st output	MLA
	F		Tailings	Retained material in the sieve of 2 nd	XRF
	G		Tailings	Retained material in the sieve of 1 st jig	XRF
TB 28	Cupola Isaac Hill	Granite	Outcrop	-	
TB 29	Isaac Hill	Primary Ore	Mineralized Granite on Isaac Hill	-	
TB 30		Concentrate	Cassiterite concentrate mined in Pirarucu Stream	MLA	
TB 31	A	São Lourenço Antena – Planta do Adenor	Concentrate	2 nd output of jig: ilmenite mined in tailings	MLA
	B		Concentrate	1 st saída do jigue: cassiterita + ilmenita – lavra de rejeito	MLA
TB 32	A	São Lourenço – Igarapé Casca- vel	Tailing	Outlet of 1 st Jig	XRF
	B		Alluvial Ore	Alluvial Ore from the Cascavel Stream	XRF
	C		Concentrate	Concentrate from 2 nd jig, 1 st output	MLA
	D		Retained material in the jig sieve	Retained material in the sieve of the jig	XRF
TB 33	A	Igarapé Saubão Jigue do Marcão	Alluvial sediment	Clay sedimentary cover	XRF
	B		Alluvial sediment	Sand layer with low content of cassiterite	XRF
	C		Alluvial sediment	"Sterile" sand layer	XRF
	D		Sedimentary Ore	Sand layer ore	XRF
	E		Sedimentary Ore	Baseline gravel	XRF
	F		Sedimentary Ore	Feriferous carapace in the interface sand/silte	XRF
	G		Concentrate	Concentrate from 2 nd jig and 2 nd output	MLA
	H		Tailing	Jig output	XRF

Sample	Local	Type of Material	Details	Analysis	
TB 34	A	Processing Plant for Regolito do Adenor	Concentrate	2 nd jig, 1 st output	MLA
	B		Concentrate	2 nd jig, 2 nd output	MLA
	C		Tailing	Output of 2 nd jig	XRF
	D		Tailing	1 st Jig Output	XRF
	E		Ore	Regolith from Isaac Hill	XRF
TB 35	Ceriumbrás	Secondary Ore	Sand layer/Secondary ore	XRF	
TB 36	A	G. Kubotani's Plant (TAK)	Concentrate	Concentrate after the spiral	MLA
	B		Tailing	Output from the spiral	XRF
	C		Tailing	Output from the Jigg	XRF
	D		Concentrate	Concentrate after the jig	MLA
	E		Tailing	Wash-out	XRF
TB 37	A	Ernst's Processing Plant	Concentrate	Milled input Mill A	MLA
	B		Concentrate	Milled input Mill B	MLA
	C		Tailing	Tailing from the first jiggling process	XRF
	D		Concentrate	Concentrate after the jig	MLA
TB 38	A	Ernst's Processing Plant	Concentrate	Input into the spiral	XRF
	B		Tailing	Output of the spiral	MLA
	C		Concentrate	Concentrate of the spiral. It is the input of the shaking table.	XRF
	D		Tailing	Output of the shaking table.	XRF
	E		Concentrate	Shaking table concentrate. Final concentrate.	MLA
TB 43	CEMAL Processing Plant	Tailing	Shaking table tailings	XRF	
TB 44		Concentrate	Columbite concentrate	MLA	
TB 45	Cassiterite Concentrate Massangana's Ore	Concentrate	2 nd Output Barreiro	Processing Tests	
TB 46		Concentrate	2 nd Output Taboca		
TB 47		Concentrate	2 nd output Renascença – Lima Stream		
TB 48		Concentrate	2 nd output – Igarapé B-3		
TB 49	ERSA's Smelter	Slag	Slag CSN	XRF	
TB 50		Slag	Slag CSN	XRF	
TB 51		Slag	Nb – Slag	–	
TB 52	Bom Futuro	Primary Ore	Hard Rock – Body 1		
TB 53		Concentrate	Concentrate	Proc. T.	
TB 54		Concentrate	Oxidized Ilmenite and Cassiterite	–	
TB 55	Cachoeirinha	Concentrate	Jig concentrate	Proc. T.	
TB 56		Sedimentary Ore	Sand layers from the Patuá region	XRF	
TB 57		Tailings	Tailings from the Queimada Stream region	XRF	
TB 58	Santa Bárbara	Concentrate	Cassiterite concentrate	MLA	
TB 59		Concentrate	Pre-concentrate (washed) input to the spirals	Proc. T.	
TB 60			Overburden of the secondary ore	XRF	

Appendix 2

Element content – grain size dependent

Tab. 2.1A: Element content – major elements.

Massangana – TB45-48								
Sample no.	Grain size [µm]	Recovery [%]	Al ₂ O ₃ [%]	SiO ₂ [%]	TiO ₂ [%]	Fe ₂ O ₃ [%]	ZrO ₂ [%]	Nb ₂ O ₅ [%]
1	< 63	0.2	14.1	51.6	4.5	5.8	2.17	0.12
2	63–100	0.5	8.2	43.8	10.5	7.7	5.64	0.24
3	100–200	14.0	2.2	14.9	42.1	18.9	1.76	1.16
4	200–300	27.4	1.5	15.0	44.5	19.3	0.44	1.42
5	300–400	22.1	2.2	24.2	39.0	17.4	0.40	1.08
6	400–500	10.2	4.6	37.0	30.2	14.3	0.91	0.71
7	500–630	7.9	7.4	42.1	23.6	12.0	1.79	0.47
8	630–800	6.2	12.0	44.1	15.8	9.2	3.31	0.30
9	800–2000	11.5	22.7	45.1	6.6	6.0	3.87	0.17

Bom Futuro – TB53								
Sample no.	Grain size [µm]	Recovery [%]	Al ₂ O ₃ [%]	SiO ₂ [%]	TiO ₂ [%]	Fe ₂ O ₃ [%]	ZrO ₂ [%]	Nb ₂ O ₅ [%]
1	< 63	0.1						
2	63–100	0.2	17.9	34.6	3.1	9.16	3.62	0.137
3	100–200	3.2	14	56.4	6.27	5.39	1.41	0.071
4	200–300	11.9	7.7	74.4	2.08	3.04	0.18	0.010
5	300–400	18.0	5	75.9	0.91	2.32	0.07	0.011
6	400–500	16.1	4.7	78.2	0.66	2.1	0.05	0.003
7	500–630	14.7	5.3	81.6	0.48	2.39	0.03	0.002
8	630–800	11.0	5.1	76.3	0.27	3.21	0.03	0.004
9	800–2000	24.8	5.3	67.1	0.18	5.52	0.01	0.007

Cachoeirinha – TB55								
Sample no.	Grain size [µm]	Recovery [%]	Al ₂ O ₃ [%]	SiO ₂ [%]	TiO ₂ [%]	Fe ₂ O ₃ [%]	ZrO ₂ [%]	Nb ₂ O ₅ [%]
1	< 63	0.1						
2	63–100	0.2	17.2	24.0	0.689	3.110	6.88	8.28
3	100–200	3.4	16.9	22.6	0.563	2.626	3.47	13.10
4	200–300	7.0	25.8	29.9	0.311	2.019	0.46	11.26
5	300–400	9.9	27.9	36.0	0.167	1.465	0.05	7.33
6	400–500	9.7	27.5	40.2	0.101	1.170	0.02	5.33
7	500–630	13.1	26.3	44.5	0.092	1.065	0.02	3.83
8	630–800	15.4	22.3	55.1	0.055	0.729	0.02	1.31
9	800–2000	41.3	17.2	58.8	0.057	0.672	0.01	0.51

Tab. 2.1A: Element content – major elements.

Santa Barbara – TB59								
Sample no.	Grain size [µm]	Recovery [%]	Al ₂ O ₃ [%]	SiO ₂ [%]	TiO ₂ [%]	Fe ₂ O ₃ [%]	ZrO ₂ [%]	Nb ₂ O ₅ [%]
1	< 63	0.1	28.4	32.5	0.64	8.9	0.306	0.134
2	63–100	1.2	25.9	32.3	0.67	10.7	0.671	0.207
3	100–200	5.9	26.0	36.0	0.68	10.6	0.234	0.128
4	200–300	11.7	21.3	41.0	0.41	8.2	0.060	0.044
5	300–400	11.7	16.8	47.7	0.30	6.4	0.032	0.022
6	400–500	9.4	15.4	53.7	0.27	6.5	0.039	0.016
7	500–630	9.8	11.2	56.1	0.23	6.4	0.028	0.012
8	630–800	10.4	10.1	66.9	0.15	6.3	0.022	0.006
9	800–2000	39.9	7.9	72.6	0.12	6.2	0.019	0.002

Massangana – TB45-48								
Sample no.	Grain size [µm]	Ta ₂ O ₅ [%]	SnO ₂ [%]	Th [%]	U [%]	Ce [%]	Y [%]	Hf [%]
1	< 63	< LOD	0.28	0.025	0.009	0.10	0.04	0.04
2	63–100	< LOD	0.79	0.059	0.013	0.21	0.06	0.14
3	100–200	0.12	1.85	0.076	0.010	0.18	0.05	0.05
4	200–300	0.15	3.33	0.090	0.006	0.19	0.05	< LOD
5	300–400	0.10	2.02	0.125	0.009	0.35	0.09	< LOD
6	400–500	0.06	1.02	0.137	0.012	0.42	0.16	0.01
7	500–630	< LOD	0.88	0.145	0.015	0.47	0.19	0.02
8	630–800	< LOD	0.96	0.169	0.032	0.59	0.26	0.09
9	800–2000	< LOD	0.04	0.094	0.036	0.36	0.19	0.10

Bom Futuro – TB53							
Sample no.	Grain size [µm]	Ta ₂ O ₅ [%]	SnO ₂ [%]	Th [%]	U [%]	Ce [%]	Y [%]
1	< 63						
2	63–100	0.113	3.73	0.026	0.0099	0.0268	0.046
3	100–200	0.063	4.65	0.01	< LOD	< LOD	0.027
4	200–300	0.048	3.37	0.0048	< LOD	< LOD	0.006
5	300–400	0.039	3.10	< LOD	< LOD	< LOD	0.005
6	400–500	0.047	3.52	< LOD	< LOD	< LOD	0.005
7	500–630	0.071	3.61	< LOD	< LOD	< LOD	0.009
8	630–800	0.036	2.33	< LOD	< LOD	< LOD	0.004
9	800–2000	0.003	1.74	< LOD	< LOD	< LOD	0.001

Tab. 2.1A: Element content – major elements.

Cachoeirinha – TB55								
Sample no.	Grain size [µm]	Ta ₂ O ₅ [%]	SnO ₂ [%]	Th [%]	U [%]	Ce [%]	Y [%]	Hf [%]
1	< 63							
2	63–100	2.04	25.8	0.147	0.073	< LOD	0.130	0.3005
3	100–200	2.89	29.9	0.089	0.0436	< LOD	0.080	0.1476
4	200–300	2.60	20.6	0.009	0.0103	< LOD	0.020	0.0131
5	300–400	1.65	17.0	0.014	< LOD	< LOD	0.004	< LOD
6	400–500	1.29	15.8	0.012	< LOD	< LOD	0.003	< LOD
7	500–630	0.98	16.3	0.013	< LOD	< LOD	0.002	< LOD
8	630–800	0.53	8.2	0.009	< LOD	< LOD	0.001	< LOD
9	800–2000	0.31	9.3	0.005	< LOD	< LOD	< LOD	< LOD

Santa Barbara – TB59						
Sample no.	Grain size [µm]	Ta ₂ O ₅ [%]	SnO ₂ [%]	Th [%]	U [%]	Ce [%]
1	< 63	0.0081	0.179	0.0270	0.0067	0.107
2	63–100	0.0159	0.448	0.0359	0.0071	0.086
3	100–200	0.0040	0.355	0.0197	< LOD	0.080
4	200–300	< LOD	0.121	0.0090	< LOD	0.041
5	300–400	< LOD	0.060	0.0053	< LOD	0.031
6	400–500	< LOD	0.067	0.0067	< LOD	0.052
7	500–630	< LOD	0.039	0.0067	< LOD	0.034
8	630–800	< LOD	0.033	0.0053	< LOD	< LOD
9	800–2000	< LOD	0.014	0.0039	< LOD	< LOD

< LOD = < detection limit

Appendix 3

Element content – heavy / light fractions of Bromoform separations

Tab. 3.1A: Major element content – heavy / light fractions.

Section no.	Sample	SiO ₂	Al ₂ O ₃	Fe ₂ O ₃	TiO ₂	MnO	Y	La
		[%]	[%]	[%]	[%]	[%]	[ppm]	[ppm]
1	TB45-48 LF	90.1	4.88	0.90	0.099	0.009	19	24.7
2	TB45-48 LF	96.0	1.70	0.82	0.090	0.012	14	16.9
3	TB45-48 LF	96.2	1.47	0.90	0.119	0.011	13	15.5
4	TB45-48 HF	3.8	0.78	41.1	43.7	1.249	772	2150
5	TB45-48 HF	3.8	1.82	42.6	42.9	1.368	1196	2640
6	TB45-48 HF	17.7	22.9	18.1	20.1	0.683	3316	3440
Total		25.7	5.52	29.1	29.7	0.947	1296	2191
7	TB53 LF	91.8	3.50	1.49	0.15	0.017	13	12.2
8	TB53 LF	96.0	1.52	1.04	0.09	0.021	7	8.4
9	TB53 LF	95.1	1.88	1.00	0.06	0.026	7	6.9
10	TB53 HF	19.9	25.7	14.6	16.2	0.55	631	87.6
11	TB53 HF	20.9	27.6	11.4	7.4	0.34	196	55.8
12	TB53 HF	30.3	26.5	21.4	1.2	0.32	29	68.2
Total		81.7	6.6	4.0	1.0	0.10	34.1	18.7
13	TB55 LF	77.9	12.78	2.41	0.133	0.008	13	7.9
14	TB55 LF	94.8	2.44	0.94	0.035	0.011	4	2.8
15	TB55 LF	97.2	1.15	0.68	0.019	0.005	3	2.3
16	TB55 HF	12.3	13.77	5.42	1.136	0.501	874	67
17	TB55 HF	19.1	31.67	3.38	0.420	0.294	94	15
18	TB55 HF	24.3	40.38	1.24	0.104	0.064	10	1.6
Total		25.7	5.52	29.1	29.7	0.947	1296	2191
19	TB59 LF	78.8	10.9	4.05	0.185	0.005	14	12.1
20	TB59 LF	83.4	8.9	2.31	0.148	0.005	15	12.5
21	TB59 LF	91.9	3.4	1.77	0.065	0.005	7	6.1
22	TB59 HF	28.1	29.2	25.5	1.431	0.039	259	145
23	TB59 HF	24.2	28.7	32.8	0.398	0.016	34	30.1
24	TB59 HF	21.5	22.6	44.7	0.331	0.012	28	30.7
Total		79.4	8.3	6.7	0.154	0.007	17.1	13.6

Tab. 3.2A: Minor element content – heavy / light fractions.

Section no.	Sample	Grain size [µm]	Density fraction	Mass rec. [%]	Ta ₂ O ₅	Nb ₂ O ₅	SnO ₂	ZrO ₂
					[%]	[%]	[%]	[%]
1	TB45-48 LF	63–200	light	0.9	< 0.003	< 0.003	0.001	0.024
2	TB45-48 LF	200–630	light	10.6	< 0.003	< 0.003	0.003	0.038
3	TB45-48 LF	630–2000	light	9.7	< 0.003	0.008	0.001	0.030
4	TB45-48 HF	63–200	heavy	6.6	0.087	0.934	2.02	4.59
5	TB45-48 HF	200–630	heavy	54.1	0.098	1.033	2.78	1.54
6	TB45-48 HF	630–2000	heavy	17.9	0.027	0.273	0.62	5.99
Total		63–2000			0.064	0.670	1.74	2.21
7	TB53 LF	63–200	light	0.9	< 0.003	< 0.003	0.004	0.013
8	TB53 LF	200–630	light	43.6	< 0.003	< 0.003	0.004	0.013
9	TB53 LF	630–2000	light	35.8	< 0.003	0.003	0.003	0.014
10	TB53 HF	63–200	heavy	1.3	0.045	0.134	7.8	4.38
11	TB53 HF	200–630	heavy	9.1	0.054	0.094	19.6	0.43
12	TB53 HF	630–2000	heavy	9.1	0.036	0.042	9.5	0.07
Total		63–2000			0.010	0.016	2.8	0.11
13	TB55 LF	63–200	light	0.2	< 0.003	0.02	0.034	0.056
14	TB55 LF	200–630	light	6.4	< 0.003	0.007	0.011	0.005
15	TB55 LF	630–2000	light	32.5	< 0.003	< 0.003	0.006	0.004
16	TB55 HF	63–200	heavy	3.1	1.37	13.0	32.3	6.13
17	TB55 HF	200–630	heavy	28.8	0.84	8.23	21.1	0.43
18	TB55 HF	630–2000	heavy	28.9	0.19	1.75	19.1	0.02
Total		63–2000			0.34	3.28	12.5	0.32
19	TB59 LF	63–200	light	2.9	0.003	0.021	0.025	0.027
20	TB59 LF	200–630	light	32.0	< 0.003	0.016	0.020	0.019
21	TB59 LF	630–2000	light	51.6	< 0.003	0.006	0.008	0.013
22	TB59 HF	63–200	heavy	1.8	0.033	0.339	0.48	1.630
23	TB59 HF	200–630	heavy	5.4	0.004	0.050	0.10	0.102
24	TB59 HF	630–2000	heavy	6.0	< 0.003	0.016	0.04	0.040
Total		63–2000			0.002	0.019	0.027	0.051

Tab. 3.3A: Trace element content – heavy / light fractions.

Section no.	Sample	Ce	Pr	Nd	Hf	W	Th	U	F
		[ppm]	[ppm]	[ppm]	[ppm]	[ppm]	[ppm]	[ppm]	[%]
1	TB45-48 LF	51	5.39	19.1	2.9	3	5.7	2.3	
2	TB45-48 LF	34	3.97	14.6	6.1	2	5.9	2.4	
3	TB45-48 LF	28	3.59	12.9	5.0	1	6.1	2.0	
4	TB45-48 HF	4290	503	1800	807	152	917	134	0.32
5	TB45-48 HF	5330	621	2190	306	130	1320	145	0.04
6	TB45-48 HF	6980	882	3200	1350	48	1990	371	4.40
Total		4426	528	1881	462	89	1133	154.3	0.83
7	TB53 LF	31	2.71	9.8	3.0	12	7.1	1.4	
8	TB53 LF	20	1.85	6.6	2.7	8	4.4	1.0	
9	TB53 LF	23	1.46	5.2	2.4	8	4.2	0.9	
10	TB53 HF	284	22.2	86.5	890	313	182	86.6	
11	TB53 HF	242	12.4	44.7	150	336	50.9	22.6	
12	TB53 HF	436	16.0	61.0	44	217	39.4	12.2	
Total		83	4.2	15.6	31	61	14.0	5.0	
13	TB55 LF	694	1.78	5.4	15.3	8	70.4	6.6	
14	TB55 LF	118	0.62	1.9	1.9	2	13.6	1.1	
15	TB55 LF	59	0.51	1.6	1.3	3	8.1	0.9	
16	TB55 HF	330	22.9	74.4	2120	2080	777	387	
17	TB55 HF	102	4.3	13.5	167	1120	73.9	68	
18	TB55 HF	59	0.4	1.0	27	443	10.6	22	
Total		85	2.3	7.1	123	516	52.2	38	
19	TB59 LF	108	2.26	6.9	6.2	14	56.4	5.6	
20	TB59 LF	97	2.40	7.6	5.2	10	40.9	3.9	
21	TB59 LF	45	1.21	3.7	3.7	6	22.8	2.6	
22	TB59 HF	588	29.2	86.4	426	127	568	95.1	
23	TB59 HF	589	5.10	15.6	27	44	217	29.5	
24	TB59 HF	425	5.11	15.1	12	40	233	34.5	
Total		125	2.6	7.9	13.7	14	63	8.1	

Appendix 4

Mineralogical composition of the different grain size fractions

Tab. 4.1A: Sample TB45-48 – Quantitative mineralogical composition of heavy and light fractions by means of Mineral Liberation Analysis – MLA (polished thin sections No. 1 to 6).

	Light fraction			Heavy fraction		
	63-200 (1)	200-630 (2)	630-2000 (3)	63-200 (4)	200-630 (5)	630-2000 (6)
	[µm]	[µm]	[µm]	[µm]	[µm]	[µm]
	[%]			[%]		
Quartz	72.15	93.58	95.52	1.11	1.76	1.87
Orthoclase	19.23	4.47	2.7	0.36	0.13	0.12
Albite	2.5	0.42	0.18			
Schoerl	2.05	0.43	0.66	0.16	0.14	0.18
Topaz	1.39	0.42	0.3	0.74	1.31	35.9
Muscovite	0.91	0.22	0.19			
Kaolinite	0.74	0.13				
Biotite	0.23		0.26			
Almandine-Spessartine	0.22				0.15	0.19
Hornblende	0.19					
Ilmenite		0.1		81.51	86.61	42.96
Zircon				9.21	2.34	8.59
Monazite				2.39	1.52	2.73
Cassiterite				1.54	3.37	0.93
Mn-Columbite				0.7	0.91	0.15
Fe-Columbite				0.11	0.15	
Xenotime				0.11		0.92
Strüverite				0.25	0.15	0.21
Goethite				0.42	0.28	1.31
Rutile				0.55	0.55	0.61
Gahnite-(Fe)						2.85
Unknown	0.11			0.18	0.11	0.15

Tab. 4.2A: Sample TB53 (Bom Futuro) – Quantitative mineralogical composition of heavy and light fractions by means of Mineral Liberation Analysis – MLA (polished thin sections No. 7 to 12).

	Light fraction			Heavy fraction		
	63-200 (7)	200-630 (8)	630-2000 (9)	63-200 (10)	200-630 (11)	630-2000 (12)
	[µm]	[µm]	[µm]	[µm]	[µm]	[µm]
	[%]			[%]		
Quartz	76.29	96.27	93.09	2.59	1.2	13.3
Orthoclase	7.82	1.61	3.83	0.77		0.24
Albite	0.76	0.31		0.13	0.12	
Schoerl	7.03	0.74	1.53	4.05	1.21	1.45
Topaz	4.11	0.43	0.58	40.34	48.76	48.5
Muscovite	0.76		0.1	0.4	0.15	0.37
Kaolinite	0.84	0.16	0.15	0.25	0.1	
Biotite	0.21			0.33	0.13	0.38
Almandine-Spessartine	1.07	0.12	0.2	1.8	1.17	2.89
Ilmenite				23.68	14.48	0.5
Zircon				8.86	1.33	
Monazite				0.09		
Cassiterite				7.33	23.48	8.32
Fe-Columbite				0.11		
Xenotime				0.11		
Strüverite				0.43	0.43	0.29
Goethite	0.65	0.12	0.25	5.22	4.85	22.35
Rutile				2.35	1.68	0.31
MnOxBa				0.11	0.1	0.23
Unknown				0.55	0.25	0.54

Tab. 4.3A: Sample TB55 – Quantitative mineralogical composition of heavy and light fractions by means of Mineral Liberation Analysis – MLA (polished thin sections No. 13 to 18).

	Light fraction			Heavy fraction		
	63-200 (13)	200-630 (14)	630-2000 (15)	63-200 (16)	200-630 (17)	630-2000 (18)
	[μm]	[μm]	[μm]	[μm]	[μm]	[μm]
	[%]			[%]		
Quartz	39.72	90.15	96.45	0.61	0.53	0.3
Albite	0.47	0.31	0.18		0.13	
Schoerl	12.4	2.21	0.75	1.89	1.41	0.89
Topaz	38.43	4.97	1.92	24.12	56.67	71.79
Muscovite	0.34			0.27		
Kaolinite	6.87	2.1	0.47	1.14	0.96	0.67
Almandine-Spessartine	0.82		0.18	0.14	0.13	0.14
Hornblende				0.25	0.1	
Ilmenite				1.25	0.24	
Zircon	0.35			14.66	1.54	
Monazite				0.12		
Cassiterite				34.01	24.47	22.23
Mn-Columbite				14.61	10.68	3.35
Fe-Columbite				3.77	1.91	0.38
Strüverite				0.11		
Goethite				0.17		
Rutile				0.13		
Pyrochlor				0.8	0.28	
(Ca, Ti, Ce, Zr)-Alu.				0.12		
Unknown				0.64	0.29	

Tab. 4.4A: Sample TB59 – Quantitative mineralogical composition of heavy and light fractions by means of Mineral Liberation Analysis – MLA (polished thin sections No. 19 to 24).

	Light fraction			Heavy fraction		
	63-200 (19)	200-630 (20)	630-2000 (21)	63-200 (22)	200-630 (23)	630-2000 (24)
	[µm]	[µm]	[µm]	[µm]	[µm]	[µm]
	[%]			[%]		
Quartz	39.72	90.15	96.45	0.61	0.53	0.3
Albite	0.47	0.31	0.18		0.13	
Schoerl	12.4	2.21	0.75	1.89	1.41	0.89
Topaz	38.43	4.97	1.92	24.12	56.67	71.79
Muscovite	0.34			0.27		
Kaolinite	6.87	2.1	0.47	1.14	0.96	0.67
Almandine-Spessartine	0.82		0.18	0.14	0.13	0.14
Hornblende				0.25	0.1	
Ilmenite				1.25	0.24	
Zircon	0.35			14.66	1.54	
Monazite				0.12		
Cassiterite				34.01	24.47	22.23
Mn-Columbite				14.61	10.68	3.35
Fe-Columbite				3.77	1.91	0.38
Strüverite				0.11		
Goethite				0.17		
Rutile				0.13		
Pyrochlor				0.8	0.28	
(Ca, Ti, Ce, Zr)-Alu.				0.12		
Unknown				0.64	0.29	

Appendix 5

Mineralogical composition of the different grain size fractions

Tab. 5.1A: Sample TB45-48 – concentrations / recovery of TiO₂.

Sample no.	Grain size		Density fraction		Magnetic fraction		TiO ₂	
	[µm]	rec. [%]	Typ	rec. [%]	Typ	rec. [%]	rec. [%]	rec. [%]
11	< 63	0.2						4.5
12	63–250	19.8						44.1
40	63–250				Para 0	4.6	7.55	53.9
37	63–250				Para 1	12.3	18.84	50.5
39	63–250				Dia	2.9	0.04	0.5
13	250–500	47.1						37.3
22	250–500		HF1	11.9				46.1
49	250–500		HF1		Para	11.0	16.58	49.7
51	250–500		HF1		Dia	0.9	0.01	0.5
23	250–500		HF2	22.7				54.9
52	250–500		HF2		Para	21.8	36.51	55.1
54	250–500		HF2		Dia	0.9	0.04	1.6
24	250–500		HF3	3.6			3.52	32.4
25	250–500		MD	4.1			0.39	3.2
26	250–500		LF	4.8			0.06	0.4
14	500–710	12.6						23.5
27	500–710		HF1	6.8				40.4
61	500–710		HF1		Para	5.9	9.11	51.3
63	500–710		HF1		Dia	0.9	0.02	0.8
28	500–710		HF2	1.5				13.6
64	500–710		HF2		Para	0.5	0.74	46.0
66	500–710		HF2		Dia	1.0	0.01	0.3
30	500–710		MD	0.8				2.1
70	500–710		MD		Para	0.1	0.05	28.9
72	500–710		MD		Dia	0.7	0.00	0.1
31	500–710		LF	3.4			0.02	0.2
15	710–2000	20.2						9.3
32	710–2000		HF1	3.4				28.4
73	710–2000		HF1		Para	2.3	3.27	47.6
75	710–2000		HF1		Dia	1.1	0.02	0.6
33	710–2000		HF2	2.9				16.0
76	710–2000		HF2		Para	1.2	1.68	47.7
78	710–2000		HF2		Dia	1.7	0.01	0.2
34	710–2000		HF3	4.1				7.4
79	710–2000		HF3		Para	0.8	1.11	44.0
81	710–2000		HF3		Dia	3.3	0.02	0.2
35	710–2000		MD	2.5				3.1
82	710–2000		MD		Para	0.2	0.22	30.1
84	710–2000		MD		Dia	2.3	0.01	0.2
36	710–2000		LF	7.7			0.15	0.6

rec.: recovery

Tab. 5.2A: Sample TB45-48 – concentrations / recovery of Fe₂O₃, ZrO₂, Nb₂O₅ and Ta₂O₅.

Sample no.	Fe ₂ O ₃		ZrO ₂		Nb ₂ O ₅		Ta ₂ O ₅	
	rec.	con.	rec.	con.	rec.	con.	rec.	con.
	[%]	[%]	[%]	[%]	[%]	[%]	[%]	[%]
11		5.8		2.17		0.12		
12		19.5		1.38		1.21		0.11
40	7.82	22.8	0.22	0.10	3.406	0.69		0.04
37	19.04	20.8	2.38	0.41	26.162	1.99		0.17
39	0.13	0.6	15.95	11.48	0.149	0.05		0.07
13		16.9		0.48		1.03		0.11
22		19.8		0.31		2.55		0.21
49	16.38	20.0	0.34	0.06	30.319	2.58		0.21
51	0.03	0.4	1.62	3.69	0.775	0.79		0.27
23		21.8		0.56		1.04		0.05
52	33.93	20.9	1.27	0.12	23.281	1.00		0.05
54	0.05	0.8	9.51	22.08	0.069	0.07		
24	3.81	14.3	1.65	0.97	1.526	0.40		
25	0.87	2.9	0.96	0.49	0.003	0.001		
26	0.35	1.0	0.18	0.08	0.004	0.001		
14		11.6		1.74		0.57		
27		16.2		2.39		1.05		
61	8.32	19.1	0.89	0.32	8.561	1.37		
63	0.03	0.5	11.61	25.70	0.176	0.17		0.19
28		9.2		2.92		0.31		
64	0.80	20.2	0.25	0.99	0.360	0.64		0.04
66	0.03	0.5	3.05	6.59	0.026	0.02		
30		3.0		0.94		0.02		
70	0.11	24.2	0.02	0.57	0.030	0.46		
72	0.03	0.5	0.18	0.51	0.001	0.00		
31	0.23	0.9	0.09	0.05	0.003	0.001		
15		7.2		3.16		0.16		
32		12.9		5.49		0.72		
73	2.99	17.7	0.94	0.87	2.388	0.99		
75	0.05	0.6	13.05	24.01	0.203	0.17		0.14
33		9.6		6.75		0.50		
76	1.68	19.5	0.68	1.22	1.001	0.81		
78	0.08	0.6	15.60	18.76	0.281	0.15		
34		6.3		4.95		0.18		
79	1.41	22.8	0.45	1.13	0.755	0.85		
81	0.12	0.5	12.70	8.15	0.349	0.10		
35		4.5		3.01		0.08		
82	0.50	27.8	0.09	0.76	0.134	0.52		
84	0.07	0.4	3.49	3.24	0.034	0.01		
36	1.13	2.0	2.84	0.77	0.006	0.001		

rec.: recovery; con.: concentration

Tab. 5.3A: Sample TB45-48 – concentrations / recovery of SnO₂, Ce, Th and U.

Sample no.	SnO ₂		Ce		Th		U	
	rec.	con.	rec.	con.	rec.	con.	rec.	con.
	[%]	[%]	[%]	[%]	[%]	[%]	[%]	[%]
11		0.28		0.10		0.025		0.009
12		6.05		0.19		0.072		0.009
40	0.41	0.20	0.37	0.03	1.13	0.025	1.02	0.004
37	9.86	1.80	16.00	0.41	13.23	0.109	7.12	0.010
39	18.78	14.47	0.23	0.03	1.05	0.036	1.93	0.011
13		7.02		0.30		0.122		0.008
22		18.83		0.58		0.196		0.013
49	15.24	3.12	19.21	0.55	17.52	0.162	7.83	0.012
51	37.33	90.93	0.07	0.03	0.15	0.017	0.24	0.004
23		0.88		0.32		0.117		0.009
52	0.65	0.07	20.42	0.29	20.91	0.097	10.99	0.009
54	3.40	8.47	0.07	0.03	0.35	0.039	1.94	0.037
24	0.17	0.11	1.50	0.13	1.83	0.052	1.97	0.010
25	0.16	0.09	0.32	0.03	2.00	0.050	1.04	0.004
26	0.03	0.02	0.38	0.03	0.14	0.003	1.23	0.004
14		2.51		0.55		0.174		0.024
27		5.09		1.00		0.288		0.038
61	1.89	0.72	22.88	1.22	18.76	0.325	11.30	0.033
63	7.01	16.63	0.08	0.03	0.63	0.067	3.20	0.058
28		0.07		0.07		0.040		0.022
64	0.02	0.10	0.20	0.12	0.29	0.056	0.51	0.017
66	0.11	0.26	0.08	0.03	0.20	0.021	1.86	0.033
30		0.10		0.03		0.006		0.005
70	0.01	0.20	0.05	0.24	0.05	0.082	0.05	0.013
72	0.02	0.06	0.06	0.03	0.02	0.003	0.19	0.004
31	0.02	0.02	0.27	0.03	0.10	0.003	0.87	0.004
15		0.77		0.32		0.103		0.028
32		2.81		1.31		0.350		0.069
73	0.46	0.46	11.02	1.52	9.89	0.444	6.45	0.049
75	3.32	6.54	0.25	0.07	1.24	0.110	6.48	0.098
33		0.57		0.57		0.157		0.067
76	0.09	0.17	3.36	0.91	3.04	0.266	3.05	0.045
78	0.44	0.57	0.30	0.05	2.17	0.126	11.70	0.116
34		0.11		0.19		0.085		0.040
79	0.09	0.25	1.13	0.42	1.43	0.175	1.76	0.036
81	0.36	0.25	0.72	0.07	2.33	0.072	12.05	0.064
35		0.19		0.08		0.039		0.027
82	0.05	0.43	0.22	0.29	0.27	0.114	0.30	0.021
84	0.03	0.03	0.18	0.03	0.75	0.034	2.98	0.023
36	0.05	0.02	0.62	0.03	0.51	0.007	1.97	0.004

rec.: recovery; con.: concentration

Appendix 6

Bom Futuro: concentrations / recovery of elements

Tab. 6.1A: Sample TB53 – concentrations / recovery of TiO₂.

Sample no.	Grain size		Density fraction		Magnetic fraction		TiO ₂	
	[µm]	rec. [%]	Typ	rec. [%]	Typ	rec. [%]	rec. [%]	
10	< 63	0.2						1.8
11	63–250	7.6						4.7
16	63–250		HF1	1.10				21.0
36	63–250		HF1		Para	0.64	27.1	46.2
38	63–250		HF1		Dia	0.46	0.6	1.4
17	63–250		HF2	0.41				14.4
39	63–250		HF2		Para	0.16	7.2	47.4
41	63–250		HF2		Dia	0.24	0.4	1.6
18	63–250		HF3	0.96				4.8
42	63–250		HF3		Para	0.08	2.5	33.6
44	63–250		HF3		Dia	0.88	0.8	1.0
19	63–250		MD	0.94				1.6
45	63–250		MD		Para	0.15	2.3	16.7
47	63–250		MD		Dia	0.79	0.3	0.4
20	63–250		LF	4.19			1.2	0.3
12	250–500	39.5						1.1
21	250–500		HF1	2.00				6.7
48	250–500		HF1		Para	0.46	18.2	42.7
50	250–500		HF1		Dia	1.54	1.0	0.7
22	250–500		HF2	2.33				4.1
51	250–500		HF2		Para	0.34	10.3	33.5
53	250–500		HF2		Dia	2.00	0.7	0.4
24	250–500		MD	12.21			5.3	0.5
25	250–500		LF	22.96			2.5	0.1
13	500–710	18.9						0.4
26	500–710		HF1	1.15				1.9
60	500–710		HF1		Para	0.14	2.5	20.0
62	500–710		HF1		Dia	1.01	0.4	0.4
27	500–710		HF2	0.58				1.8
63	500–710		HF2		Para	0.07	1.2	18.9
65	500–710		HF2		Dia	0.51	0.1	0.2
29	500–710		MD	5.03			1.8	0.4
30	500–710		LF	12.15			1.2	0.1
14	710–2000	33.8						0.2
31	710–2000		HF1	3.91				0.7
72	710–2000		HF1		Para	0.95	2.2	2.6
74	710–2000		HF1		Dia	2.96	0.8	0.3
32	710–2000		HF2	5.23				0.2
75	710–2000		HF2		Para	0.70	0.7	1.0
77	710–2000		HF2		Dia	4.52	2.0	0.5
34	710–2000		MD	5.82			0.8	0.2
35	710–2000		LF	18.82			5.7	0.3

rec.: recovery

Tab. 6.2A: Sample TB53 – concentrations / recovery of Fe₂O₃, ZrO₂, Nb₂O₅ and Ta₂O₅.

Sample no.	Fe ₂ O ₃		ZrO ₂		Nb ₂ O ₅		Ta ₂ O ₅	
	rec.	con.	rec.	con.	rec.	con.	rec.	con.
	[%]	[%]	[%]	[%]	[%]	[%]	[%]	[%]
10		11.4		0.513		0.048		0.04
11		4.8		1.243		0.586		0.28
16		9.9		3.621		0.374		0.16
36	3.6	20.0	8.4	1.283	14.6	0.484	2.9	0.12
38	0.1	0.4	38.9	8.228	4.8	0.222	5.1	0.29
17		8.0		2.081		0.166		0.03
39	1.0	20.7	1.8	1.054	2.4	0.308	0.4	0.06
41	0.0	0.6	11.3	4.512	0.6	0.055	0.1	0.01
18		4.4		0.554		0.072		0.03
42	0.5	20.5	0.5	0.608	1.0	0.248	0.1	0.03
44	0.1	0.6	5.6	0.621	1.0	0.025	0.3	0.01
19		3.0		0.068		0.012		0.01
45	1.2	27.9	0.3	0.162	0.9	0.129	0.0	0.01
47	0.1	0.6	0.3	0.041	0.1	0.003	0.2	0.01
20	2.6	2.2		0.014	0.10	0.001	1.3	0.01
12		2.4		0.095		0.019		0.09
21		3.8		0.270		0.307		0.22
48	2.7	20.9	1.0	0.216	11.22	0.511	2.7	0.15
50	0.2	0.5	5.2	0.328	18.57	0.255	15.2	0.26
22		4.3		0.135		0.080		0.12
51	2.1	22.2	0.6	0.164	5.20	0.327	1.2	0.09
53	0.3	0.5	2.6	0.128	5.27	0.056	8.5	0.11
24	7.5	2.2	4.1	0.033	0.41	0.000716	3.8	0.01
25	10.3	1.6	6.4	0.027	0.54	0.001	7.1	0.01
13		2.4		0.041		0.000		0.06
26		2.6		0.068		0.307		0.29
60	1.2	30.7	0.1	0.062	3.85	0.600	1.5	0.28
62	0.1	0.4	0.7	0.070	11.55	0.241	10.2	0.26
27		5.0		0.041		0.052		0.09
63	0.6	33.2	0.1	0.084	0.90	0.280	0.5	0.18
65	0.1	0.5	0.3	0.052	1.27	0.052	1.9	0.10
29	4.4	3.2	0.7	0.014	0.12	0.001	1.5	0.01
30	6.7	2.0	1.7	0.014	0.29	0.001	3.7	0.01
14		5.2		0.014		0.005		0.04
31		11.2		0.027		0.091		0.16
72	14.0	52.5	0.3	0.029	4.67	0.103	3.7	0.10
74	0.5	0.6	1.8	0.058	8.49	0.061	18.6	0.16
32		6.8		0.014		0.003		0.03
75	8.6	43.7	0.2	0.029	0.49	0.015	0.5	0.02
77	1.6	1.3	0.8	0.016	0.95	0.004	1.4	0.01
34	9.7	5.9	0.8	0.014	0.14	0.001	1.8	0.01
35	20.2	3.8	5.2	0.027	0.45	0.001	5.8	0.01

rec.: recovery; con.: concentration

Tab. 6.3A: Sample TB53 – concentrations / recovery of SnO₂, Th and U.

Sample no.	SnO ₂		Th		U	
	rec.	con.	rec.	con.	rec.	con.
	[%]	[%]	[%]	[%]	[%]	[%]
10		1.61		0.004		0.002
11		10.15		0.014		0.005
16		41.96		0.030		0.013
36	1.2	7.99	12.1	0.030	2.8	0.009
38	7.5	67.22	7.6	0.026	3.7	0.016
17		5.09		0.012		0.009
39	0.04	0.95	2.9	0.029	0.7	0.008
41	0.45	7.52	1.6	0.010	2.0	0.016
18		0.46		0.004		0.002
42	0.01	0.52	1.0	0.020	0.2	0.005
44	0.13	0.61	0.4	0.001	0.8	0.002
19		0.18		0.001		0.002
45	0.01	0.32	1.8	0.019	0.3	0.004
47	0.01	0.08	0.4	0.001	0.7	0.002
20	0.03	0.0250	2.1	0.001	3.7	0.002
12		7.71		0.001		0.002
21		66.75		0.010		0.002
48	2.05	18.17	7.5	0.026	1.1	0.005
50	28.57	76.30	0.8	0.001	1.3	0.002
22		24.10		0.004		0.002
51	0.51	6.22	4.0	0.019	1.2	0.007
53	12.97	26.72	1.0	0.001	1.7	0.002
24	0.25	0.09	6.1	0.001	10.7	0.002
25	0.14	0.0250	11.5	0.001	20.0	0.002
13		7.68		0.001		0.002
26		69.46		0.001		0.002
60	0.67	20.19	2.0	0.024	0.5	0.007
62	17.34	70.46	0.5	0.001	0.9	0.002
27		16.92		0.004		0.002
63	0.09	5.70	0.8	0.018	0.2	0.007
65	2.84	22.79	0.3	0.001	0.4	0.002
29	1.09	0.89	5.0	0.002	4.4	0.002
30	0.15	0.05	6.1	0.001	10.6	0.002
14		3.45		0.001		0.002
31		24.43		0.001		0.002
72	0.47	2.04	5.3	0.009	2.8	0.006
74	20.51	28.52	1.5	0.001	2.6	0.002
32		0.55		0.001		0.002
75	0.05	0.31	2.9	0.007	1.2	0.003
77	2.06	1.88	2.3	0.001	3.9	0.002
34	0.07	0.05	2.9	0.001	5.1	0.002
35	0.70	0.15	9.4	0.001	16.4	0.002

rec.: recovery; con.: concentration

Appendix 7

Cachoeirinha: concentrations / recovery of elements

Tab. 7.1A: Sample TB55 – concentrations / recovery of TiO₂.

Sample no.	Grain size		Density fraction		Magnetic fraction		TiO ₂	
	[µm]	rec. [%]	Typ	rec. [%]	Typ	rec. [%]	rec. [%]	rec. [%]
10	< 63	0.1						
11	63–250	6.5						0.46
16	63–250		HF1	3.2				0.63
32	63–250		HF1		Para	1.54	14.5	1.35
34	63–250		HF1		Dia	1.71	2.4	0.20
17	63–250		HF2	1.0				0.95
35	63–250		HF2		Para	0.49	6.2	1.81
37	63–250		HF2		Dia	0.55	1.0	0.26
18	63–250		MD	0.7				0.36
38	63–250		MD		Para	0.06	1.0	2.30
40	63–250		MD		Dia	0.63	0.7	0.15
19	63–250		LF	1.5			1.3	0.13
12	250–500	25.5						0.19
20	250–500		HF1	4.9				0.41
41	250–500		HF1		Para	1.90	14.4	1.08
43	250–500		HF1		Dia	3.01	3.9	0.19
21	250–500		HF2	3.4				0.33
44	250–500		HF2		Para	0.97	8.1	1.20
46	250–500		HF2		Dia	2.46	1.6	0.09
22	250–500		MD	2.0				0.09
47	250–500		MD		Para	0.04	0.8	2.92
49	250–500		MD		Dia	1.91	0.7	0.05
23	250–500		LF	15.2			6.1	0.06
13	500–710	20.0						0.09
24	500–710		HF1	3.2				0.23
50	500–710		HF1		Para	0.80	3.9	0.70
52	500–710		HF1		Dia	2.37	2.3	0.14
25	500–710		HF2	2.0				0.07
53	500–710		HF2		Para	0.12	0.7	0.90
55	500–710		HF2		Dia	1.93	0.7	0.05
26	500–710		MD	4.4				0.03
56	500–710		MD		Para	0.03	0.3	1.27
58	500–710		MD		Dia	4.35	1.7	0.06
27	500–710		LF	10.4			3.3	0.04
14	710–2000	48.0						0.05
28	710–2000		HF1	5.4				0.14
59	710–2000		HF1		Para	0.42	1.5	0.51
61	710–2000		HF1		Dia	4.99	5.2	0.15
29	710–2000		HF2	4.8				0.08
62	710–2000		HF2		Para	0.13	0.6	0.65
64	710–2000		HF2		Dia	4.69	3.6	0.11
30	710–2000		MD	10.7			4.8	0.06
31	710–2000		LF	27.0			8.7	0.05

rec.: recovery

Tab. 7.2A: Sample TB55 – concentrations / recovery of Fe₂O₃, ZrO₂, Nb₂O₅ and Ta₂O₅.

Sample no.	Fe ₂ O ₃		ZrO ₂		Nb ₂ O ₅		Ta ₂ O ₅	
	rec.	con.	rec.	con.	rec.	con.	rec.	con.
	[%]	[%]	[%]	[%]	[%]	[%]	[%]	[%]
10								
11		2.52		2.97		13.12		2.97
16		2.94		1.95		22.52		3.58
32	11.1	7.28	13.3	2.27	21.9	43.27	21.3	8.28
34	0.9	0.56	10.4	1.60	0.8	1.43	1.6	0.55
17		3.65		10.32		17.98		4.23
35	3.3	6.86	21.8	11.63	5.1	31.79	5.5	6.73
37	0.3	0.48	19.8	9.52	0.0	0.20	0.2	0.21
18		0.94		6.70		1.32		0.11
38	0.3	5.15	7.0	30.39	0.1	7.14	0.1	1.44
40	0.3	0.42	6.7	2.81	0.0	0.07	0.0	0.009
19	1.7	1.15	3.9	0.67	0.1	0.11	0.0	0.009
12		1.56		0.17		7.94		1.83
20		2.61		0.23		21.87		3.18
41	15.6	8.32	1.6	0.23	30.6	49.20	29.2	9.20
43	1.6	0.55	2.5	0.21	1.7	1.71	2.9	0.58
21		2.52		0.23		19.32		3.03
44	8.4	8.74	1.4	0.39	15.4	48.51	13.3	8.17
46	0.9	0.36	1.6	0.17	0.5	0.60	1.2	0.29
22		0.69		0.20		2.21		0.31
47	0.6	16.65	0.3	1.80	0.4	35.37	0.4	6.15
49	0.6	0.32	1.1	0.15	0.0	0.04	0.0	0.009
23	10.2	0.68	1.8	0.03	0.7	0.14	1.0	0.04
13		0.95		0.02		3.24		0.97
24		1.74		0.05		15.48		2.07
50	5.5	6.98	0.2	0.07	12.2	46.37	10.0	7.45
52	1.1	0.48	1.6	0.18	1.2	1.48	1.8	0.46
25		0.90		0.02		6.27		0.99
53	1.1	9.30	0.0	0.08	1.6	42.97	1.4	7.08
55	0.7	0.35	0.2	0.02	0.2	0.34	0.5	0.14
26		0.50		0.01		0.98		0.12
56	0.6	18.27	0.0	0.18	0.3	29.51	0.3	5.16
58	1.4	0.34	0.4	0.03	0.1	0.04	0.1	0.02
27	6.5	0.63	0.4	0.01	0.1	0.01	0.2	0.009
14		0.57		0.01		0.36		0.25
28		0.70		0.13		3.96		0.74
59	1.4	3.47	0.2	0.11	3.3	24.22	2.8	3.99
61	1.8	0.37	0.7	0.04	1.3	0.81	2.5	0.30
29		0.65		0.04		2.13		0.48
62	0.9	6.92	0.0	0.08	1.2	28.03	0.9	4.44
64	1.7	0.37	0.5	0.03	1.0	0.65	2.1	0.26
30	5.1	0.48	0.6	0.01	0.1	0.02	0.3	0.02
31	16.5	0.62	2.0	0.02	0.1	0.007	0.4	0.009

rec.: recovery; con.: concentration

Tab. 7.3A: Sample TB55 – concentrations / recovery of SnO₂, Th and U.

Sample no.	SnO ₂		Th		U	
	rec.	con.	rec.	con.	rec.	con.
	[%]	[%]	[%]	[%]	[%]	[%]
10						
11		32.5		0.088		0.0331
16		53.5		0.054		0.0313
32	1.7	17.7	18.3	0.082	14.8	0.0581
34	9.3	87.2	0.4	0.0015	3.3	0.0117
17		8.2		0.262		0.1234
35	0.1	3.2	26.0	0.366	14.3	0.1762
37	0.7	21.4	9.5	0.120	6.0	0.0669
18		1.3		0.081		0.0816
38	0.0	2.2	5.8	0.661	3.9	0.3903
40	0.1	1.5	3.1	0.035	3.1	0.0301
19	0.0	0.3	3.9	0.018	2.5	0.0098
12		26.7		0.0015		0.0058
20		59.4		0.009		0.017
41	2.0	16.7	0.4	0.0015	10.8	0.0346
43	17.0	90.6	2.9	0.007	1.0	0.002
21		38.7		0.011		0.0105
44	0.5	9.1	3.1	0.022	5.4	0.0335
46	9.2	59.6	3.3	0.009	0.8	0.002
22		2.1		0.011		0.007
47	0.0	4.5	0.6	0.121	0.3	0.0519
49	0.3	2.7	2.3	0.008	0.6	0.002
23	0.4	0.4	3.3	0.0015	5.0	0.002
13		23.3		0.011		0.002
24		61.5		0.0015		0.0093
50	1.4	28.4	0.2	0.0015	3.6	0.0276
52	11.0	74.2	0.5	0.0015	0.8	0.002
25		37.2		0.006		0.0046
53	0.1	20.3	0.0	0.0015	0.5	0.0274
55	5.1	42.5	0.4	0.0015	0.6	0.002
26		3.7		0.005		0.002
56	0.0	8.4	0.1	0.029	0.1	0.0221
58	1.3	4.8	0.9	0.0015	1.4	0.002
27	0.2	0.2	4.3	0.003	3.4	0.002
14		17.9				0.002
28		62.8		0.008		0.0065
59	1.7	63.4	0.1	0.0015	1.4	0.0198
61	20.9	67.2	1.1	0.0015	1.7	0.002
29		53.7		0.0015		0.002
62	0.4	44.2	0.0	0.0015	0.5	0.0222
64	15.3	52.2	1.0	0.0015	1.5	0.002
30	0.7	1.0	2.3	0.0015	3.5	0.002
31	0.5	0.3	5.9	0.0015	8.9	0.002

rec.: recovery; con.: concentration

Appendix 8

Santa Barbara: concentrations / recovery of elements

Tab. 8.1A: Sample TB59 – concentrations / recovery of Al₂O₃.

Sample no.	Grain size		Density fraction		Magnetic fraction		Al ₂ O ₃	
	[µm]	rec.	Typ	rec.	Typ	rec.	rec.	
		[%]		[%]		[%]	[%]	
42.0	< 20	14.0					19.7	
42.1	20-63	0.3					16.9	
42.2	63-200	5.5					16.0	
45	63-200		HF1	0.75			1.5	18.1
46	63-200		HF2	1.25			1.7	12.7
47	63-200		MD	1.20			1.8	13.7
48	63-200		LF	2.31			4.8	19.4
11	200-630	33.00						17.9
13	200-630		HF1	2.22			3.5	14.7
21	200-630		HF1		Para 1	0.52	0.6	13.4
23	200-630		HF1		Dia	1.71	2.4	15.0
14	200-630		HF2	5.34			4.9	8.5
24	200-630		HF2		Para 1	0.91	1.5	17.4
26	200-630		HF2		Dia	4.43	2.5	6.0
15	200-630		MD	12.63			14.1	10.4
27	200-630		MD		Para 1	7.34	17.9	26.4
29	200-630		MD		Dia	5.29	2.5	5.2
16	200-630		LF	12.80			28.0	20.2
12	630-2000	47.20						7.7
17	630-2000		HF1	2.88			3.2	10.4
30	630-2000		HF1		Para 1	0.58	0.8	14.5
32	630-2000		HF1		Dia	2.30	1.6	7.6
18	630-2000		HF2	6.59			4.2	5.9
33	630-2000		HF2		Para 1	1.15	1.8	17.3
35	630-2000		HF2		Dia	5.44	1.4	2.7
19	630-2000		MD	13.16			8.7	6.1
36	630-2000		MD		Para 1	6.21	12.6	21.9
38	630-2000		MD		Dia	6.96	2.0	3.1
20	630-2000		LF	24.56			23.5	8.9

rec.: recovery; con.: concentration

Tab. 8.2A: Sample TB59 – concentrations / recovery of SiO₂, Fe₂O₃, Nb₂O₅ and Ta₂O₅.

Sample no.	SiO ₂		Fe ₂ O ₃		Nb ₂ O ₅		Ta ₂ O ₅	
	rec.	con.	rec.	con.	rec.	con.	rec.	con.
	[%]	[%]	[%]	[%]	[%]	[%]	[%]	[%]
42.0		25.1		8.3		0.081		0.058
42.1		42.8		15.3		0.308		0.042
42.2		46.7		10.7		0.095		0.027
45	0.47	33.7	2.1	16.5	30.14	0.590	6.66	0.089
46	1.18	50.9	3.1	14.6	2.02	0.024	0.25	0.002
47	1.21	54.2	2.0	9.7	1.14	0.014	2.21	0.019
48	1.77	41.3	2.9	7.4	4.48	0.029	6.09	0.027
11		48.2		7.5		0.028		0.017
13	2.18	52.9	4.8	12.7	16.65	0.110	6.06	0.027
21	0.1	14.4	2.9	49.9	11.77	0.407	2.78	0.059
23	2.2	65.6	0.2	0.9	0.38	0.004	0.31	0.002
14	6.81	68.7	7.6	8.4	2.08	0.006	1.06	0.002
24	0.3	19.3	4.9	48.3	1.68	0.033	0.17	0.002
26	7.0	80.4	0.3	0.7	0.02	0.0001	0.81	0.002
15	14.27	60.8	13.5	6.3	6.99	0.008	20.50	0.016
27	4.1	28.6	21.9	26.7	17.66	0.043	20.93	0.031
29	8.2	78.4	0.5	0.9	0.08	0.000	0.96	0.002
16	10.57	44.5	13.7	6.3	25.87	0.030	44.36	0.035
12		70.0		6.1		0.003		0.016
17	3.19	59.6	5.3	10.9	2.24	0.011	4.26	0.015
30	0.2	16.0	3.4	52.0	2.31	0.071	1.16	0.022
32	3.6	79.8	0.2	0.7	0.01	0.0001	0.42	0.002
18	8.43	68.9	11.8	10.6	1.02	0.002	1.31	0.002
33	0.4	19.3	6.3	48.8	1.57	0.024	1.99	0.019
35	9.4	87.9	0.5	0.9	0.03	0.0001	0.99	0.002
19	18.18	74.4	12.8	5.8	1.15	0.001	2.61	0.002
36	3.0	24.9	29.0	41.9	6.95	0.020	9.19	0.016
38	11.6	84.5	0.9	1.2	0.04	0.0001	1.27	0.002
20	31.75	69.6	20.4	4.9	6.20	0.004	4.87	0.002

rec.: recovery; con.: concentration

Tab. 8.3A: Sample TB59 – concentrations / recovery of SnO₂, Th and U.

Sample no.	SnO ₂		Th		U	
	rec.	con.	rec.	con.	rec.	con.
	[%]	[%]	[%]	[%]	[%]	[%]
42.0		0.046		0.0154		0.0015
42.1		0.653		0.0818		0.0190
42.2		0.277		0.0193		0.0045
45	26.74	1.658	7.11	0.05345	9.41	0.0176
46	0.88	0.033	2.81	0.0127	1.33	0.0015
47	0.18	0.007	1.44	0.0068	1.28	0.0015
48	1.77	0.036	4.49	0.011	2.46	0.0015
11		0.045		0.0087		0.0015
13	26.76	0.561	5.15	0.0131	2.37	0.0015
21	4.09	0.355	2.38	0.0378	2.37	0.009
23	21.99	0.578	0.85	0.0041	1.30	0.0015
14	7.43	0.065	4.06	0.0043	5.70	0.0015
24	0.75	0.037	3.32	0.0298	2.98	0.0064
26	0.69	0.007	0.38	0.0007	3.38	0.0015
15	1.90	0.007	10.95	0.0049	13.47	0.0015
27	3.64	0.022	23.38	0.02615	16.07	0.0043
29	0.83	0.007	0.45	0.0007	4.04	0.0015
16	7.64	0.028	21.07	0.0093	13.65	0.0015
12		0.041		0.0041		0.0015
17	20.04	0.324	3.67	0.0072	3.07	0.0015
30	1.58	0.122	2.12	0.03005	2.30	0.0078
32	15.24	0.297	0.20	0.0007	1.76	0.0015
18	0.99	0.007	7.11	0.0061	7.03	0.0015
33	2.65	0.103	4.09	0.02915	3.17	0.0054
35	0.85	0.007	0.93	0.0014	4.15	0.0015
19	1.98	0.007	9.08	0.0039	14.04	0.0015
36	4.09	0.030	20.03	0.0265	14.22	0.0045
38	1.09	0.007	0.59	0.0007	5.32	0.0015
20	3.69	0.007	23.03	0.0053	26.19	0.0015

rec.: recovery; con.: concentration

Appendix 9

Radiation measurements

Tab. 9.1A: Massangana TB45-48 – radiation measurements.

Sample no.	Grain size	Density fraction	Magnetic fraction	Mass	Dose rate	Alpha	beta + gamma
	[μm]			[g]	[nSv/h]	[ips]	[ips]
	Background				120	0.13	17.2
1	< 63			18.9	129	0.32	24.0
2	63–100			91.6	173	0.90	40.2
3	100–200			81.0	189	0.80	38.5
4	200–300			91.6	206	1.40	38.4
5	300–400			85.7	223	1.70	47.7
6	400–500			57.5	223	1.40	53.5
7	500–630			42.9	198	1.00	46.2
8	630–800			29.3	173	1.00	41.9
9	800–2000			67.9	212	1.30	50.3
10	63–200			91.6	200	0.90	40.2
11	< 63			18.9	129	0.32	24.0
12	63–250			94.8	202	1.30	40.1
13	250–500			87.5	225	1.40	52.8
14	500–710			72.2	256	2.40	71.0
15	710–2000			66.9	194	1.30	51.7
22	250–500	HF1		105.9	303	2.20	68.0
23	250–500	HF2		102.0	250	2.00	54.5
25	250–500	MD		61.8	125	0.20	19.5
26	250–500	LF		56.2	123	0.12	18.8
27	500–710	HF1		95.3	406	3.50	107.0
28	500–710	HF2		78.7	157	0.80	36.3
30	500–710	MD		54.9	122	0.28	18.2
31	500–710	LF		53.5	120	0.23	16.0
32	710–2000	HF1		87.9	433	3.50	120.0
33	710–2000	HF2		81.2	270	2.40	77.0
35	710–2000	MD		67.3	146	0.60	30.4
36	710–2000	LF		55.1	130	0.28	19.8
40	63–250		Para 0	101.1	144	0.40	24.0
37	63–250		Para 1	102.6	241	1.50	53.0
39	63–250		Dia	71.3	142	0.42	28.6
49	250–500	HF1	Para	106.1	324	2.00	69.0
51	250–500	HF1	Dia	143.8	139	0.70	28.3
52	250–500	HF2	Para	101.7	244	1.40	51.2
54	250–500	HF2	Dia	81.8	200	1.10	44.8

Tab. 9.1A: Massangana TB45-48 – radiation measurements.

Sample no.	Grain size	Density fraction	Magnetic fraction	Mass	Dose rate	Alpha	beta + gamma
	[μm]			[g]	[nSv/h]	[ips]	[ips]
55	250–500	HF3	Para	96.8	182	1.10	35.8
57	250–500	HF3	Dia	65.4	137	0.27	25.9
58	250–500	MD	Para	80.1	150	1.50	28.3
60	250–500	MD	Dia	59.7	117	0.15	16.2
61	500–710	HF1	Para	96.8	440	4.50	114.0
63	500–710	HF1	Dia	87.8	227	1.70	60.8
64	500–710	HF2	Para	87.6	200	1.60	47.8
66	500–710	HF2	Dia	72.4	150	0.42	31.1
73	710–2000	HF1	Para	101.0	554	5.10	156.0
75	710–2000	HF1	Dia	85.3	244	1.90	73.0
76	710–2000	HF2	Para	93.7	375	2.80	99.0
78	710–2000	HF2	Dia	76.8	226	1.70	65.1
79	710–2000	HF3	Para	85.2	300	2.80	83.0
81	710–2000	HF3	Dia	83.8	170	0.60	35.7
82	710–2000	MD	Para	81.1	227	1.50	54.5
84	710–2000	MD	Dia	68.2	138	0.47	23.7

Tab. 9.2A: Bom Futuro TB53 – radiation measurements.

Sample no.	Grain size	Density fraction	Magnetic fraction	Mass	Dose rate	Alpha	beta + gamma
	[μm]			[g]	[nSv/h]	[ips]	[ips]
	Background				120	0.13	17.2
1	< 63			35.3	119	0.23	18.6
2	63–100						
3	100–200			22.5	126	0.28	20.3
4	200–300			60.4	127	0.15	17.8
5	300–400			56.6	126	0.13	17.8
6	400–500			55.5	127	0.13	16.0
7	500–630			54.4	128	0.12	18.8
8	630–800			54.2	121	0.27	17.2
9	800–2000			50.3	126	0.07	17.2
10	< 63			36.9	115	0.17	18.8
11	63–250			63.4	125	0.17	19.7
12	250–500			55.8	120	0.22	15.6
13	500–710			53.1	117	0.15	18.4
14	710–2000			53.1	110	0.05	17.7
16	63–250	HF1		112.9	162	1.90	30.1
17	63–250	HF2		77.0	121	0.20	18.8

Tab. 9.2A: Bom Futuro TB53 – radiation measurements.

Sample no.	Grain size	Density fraction	Magnetic fraction	Mass	Dose rate	Alpha	beta + gamma
	[μm]			[g]	[nSv/h]	[ips]	[ips]
19	63–250	MD		66.8	115	0.15	15.7
20	63–250	LF		58.1	111	0.07	16.4
21	250–500	HF1		114.8	128	0.32	20.6
22	250–500	HF2		76.3	125	0.25	18.0
24	250–500	MD		60.0	120	0.08	15.8
25	250–500	LF		53.5	115	0.07	17.3
26	500–710	HF1		106.3	131	0.18	18.4
27	500–710	HF2		77.4	127	0.16	18.0
29	500–710	MD		57.3	119	0.05	17.4
30	500–710	LF		52.4	116	0.05	17.5
31	710–2000	HF1		66.4	120	0.48	20.4
32	710–2000	HF2		55.6	132	0.25	15.3
34	710–2000	MD		52.0	118	0.05	17.7
35	710–2000	LF		49.7	110	0.07	16.7
36	63–250	HF1	Para	105.3	163	0.90	29.7
38	63–250	HF1	Dia	100.5	155	1.00	27.5
39	63–250	HF2	Para	47.6	132	0.80	24.8
41	63–250	HF2	Dia	74.2	126	0.33	22.9
42	63–250	HF3	Para	30.7	131	0.45	20.0
44	63–250	HF3	Dia	76.1	123	0.10	17.9
45	63–250	MD	Para	16.2	124	0.17	21.7
47	63–250	MD	Dia	67.2	125	0.08	16.3
48	250–500	HF1	Para	97.0	140	0.60	26.8
50	250–500	HF1	Dia	120.1	125	0.33	18.6
51	250–500	HF2	Para	89.0	144	0.70	25.4
53	250–500	HF2	Dia	74.6	118	0.12	17.7
60	500–710	HF1	Para	30.2	136	0.30	24.1
62	500–710	HF1	Dia	108.2	120	0.18	17.0
63	500–710	HF2	Para	22.2	116	0.30	22.6
65	500–710	HF2	Dia	73.5	125	0.08	18.1
72	710–2000	HF1	Para	63.2	123	0.17	21.3
74	710–2000	HF1	Dia	68.8	116	0.17	16.3
75	710–2000	HF2	Para	58.2	118	0.18	17.7
77	710–2000	HF2	Dia	55.3	116	0.13	17.1

Tab. 9.3A: CachoeirinhaTB 55 – radiation measurements.

Sample no.	Grain size	Density fraction	Magnetic fraction	Mass	Dose rate	Alpha	beta + gamma
	[µm]			[g]			
	Background				120	0.13	17.2
1	< 63						
2	63–100						
3	100–200			21.2	140	0.90	34.0
4	200–300			57.4	135	0.60	21.5
5	300–400			76.3	132	0.30	19.0
6	400–500			69.8	128	0.33	18.8
7	500–630			69.4	132	0.20	18.2
8	630–800			66.0	125	0.27	16.3
9	800–2000			56.8	131	0.22	16.6
10	< 63						
11	63–250			91.4	175	1.80	39.4
12	250–500			78.5	123	0.18	19.6
13	500–710			69.3	131	0.03	16.0
14	710–2000			65.1	127	0.05	17.4
16	63–250	HF1		128.5	183	2.40	38.7
17	63–250	HF2		92.8	264	6.30	80.0
18	63–250	MD		76.7	160	2.10	38.8
19	63–250	LF		68.0	133	0.30	16.4
20	250–500	HF1		129.2	151	0.60	26.4
21	250–500	HF2		104.6	139	0.45	22.8
22	250–500	MD		77.4	123	0.08	19.0
23	250–500	LF		74.6	130	0.13	16.0
24	500–710	HF1		119.2	143	0.38	24.0
25	500–710	HF2		85.1	130	0.08	17.1
26	500–710	MD		73.0	124	0.12	15.4
27	500–710	LF		58.0	130	0.07	14.6
28	710–2000	HF1		104.7	130	0.30	19.3
29	710–2000	HF2		88.4	126	0.10	17.8
30	710–2000	MD		58.4	119	0.07	17.0
31	710–2000	LF		61.4	124	0.07	16.3
32	63–250	HF1	Para	119.4	220	2.90	51.7
34	63–250	HF1	Dia	138.5	138	0.80	24.7
35	63–250	HF2	Para	104.5	362	10.70	128.0
37	63–250	HF2	Dia	82.5	172	1.80	40.5
38	63–250	MD	Para	13.2	183	4.80	132.0
40	63–250	MD	Dia	75.8	130	0.70	22.8

Tab. 9.3A: CachoeirinhaTB 55 – radiation measurements.

Sample no.	Grain size	Density fraction	Magnetic fraction	Mass	Dose rate	Alpha	beta + gamma
	[μm]			[g]	[nSv/h]	[ips]	[ips]
41	250–500	HF1	Para	119.8	186	1.20	36.7
43	250–500	HF1	Dia	138.2	128	0.33	23.1
44	250–500	HF2	Para	120.2	178	1.40	43.2
46	250–500	HF2	Dia	96.1	125	0.25	19.3
47	250–500	MD	Para	13.3	133	1.10	43.0
49	250–500	MD	Dia	74.8	112	0.08	16.3
50	500–710	HF1	Para	120.4	170	1.00	36.1
52	500–710	HF1	Dia	115.7	120	0.23	18.1
53	500–710	HF2	Para	43.7	135	0.60	34.1
55	500–710	HF2	Dia	83.6	116	0.08	16.9
56	500–710	MD	Para	11.6	120	0.28	28.2
58	500–710	MD	Dia	73.2	120	0.10	16.7
59	710–2000	HF1	Para	127.9	160	1.00	38.0
61	710–2000	HF1	Dia	98.3	125	0.25	18.6
62	710–2000	HF2	Para	54.1	141	0.60	32.8
64	710–2000	HF2	Dia	86.0	118	0.12	17.6

Tab. 9.4A: Santa Barbara TB59 – radiation measurements.

Sample no.	Grain size	Density fraction	Magnetic fraction	Mass	Dose rate	Alpha	beta + gamma
	[μm]			[g]			
	Background				120	0.13	17.2
1	< 63						
2	63–100						
3	100–200			44.6	129	0.48	18.8
4	200–300			48.6	123	0.18	18.6
5	300–400			50.0	120	0.22	17.9
6	400–500			48.9	126	0.32	17.4
7	500–630			49.9	126	0.27	18.5
8	630–800			48.8	123	0.22	15.7
9	800–2000			51.6	123	0.17	18.0
10.0	< 63			30.1	116	0.43	20.7
10.1	63–200			52.4	133	0.47	21.3
11	200–630			51.1	122	0.20	18.3
12	630–2000			50.4	122	0.23	18.1
13	200–630	HF1		65.4	120	0.47	19.7
14	200–630	HF2		60.7	126	0.20	18.2
15	200–630	MD		55.4	122	0.30	17.1
16	200–630	LF		48.0	131	0.30	17.2
17	630–2000	HF1		62.1	125	0.22	17.1
18	630–2000	HF2		56.2	123	0.23	17.9
19	630–2000	MD		53.0	120	0.23	16.6
20	630–2000	LF		49.0	120	0.15	16.6
21	200–630	HF1	Para	21.6	123	0.60	22.0
23	200–630	HF1	Dia	64.1	119	0.07	18.4
24	200–630	HF2	Para	58.0	128	0.50	23.2
26	200–630	HF2	Dia	61.6	124	0.07	15.8
27	200–630	MD	Para	46.6	134	0.47	23.1
29	200–630	MD	Dia	55.5	123	0.10	17.6
30	630–2000	HF1	Para	30.7	137	0.25	23.8
32	630–2000	HF1	Dia	57.5	124	0.08	16.9
33	630–2000	HF2	Para	61.8	136	0.47	24.7
35	630–2000	HF2	Dia	55.1	121	0.10	15.8
36	630–2000	MD	Para	51.1	133	0.60	20.6
38	630–2000	MD	Dia	54.6	120	0.07	16.8
39	> 2000	500 g	Para	54.1	129	0.60	24.2

All masses refer to a volume of 38 cm³ (Petri dish 76 mm diameter, 8.4 mm height).

Appendix 10

Optical microscopy and SEM-BSE of polished thin sections

Tab. 10.1A: Topography of polished thin sections.

	Light fraction <2,89 g/cm ³			Heavy fraction >2,89 g/cm ³		
	63–200 μm	200–630 μm	630–2000 μm	63–200 μm	200–630 μm	630–2000 μm
TB 45-48						
TB 53						
TB 55						
TB 59						

RM: reflection mode/light

TM: transmitted light

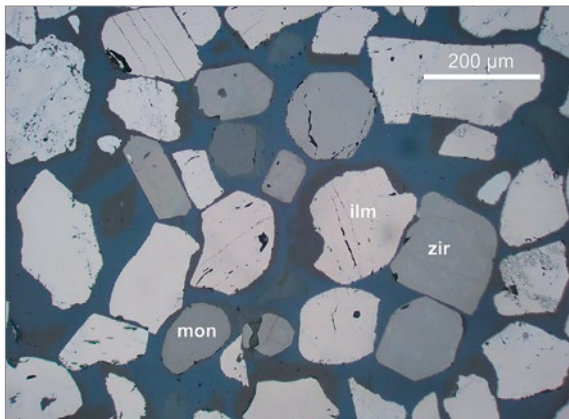


Fig. 10.1A: Section #04, RM, 200x, ||: Bulk of different heavy mineral grains, mostly ilmenite.

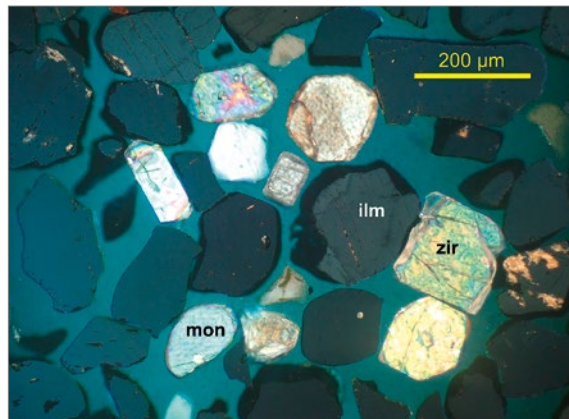


Fig. 10.2A: Section #04, RM, 200x, #: Same in polarized light.

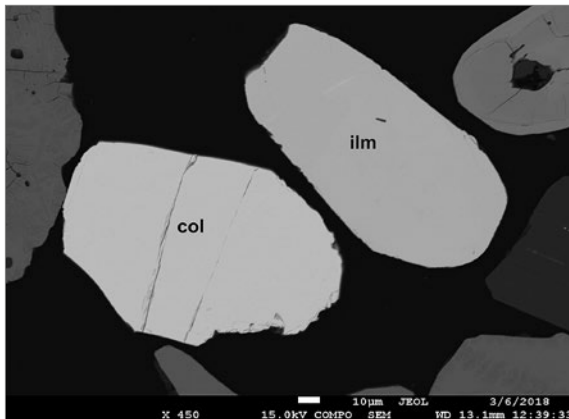


Fig. 10.3A: Section #04, SEM-BSE: Columbite and ilmenite with different brightness by reason of atomic weight.

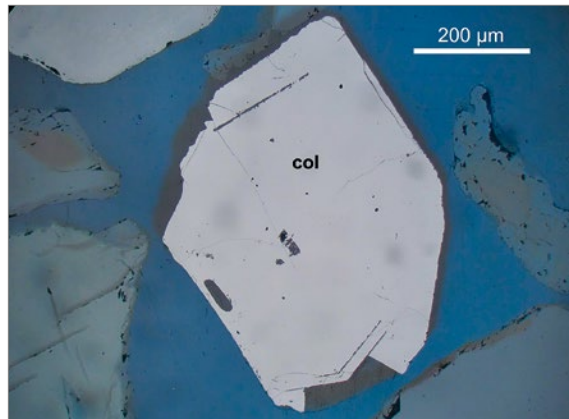


Fig. 10.4A: Section #18, RM, 200x, ||: Columbite crystal.

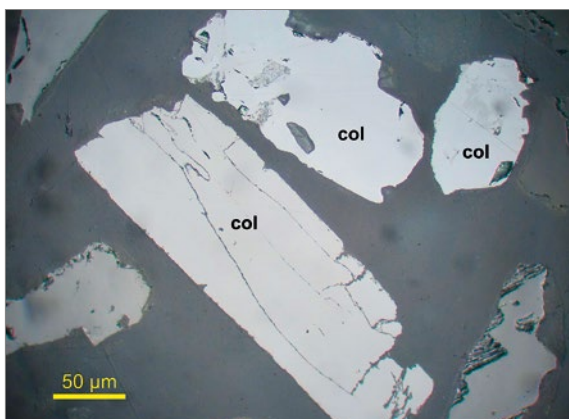


Fig. 10.5A: Section #16, RM, 500x, ||: Columbite grains with different reflection colours by reflection anisotropy.

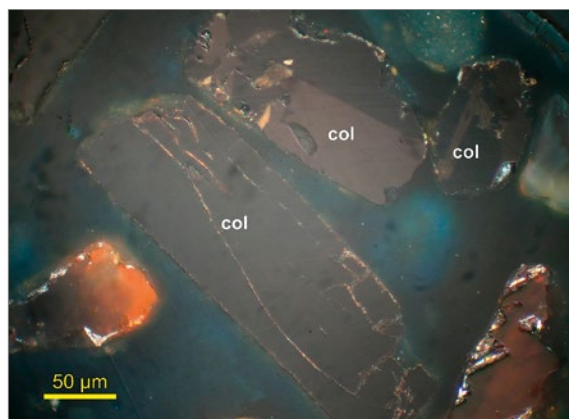


Fig. 10.6A: Section #16, RM, 500x, #: Anisotropy colours in polarized light.

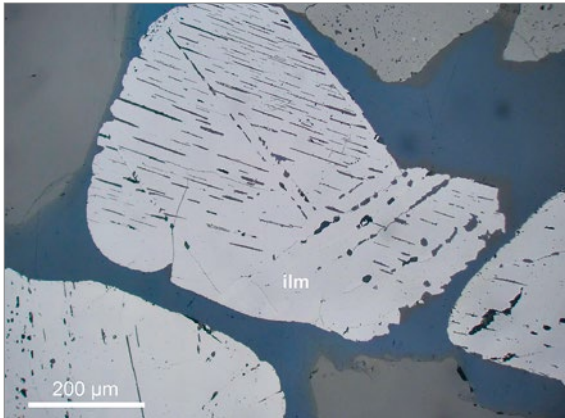


Fig. 10.7A: Section #06, RM, 200x, ||: Corroded ilmenite with oriented lamellae.

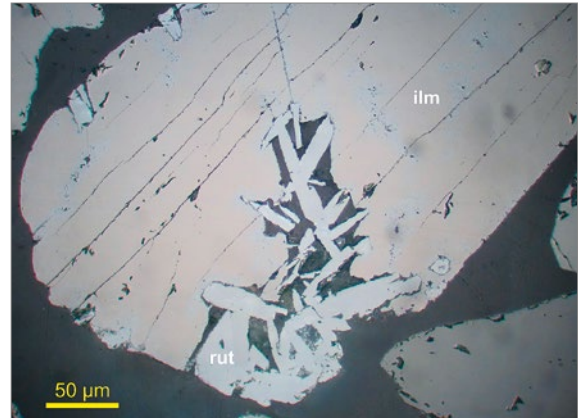


Fig. 10.8A: Section #05, RM, 500x, ||: Ilmenite, partial changed into rutile.

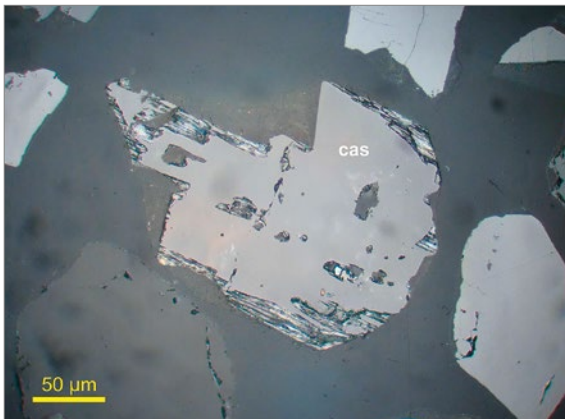


Fig. 10.9A: Section #16, RM, 500x, ||: Cassiterite grain.

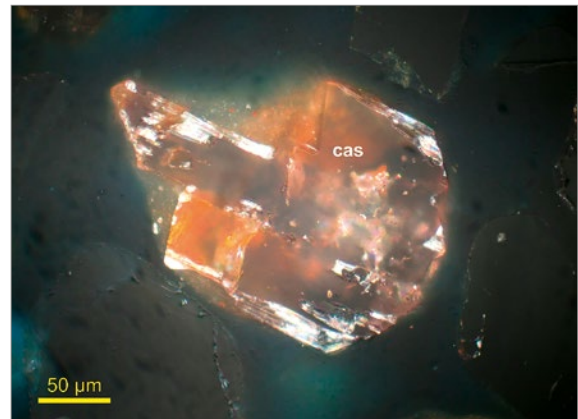


Fig. 10.10A: Section #16, RM, 500x, #: Same grain with orange-brown internal reflections.

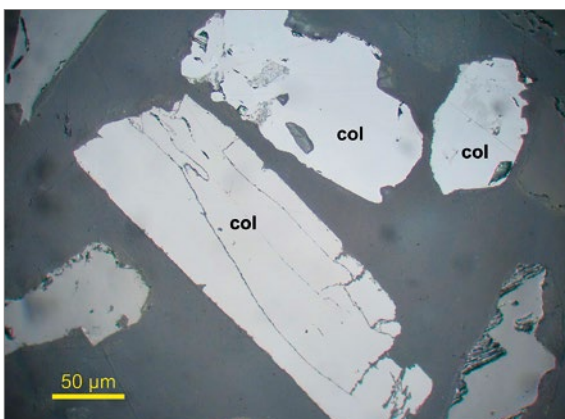


Fig. 10.11A: Section #18, TM, 125x, ||: Grain of cassiterite, zoned by growth.

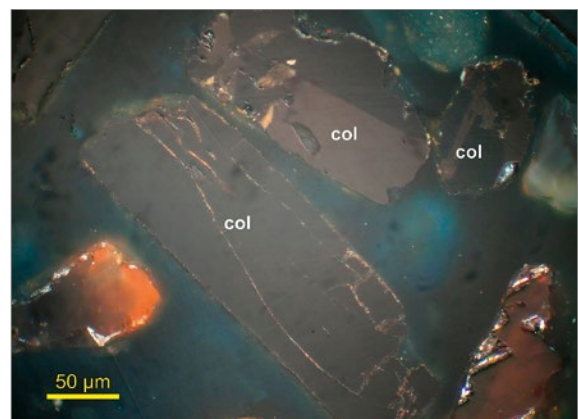


Fig. 10.12A: Section #11, TM, 250x, ||: Colourless cassiterite with reddish brown stripes.

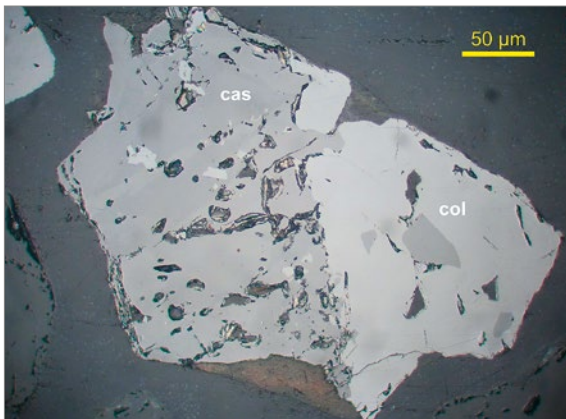


Fig. 10.13A: Section #17, RM, 500x, ||: Cassit-
erite – columbite intergrowth.

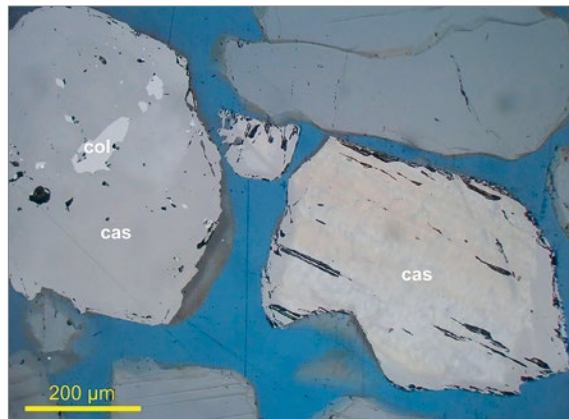


Fig. 10.14A: Section #17, RM, 200x, ||: Cassit-
erite with bodies of columbite and
pure cassiterite.

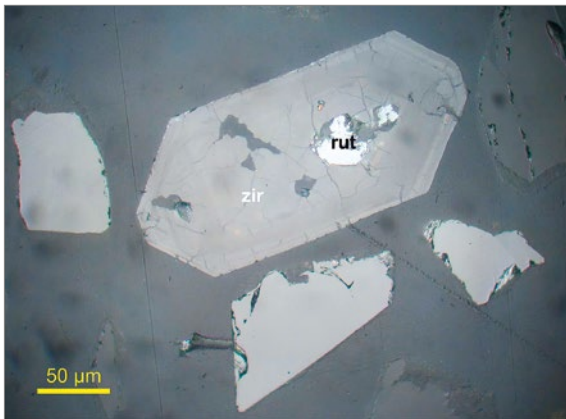


Fig. 10.15A: Section #16, RM, 500x, ||: Zircon
crystal with rutile inclusion.



Fig. 10.16A: Section #16, RM, 500x, #: Different
Zircons with inclusions and with
disseminated Fe-phases.

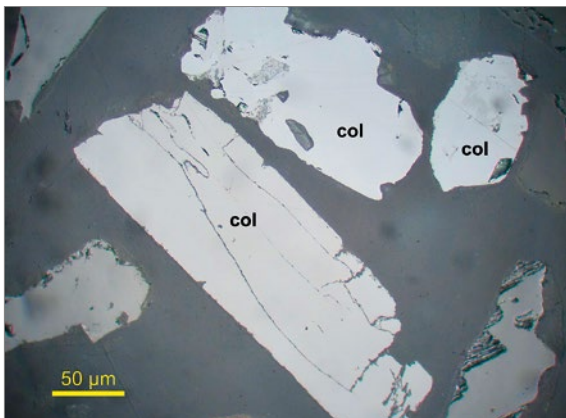


Fig. 10.17A: Section #05, TM, 125x, ||: Monazite
common with cassiterite and
opaque grains.

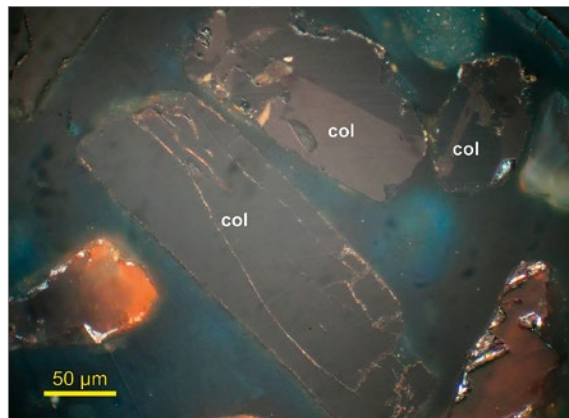


Fig. 10.18A: Section #05, TM, 125x, #: Charac-
teristic greenish interference
colour of monazite.

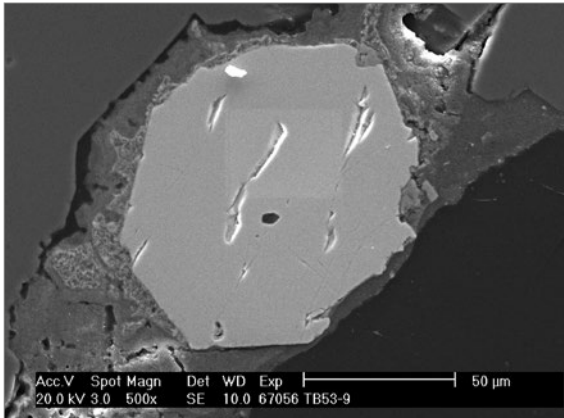


Fig. 10.19A: Section #09, SEM-SEI: Crystal of xenotime in clay mineral – goethite mass on quartz.



Fig. 10.20A: Section #06, RM, 125x, ||: Isolated euxenite grain with pyrochlore alterations (darker zones).

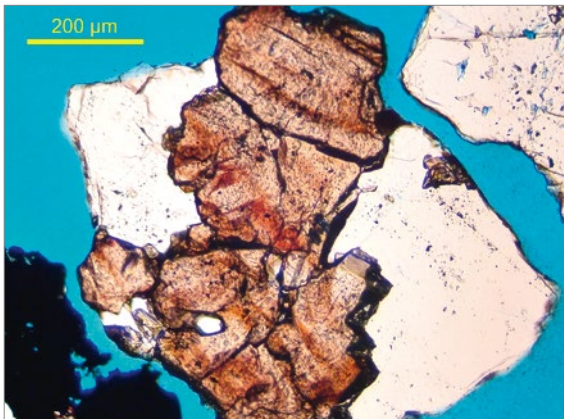


Fig. 10.21A: Section #12, RM, 125x, ||: Single intergrowth between quartz and cassiterite.

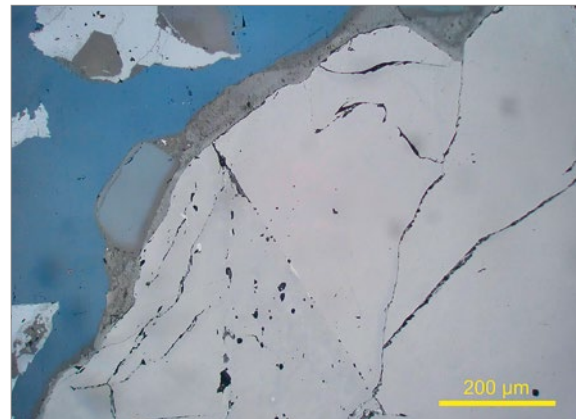


Fig. 10.22A: Section #12, RM, 200x, ||: Coatings of clay minerals on cassiterite.

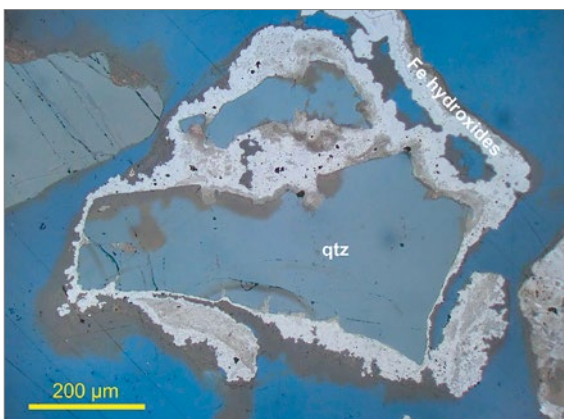


Fig. 10.23A: Section #24, RM, 200x, ||: Agglomerates of quartz and Fe-Hydroxides.

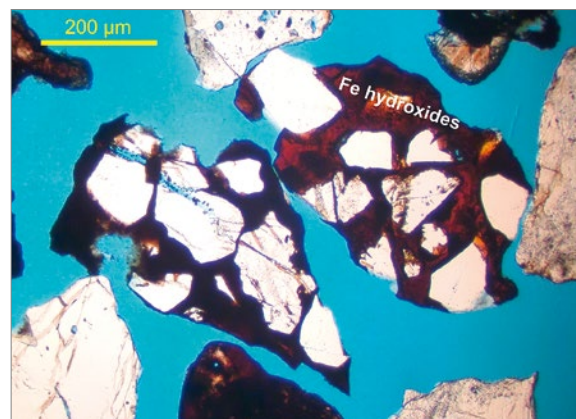


Fig. 10.24A: Section #12, TM, 125x, ||: Agglomerates of Fe-Hydroxides and quartz and topaz in heavy fraction.

Appendix 11

Mineral liberation analysis – MLA

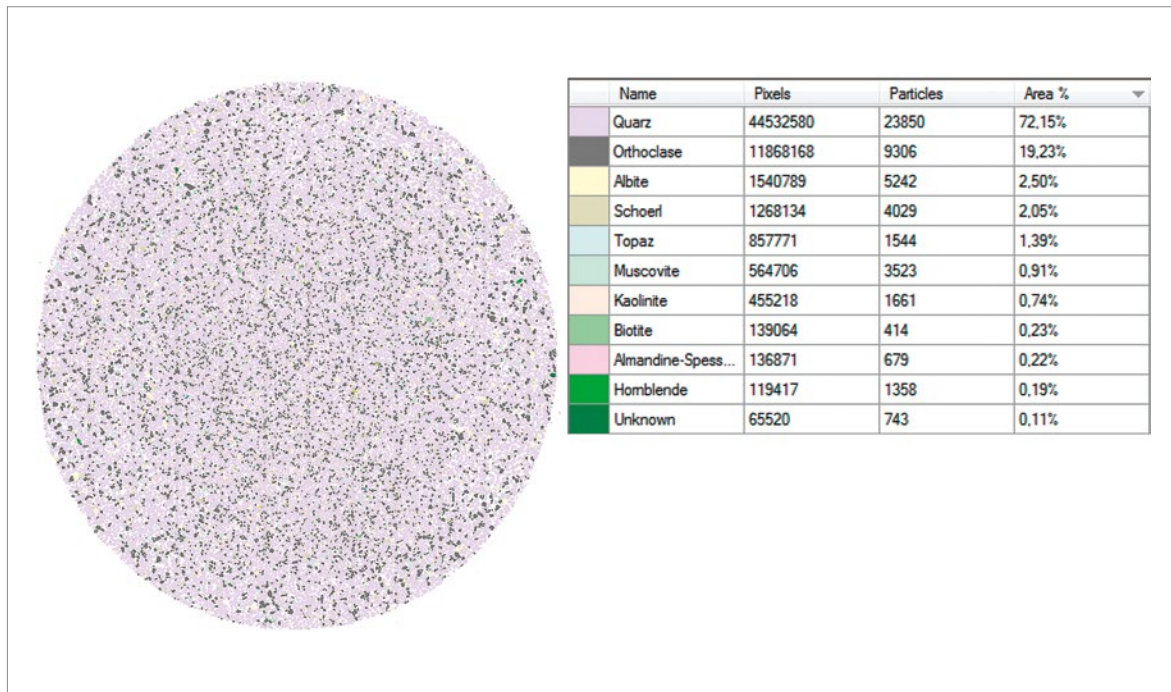


Fig. 11.1A: Thin section of sample TB45-48, grain size range 63–200 μm , light fraction.

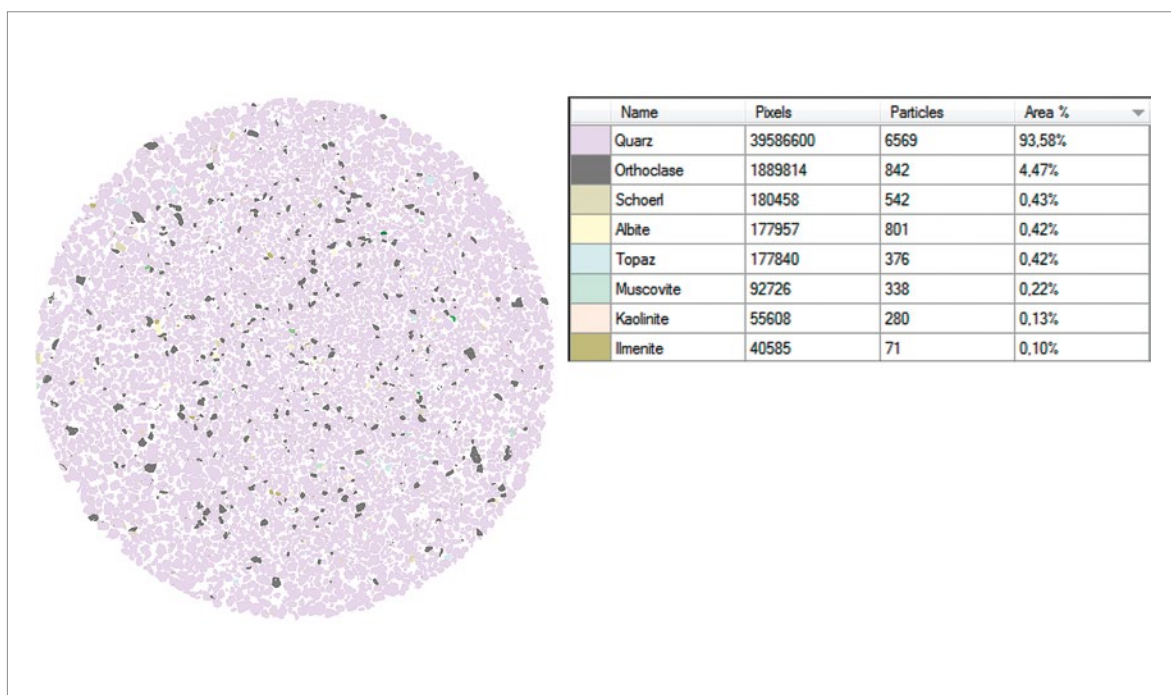


Fig. 11.2A: Thin section of sample TB45-48, grain size range 200–630 μm , light fraction.

Mineral liberation analysis – MLA

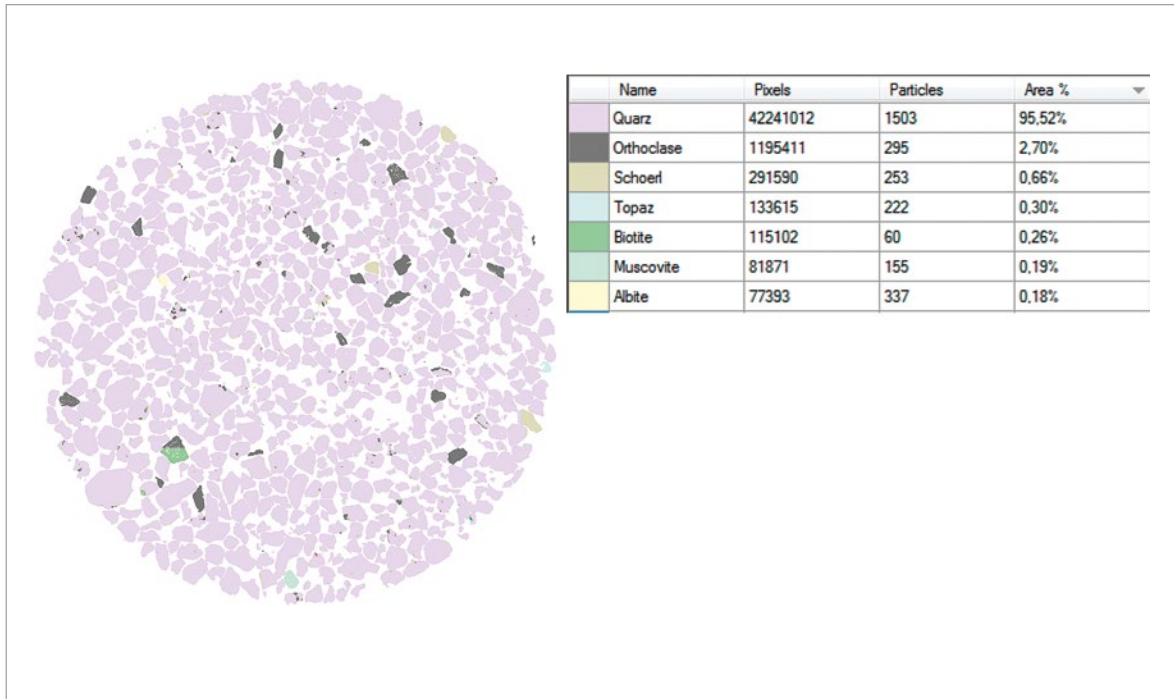


Fig. 11.3A: Thin section of sample TB45-48, grain size range 630–2000 µm, light fraction.

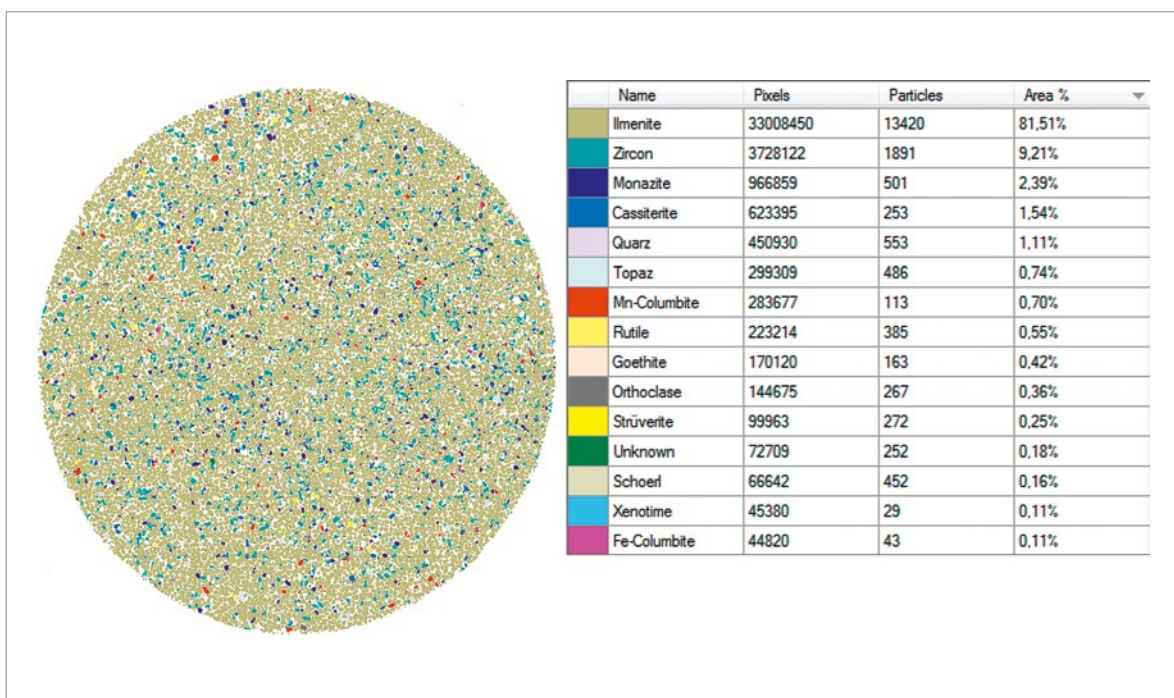


Fig. 11.4A: Thin section of sample TB45-48, grain size range 200–630 µm, light fraction.

Mineral liberation analysis – MLA

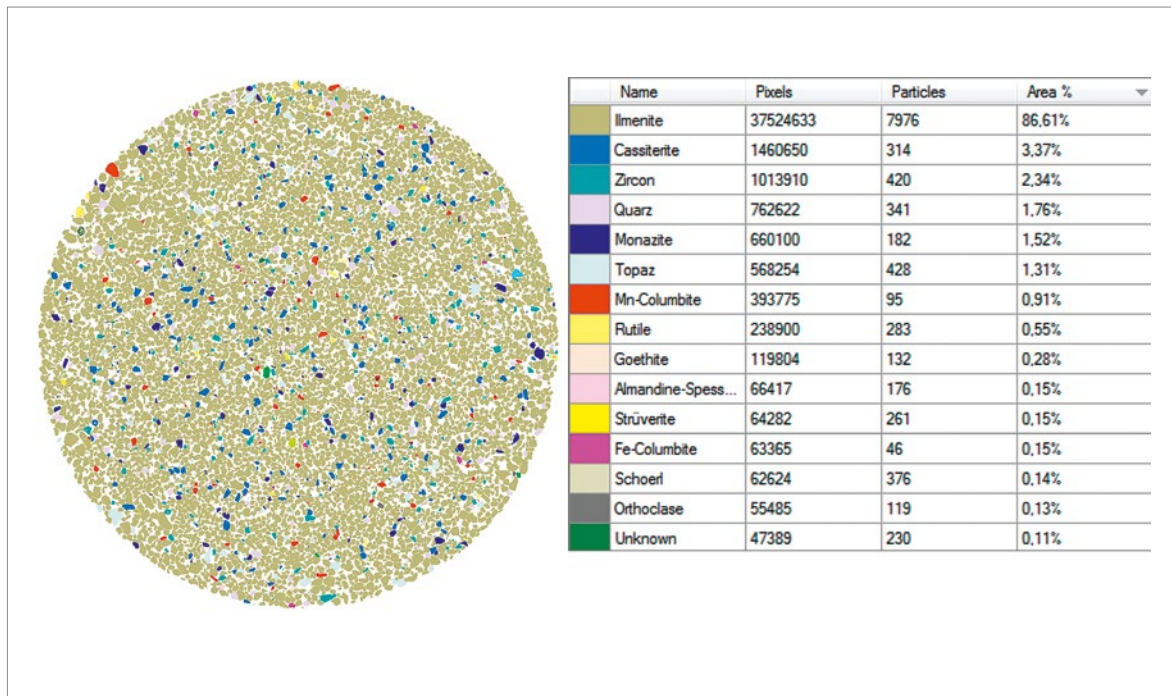


Fig. 11.5A: Thin section of sample TB45-48, grain size range 200–630 μm , heavy fraction.

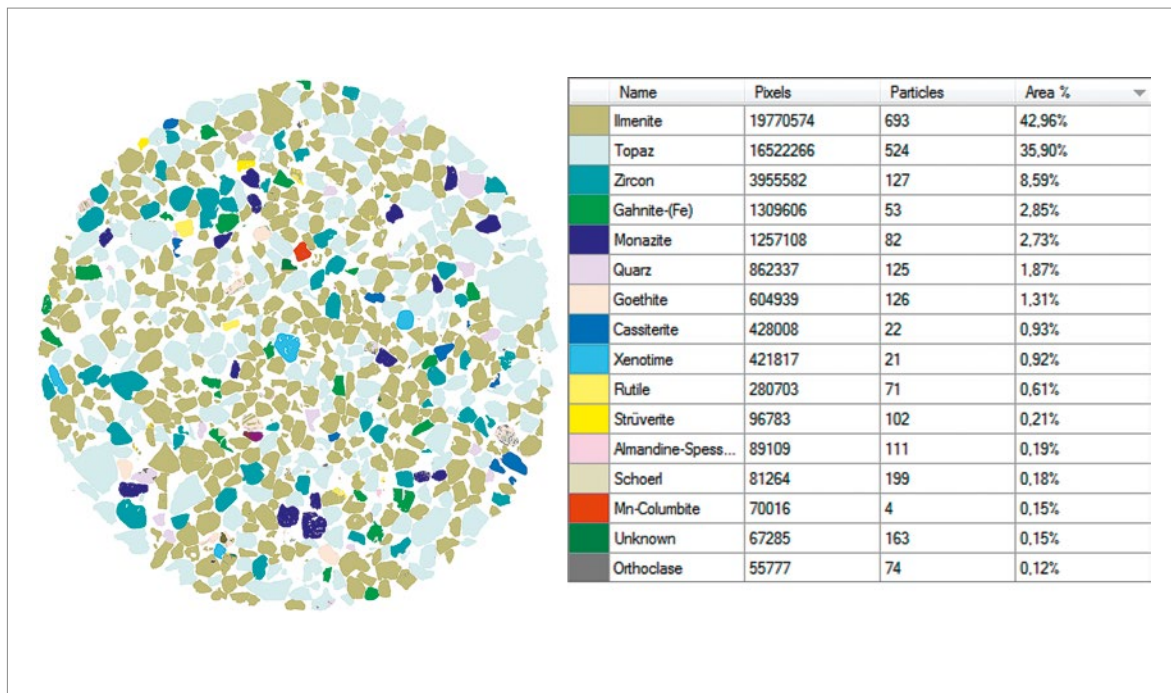


Fig. 11.6A: Thin section of sample TB45-48, grain size range 630–2000 μm , heavy fraction.

Mineral liberation analysis – MLA

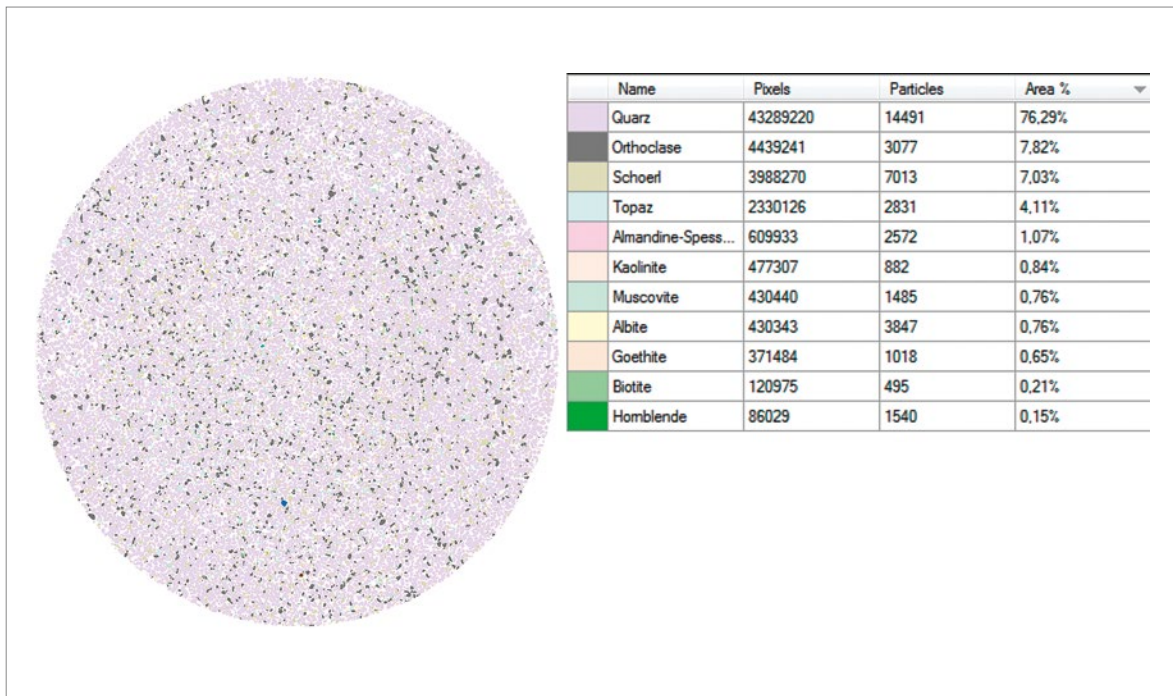


Fig. 11.7A: Thin section of sample TB53, grain size range 63–200 μm , light fraction.

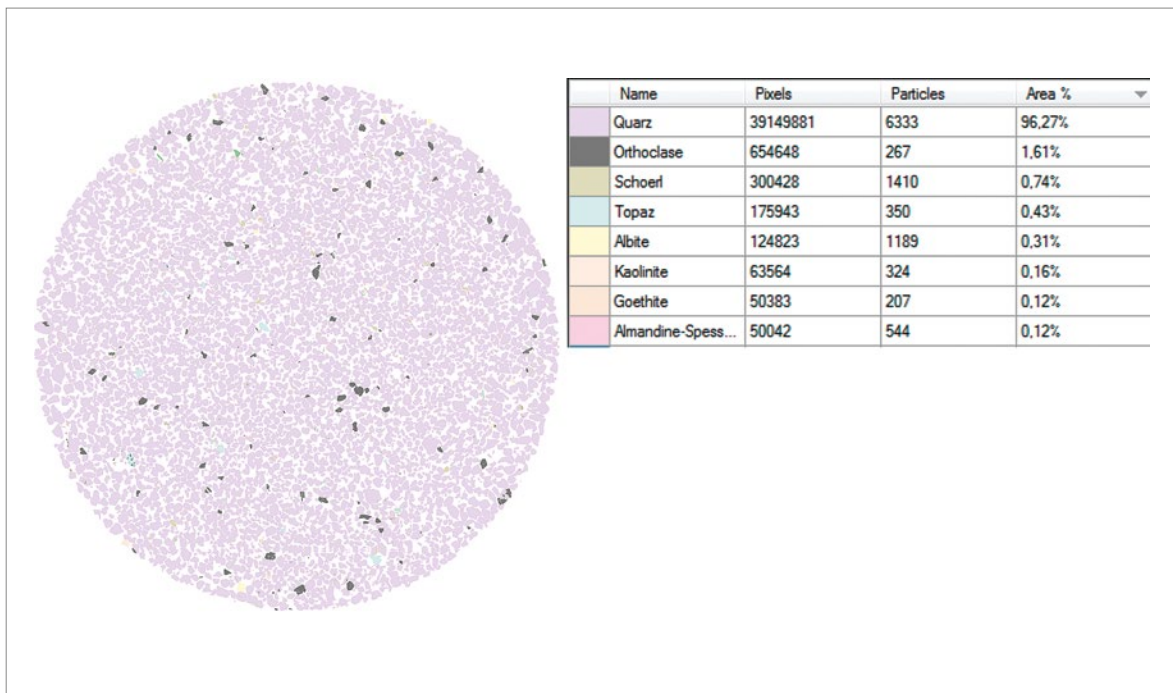


Fig. 11.8A: Thin section of sample TB53, grain size range 200–630 μm , light fraction.

Mineral liberation analysis – MLA

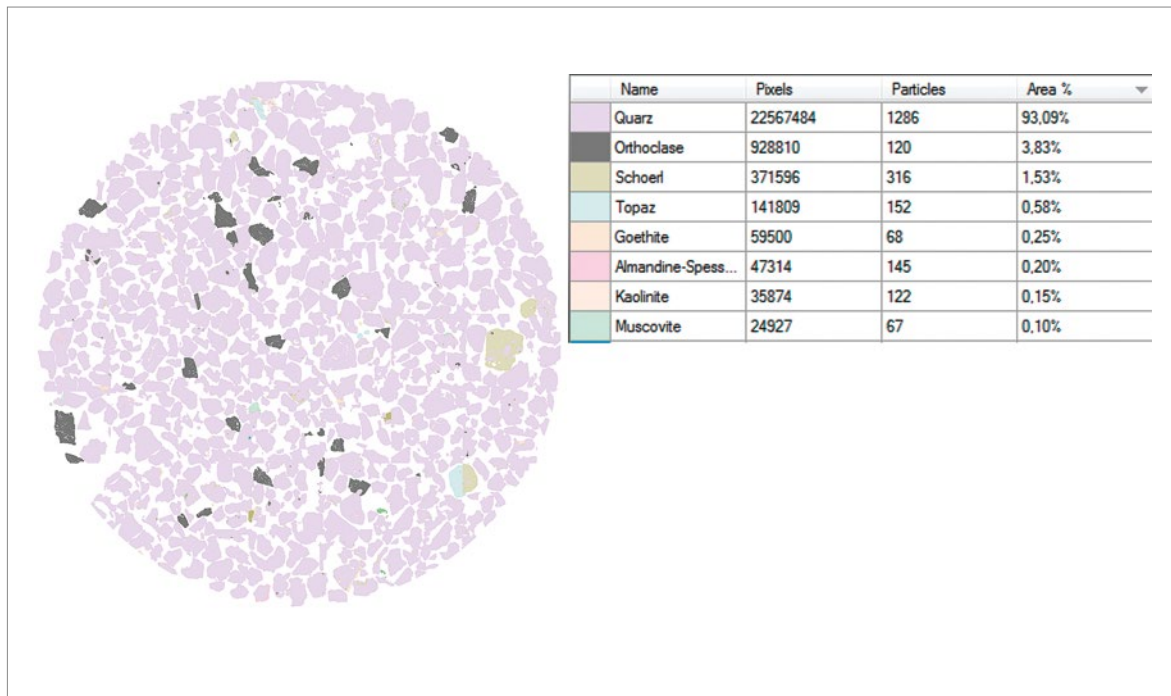


Fig. 11.9A: Thin section of sample TB53, grain size range 630–2000 μm , light fraction.

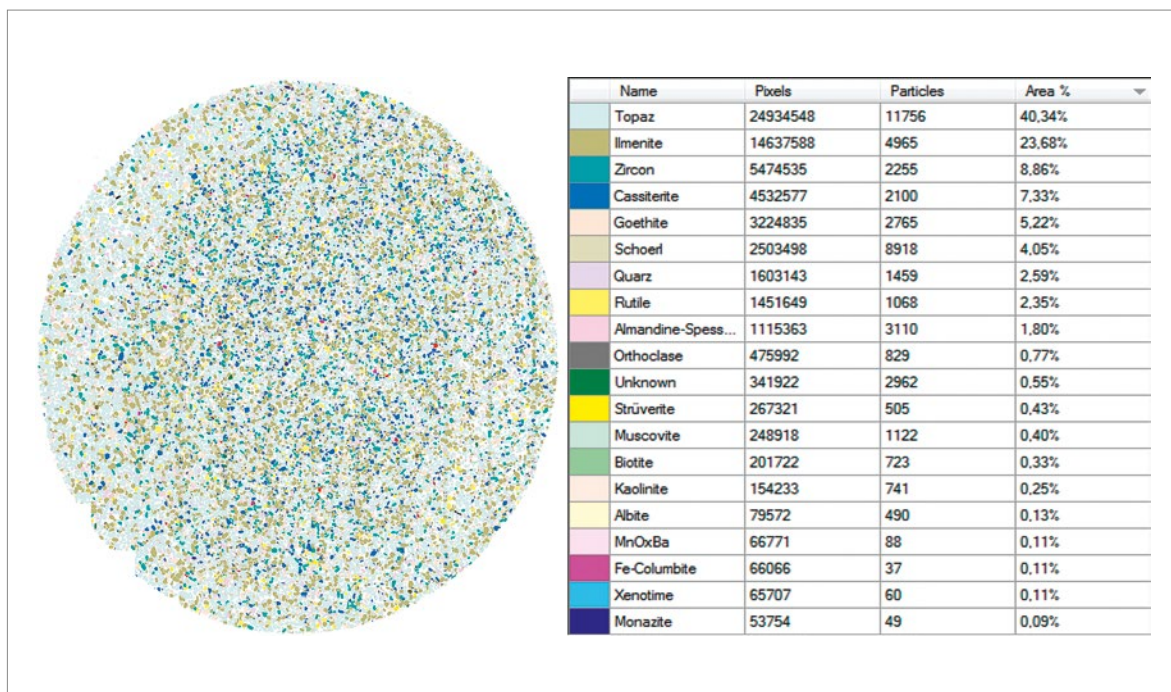


Fig. 11.10A: Thin section of sample TB53, grain size range 63–200 μm , heavy fraction.

Mineral liberation analysis – MLA

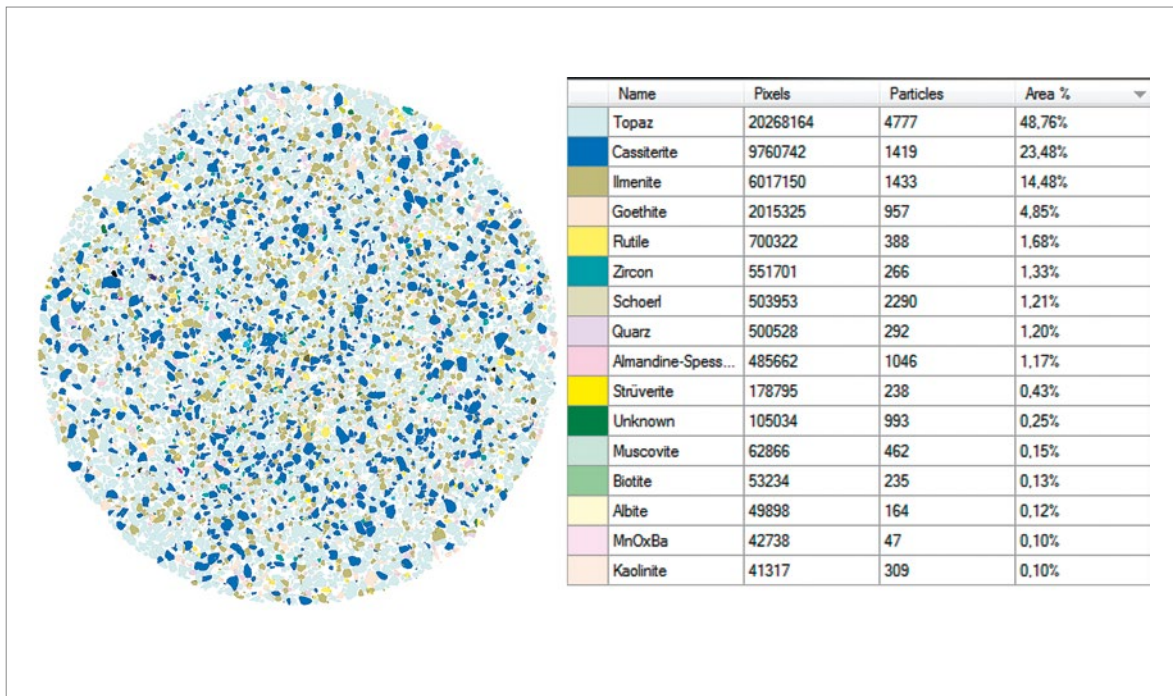


Fig. 11.11A: Thin section of sample TB53, grain size range 200–630 μm , heavy fraction.

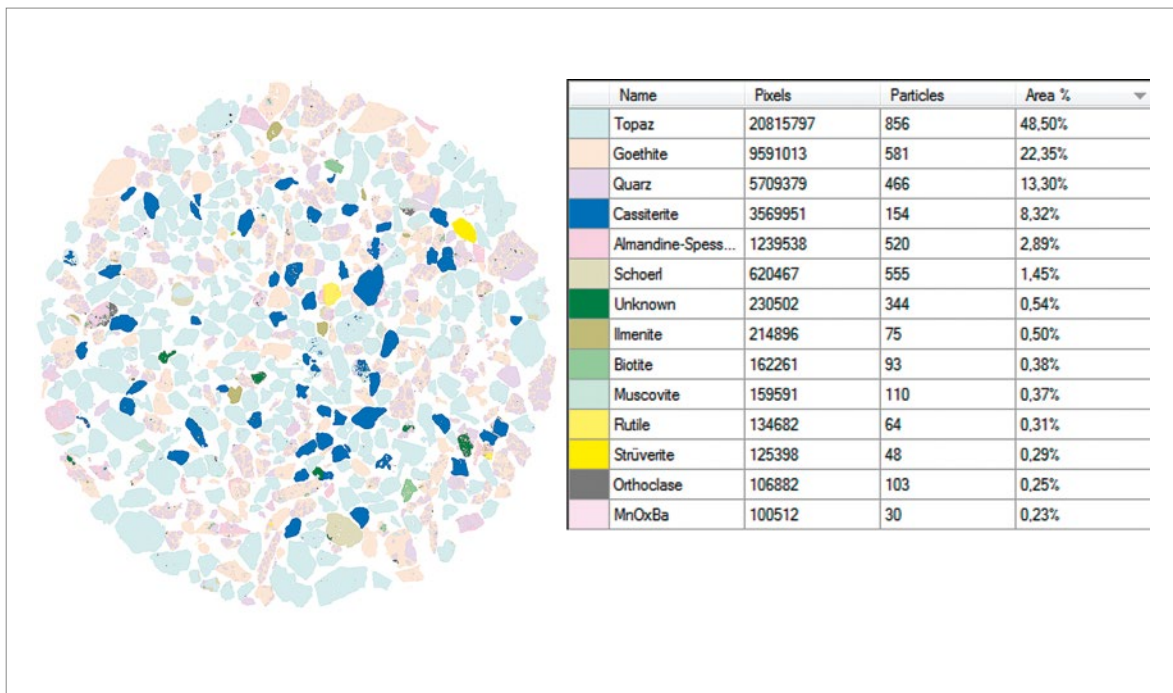


Fig. 11.12A: Thin section of sample TB53, grain size range 630–2000 μm , heavy fraction.

Mineral liberation analysis – MLA

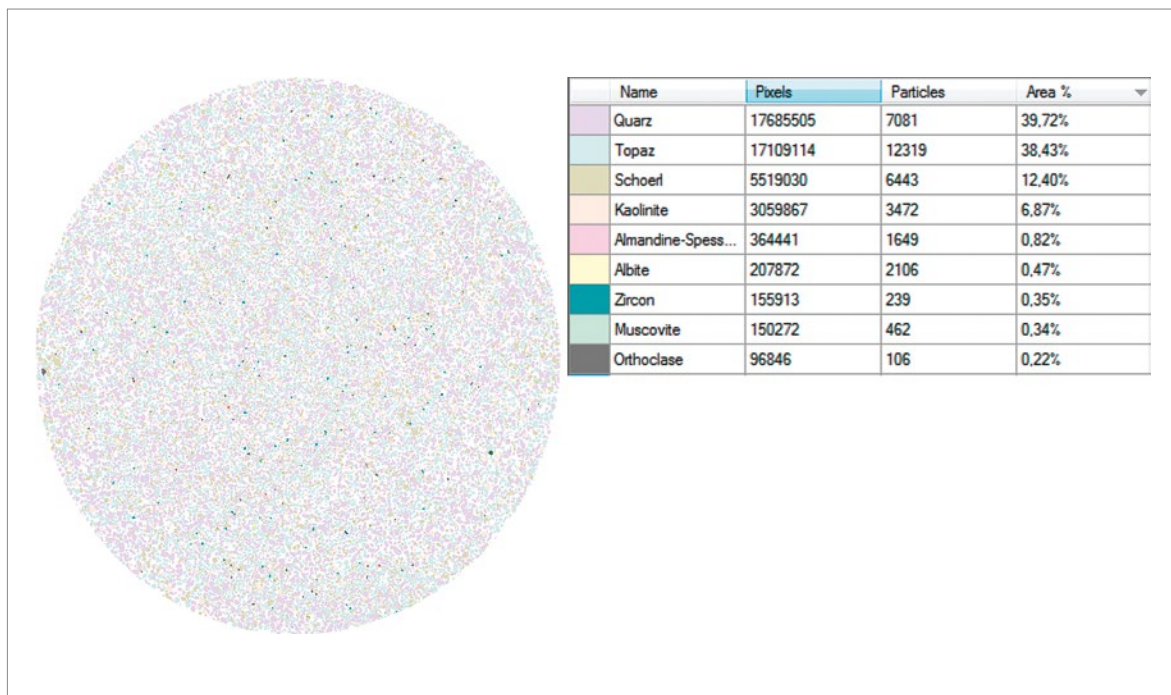


Fig. 11.13A: Thin section of sample TB55, grain size range 63–200 μm , light fraction.

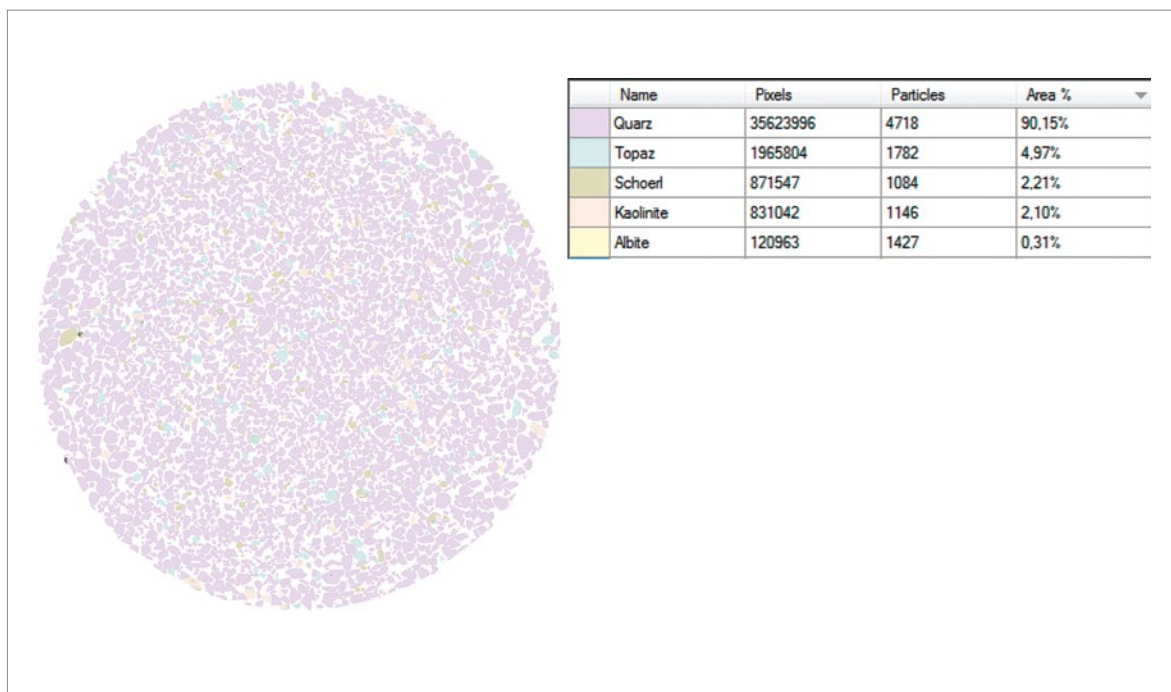


Fig. 11.14A: Thin section of sample TB55, grain size range 200–630 μm , light fraction.

Mineral liberation analysis – MLA

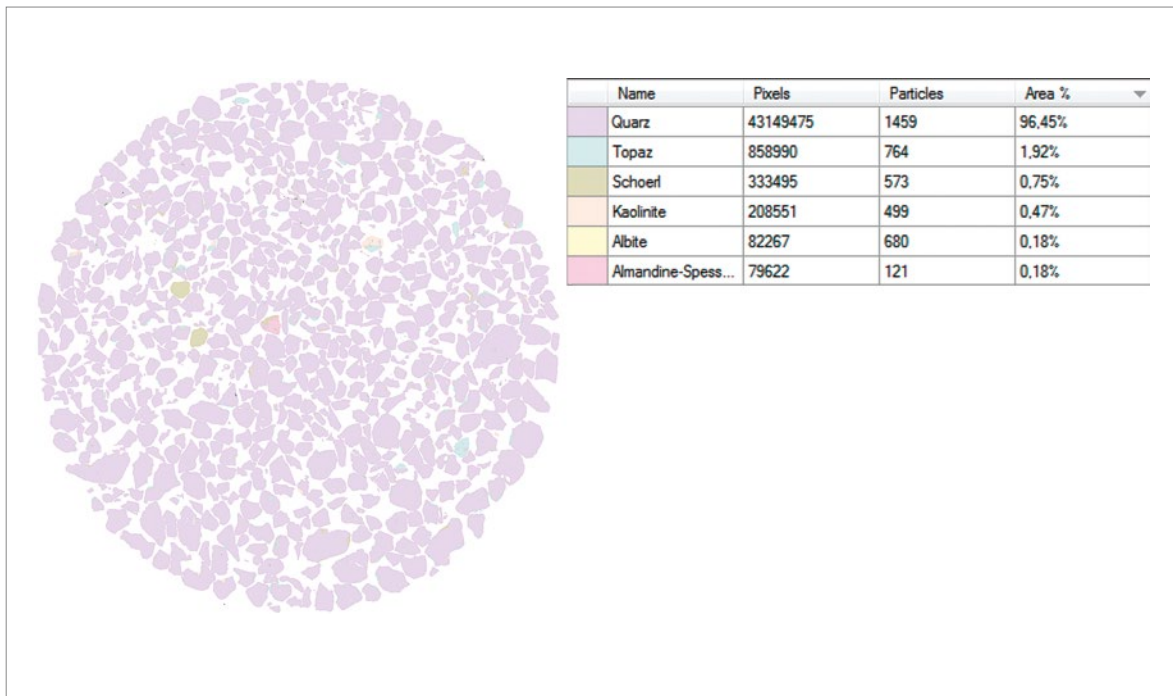


Fig. 11.15A: Thin section of sample TB55, grain size range 630–2000 μm , light fraction.

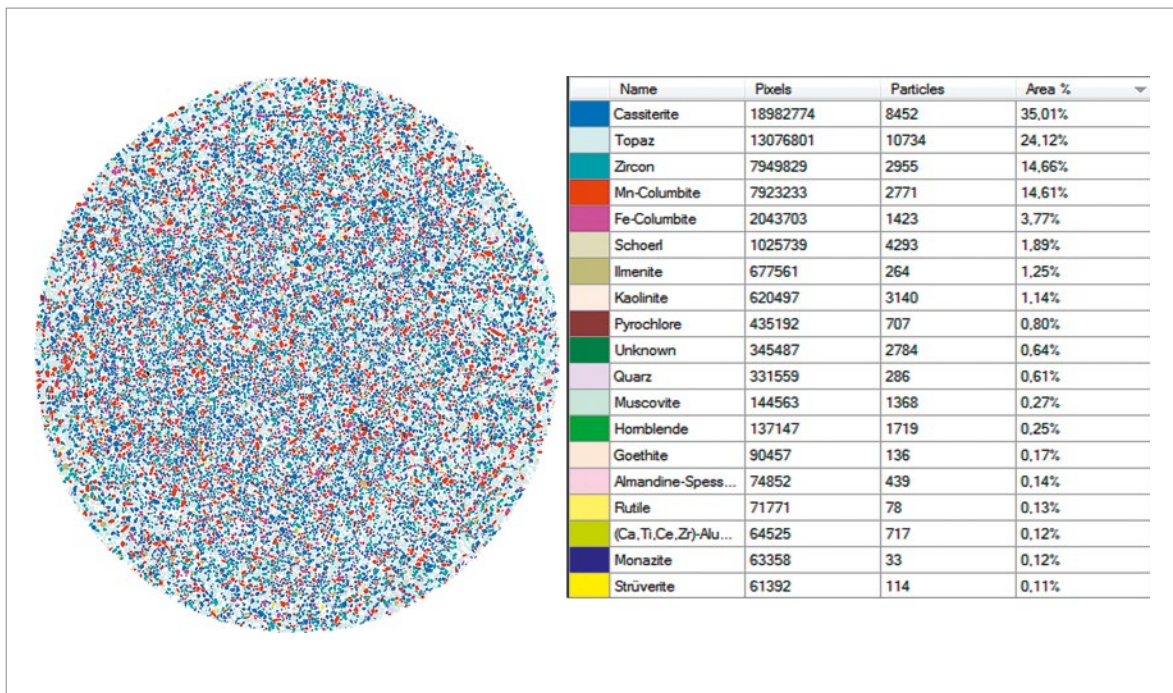


Fig. 11.16A: Thin section of sample TB55, grain size range 63–200 μm , heavy fraction.

Mineral liberation analysis – MLA

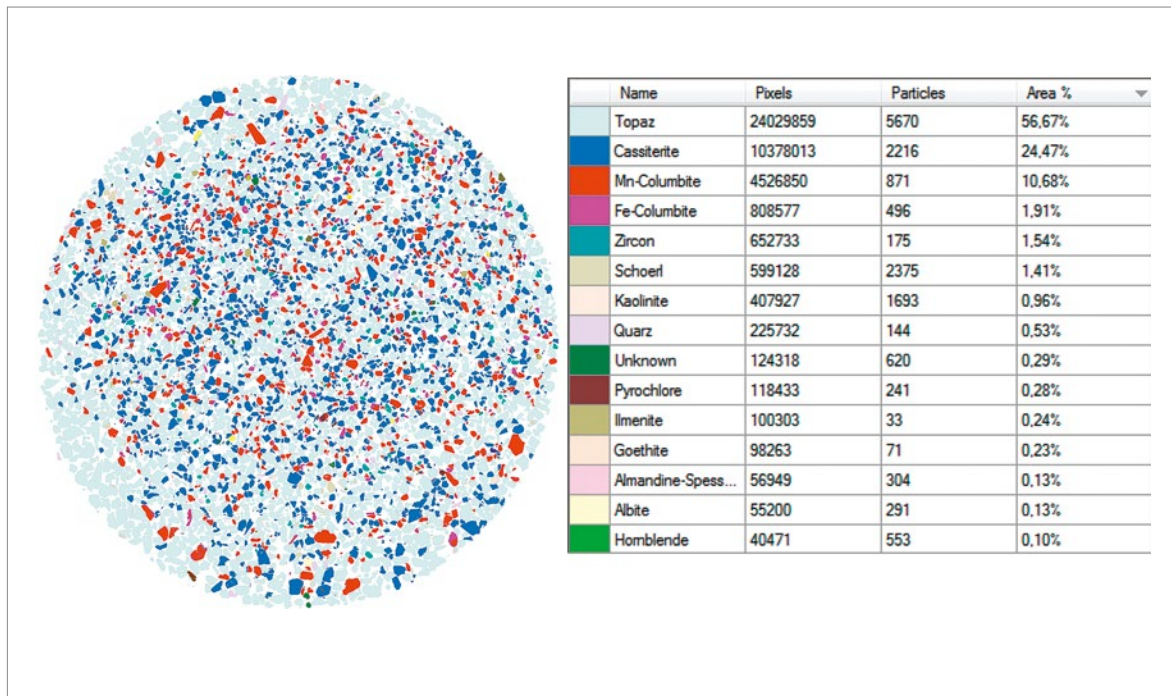


Fig. 11.17A: Thin section of sample TB55, grain size range 200–630 μm , heavy fraction.

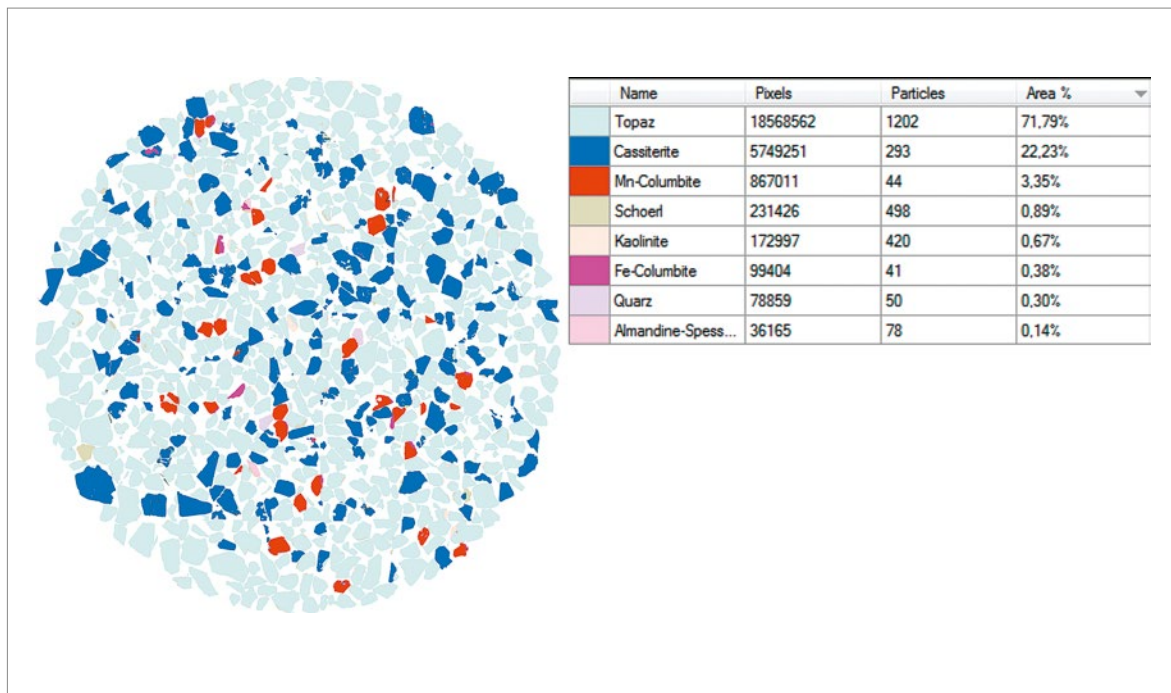


Fig. 11.18A: Thin section of sample TB55, grain size range 630–2000 μm , heavy fraction.

Mineral liberation analysis – MLA

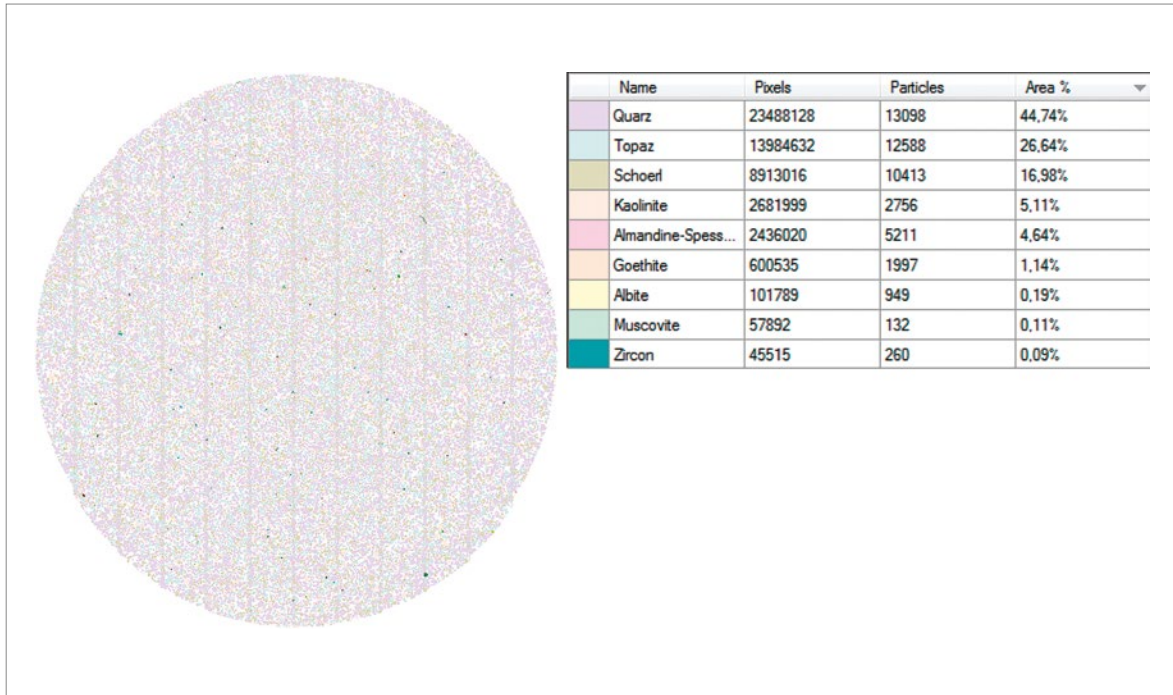


Fig. 11.19A: Thin section of sample TB59, grain size range 63–200 μm , light fraction.

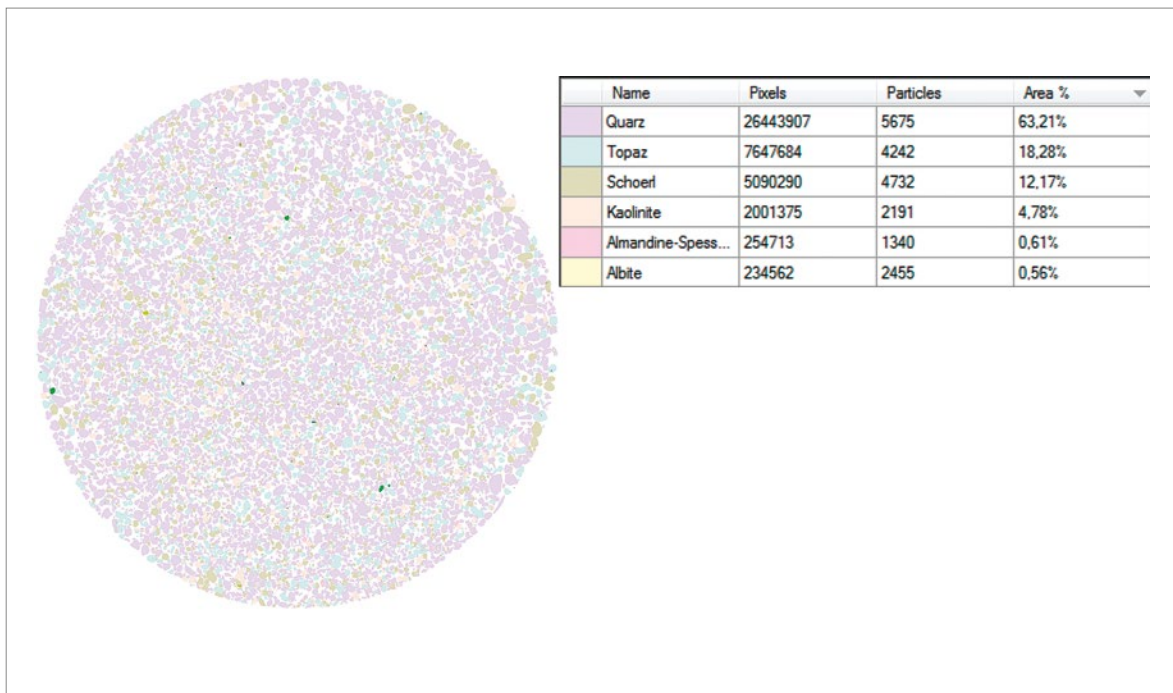


Fig. 11.20A: Thin section of sample TB59, grain size range 200–630 μm , light fraction.

Mineral liberation analysis – MLA

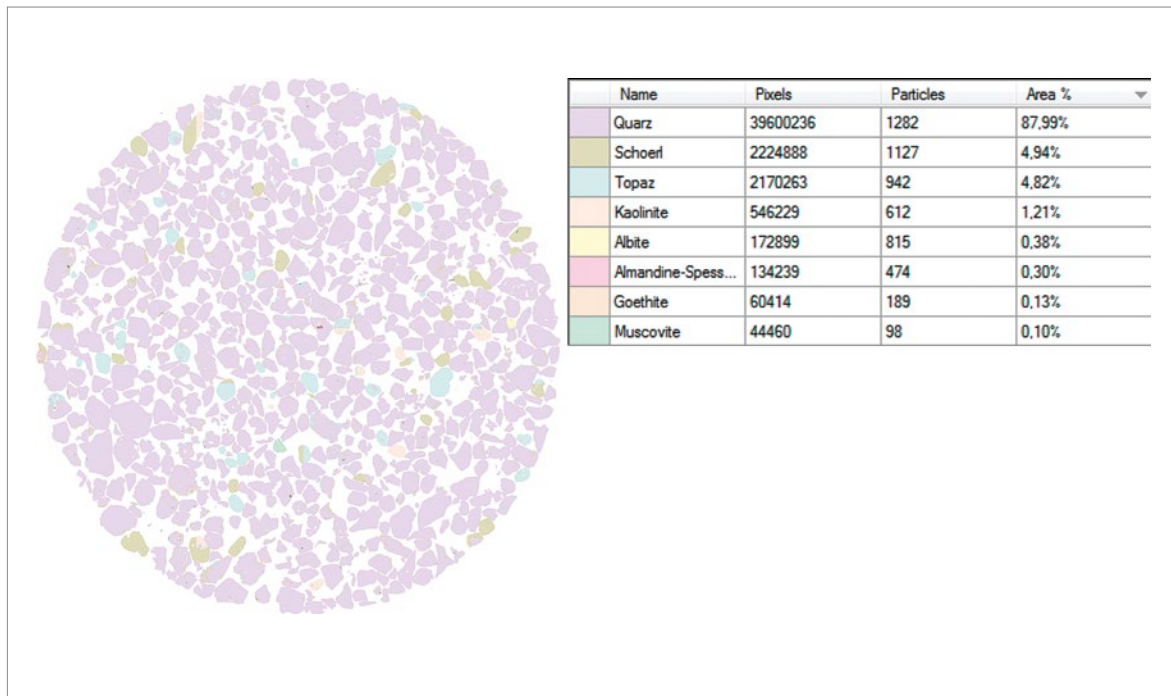


Fig. 11.21A: Thin section of sample TB59, grain size range 630–2000 μm , light fraction.

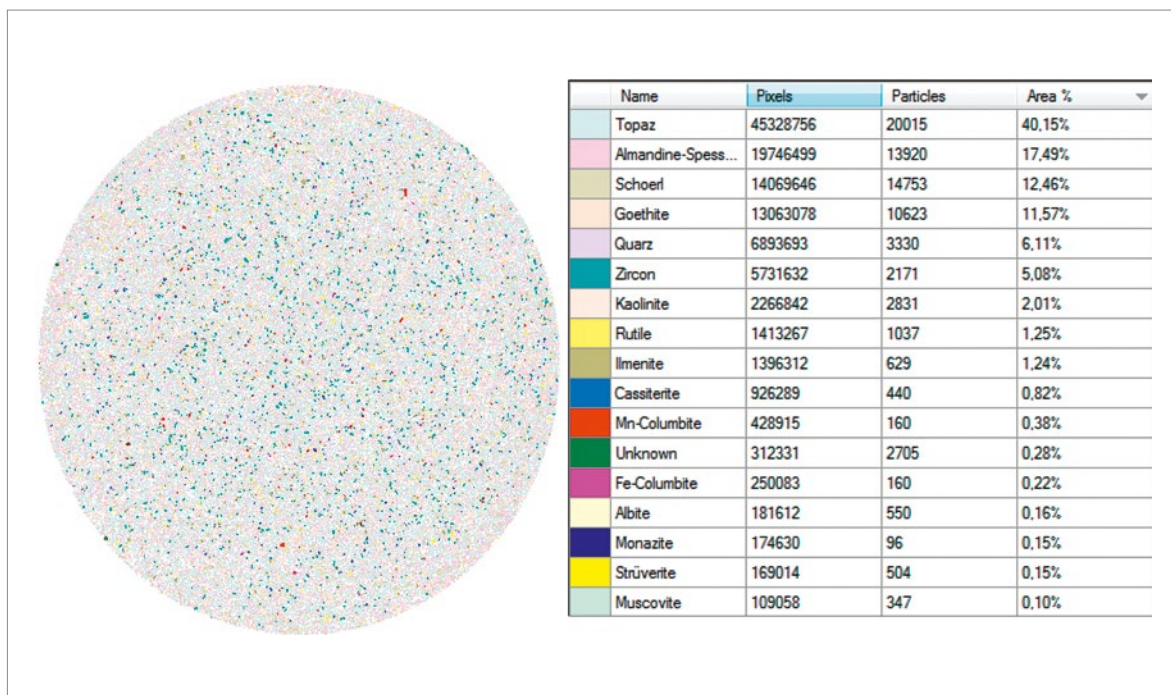


Fig. 11.22: Thin section of sample TB59, grain size range 63–200 μm heavy fraction.

Mineral liberation analysis – MLA

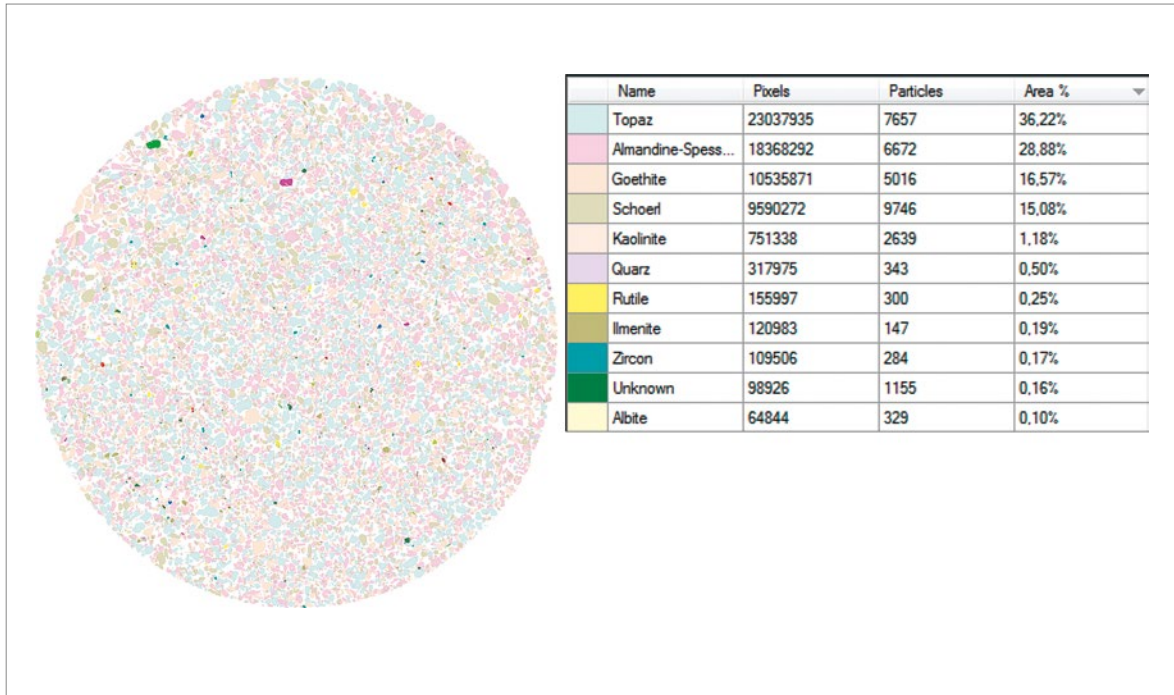


Fig. 11.23A: Thin section of sample TB59, grain size range 200–630 μm , heavy fraction.

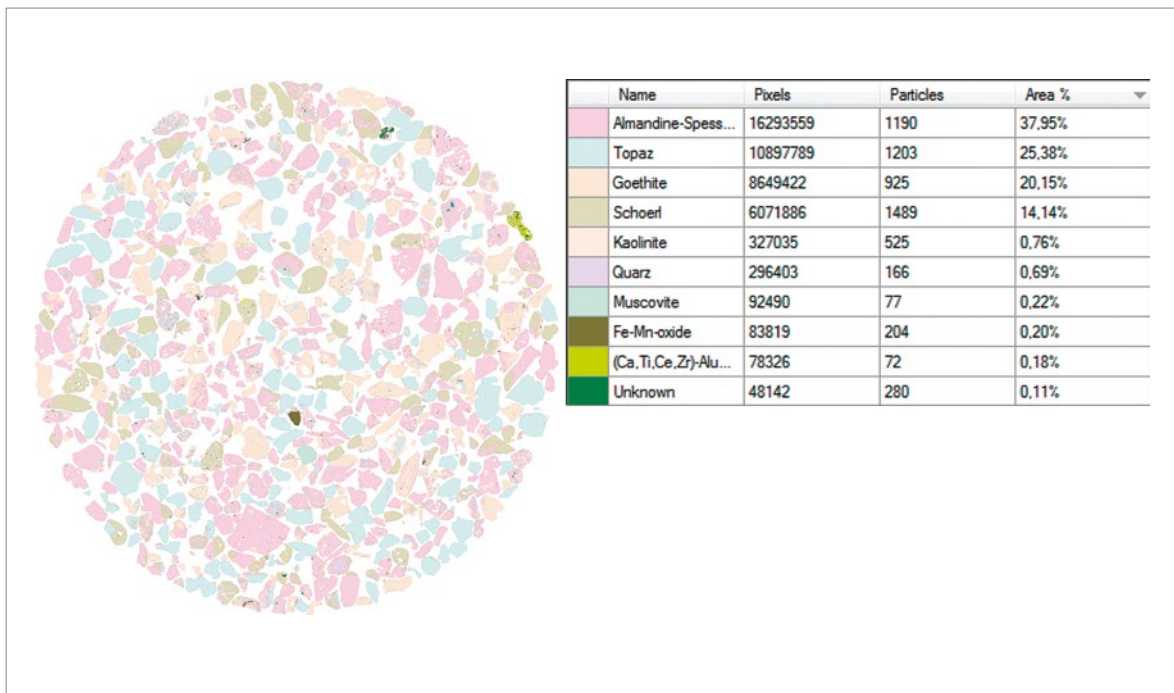


Fig. 11.24A: Thin section of sample TB59, grain size range 630–2000 μm , heavy fraction.

**Deutsche Rohstoffagentur (DERA) in der
Bundesanstalt für Geowissenschaften und Rohstoffe (BGR)**

Wilhelmstraße 25–30
13593 Berlin
Tel.: +49 30 36993 226
dera@bgr.de
www.deutsche-rohstoffagentur.de

ISBN: 978-3-943566-83-3 (Druckversion)
ISBN: 978-3-943566-84-0 (PDF)
ISSN: 2193-5319